

12-2012

# Determination of the Maximum MGS Mounting Height Phase II Detailed Analysis

Ramen D. Julin

*University of Nebraska-Lincoln, r.d.julin@gmail.com*

Ronald K. Faller

*University of Nebraska - Lincoln, rfaller1@unl.edu*

John D. Reid

*University of Nebraska - Lincoln, jreid@unl.edu*

Mario Mongiardini

*university of Nebraska - Lincoln*

Follow this and additional works at: <http://digitalcommons.unl.edu/ndor>



Part of the [Transportation Engineering Commons](#)

Julin, Ramen D.; Faller, Ronald K.; Reid, John D.; and Mongiardini, Mario, "Determination of the Maximum MGS Mounting Height Phase II Detailed Analysis" (2012). *Nebraska Department of Transportation Research Reports*. 122.  
<http://digitalcommons.unl.edu/ndor/122>

This Article is brought to you for free and open access by the Nebraska LTAP at DigitalCommons@University of Nebraska - Lincoln. It has been accepted for inclusion in Nebraska Department of Transportation Research Reports by an authorized administrator of DigitalCommons@University of Nebraska - Lincoln.



*Midwest States Regional Pooled Fund Research Program  
Fiscal Year 2009-2010 (Year 20)  
Research Project Number TPF-5(193)  
NDOR Sponsoring Agency Code RFPF-10-MGS*

# **DETERMINATION OF THE MAXIMUM MGS MOUNTING HEIGHT – PHASE II DETAILED ANALYSIS WITH LS-DYNA<sup>®</sup>**

Submitted by

Ramen D. Julin, B.S.M.E., E.I.T.  
Former Graduate Research Assistant

John D. Reid, Ph.D.  
Professor

Ronald K. Faller, Ph.D., P.E.  
Research Assistant Professor  
Interim MwRSF Director

Mario Mongiardini, Ph.D.  
Former Post-Doctoral Research Assistant

## **MIDWEST ROADSIDE SAFETY FACILITY**

Nebraska Transportation Center  
University of Nebraska-Lincoln  
130 Whittier Research Center  
2200 Vine Street  
Lincoln, Nebraska 68583-0853  
(402) 472-0965

Submitted to

## **MIDWEST STATES REGIONAL POOLED FUND PROGRAM**

Nebraska Department of Roads  
1500 Nebraska Highway 2  
Lincoln, Nebraska 68502

MwRSF Research Report No. TRP-03-274-12

December 5, 2012

## TECHNICAL REPORT DOCUMENTATION PAGE

1. Report No. <b>TRP-03-274-12</b>	2.	3. Recipient's Accession No.	
4. Title and Subtitle <b>Determination of the Maximum MGS Mounting Height – Phase II Detailed Analysis Using LS-DYNA<sup>®</sup></b>		5. Report Date <b>December 5, 2012</b>	
7. Author(s) <b>Julin, R.D., Reid, J.D., Faller, R.K., and Mongiardini, M.</b>		8. Performing Organization Report No. <b>TRP-03-274-12</b>	
9. Performing Organization Name and Address <b>Midwest Roadside Safety Facility (MwRSF) Nebraska Transportation Center University of Nebraska-Lincoln 130 Whittier Research Center 2200 Vine Street Lincoln, Nebraska 68583-0853</b>		10. Project/Task/Work Unit No.	
		11. Contract © or Grant (G) No. <b>TPF-5(193)</b>	
12. Sponsoring Organization Name and Address <b>Midwest States Regional Pooled Fund Program Nebraska Department of Roads 1500 Nebraska Highway 2 Lincoln, Nebraska 68502</b>		13. Type of Report and Period Covered <b>Final Report: 2010 – 2012</b>	
		14. Sponsoring Agency Code <b>RPPF-10-MGS</b>	
15. Supplementary Notes <b>Prepared in cooperation with U.S. Department of Transportation, Federal Highway Administration.</b>			
16. Abstract (Limit: 200 words) <p>Determination of the maximum Midwest Guardrail System (MGS) mounting height was performed in two phases. Phase I concentrated on crash testing: two full-scale crash tests were performed on the MGS with top-rail mounting heights of 34 in. (864 mm) and 36 in. (914 mm), each impacted by 1100C vehicles. Both system heights satisfied the Manual for Assessing Safety Hardware (MASH) Test Level 3 (TL-3) evaluation criteria for test no. 3-10. Phase I was documented in the Midwest Roadside Safety Facility (MwRSF) Report No. TRP-03-255-12.</p> <p>Phase II, the subject of this report, concentrated on a detailed analysis of an increased-height MGS using computer simulation (Barrier VII and LS-DYNA). It was shown that on level terrain the MGS would satisfy MASH TL-3 evaluation criteria with rail heights up to 36 in. Also, errant passenger vehicles were successfully contained on approach slopes as steep as 6:1 when the rail was mounted at 36 in. Also, the 820C vehicle redirection was improved on 8:1 approach slopes with rail mounting heights as large as 36 in. (914 mm). Furthermore, the effects of various vehicle geometries and their associated complications were investigated.</p> <p>Additional full-scale vehicle crash tests are necessary to confirm the simulation results before these taller systems can be deemed crashworthy according to MASH. Nonetheless, there appeared to be a considerable amount of upside tolerance for the rail height on the MASH-approved MGS. Evidence of this was given in a prior high-flare-rate study and the current study.</p>			
17. Document Analysis/Descriptors <b>Highway Safety, Crash Test, Roadside Appurtenances, Compliance Test, MASH, MGS, Maximum Height, Embedment Depth, Approach Slopes</b>		18. Availability Statement <b>No restrictions. Document available from: National Technical Information Services, Springfield, Virginia 22161</b>	
19. Security Class (this report) <b>Unclassified</b>	20. Security Class (this page) <b>Unclassified</b>	21. No. of Pages <b>211</b>	22. Price

### **DISCLAIMER STATEMENT**

This report was completed with funding from the Federal Highway Administration, U.S. Department of Transportation. The contents of this report reflect the views and opinions of the authors who are responsible for the facts and the accuracy of the data presented herein. The contents do not necessarily reflect the official views or policies of the state highway departments participating in the Midwest States Regional Pooled Fund Program nor the Federal Highway Administration, U.S. Department of Transportation. This report does not constitute a standard, specification, regulation, product endorsement, or an endorsement of manufacturers.

### **UNCERTAINTY OF MEASUREMENT STATEMENT**

The Midwest Roadside Safety Facility (MwRSF) has determined the uncertainty of measurements for several parameters involved in standard full-scale crash testing and non-standard testing of roadside safety features. Information regarding the uncertainty of measurements for critical parameters is available upon request by the sponsor and the Federal Highway Administration.

### **INDEPENDENT APPROVING AUTHORITY**

The Independent Approving Authority (IAA) for the data contained herein was Ms. Karla Lechtenberg, Research Associate Engineer.

## **ACKNOWLEDGEMENTS**

The authors wish to acknowledge several sources that made a contribution to this project: (1) the Midwest States Regional Pooled Fund Program funded by the Illinois Department of Transportation, Iowa Department of Transportation, Kansas Department of Transportation, Minnesota Department of Transportation, Missouri Department of Transportation, Nebraska Department of Roads, Ohio Department of Transportation, South Dakota Department of Transportation, Wisconsin Department of Transportation, and Wyoming Department of Transportation for sponsoring this project; and (2) MwRSF personnel for constructing the barriers and conducting the crash tests.

Acknowledgement is also given to the following individuals who made a contribution to the completion of this research project.

### **Midwest Roadside Safety Facility**

J.C. Holloway, M.S.C.E., E.I.T., Test Site Manager  
K.A. Lechtenberg, M.S.M.E., E.I.T., Research Associate Engineer  
R.W. Bielenberg, M.S.M.E., E.I.T., Research Associate Engineer  
S.K. Rosenbaugh, M.S.C.E., E.I.T., Research Associate Engineer  
C.L. Meyer, B.S.M.E., E.I.T., Research Associate Engineer  
A.T. Russell, B.S.B.A., Shop Manager  
K.L. Krenk, B.S.M.A., Maintenance Mechanic  
Undergraduate and Graduate Research Assistants

### **Illinois Department of Transportation**

Tim Sheehan, P.E., Safety Design Engineer  
David Piper, P.E., Safety Implementation Engineer (Retired)

### **Iowa Department of Transportation**

David Little, P.E., Assistant District Engineer  
Deanna Maifield, P.E., Methods Engineer  
Chris Poole, P.E., Roadside Safety Engineer

**Kansas Department of Transportation**

Ron Seitz, P.E., Bureau Chief  
Rod Lacy, P.E., Metro Engineer  
Scott King, P.E., Road Design Leader

**Minnesota Department of Transportation**

Michael Elle, P.E., Design Standard Engineer

**Missouri Department of Transportation**

Joseph G. Jones, P.E., Engineering Policy Administrator

**Nebraska Department of Roads**

Amy Starr, P.E., Research Engineer  
Phil TenHulzen, P.E., Design Standards Engineer  
Jodi Gibson, Research Coordinator

**Ohio Department of Transportation**

Michael Bline, P.E., Standards and Geometrics Engineer  
Maria E. Ruppe, P.E., Roadway Standards Engineer

**South Dakota Department of Transportation**

David Huft, Research Engineer  
Bernie Clocksin, Lead Project Engineer

**Wisconsin Department of Transportation**

Jerry Zogg, P.E., Chief Roadway Standards Engineer  
John Bridwell, P.E., Standards Development Engineer  
Erik Emerson, P.E., Standards Development Engineer

**Wyoming Department of Transportation**

William Wilson, P.E., Architectural and Highway Standards Engineer

**Federal Highway Administration**

John Perry, P.E., Nebraska Division Office  
Danny Briggs, Nebraska Division Office

**TABLE OF CONTENTS**

TECHNICAL REPORT DOCUMENTATION PAGE ..... i

DISCLAIMER STATEMENT ..... ii

UNCERTAINTY OF MEASUREMENT STATEMENT ..... ii

INDEPENDENT APPROVING AUTHORITY ..... ii

ACKNOWLEDGEMENTS ..... iii

TABLE OF CONTENTS ..... v

LIST OF FIGURES ..... ix

LIST OF TABLES ..... xii

1 INTRODUCTION ..... 1

    1.1 Problem Statement ..... 1

    1.2 Objectives ..... 2

    1.3 Scope ..... 2

2 LITERATURE REVIEW ..... 4

    2.1 Overview of Increased Top-Rail Mounting Heights ..... 4

    2.2 Midwest Roadside Safety Facility Research ..... 5

    2.3 Terminals ..... 10

    2.4 Discussion of Full-Scale Tests ..... 10

    2.5 Simulation Studies ..... 14

3 BARRIER VII ANALYSIS AND COMPARISON ..... 16

    3.1 Brief Background and Application ..... 16

    3.2 MGS Standard Height, 175-ft (53.3-m) Long System ..... 16

    3.3 Baseline BARRIER VII 2270P Model ..... 17

        3.3.1 Development and Validation of the 2214MG-2 Model ..... 17

        3.3.2 Comparison of Test Conditions and Simulation Results ..... 22

        3.3.3 Anchor Analysis ..... 23

    3.4 Baseline BARRIER VII 1100C Model ..... 28

        3.4.1 Development and Validation of the 2214MG-3 Model ..... 28

        3.4.2 Comparison of Test Conditions and Simulation Results ..... 32

        3.4.3 Anchor Analysis ..... 34

    3.5 Maximum Rail Height Models ..... 37

        3.5.1 Development and Validation of the Test No. MGSMRH-1 Model ..... 37

        3.5.2 Comparison of Test Conditions and Simulation Results ..... 41

        3.5.3 Development and Validation of the Test No. MGSMRH-2 Model ..... 41

        3.5.4 Comparison of Test Conditions and Simulation Results ..... 45

    3.6 Discussion ..... 46

4 MODELING AND SIMULATION.....	48
4.1 Introduction.....	48
4.2 Midwest Guardrail System Model.....	48
4.2.1 Increased Mounting Height Modeling.....	51
4.2.2 Anchor Geometry Effects at Increased Mounting Height.....	51
4.3 Vehicle Models.....	52
4.3.1 Geo Metro Vehicle Model.....	52
4.3.2 Dodge Neon Vehicle Model.....	54
4.3.3 Chevrolet Silverado Vehicle Model.....	54
4.4 Modeling Issues.....	55
4.4.1 Surface Contact Scale Factors.....	55
4.4.1.1 Simulation at 34-in. (864-mm) Rail Height.....	56
4.4.1.2 Simulation at 36-in. (914-mm) Rail Height.....	56
4.4.2 Contact Formulation.....	58
4.4.2.1 SOFT=0.....	59
4.4.2.2 SOFT=2.....	59
4.4.2.3 Graphical Comparison of Cases.....	59
4.4.3 Blockout Bolt Failure Deflection.....	60
4.4.3.1 Failure Deflection = 0.3.....	63
4.4.3.2 Failure Deflection = 0.5.....	63
4.4.3.3 Failure Deflection= 0.75.....	64
4.4.3.4 Graphical Comparison of Failure Deflections.....	65
4.5 Modeling Instabilities of 1100C (Neon) Vehicle Model.....	66
4.6 Summary of Parameters.....	66
5 BASELINE SIMULATION AT 32-IN. (813-MM) RAIL HEIGHT.....	68
5.1 Introduction.....	68
5.2 Simulation at 32-in. (813-mm) Rail Height.....	68
5.3 Comparison of Test Conditions and Simulation Results.....	69
5.3.1 Anchor Displacement.....	69
5.3.2 Vehicle-Rail Interaction.....	72
5.3.3 Energy Balance.....	74
5.4 Discussion.....	74
6 MAXIMUM SAFE GUARDRAIL HEIGHT EVALUATION WITH LS-DYNA.....	75
6.1 Introduction.....	75
6.2 Simulation at 34-in. (864-mm) Rail Height.....	75
6.3 Simulation at 36-in. (914-mm) Rail Height.....	79
6.4 Simulation at 37-in. (940-mm) Rail Height.....	79
6.5 Comparison of Test Conditions and Simulation Results.....	83
6.5.1 Rail Deflection Analysis.....	83
6.5.2 Lateral Velocity.....	86
6.5.3 Longitudinal Velocity.....	86
6.5.4 Yaw.....	88
6.5.5 Roll.....	88
6.5.6 Pitch.....	89
6.5.7 Energy Balance.....	92



6.6 Discussion.....	93
7 ANALYSIS OF GEOMETRY AND RAIL HEIGHT EFFECTS.....	94
7.1 Vehicle-to-Rail Geometry Effects.....	94
7.2 Front-End Geometry Comparison.....	97
8 ANCHORAGE AND RAIL DEFLECTION ANALYSIS.....	100
8.1 Purpose of 2270P Pickup Truck Analysis.....	100
8.2 Anchorage Force Analysis.....	100
8.3 Anchorage Displacement Analysis.....	106
8.4 Impact Variations Due to Suspension Failure.....	107
8.5 Comparison of Test Conditions and Simulation Results.....	109
8.6 Discussion.....	111
9 CRITICAL HEIGHT WITH APPROACH SLOPES.....	114
9.1 Background on Approach Slopes.....	114
9.2 Overview of Simulation Study.....	115
9.3 Underride on 8:1 Approach Slope with 820C.....	116
9.3.1 Simulation at 31-in. (787-mm) Rail Height.....	116
9.3.2 Simulation at 34-in. (864-mm) Rail Height.....	119
9.3.3 Simulation at 36-in. (914-mm) Rail Height.....	120
9.3.4 Comparison of Test Conditions and Simulation Results.....	125
9.4 Underride on 6:1 Approach Slope with 820C.....	127
9.4.1 Simulation at 31-in. (787-mm) Rail Height.....	128
9.4.2 Simulation at 34-in. (864-mm) Rail Height.....	130
9.4.3 Simulation at 36-in. (914-mm) Rail Height.....	130
9.4.4 Comparison of Test Conditions and Simulation Results.....	133
9.5 Override on 6:1 Approach Slope with 2270P at 5-ft (1.5-m) Offset.....	135
9.5.1 Simulation at 31-in. (787-mm) Rail Height.....	136
9.5.2 Simulation at 34-in. (864-mm) Top-Rail Height.....	138
9.5.3 Simulation at 36-in. (914-mm) Top-Rail Height.....	138
9.5.1 Comparison of Test Conditions and Simulation Results.....	143
9.6 Override on 6:1 Approach Slope with 2270P at 9-ft (2.7-m) Offset.....	145
9.6.1 Simulation at 36-in. (914-mm) Rail Height.....	145
9.6.1 Comparison of Test Conditions and Simulation Results.....	148
9.7 Discussion.....	151
10 SUMMARY, CONCLUSIONS, AND RECOMMENDATIONS.....	154
10.1 BARRIER VII.....	154
10.2 Maximum Height Determination on Flat Ground.....	154
10.3 Maximum Height Determination on Approach Slopes Summary.....	158
10.4 Discussion Summary.....	160
10.5 Guidelines.....	162
10.6 Future Research.....	162
11 REFERENCES.....	165
12 APPENDICES.....	169

Appendix A. - MGS 31-in. (787-mm) BARRIER VII Input Deck (2270P)..... 170  
Appendix B. - MGS 32-in. (813-mm) BARRIER VII Input Deck (1100C)..... 172  
Appendix C. - MGS 34-in. (864-mm) BARRIER VII Input Deck (1100C)..... 174  
Appendix D. - MGS 36-in. (914-mm) BARRIER VII Input Deck (1100C) ..... 176  
Appendix E. - Validation for Small Car Striking a 32-in. MGS..... 178  
Appendix F. - Validation for Pickup Truck Striking a 31-in. MGS..... 189  
Appendix G. - Validation for Small Car Striking a 31-in. MGS on Approach Slope . 200

## LIST OF FIGURES

Figure 1. 820C Impact with MGS, test no. NPG-1.....	6
Figure 2. Underride in 1100C Impact of MGS, test no. 2214MG-3.....	7
Figure 3. Vehicle Yaw Towards Barrier, test no. 2214MG-3 .....	7
Figure 4. Test No. MGSMRH-1 Penetration.....	9
Figure 5. Test No. MGSMRH-2 Penetration.....	9
Figure 6. Rail Snag Under Hood of Test No. 2214MG-3.....	11
Figure 7. Test No. MGSMRH-1 Vehicle Damage .....	12
Figure 8. Test No. MGSMRH-2 Vehicle Damage .....	12
Figure 9. Sequential Figures from Simulations and Test No. 2214MG-2.....	19
Figure 9. Sequential Figures from Simulations and Test No. 2214MG-2 (continued).....	20
Figure 9. Sequential Figures from Simulations and Test No. 2214MG-2 (continued).....	21
Figure 10. Anchor Displacement Results from Simulation.....	25
Figure 11. Differences in X and Y Coordinates at Post No. 11.....	26
Figure 12. Simulated Forces in Anchors.....	27
Figure 13. Sequential Figures from BARRIER VII and Test No. 2214MG-3 .....	30
Figure 13. Sequential Figures from BARRIER VII and Test No. 2214MG-3 (continued).....	31
Figure 14. Upstream and Downstream Anchor Displacements.....	36
Figure 15. Force through Anchor Members .....	37
Figure 16. Sequential Figures from BARRIER VII and Test No. MGSMRH-1 .....	39
Figure 16. Sequential Figures from BARRIER VII and Test No. MGSMRH-1 (continued) .....	40
Figure 17. Sequential Figures from BARRIER VII and Test No. MGSMRH-2.....	43
Figure 17. Sequential Figures from BARRIER VII and Test No. MGSMRH-2 (continued) .....	44
Figure 18. (a) Actual End Anchorage and (b) Finite Element Model .....	50
Figure 19. (a) Actual Overall System and (b) Simulation Model.....	50
Figure 20. Post Scaling.....	53
Figure 21. Anchor Cable Geometry Changes.....	53
Figure 22. Geo Metro Vehicle Model.....	54
Figure 23. Dodge Neon Vehicle Model.....	54
Figure 24. Chevrolet Silverado Vehicle Model .....	55
Figure 25. Comparison of 820C impact with SFS=1.0 and 0.5 at 34 in. (864 mm).....	57
Figure 26. Comparison of 820C impact with SFS=1.0 and 0.5 at 36 in. (914 mm).....	58
Figure 27. Contact Formulation Differences .....	60
Figure 28. Blockout Bolt Failure Modes .....	62
Figure 29. Blockout and Bolt from Test No. MGSMRH-1 and Simulation.....	62
Figure 30. Anchor Displacement for 820C with FD=0.3 .....	63
Figure 31. Anchor Displacement for 820C with FD=0.5 .....	64
Figure 32. Blockout Bolt Failure Deflection Comparison.....	65
Figure 33. Sequential Figures from Simulation and Test No. NPG-1 .....	70
Figure 33. Sequential Figures from Simulation and Test No. NPG-1 (continued).....	71
Figure 34. Anchor Displacement for 32-in. (813-mm) Top-Rail Height MGS.....	72
Figure 35. Energy Balance of 820C Vehicle Simulation.....	74
Figure 36. Backside Sequential Figures from Simulation and Test No. MGSMRH-1 .....	77
Figure 37. Overhead Sequential Figures from Simulation and Test No. MGSMRH-1.....	78
Figure 38. Back Side Sequential Figures from Simulation and Test No. MGSMRH-2.....	80
Figure 39. Overhead Sequential Figures from Simulation and Test No. MGSMRH-2.....	81

Figure 40. Sequential Figures from 37-in. (940-mm) Top-Rail Height Simulation .....	82
Figure 41. Simulated Rail Deflection Comparison at 600 ms for 820C Vehicle Impact .....	85
Figure 42. Comparison of Lateral CG Velocity of 820C Vehicle .....	86
Figure 43. Comparison of Longitudinal CG Velocity of 820C Vehicle.....	87
Figure 44. Comparison of Resultant CG Velocity of 820C.....	87
Figure 45. Yaw of 820C in Relation to Rail .....	88
Figure 46. Roll of 820C .....	89
Figure 47. Pitch of 820C.....	90
Figure 48. Roll Behavior of 820C Vehicle .....	91
Figure 49. Energy Balance of 820C Vehicle Simulations .....	93
Figure 50. Vehicle-to-Rail Geometry - 820C and 1100C Profiles .....	94
Figure 51. 1100C Neon Underride Comparison at 130 ms .....	96
Figure 52. 820C Geo Metro Underride Comparison at 130 ms.....	96
Figure 53. Simulation Model Vehicle and Test Vehicle Dimension Comparison .....	98
Figure 54. US Anchor Cable Cross Section Forces.....	101
Figure 55. Downstream Anchor Cable Cross Section Forces.....	102
Figure 56. Upstream Anchor Cross-Sections.....	102
Figure 57. Force through Rail from a 2270P Impact.....	105
Figure 58. Upstream Anchor Displacement (2270P Pickup Truck).....	106
Figure 59. Downstream Anchor Displacement (2270P Pickup Truck).....	106
Figure 60. 2270P Pickup Truck Impact without Prescribed Suspension Failure .....	108
Figure 61. Prescribed Suspension Failure Impact Variations.....	108
Figure 62. Simulated Rail Deflection Comparison at 600 ms for 2270P Pickup Truck Impact.	112
Figure 63. Anchor Post No. 2 Displacement .....	113
Figure 64. Time Sequential of Test No. MGSAS-2 and Simulation .....	117
Figure 64. Time Sequential of Test No. MGSAS-2 and Simulation (continued).....	118
Figure 64. Time Sequential of Test No. MGSAS-2 and Simulation (continued).....	119
Figure 65. Sequential of 20- and 25-degree Impacts at 34-in. (864-mm) Top-Rail Height .....	122
Figure 66. Sequential of 20- and 25-degree Impacts at 36-in. (914-mm) Top-Rail Height .....	123
Figure 67. Crushing of A-Pillar .....	124
Figure 68. Vehicle Trajectory Across Approach Slope .....	124
Figure 69. Vehicle Underride at 36 in. (914 mm).....	125
Figure 70. Sequential of 20- and 25-degree Impacts at 31-in. (787-mm) Top-Rail Height .....	129
Figure 71. Sequential of 20- and 25-degree Impacts at 34-in. (864-mm) Top-Rail Height .....	131
Figure 72. Sequential of 20- and 25-degree Impacts at 36-in. (914-mm) Top-Rail Height .....	132
Figure 73. MGS on Approach Slope in Relation to Road Grade.....	135
Figure 74. 2270P Simulation at 31-in. (787-mm) Top-Rail Height on 6:1 Approach Slope .....	137
Figure 75. 2270P Override at 31-in. (787-mm) Rail Height on 6:1 Approach Slope.....	138
Figure 76. 2270P Simulation at 34-in. (864-mm) Top-Rail Height on 6:1 Approach Slope .....	139
Figure 76. 2270P Simulation at 34-in. (864-mm) Top-Rail Height on 6:1 Approach Slope (continued) .....	140
Figure 77. Wheel Contacting Undercarriage of Truck .....	140
Figure 78. 2270P Simulation at 36-in. (914-mm) Top-Rail Height on 6:1 Approach Slope .....	141
Figure 78. 2270P Simulation at 36-in. (914-mm) Top-Rail Height on 6:1 Approach Slope (continued) .....	142
Figure 79. 2270P Vehicle Simulation at 36-in. (914-mm) Top-Rail Height and 9-ft (2.7-m) Offset on 6:1 Approach Slope.....	146

Figure 79. 2270P Vehicle Simulation at 36-in. (914-mm) Top-Rail Height and 9-ft (2.7-m) Offset on 6:1 Approach Slope (continued) ..... 147

Figure 80. MGS on Approach Slope in Relation to Road Grade..... 150

Figure E-1. X-Channel (a) acceleration-time history data used to compute metrics and (b) integration of acceleration-time history data ..... 187

Figure F-1. X-Channel (a) acceleration-time history data used to compute metrics and (b) integration of acceleration-time history data ..... 198

Figure G-1. X-Channel (a) acceleration-time history data used to compute metrics and (b) integration of acceleration-time history data ..... 209

**LIST OF TABLES**

Table 1. Small Car Testing Performed on W-Beam Guardrail  $\geq$  32 in. (813 mm) ..... 13

Table 2. Performance Limits Found by Texas Transportation Institute Research [22]..... 15

Table 3. Effective Top Rail Height Using Texas Transportation Institute Research ..... 15

Table 4. BARRIER VII Simulation Parameters [23, 24]..... 17

Table 5. Test and Simulation Results for 2270P Vehicle on Level Terrain ..... 22

Table 6. Simulation Anchorage Calculations with 2270P ..... 24

Table 7. BARRIER VII Simulation Parameters ..... 29

Table 8. Test and Simulation Results for 1100C Vehicle on Level Terrain..... 33

Table 9. Simulation Anchorage Calculations with 1100C..... 35

Table 10. BARRIER VII Simulation Parameters for Test No. MGSMRH-1 [23, 24] ..... 38

Table 11. Test and BARRIER VII Simulation Results..... 42

Table 12. BARRIER VII Simulation Parameters for Test No. MGSMRH-2..... 42

Table 13. Test and BARRIER VII Simulation Results..... 46

Table 14. Summary of MGS Model Part Properties..... 49

Table 15. Summary of 820C - Barrier Model..... 67

Table 16. Test No. NPG-1 and Simulation Conditions ..... 68

Table 17. Test No. NPG-1 and Simulation Results ..... 71

Table 18. Event History of Test No. NPG-1 and Simulation ..... 73

Table 19. Test and Simulation Conditions and Results Comparison..... 84

Table 20. Recent Model Year Vehicle Front-End Geometry Profiles..... 99

Table 21. Comparison of Test Conditions and Simulation Results ..... 110

Table 22. Simulation Results for 820C Vehicle on 8:1 Approach Slope ..... 126

Table 23. Simulation Results for 820C Vehicle on 6:1 Approach Slope ..... 134

Table 24. Simulation Results for 2270P Vehicle on 6:1 Approach Slope..... 144

Table 25. Simulation Results for 2270P Vehicle on 6:1 Approach Slope..... 149

Table 26. Recommended MASH Testing for Longitudinal Barriers..... 163

Table E-1. Analysis Solution Verification Table..... 180

Table E-2. Roadside Safety Validation Metrics Rating Table – Time History Comparisons  
(single channel option)..... 181

Table E-3. Roadside Safety Validation Metrics Rating Table – Time History Comparisons  
(multi-channel option) ..... 182

Table E-4. Evaluation Criteria Test Applicability Table ..... 183

Table E-5. (a) Roadside Safety Phenomena Importance Ranking Table (Structural Adequacy) 184

Table E-5. (b) Roadside Safety Phenomena Importance Ranking Table (Occupant Risk) ..... 185

Table E-5. (c) Roadside Safety Phenomena Importance Ranking Table (Vehicle Trajectory).. 186

Table F-1. Analysis Solution Verification Table..... 191

Table F-2. Roadside Safety Validation Metrics Rating Table – Time History Comparisons  
(single channel option)..... 192

Table F-3. Roadside Safety Validation Metrics Rating Table – Time History Comparisons  
(multi-channel option) ..... 193

Table F-4. Evaluation Criteria Test Applicability Table ..... 194

Table F-5. (a) Roadside Safety Phenomena Importance Ranking Table (Structural Adequacy) 195

Table F-5. (b) Roadside Safety Phenomena Importance Ranking Table (Occupant Risk) ..... 196

Table F-5. (c) Roadside Safety Phenomena Importance Ranking Table (Vehicle Trajectory).. 197

Table G-1. Analysis Solution Verification Table ..... 202

Table G-2. Roadside Safety Validation Metrics Rating Table – Time History Comparisons  
(single channel option)..... 203

Table G-3. Roadside Safety Validation Metrics Rating Table – Time History Comparisons  
(multi-channel option) ..... 204

Table G-4. Evaluation Criteria Test Applicability Table..... 205

Table G-5. (a) Roadside Safety Phenomena Importance Ranking Table (Structural Adequacy)  
..... 206

Table G-5. (b) Roadside Safety Phenomena Importance Ranking Table (Occupant Risk)..... 207

Table G-5. (c) Roadside Safety Phenomena Importance Ranking Table (Vehicle Trajectory) . 208

## 1 INTRODUCTION

### 1.1 Problem Statement

In post-and-rail guardrail systems, rail height played a crucial role in the way an errant vehicle interacts with the barrier. Low rail heights increased the propensity for vehicle rollover or override, while an excessively tall rail promoted vehicle snagging and underride in small cars. The rail mounting height and the post embedment depth may be altered by various installation or environmental deviations, such as soil erosion, frost heave, human error, and future roadway overlays. Therefore, the range of rail mounting heights that facilitated safe vehicular redirection needs to be known to mitigate the concerns of mounting height variability.

The Midwest Guardrail System (MGS) was originally developed according to the standards set forth by the National Cooperative Highway Research Program (NCHRP) Report No. 350 [1]. As a W-beam post-and-rail guardrail system, it was designed to capture and redirect larger vehicles, specifically the  $\frac{3}{4}$ -ton pickup truck, while minimizing the potential for barrier underride by the small car [2].

Then, crash testing standards were updated in the Manual for Assessing Safety Hardware (MASH) [3]. The MGS was successfully tested according to the Test Level 3 (TL-3) crash testing procedures provided in MASH for both the 1100C passenger car and the 2270P pickup truck [4,5]. During both NCHRP Report No. 350 and MASH testing, the W-beam's top rail mounting height was 32 in. (813 mm) for the passenger car tests and 31 in. (787 mm) for the pickup truck tests. Prior research using a 2270P pickup truck has determined the minimum recommended top rail mounting height to be  $27\frac{3}{4}$  in. (706 mm) [6].

In 2005, the Midwest Roadside Safety Facility (MwRSF) completed a flare-rate study for the MGS. During that project, the MGS was successfully simulated and crash tested with the 820C small car and flare rates as high as 5:1 [7,8]. The increased impact severity of this



particular configuration did not result in barrier underride and indicated that the upper-height tolerance for the MGS may be significantly higher than 32 in. (813 mm).

Raising the height of the rail led to the following four issues regarding system performance of the MGS: (1) vehicle underride for small cars; (2) post snagging for small cars; (3) excessive deflection due to reduced lateral resistance for pickup trucks; and (4) overloaded anchors that were designed with shorter rail heights for pickup trucks. Before the larger deflections were quantified or the anchorages were evaluated with new rail heights, the rail-height limit for acceptable small car interaction was defined. Although many full-scale crash tests have utilized a small car impacting the MGS guardrail system, there have been no recent underride issues and, therefore, no useful insights into the upper rail-height limits for the MGS.

## **1.2 Objectives**

The objective of this research project was to evaluate the safety performance of an increased-height MGS with respect to underride and post snagging for small cars and to evaluate anchorage loading and deflection, lateral barrier resistance, and rail deflection using a pickup truck. The guardrail systems were to be evaluated according to MASH TL-3 safety performance criteria [3]. The objective was accomplished using a combination of full-scale crash testing and computer simulation.

## **1.3 Scope**

The research objective was achieved in two phases. Phase I concentrated on crash testing; two full-scale crash tests were performed on the MGS with a top rail mounting height of 34 in. (864 mm) and 36 in. (914 mm), respectively, using 1100C vehicles. Both system heights satisfied MASH TL-3 evaluation criteria for test no. 3-10. Phase I was documented in *Determination of Maximum MGS Mounting Height - Phase I Crash Testing* [9].

This report, phase II, contains a detailed analysis of the increased-height MGS, which required several tasks. First, researchers performed a literature review of recent W-beam tests to examine the interaction between small cars and varying height guardrails. Then, a computer simulation effort was used to predict a maximum acceptable rail height using a 3-D nonlinear finite element program, LS-DYNA [10], and a 2-D finite element program, BARRIER VII, by incrementally raising the rail height in the MGS model until a performance limit was reached. Additionally, LS-DYNA simulations were used to determine a critical rail height on various approach slopes. Finally, conclusions and recommendations were made pertaining to the safety performance of the maximum-height MGS.

## **2 LITERATURE REVIEW**

### **2.1 Overview of Increased Top-Rail Mounting Heights**

The majority of current W-Beam guardrail systems have been modified by raising rail mounting heights to improve system performance with high center-of-gravity (CG) vehicles. The previous standard mounting heights were 27 or 27 ¾ in. (686 or 706 mm), and current standards have increased this to a 31-in. (787-mm) nominal top rail mounting height. Several systems have been tested and validated at 31 in. (787 mm) [2,4,11]. In limited cases, systems have been tested at 32 in. (813 mm) or higher [5,9]. Raising the rail height can lead to four potential performance issues including: (1) vehicle underride for small cars; (2) post snagging for small cars; (3) excessive deflection due to reduced lateral resistance for trucks; and (4) overloaded anchors which were designed for shorter rail heights. There have been many full-scale guardrail crash tests utilizing small cars. However, there have been no underride issues that could provide knowledge of the upper rail mounting height limit for the MGS. Additionally, wheel snag on posts has not caused reduced rail performance in redirecting small cars. There are two prevailing theories in regard to wheel snag on posts: (1) it can increase occupant risk and cause vehicular instabilities in small cars, and (2) it is negligible as the vehicle impacts the weak axis of the post, causing the post to bend to the ground. Additionally, post snagging may increase vehicle stability by tearing the impacting wheel assembly from the vehicle. This action may cause significant yaw towards the barrier or be redirected close to the barrier. However, this behavior did not prevent the barrier from meeting crash test standards.

There are no data or sources for tests performed outside of MwRSF for systems with top rail mounting heights above 32 in. (813 mm). A small number of tests have been performed at 32 in. (813 mm) at the MwRSF, and one test has been performed at both 34 in. (864 mm) and 36 in. (914 mm). The 32-in. (813 mm) rail height modified systems have been tested to NCHRP Report

No. 350 standards and MASH standards [1]. The 34- and 36-in. (864- and 914-mm) systems have been tested in accordance with MASH standards, having been tested with the 2,245-lb (1,100-kg) 1100C small car [9]. Systems that have been validated by these standards, with the 820C or 1100C small car, at or above standard top rail mounting heights will be discussed in detail.

## **2.2 Midwest Roadside Safety Facility Research**

Researchers at MwRSF have developed a revised guardrail system called the Midwest Guardrail System, or MGS. This system was developed in order to improve performance for high CG light trucks. The new guardrail design incorporated a 31-in. (787-mm) nominal top rail height, splices located between posts, and an increased blockout depth of 12 in. (305 mm).

The MwRSF performed test no. 3-10 with an 820C vehicle on the MGS while in development and called the test NPG-1. For this test, the top of the rail was placed at 32 in. (813 mm) above the ground to demonstrate the barrier's performance at the maximum allowable rail height. In crash test film analysis, minor vehicle underride occurred when the left-front corner of the vehicle slightly penetrated below the rail element. This penetration caused the left-front tire to slightly snag on post no. 15 and partially disconnect from the vehicle, as shown in Figure 1. This snagging caused the vehicle to yaw towards the barrier after leaving the exit box. This behavior did not cause any additional occupant risk or vehicle instability, and the barrier passed in accordance with NCHRP Report No. 350 standards [12].

The MwRSF published a report in 2004 that provided test results for the MGS in standard and special applications, including reduced post spacing and in combination with curbs [2]. FHWA acceptance for the MGS was received in 2005 [13].



Figure 1. 820C Impact with MGS, test no. NPG-1

Project NCHRP 22-14(2) was undertaken by MwRSF to evaluate current roadside safety devices. One of the selected barriers was the strong-post W-beam guardrail system. Test no. 2214MG-3 evaluated the MGS barrier mounted at the top rail height of 32 in. (813 mm), and utilized a 2,245-lb (1,100-kg) small car, an impact angle of 25 degrees, and an impact velocity of 62.1 mph (100 km/h). No significant vehicle underride was observed, as shown in Figure 2. However, post nos. 15 through 17 slightly deflected the right-front wheel of the vehicle. The passenger side frame, which was connected to the wheel, was bent back, and the right-front wheel assembly was pushed up and back into the wheel well, crushing the quarter panel on the right-front side; this was deemed insignificant.

Wheel snag caused the vehicle to yaw towards the barrier, as shown in Figure 3, but it did not abruptly stop the vehicle. The barrier passed the test successfully, meeting the proposed TL-3 requirements presented in MASH [5].



Figure 2. Underride in 1100C Impact of MGS, test no. 2214MG-3



Figure 3. Vehicle Yaw Towards Barrier, test no. 2214MG-3

In 2008, MwRSF published a report that examined critical flare rates for the MGS. Two tests were performed with an 820C small car and a 31-in. (787-mm) nominal rail mounting height. The first of the two tests, test no. FR-3, was performed on the MGS with a flare rate of 7:1. The second, test no. FR-5, had a flare rate of 5:1. Both tests were successful, indicating that the critical flare rate for the MGS was 5:1 or steeper. Tests with vehicles in the light truck category were also performed and reported [14]. Barrier underride was not prevalent despite the

increased impact severity of the higher-flare-rate configuration, indicating that the upper-height tolerance for the MGS may be increased from the current maximum height.

Earlier in 2012, MwRSF published a report that examined maximum height parameters for the MGS [9]. Two tests were performed on 175-ft (53.3-m) systems with an 1100C small car and rail mounting heights above the 32-in. (813-mm) nominal mounting height. Test no. MGSMRH-1 was performed on the MGS with a 34-in. (864-mm) nominal rail mounting height, and test no. MGSMRH-2 had a 36-in. (914-mm) nominal rail mounting height.

Barrier damage in test no. MGSMRH-1 was moderate. The bottom corrugation was flattened through the impact zone, and the bottom edge of the rail was folded upward at post no. 14. The vehicle did not penetrate or underride the barrier and remained upright throughout and after the impact event, as shown in Figure 4. The vehicle's right A-pillar was crushed at its base, the right-front corner of the hood was crushed inward, the side panels were scraped from front to back, and the windshield was cracked in a spider-web pattern.

Test no. MGSMRH-2 also exhibited moderate barrier damage with similar bottom corrugation flattening as the previous test. Vehicle damage was similar as well. However, the vehicle did not suffer damage exceeding that of MASH established deformation limits. Again, the vehicle did not penetrate or underride the system and remained upright throughout the test, as shown in Figure 5 [9].

Both tests were determined to be successful according to MASH safety performance criteria, indicating that the MGS can successfully be raised above the standard rail mounting height with respect to the small car performance [9].



Figure 4. Test No. MGSMRH-1 Penetration

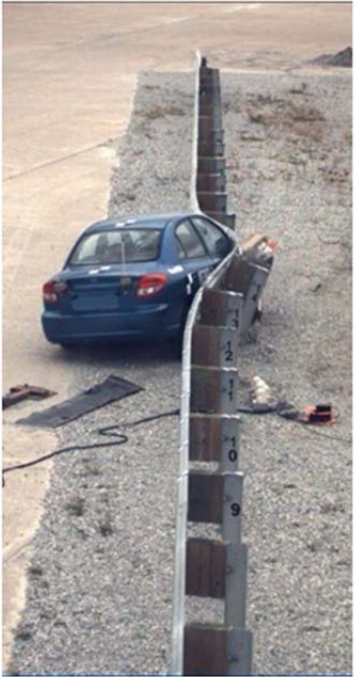


Figure 5. Test No. MGSMRH-2 Penetration



## **2.3 Terminals**

Terminals are also affected by the increased rail mounting heights applied to the standard barriers. The Federal Highway Administration (FHWA) has approved several terminals for use with strong-post, W-beam systems. SKT and FLEAT terminals were approved for use with the GMS-WB31 system through similarities to the MGS system [15]. The SRT-31 terminal was approved for use with the MGS, T-31, and GMS-WB31 systems through test no. 220541-2 [16]. Other terminals that were approved for the MGS system are the SKT (test no. SMG-1), the SKT-LITE, the FLEAT (test nos. FLEAT-5,-6,-8), and the ET-Plus 31 (test no. 220601-2) [16-20]. Also, researchers at MwRSF tested a SKT-MGS Tangent End Terminal while working on NCHRP Project 22-14(2) (test no. 2214TT-1). The top of the rail was mounted at 32 in. (813 mm) and met the proposed standards of MASH [21].

## **2.4 Discussion of Full-Scale Tests**

Wheel snag can push the wheel rearward against the wheel well, potentially deforming the floorpan. Additionally, wheel snag may increase the longitudinal force on the wheel and slow the vehicle too quickly, increasing occupant risk. In the case of test no. 2214MG-3, the wheel was pushed into the wheel well, but floorpan deformation was not significant. In this case, wheel snag did not stop the vehicle, but it did cause the vehicle to yaw into the barrier. In some cases, wheel snag stabilized the vehicle by disconnecting the wheel from the vehicle. In the reviewed tests, wheel snag was not a significant concern.

Barrier underide posed two primary risks to the vehicle and occupants: (1) rail contact with the windshield could cause occupant compartment intrusion, and (2) vehicle penetration through the barrier may result in secondary impacts with hazards behind the barrier. None of these tests, including the 34-in. (864-mm) and 36-in. (914-mm) tests, displayed significant barrier underide.

However, the potential for underride was apparent as the rail was raised. In test no. 2214MG-3, the rail contacted the right-front corner of the vehicle and began to slide up the vehicle frame. The rail pushed the hood upward, causing the rail to become trapped between the hood and right-front bumper section of the vehicle, shown in Figure 6. This caused the vehicle to roll away from the barrier, limited vehicle penetration, and prevented vehicle underride of the guardrail.



Figure 6. Rail Snag Under Hood of Test No. 2214MG-3

In test nos. MGSMRH-1 and MGSMRH-2, the right front corners of the vehicles' hoods apparently slid into the valley of the W-beam guardrail, which trapped the hood corners and caused significant deformation in that region of the vehicles. The rail did not slide up the A-pillar or cause significant occupant compartment deformation, as shown in Figures 7 and 8. A summary of relevant full-scale vehicle crash tests and parameters is given in Table 1.



Figure 7. Test No. MGSMRH-1 Vehicle Damage



Figure 8. Test No. MGSMRH-2 Vehicle Damage

Table 1. Small Car Testing Performed on W-Beam Guardrail  $\geq$  32 in. (813 mm)

Test Number	Test Date	System Type	Rail Height	Vehicle	Vehicle Mass	Speed		Angle		Test Standard Used	Pass/Fail	Ref. No.
			in. (mm)			lb (kg)	Target mph (km/h)	Test mph (km/h)	Target deg			
NPG-1	6/29/2001	MGS	32 (813)	820C	1,956 (887)	62.1 (100)	63.9 (102.9)	20	18.74	NCHRP 350	Pass	2,12
										3-10		
2214 MG-3	11/8/2004	MGS	32 (813)	1100C	2,588 (1,174)	62.1 (100)	60.8 (97.8)	25	25.36	MASH	Pass	5,6
										3-10		
MGS MRH-1	6/29/2010	MGS	34 (864)	1100C	2,599 (1,179)	62.1 (100)	63.6 (102.4)	25	24.97	MASH	Pass	9
										3-10		
MGS MRH-2	9/9/2010	MGS	36 (914)	1100C	2,584 (1,172)	62.1 (100)	64.1 (103.1)	25	25.6	MASH	Pass	9
										3-10		
FR-3	8/17/2005	MGS 7:1 Flare	31 (787)	820C	1,971 (894)	62.1 (100)	63.5 (102.2)	28.13	28.7	NCHRP 350	Pass	14
										3-10		
FR-5	7/6/2006	MGS 5:1 Flare	31 (787)	820C	2,002 (908)	62.1 (100)	59.3 (95.5)	31.3	31.8	NCHRP 350	Pass	14
										3-10		
2214 TT-1	7/1/2005	SKT-MGS Tangent Terminal	32 (813)	1100C	2,597 (1,178)	62.1 (100)	64.4 (103.6)	15	14.49	NCHRP 350	Pass	21
										3-10		

## 2.5 Simulation Studies

The Texas Transportation Institute (TTI) analyzed the performance limit for common roadside and median barriers using LS-DYNA, including the MGS [22]. In this study, simulations were used to determine acceptable vehicle impact heights by incrementally varying them. Underride was examined using an 820C Geo small car model, and the initiation of override and rollover was examined using a 2000P C2500 pickup truck model.

The study examined the effects of suspension compression on system redirection by lowering the 820C vehicle model with respect to the standard position of the guardrail. This task was completed by lowering the ground level for the vehicle. In this research, the increased vehicle impact heights were obtained by lowering the vehicle below the defined guardrail soil level and removing contacts between the vehicle and the soil. Additionally, contacts between the vehicle and the below-ground portions of the posts were removed. This gave a similar effect to raising the rail height without actually re-modeling the system or re-meshing any parts. However, there was no effective change in the post-in-soil embedment depth or any difference in the rotation point of the post in the soil.

In the underride limit analysis, the vehicle impacted the barrier at reduced bumper heights, or effectively at increased rail heights. In the override analysis, the vehicle impacted the barrier at increased bumper heights. The limits found by these methods for the MGS, a Modified G4(1S) W-beam, and a modified weak post W-beam guardrail system are shown in Table 2 [22].

This research shows the underride and override at varying vehicle impact heights which is analogous to varying guardrail mounting heights. The analogous effective top rail mounting height calculated from the center of the corrugated guardrail is shown in Table 3.

Table 2. Performance Limits Found by Texas Transportation Institute Research [22]

Guardrail Type	Rail Center Height		Bumper Top Height above Ground Level	
			Override Limit	Underride Limit
	Upper	Lower	Ferdous et al. [22]	Ferdous et al. [22]
	in. (mm)	in. (mm)	in. (mm)	in. (mm)
<b>Midwest Guardrail System</b>	28.7 (728)	21 (535)	32.2 (818)	16 (410)
<b>Modified G4(1S) W-beam</b>	25.6 (651)	17.8 (453)	28.6 (726)	15.9 (403)
<b>Modified Weak Post W-beam</b>	29.8 (757)	22 (557)	29.8 (757)	16.6 (421)

Table 3. Effective Top Rail Height Using Texas Transportation Institute Research

Guardrail Type	Effective Top Rail Height	
	Upper Limit	Lower Limit
	in. (mm)	in. (mm)
<b>Midwest Guardrail System</b>	34.7 (881)	27.1 (688)
<b>Modified G4(1S) W-beam</b>	31.7 (805)	24.0 (610)
<b>Modified weak post W-beam</b>	35.9 (912)	28.1 (714)

The results in Table 3 suggested that the maximum top rail mounting height for the MGS with respect to the 820C small car should be 34.7 in. (881 mm). However, this research, as mentioned previously, did not take into account the reduced soil stiffness from decreasing the post embedment depth. In fact, the weak-post guardrail system was shown to have an effective maximum height closer to 36 in. (914 mm). This suggested that the post reaction, rotation, and reduced soil embedment played a significant role in determining the maximum guardrail height.

### **3 BARRIER VII ANALYSIS AND COMPARISON**

#### **3.1 Brief Background and Application**

BARRIER VII is a computer program used extensively to model and analyze vehicle crashes into guardrail systems. In this program, the barrier was idealized as a two-dimensional structural framework of arbitrary shape. The analysis was done in the horizontal plane, meaning that vertical displacements of the barrier or the vehicle were not considered. In these simulations, the vehicle was idealized as a rigid body of prescribed shape surrounded by a cushion of discrete springs.

A baseline BARRIER VII model was developed to study the performance of the MGS guardrail, and specifically the anchorages, at a 175-ft (53.3-m) system length and validated with corresponding full-scale crash tests. This model was used for parametric studies to determine the effect that height had on guardrail post capacity and safety performance, provide a basis of comparison with LS-DYNA results, and determine the effectiveness of LS-DYNA models in simulating guardrail behavior at raised rail heights.

#### **3.2 MGS Standard Height, 175-ft (53.3-m) Long System**

Two full-scale crash tests were performed on 175-ft (53.3-m) long standard-height systems. Test no. 2214MG-2 involved a 2270P pickup truck impacting a system with a 31-in. (787-mm) top rail mounting height at an angle of 25.5 degrees and a speed of 62.9 mph (101.2 km/h) [4]. The second test, test no. 2214MG-3, involved an 1100C small car impacting a system with a 32-in. (813-mm) top rail mounting height at an angle of 25.4 degrees and a speed of 60.8 mph (97.8 km/h) [5]. These impact conditions fell within the allowable range for the successful evaluation of the barrier's performance.

The data acquired during test no. 2214MG-2 and test no. 2214MG-3 from the overhead high-speed film, onboard vehicle accelerometers, and speed traps were used to calibrate the

models to the physical tests [24]. Furthermore, a previously developed LS-DYNA model with the same test conditions was analyzed to validate its use and to determine if updating the MGS barrier model was justified. The BARRIER VII model, first-generation LS-DYNA model, and full-scale tests were analyzed and compared, the results of which are outlined hereafter.

### 3.3 Baseline BARRIER VII 2270P Model

#### 3.3.1 Development and Validation of the 2214MG-2 Model

The BARRIER VII model had a single beam and three different posts. The model had a total length of 175 ft (53.3 m). Two of the posts represented the two breakaway cable terminal (BCT) anchor posts on both the upstream and downstream ends for test nos. 2214MG-2 and 2214MG-3 [4,5]. The post parameters for the W6x9 (W152x13.4) post used in the BARRIER VII simulation are shown in Table 4 [23, 24]. The ground-line strut and cable are not modeled in BARRIER-VII. Thus, the anchor post strength was given particular attention. The kinetic friction value was calibrated according to the physical test exit times and length of contact in order to provide the best results.

Table 4. BARRIER VII Simulation Parameters [23, 24]

<b>BARRIER VII Parameters</b>	<b>Units</b>	<b>Input Values</b>
<b>K<sub>B</sub> - Post Stiffness Along B (strong axis)</b>	kip/in. (kN/m)	3.00 (525.38)
<b>K<sub>A</sub> - Post Stiffness Along A (weak axis)</b>	kip/in. (kN/m)	2.60 (455.33)
<b>M<sub>A</sub> - Moment About A (strong axis)</b>	kip-in. (kN-m)	164.18 (18.5)
<b>M<sub>B</sub> - Moment About B (weak axis)</b>	kip-in. (kN-m)	61.90 (6.99)
<b>δ<sub>F</sub> - Failure Displacement Along B</b>	in. (mm)	15 (381)
<b>μ<sub>k</sub> - Kinetic Friction Coefficient</b>	Vehicle to Barrier	0.40



One important validation method was the graphical comparison of the two simulations and physical crash test barrier profiles. The input parameters were calibrated if BARRIER VII was able to accurately predict the barrier profile. The LS-DYNA profile was obtained by tracking the x-y location of various nodes along the barrier model. The barrier profile during the physical crash test was obtained from the overhead film analysis. In the actual full-scale crash test, the right-front corner of the vehicle impacted the barrier. However, to generate a visual comparison with the models, sequential photos of the full-scale test were mirrored about the vertical axis, giving the indication of a left-front impact. It was assumed that an actual right-front wheel separation was identical to a virtual left-front wheel separation.

BARRIER VII had some difficulty fully reproducing the guardrail shape between 250 ms and 350 ms. However, it should be noted that during the BARRIER VII run, the path followed a similar trajectory but was slightly offset during this time period. In the actual full-scale crash test, the right-front wheel snagged on post nos. 12 and 13, pulling the wheel away from the hub of the truck. From 250 to 350 ms, the front wheel snagged on post no. 14 and was pulled from the vehicle. This behavior deflected the vehicle in a slightly different path, leading to the difference noted in the BARRIER VII simulation results. Since BARRIER VII was limited to planar motion and because tire separation could not be modeled, the deflection could not be precisely reproduced. Without snagging, it calculated a smoother deflection of the rail in this area. By 350 ms, the tire was torn away, and the rail deflection evened out as the vehicle moved along the rest of the rail.

LS-DYNA replicated the full-scale crash test barrier deflection profile reasonably well. The 3-D non-linear finite element program was capable of modeling tail slap, similar to the full-scale test, and it was also capable of modeling the separation of the left-front wheel, similar to the right-front wheel separation of the full-scale test. A graphical comparison of the simulated

BARRIER VII results, discretized barrier shape data from the LS-DYNA results, and full-scale testing for test no. 2214MG-2 is shown in Figure 9.

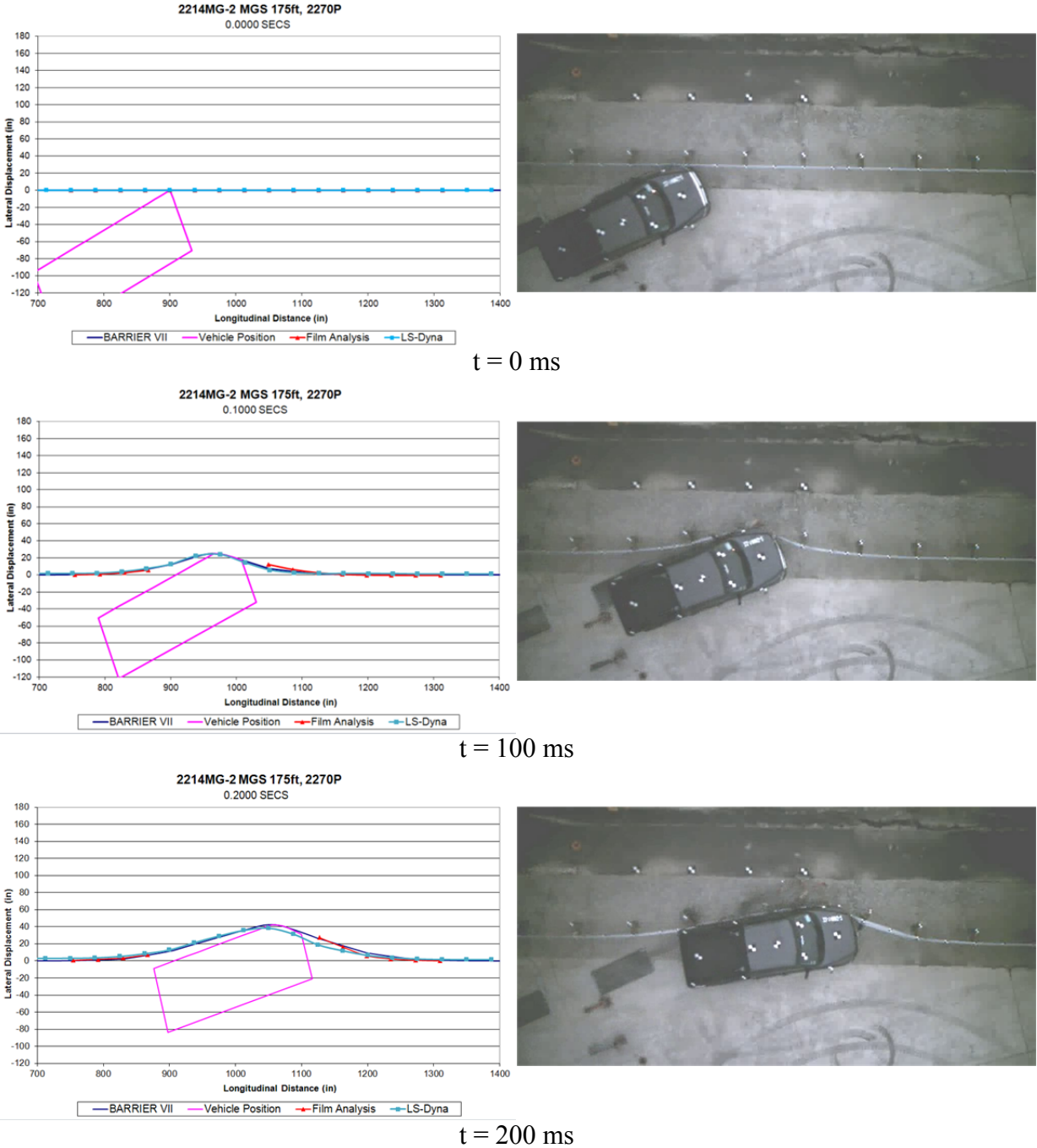


Figure 9. Sequential Figures from Simulations and Test No. 2214MG-2

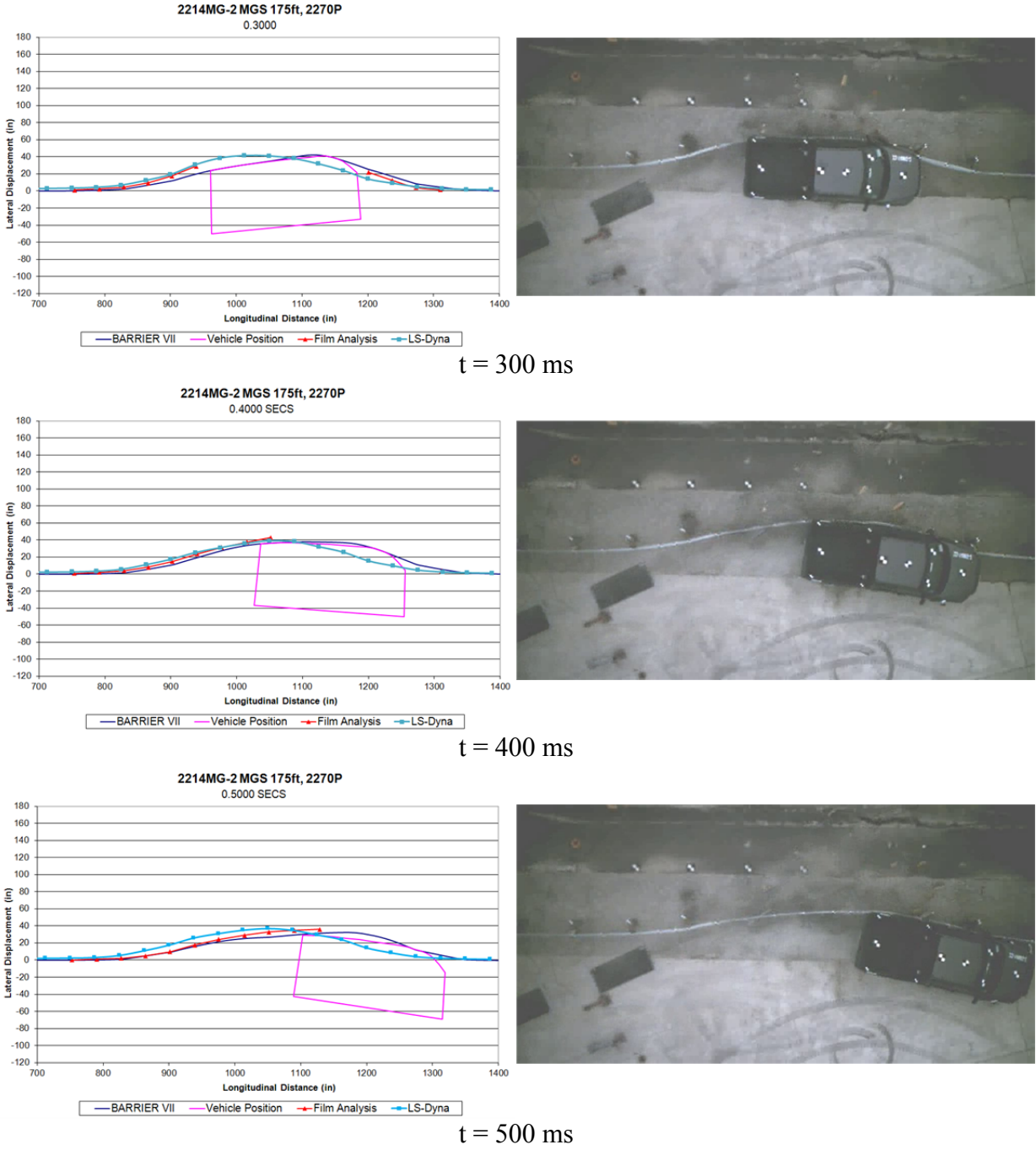


Figure 9. Sequential Figures from Simulations and Test No. 2214MG-2 (continued)

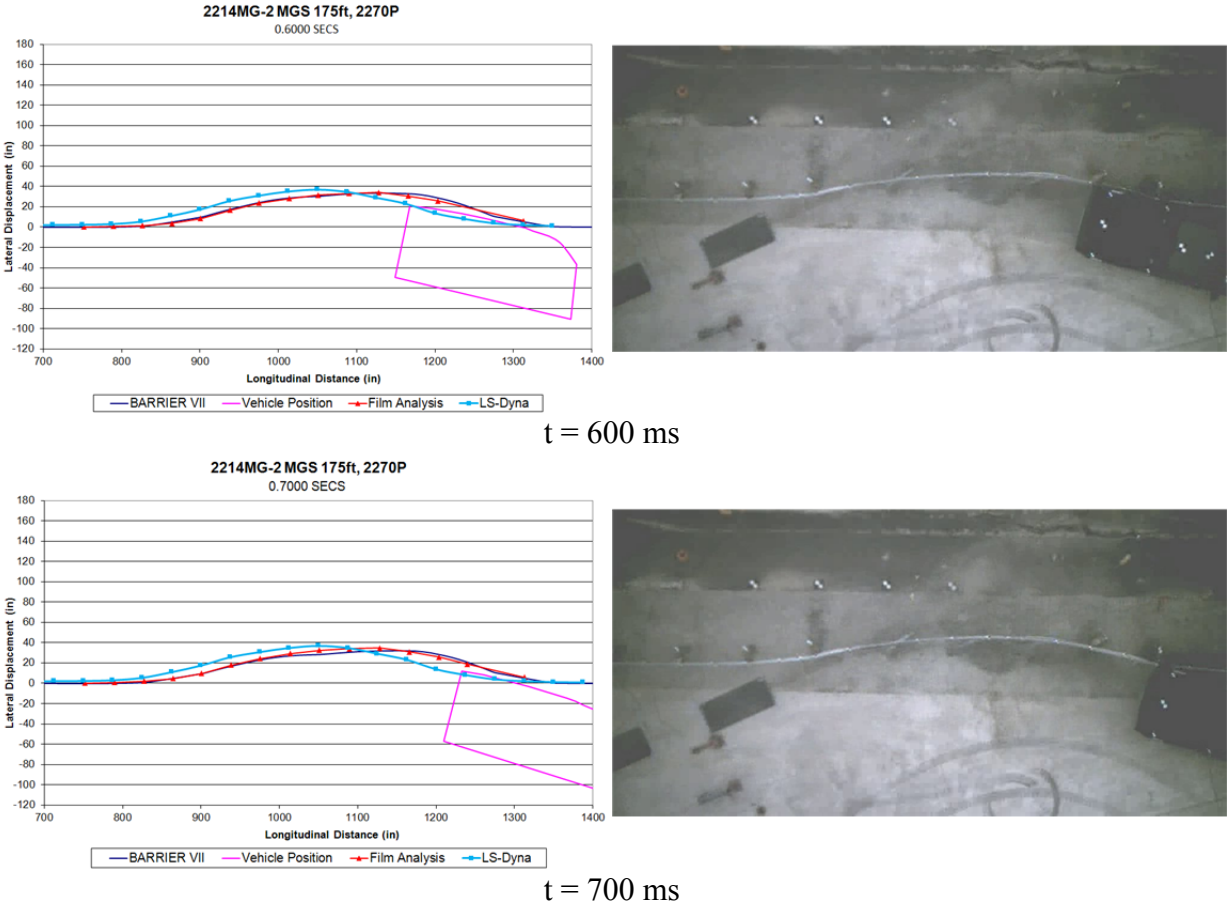


Figure 9. Sequential Figures from Simulations and Test No. 2214MG-2 (continued)

The LS-DYNA modeled an impact at post no. 12, whereas the BARRIER VII model and full-scale tests used an impact at post no. 13, which can explain some of the differences outlined in this report. For comparison in this report, all LS-DYNA simulation results were assumed to be the same as those of the corresponding BARRIER VII simulation and full-scale vehicle crash test results had they impacted at the same point. Therefore, post no. 12 of the LS-DYNA model was assumed to be post no. 13 of the full-scale vehicle crash test so comparisons could be made between the two.

### 3.3.2 Comparison of Test Conditions and Simulation Results

A second validation method incorporated different evaluation parameters which were measured in the full-scale test and calculated using BARRIER VII and LS-DYNA. Tabulated validation results for vehicle behavior, barrier displacements, and working width for the calibration are listed in Table 5. Both LS-DYNA and BARRIER VII modeled the full-scale vehicle crash test fairly well.

Table 5. Test and Simulation Results for 2270P Vehicle on Level Terrain

Evaluation Parameters	Units	Test No. 2214MG-2 [4]	Simulation Results	
			BARRIER VII Simulation	LS-DYNA Simulation
<b>Parallel Time</b>	ms	282	324	260
<b>Parallel Velocity</b>	mph (km/h)	45.8 (73.7)	39.8 (64.1)	53.1 (85.5)
<b>Dynamic Rail Deflection</b>	in. (mm)	-43.9 (-1114)	-46.1 (-1172)	-43.9 (-1116)
<b>Working Width</b>	in. (mm)	48.6 (1234)	52.1 (1324)	66.5 (1690)
<b>Working Width Indicator</b>	-	Hood Corner	Post*	Hood Corner
<b>Exit Time</b>	ms	718	535	580
<b>Exit Angle</b>	deg	-13.47	-8.1	-14.08
<b>Resultant Velocity at Exit</b>	mph (km/h)	39.6 (63.7)	35.8 (57.6)	48.9 (78.7)

\*Although the post was the working width indicator, it was unlikely that the post would remain attached to the rail for that displacement.

The largest differences between the full-scale test, BARRIER VII model, and LS-DYNA model were the parallel times (282 ms, 324 ms, 260 ms) and exit times (718 ms, 535 ms, 580 ms). This 183-ms difference in exit time between BARRIER VII and the full-scale test was attributed to differences in film analysis and computer simulation. BARRIER VII was able to

exactly detect any loss of contact from the barrier, while this may not be observable during film analysis. In addition, the right-front tire was detached from the vehicle in the actual crash test, causing the vehicle to penetrate farther into the rail, increasing contact time. BARRIER VII was unable to model the detachment of the tire and, thus, predicted vehicle redirection sooner. A 13 percent difference was observed in the parallel times between the full-scale vehicle crash test and the BARRIER VII simulation. This difference was attributed to the inability of BARRIER VII to accurately model the roll of the vehicle and the detachment of the tire, which caused a slightly different redirection angle between 250 ms and 350 ms. LS-DYNA did model these events, and had a 7.8 percent difference in parallel time relative to the full-scale test.

The other observable difference was in the exit angle of the center of gravity of the vehicle (13.47 degrees for the physical test [4] versus 8.1 degrees for the BARRIER VII simulation). This 39 percent difference was attributed to the 2-D limitation that under estimated the exit vector. However, the exit angle simulated by LS-DYNA was only 4.3 percent different than the full-scale crash test exit angle.

### **3.3.3 Anchor Analysis**

Particular attention was paid in this analysis to the deflection and forces imparted to the anchor posts in the system. As the barrier height increased, the post embedment decreased, causing the anchors to absorb more of the force imparted on the barrier by the vehicle. Values for the maximum deflection and force through the anchors for the simulations are shown in Table 6. As previously noted, the LS-DYNA simulation modeled an impact at post no. 12, whereas BARRIER VII modeled an impact at post no. 13. This explained some of the slight differences in the maximum forces and displacements between the two simulation methods. Despite this discrepancy, the anchor forces and displacements of BARRIER VII and LS-DYNA models were very similar.

Table 6. Simulation Anchorage Calculations with 2270P

Measurement	Units	B. VII U.S. Anchor	LS-DYNA U.S. Anchor	B. VII D.S. Anchor	LS-DYNA D.S. Anchor
Time of Maximum Deflection	ms	184	140	203	179
Maximum Deflection	in. (mm)	2.91 (74)	3.11 (79)	-1.11 (-28)	-0.91 (-23)
Maximum Force Through Anchor	kips (kN)	27.32 (121.5)	31.47 (139.9)	13.37 (59.5)	10.49 (46.7)

The upstream anchor was calibrated by using two measurements: (1) post-test field book measurements versus the simulation displacements and (2) the farthest visible upstream target in the overhead film. Since there was no high-speed camera above the upstream or downstream anchor post, some extrapolation was needed to find the maximum rail displacement at the anchors for the full-scale test.

From field observations for test no. 2214MG-2, the maximum soil displacement was approximately 1 in. (25 mm) on the upstream side of post no. 1. Extrapolating this 1-in. (25-mm) displacement to the top rail height of 31 in. (787 mm), the maximum upstream anchor displacement was 2.134 in. (54 mm) during test no. 2214MG-2. The estimation for the anchor post displacement was done assuming a 2/3 embedment depth rotation point and was based on estimated measurements from post-test documentation. The post rotation point assumption may explain the discrepancy between the full-scale test and the simulation results. BARRIER VII predicted a maximum displacement of 2.91 in. (74 mm), resulting in a 27 percent difference. LS-DYNA predicted a maximum displacement of 3.11-in. (79 mm), resulting in a 31 percent difference. Overall, both models predicted very similar anchor displacements.

BARRIER VII and LS-DYNA estimated maximum displacements of -1.11 and -0.91 in. (-28 and -23 mm) for the downstream anchor. Simulation results are shown in Figure 10 for anchor displacements on both the upstream and downstream ends.

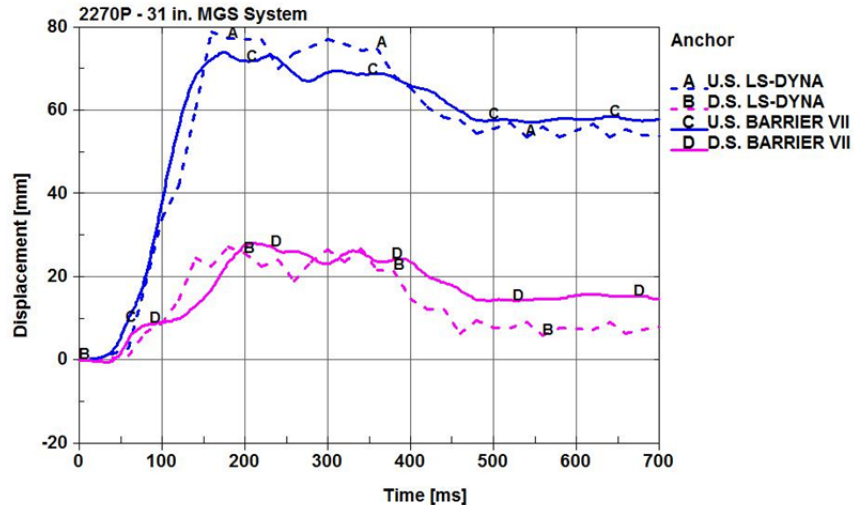


Figure 10. Anchor Displacement Results from Simulation

The upstream anchor displacements were measured at node no. 1, and the downstream anchor displacements were measured at node no. 225 in BARRIER VII. These nodes correspond to the extreme ends of the 31-in. (787-mm) tall system at an impact height of 24.875 in. (632 mm). A central node was tracked in LS-DYNA on the top of both the upstream and downstream anchorages for comparison. BARRIER VII and LS-DYNA predicted very similar displacement curves for both anchorages.

The difference in distance between simulations and film analysis for the farthest visible upstream target, post no. 11, is shown in Figure 11. This calibration effort, therefore, shows the calibration of the displacement of post no. 11. This post was tracked in both BARRIER VII and LS-DYNA.

Some similarities were observed in the plots of the differences in the x- and y-directions. However, for this calibration BARRIER VII was better calibrated than LS-DYNA at post no. 11 for displacement in the x- and y-directions. A greater discrepancy in the x-direction between the full-scale data and the LS-DYNA results for this post displacement was shown.



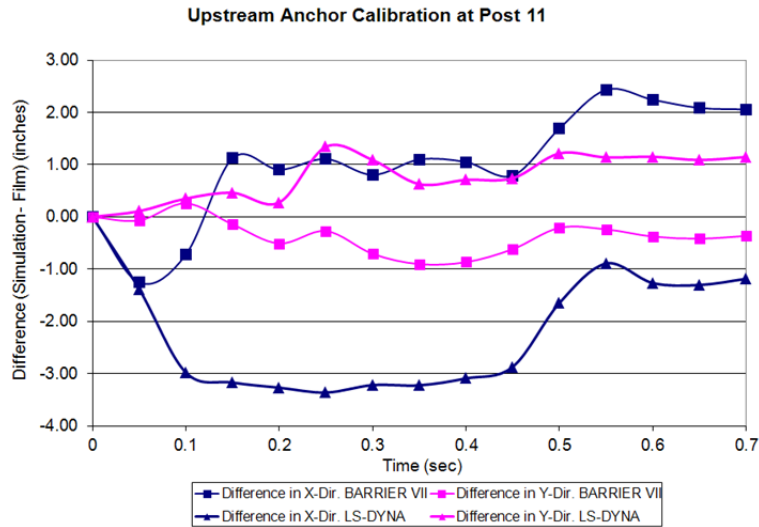


Figure 11. Differences in X and Y Coordinates at Post No. 11

BARRIER VII had minor difficulty replicating the displacements of the farthest visible upstream target, post no. 11. Initially, BARRIER VII under-predicted the x-displacement of the target, but this quickly switched to an over-prediction. The initial under-prediction of the target by the simulation was attributed to the simulation being able to calculate exactly when the vehicle deflects this post at this time. The over-prediction was attributed to how BARRIER VII observed post failure. In full-scale tests, the post provided slight resistance which was not modeled in BARRIER VII. Also, in the full-scale test, the wheel became detached from the vehicle, potentially causing a difference in the deflection of the vehicle and creating slight differences in the deflection of the target. This calibration verified that BARRIER VII can calculate displacements of posts and can validate results from the anchor post displacements.

Because LS-DYNA is a 3-dimensional modeling tool, it was expected to be more accurate than BARRIER VII. However, this was not the case. In the LS-DYNA simulation, the vehicle pulled the post and rail more than in the full-scale tests, and the posts bent downstream to a greater extent. In the model, it appears as though the blockout and post connection was more

rigid than in reality, causing the blockout and post to twist together rather than allowing the blockout to be pulled away from the post or rail.

Further analysis was performed to determine the upstream and downstream anchor forces. A plot of the anchor force in the upstream and downstream anchors during the impact event is shown in Figure 12. The upstream anchor forces were measured in BARRIER VII at member no. 1, and the downstream anchor forces were measured at member no. 224. In LS-DYNA, a plane section was created through the anchor posts at the lowest measurable level (immediately above the ground-line hole in the BCT post), and the normal force was plotted through the center of the post. These locations corresponded to the furthest upstream and downstream ends of the system at an impact height of 24.875 in. (632 mm). The members were measured at 0 and 24.875 in. (0 and 632 mm) for the ground level and impact height. In BARRIER VII and LS-DYNA, the peak forces through the upstream anchor post were 27.32 kips (121.5 kN) and 31.47 kips (139.9 kN), respectively. The peak forces through the downstream anchor post were 13.37 kips (59.5 kN) and 10.49 kips (46.7 kN), respectively.

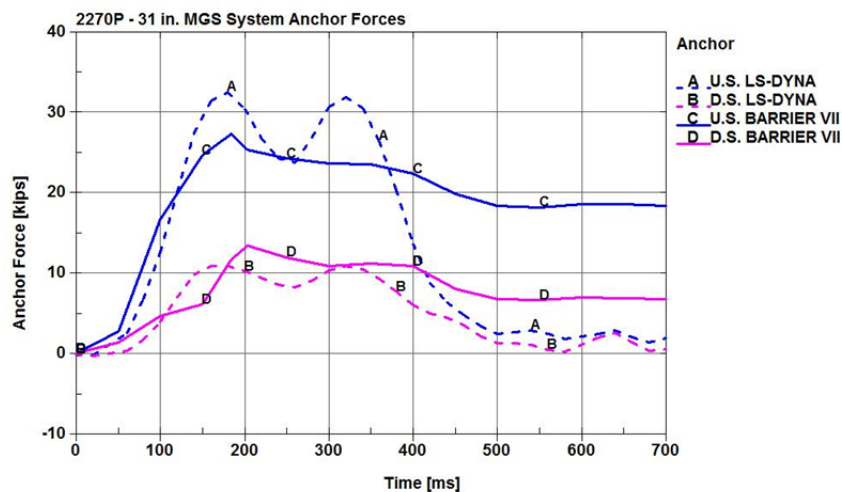


Figure 12. Simulated Forces in Anchors

These force plots provided similar results. There was a force plateau between 200 and 400 ms on both plots for the upstream and downstream anchors. In LS-DYNA, the anchor forces returned to approximately zero after impact, while in BARRIER VII, residual forces were left in the posts due to the displacements. Overall, the similarity of the two plots provide good agreement between the two models and results, however, anchor force data for the full-scale test were not available for comparison.

### **3.4 Baseline BARRIER VII 1100C Model**

#### **3.4.1 Development and Validation of the 2214MG-3 Model**

Similar to the 2214MG-2 test, a finite element model of the 2214MG-3 test was developed for use in BARRIER VII and LS-DYNA. The BARRIER VII model had a single beam type, and 3 different post types and a total length of 175 ft (53.3 m). The difference between the two BARRER VII simulations and LS-DYNA simulations, aside from the utilization of an 1100C model for the 2214MG-3 versus the 2270P model for the 2214MG-2, was the impact height of the barrier. The impact height was increased by 1 in. to 25.875 in. (657 mm) to correlate with the top rail mounting height of 32 in. (813 mm) for this system [5].

As before, two of the post types represented the two BCT anchor posts on both the upstream and downstream ends. The ground-line strut and cable were not modeled for simplicity. Thus, the anchor post strength was given particular attention and is discussed further in Section 3.4.3. The other post type represented the W6x9 (W152x13.4) system posts for the MGS.

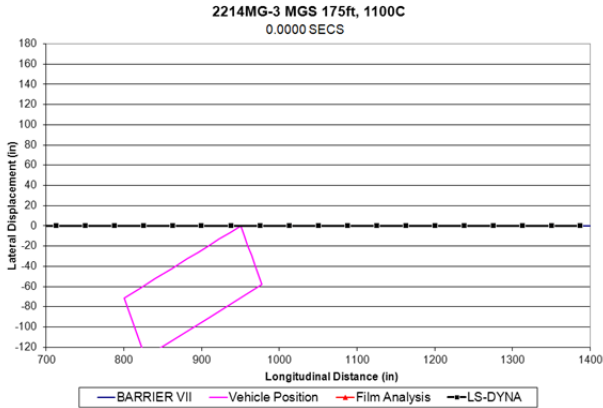
Similar to the validation of the 2214MG-2 model, the validation method for the 2214MG-3 model involved a graphical comparison of the simulations, using discretized LS-DYNA rail displacement data, BARRIER VII data, and the physical crash test barrier profile. The barrier profile during the physical crash test was obtained from the overhead film analysis, the LS-DYNA profile came from node tracking of the barrier throughout the simulation, and BARRIER

VII results were from the rail deflection calculation. The validated BARRIER VII input parameters are provided in Table 7 [23,24]. The kinetic friction coefficient was calibrated using the full-scale crash test results.

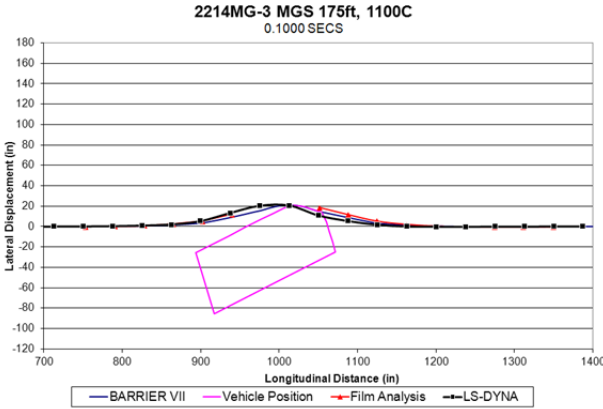
Table 7. BARRIER VII Simulation Parameters

<b>BARRIER VII Parameters [23, 24]</b>	<b>Units</b>	<b>Input Values</b>
<b>K<sub>B</sub> - Post Stiffness Along B (strong axis)</b>	kip/in. (kN/m)	3.00 (525.38)
<b>K<sub>A</sub> - Post Stiffness Along A (weak axis)</b>	kip/in. (kN/m)	2.60 (455.33)
<b>M<sub>A</sub> - Moment About A (strong axis)</b>	kip-in. (kN-m)	142.05 (16.05)
<b>M<sub>B</sub> - Moment About B (weak axis)</b>	kip-in. (kN-m)	61.90 (6.99)
<b>δ<sub>F</sub> - Failure Displacement Along B</b>	in. (mm)	15 (381)
<b>μ<sub>k</sub> - Kinetic Friction Coefficient</b>	Vehicle to Barrier	0.30

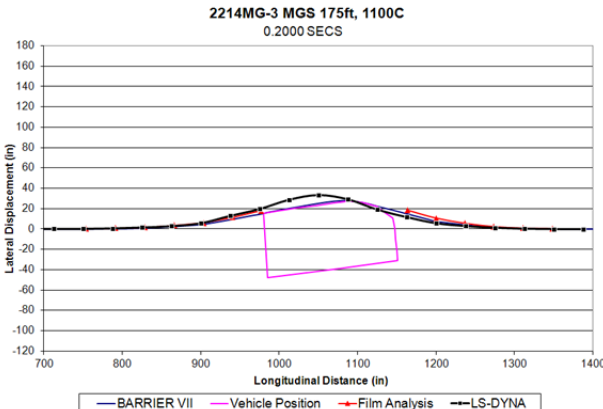
LS-DYNA and BARRIER VII simulations were compared directly with full-scale crash test data to examine the effectiveness of the programs in simulating the crashes. A graphical comparison of the simulations and test no. 2214MG-3 is shown in Figure 13. In the actual full-scale crash test, the right-front corner of the vehicle impacted the barrier. However, to generate a visual comparison with the models, sequential photos of the full-scale test were mirrored about the vertical axis, giving the indication of a left-front impact. It was assumed that an actual right-front wheel separation was identical to a virtual left-front wheel separation.



t = 0 ms



t = 100 ms



t = 200 ms

Figure 13. Sequential Figures from BARRIER VII and Test No. 2214MG-3

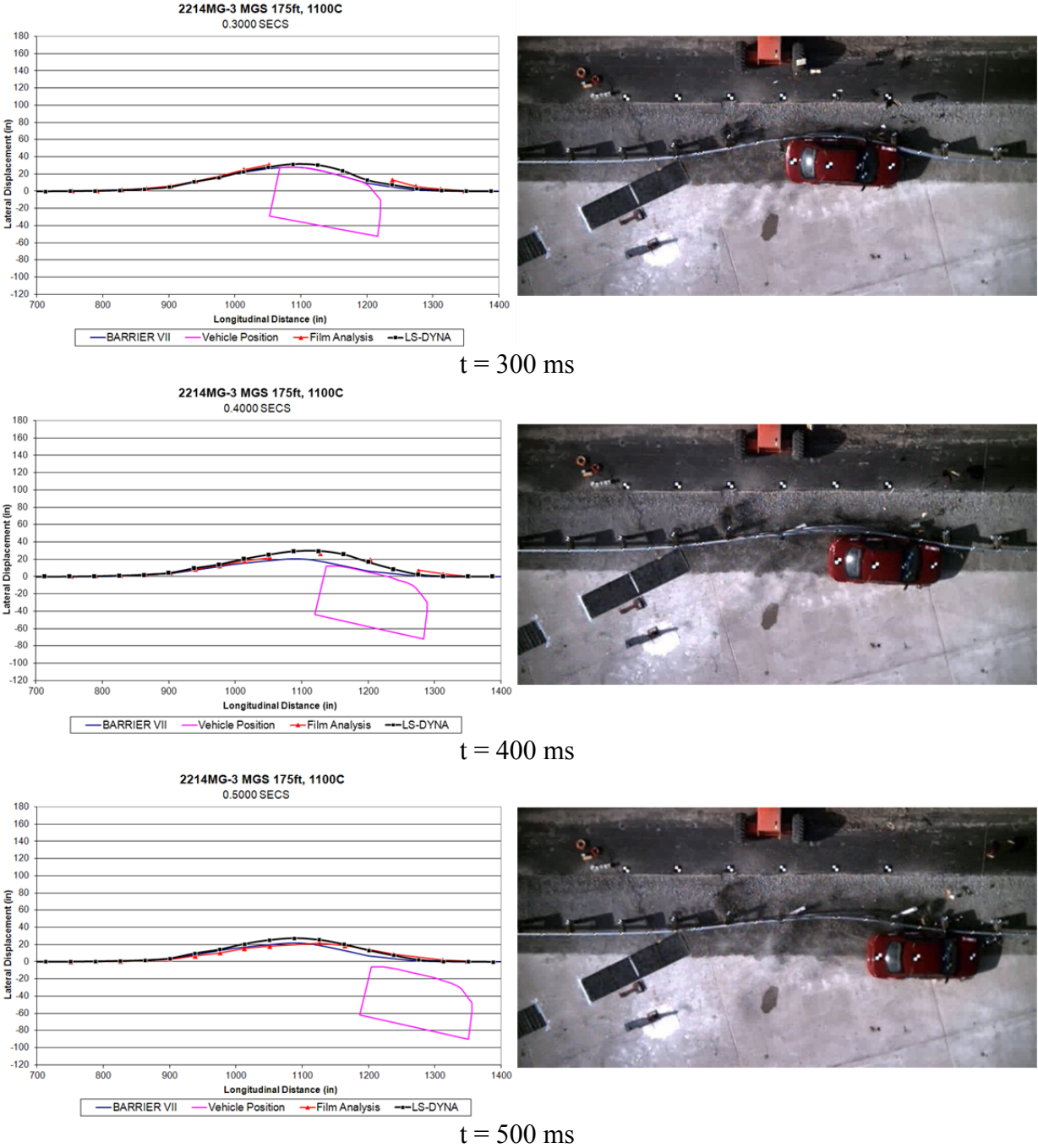


Figure 13. Sequential Figures from BARRIER VII and Test No. 2214MG-3 (continued)

BARRIER VII had some difficulty fully reproducing the guardrail shape after 200 ms. An “overly stiff” condition appeared to occur in the system as BARRIER VII under-predicted the path of the vehicle relative to the full-scale test. When the full-scale test video footage was evaluated, it was apparent that some slight underride of the vehicle into the barrier occurred. The lowest portion of the rail deflected laterally farther than the top portion. The targets were located on the top of the rail for the film analysis, so it was expected that BARRIER VII would under-predict the deflection from the point where the vehicle began to underride the barrier – approximately 200 ms.

LS-DYNA outperformed BARRIER VII in predicting guardrail behavior. LS-DYNA had the advantage of being able to simulate, and closely predict, vehicle behavior at exit. The full-scale crash test resulted in wheel snag near the vehicle’s exit from the system, causing the vehicle to yaw towards the barrier rather than being redirected away from it. LS-DYNA simulated this snag and yaw, whereas BARRIER VII predicted a smooth redirection away from the system at exit.

### **3.4.2 Comparison of Test Conditions and Simulation Results**

The second comparison method incorporated different evaluation parameters which were measured in the full-scale test and calculated using both BARRIER VII and LS-DYNA. Tabulated validation results for vehicle behavior, barrier displacements, and working width for the comparison are listed in Table 8.

A relatively small difference occurred in the parallel times for the full-scale vehicle crash test, the BARRIER VII model, and the LS-DYNA model (216 ms, 230 ms, and 222 ms). A larger discrepancy occurred in the exit times (530 ms 381 ms, and 540 ms). The 28-percent difference in exit time between BARRIER VII and the full-scale test was attributed to wheel snag. In the full-scale vehicle test, the right-front corner of the vehicle slightly underrode the

system. This caused snagging which slowed the vehicle and created a longer vehicle-to-barrier contact time. The tire deflated, the right-front corner of the vehicle dropped, and the vehicle yawed into the barrier. BARRIER VII was unable to model the tire deflation and therefore allowed the vehicle to redirect more quickly. LS-DYNA did simulate the underride, and, subsequently, the simulation results were very close to the full-scale crash results.

Table 8. Test and Simulation Results for 1100C Vehicle on Level Terrain

Evaluation Parameters	Units	Test No. 2214MG-3	Simulation Results	
			BARRIER VII Simulation	LS-DYNA Simulation
<b>Parallel Time</b>	ms	216	230	222
<b>Dynamic Rail Deflection</b>	in. (mm)	-35.9 (-913)	-28.8 (-731)	-32.7 (-830)
<b>Working Width</b>	in. (mm)	48.3 (1227)	32.8 (832*)	46.2 (1174)
<b>Working Width Indicator</b>	-	Hood Corner	Post*	Hood Corner
<b>Exit Time</b>	ms	530	381	540
<b>Exit Angle</b>	deg	-14.1	-9.7	-15.78
<b>Exit Velocity Vector</b>	deg	-	-15.7	-
<b>Resultant Velocity at Exit</b>	mph (km/h)	30.1 (48.4)	39.5 (63.5)	20.8 (33.5)

\*Although the post was the working width indicator, it was unlikely that the post would remain attached to the rail for that displacement.

Another significant difference between BARRIER VII and the full-scale test results was the exit angle of the vehicle (14.1 degrees for the physical test versus 9.7 degrees for the BARRIER VII simulation). The 31-percent difference was attributed to the inability of the program to correctly simulate wheel snag calculated by BARRIER VII which was previously discussed, leading to the under-prediction of the exit vector as the vehicle maintained a longer



contact time. The difference in exit velocity was attributed to the differences between the 2-D BARRIER VII simulation and the full-scale vehicle test. As the vehicle maintained longer contact time with the barriers, the vehicle slowed more drastically, causing the difference. The consistent parallel times and similar graphical sequential figures from 0 ms to 200 ms for BARRIER VII validates that the longer contact time was the cause of the differences. Post snag increased the exit time and decreased the exit velocity. LS-DYNA simulated these results more closely and, thus, was more capable of modeling wheel snag and the yaw of the vehicle into the barrier.

### **3.4.3 Anchor Analysis**

Particular attention was given to the deflection and forces imparted to the anchor posts in the system. It was important to calibrate anchor system behavior with existing tests before the model could be confidently used to investigate increased rail heights of the MGS. As with test no. 2241MG-2, there was no high-speed camera above the upstream or downstream anchor posts. Therefore, extrapolation was needed to find the maximum rail displacement for the full-scale test. From the fieldbook for test no. 2214MG-3, a maximum soil displacement of approximately 9/16 in. (14 mm) was measured on the upstream side of post no. 1. By extrapolating this displacement to the top rail height of 32 in. (813 mm), the estimated maximum upstream anchor displacement was 1.323 in. (34 mm). The estimation for the anchor post displacement was done using a 2/3 embedment depth rotation point and was based on measurements from post-test documentation, where the precision of the documentation may explain the discrepancy between the full-scale test and the simulation results.

Calibration of the upstream anchor in BARRIER VII was again satisfied by using two measurements: (1) post-test field book measurements versus the simulation displacements and (2) the farthest visible upstream target in the overhead film analysis. BARRIER VII predicted a

maximum displacement of 1.31 in. (33 mm), resulting in a 1.0-percent difference compared to the full-scale test. The simulated downstream anchor displacement was -0.62 in. (-16 mm). Values for the x- and y-deflection for the BARRIER VII simulation are shown in Table 9. Likewise, LS-DYNA was also used to calculate anchor displacement; those values are also shown in Table 9. LS-DYNA did a considerably poorer job predicting anchor displacement than BARRIER VII with approximately twice the anchor deflection calculated in the full-scale test.

Table 9. Simulation Anchorage Calculations with 1100C

<b>Measurement</b>	<b>Units</b>	<b>B. VII U.S. Anchor</b>	<b>LS-DYNA U.S. Anchor</b>	<b>B. VII D.S. Anchor</b>	<b>LS-DYNA D.S. Anchor</b>
<b>Time of Maximum Deflection</b>	ms	130	220	171	180
<b>Maximum Deflection</b>	in. (mm)	1.31 (33)	2.92 (74)	-0.62 (-16)	-1.03 (-26)
<b>Maximum Force through Anchor</b>	kips (kN)	15.76 (70.1)	12.34 (54.9)	7.17 (31.9)	9.3 (41.4)

The BARRIER VII and LS-DYNA simulation results are shown in Figure 14 for anchor displacements on both the upstream and downstream ends. For BARRIER VII, the upstream anchor displacements were measured at node no. 1 and the downstream anchor displacements were measured at node no. 225. These nodes corresponded to the furthest ends of the system at an impact height of 25.875 in. (657 mm) for the 32-in. (813-mm) tall system.

When the small car impacted a guardrail, a decreased lateral load was imparted on the rail compared to impacts involving pickup trucks; thus a decreased force was transmitted to the anchorage, leading to decreased anchorage deflection. However, the anchor deflections exhibited by the LS-DYNA model were closer to that of the expected anchorage deflection caused by the 2270P impact rather than the 1100C impact. Anchor deflections and forces need to be modeled

properly in order to simulate guardrails at increased rail heights. Therefore, a redesign of the LS-DYNA anchorage model was necessary before increased rail heights could be simulated.

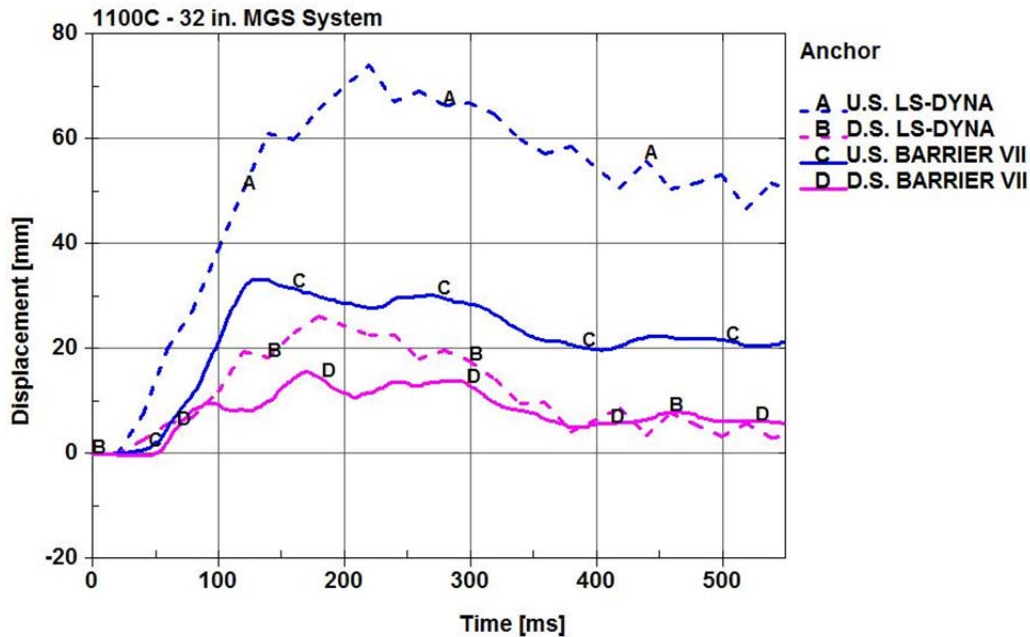


Figure 14. Upstream and Downstream Anchor Displacements

Further analysis was performed to determine the upstream and downstream anchor force. The anchor force in the upstream and downstream anchor versus time for both LS-DYNA and BARRIER VII is shown in Figure 15. For BARRIER VII, the upstream anchor forces were measured at member no. 1, and the downstream anchor forces were measured at member no. 224. These locations corresponded to the farthest upstream and downstream ends of the system at an impact height of 25.875 in. (657 mm). The members were measured at 0 and 25.875 in. (0 and 657 mm) which corresponded to the ground level and the impact height. In BARRIER VII, the peak force through the upstream anchor post was 15.76 kips (70.1 kN), while the downstream anchor post experienced a peak force of 7.17 kips (31.9 kN). These values did not correspond as well to the LS-DYNA simulation results as would be expected considering the difference in displacements that was previously noted.

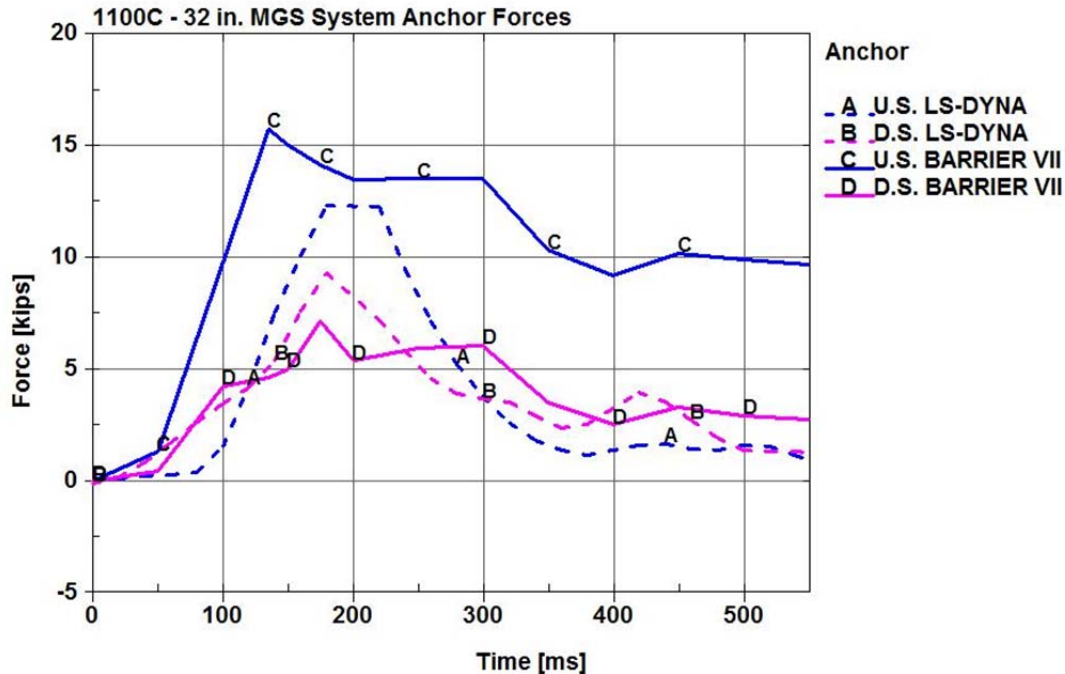


Figure 15. Force through Anchor Members

Because LS-DYNA did not predict anchor displacements well, it was believed that the BARRIER VII force results were more accurate. However, anchor force data for the full-scale test were not available for comparison.

### 3.5 Maximum Rail Height Models

#### 3.5.1 Development and Validation of the Test No. MGSMRH-1 Model

Similar to the 2214MG-3 model, a BARRIER VII model of test no. MGSMRH-1 was developed. This model allowed for comparison with LS-DYNA to validate another model's results for parameters such as anchor force and displacement. The top rail height was increased to 34 in. (864 mm) for this system [9]. The validation method for this model involved a graphical comparison of the simulations, using BARRIER VII and physical crash test barrier overhead photos. The BARRIER VII input parameters are provided in Table 10 [23, 24]. The kinetic friction coefficient was calibrated using full-scale results for the length of contact and exit times.

It should be noted that as the soil compaction methods at the MwRSF became more stringent with the introduction of MASH performance specifications. In test nos. 2214MG-2 and 2214MG-3, the guardrail posts were embedded in a moderately compacted soil. However, in test nos. MGSMRH-1 and MGSMRH-2, the posts were embedded in a highly compacted soil. Therefore, although the increased rail height would suggest a reduced strong axis bending moment, in reality the strong axis bending moment increased due to the denser soil and resulting increased post-soil resistance.

Table 10. BARRIER VII Simulation Parameters for Test No. MGSMRH-1 [23, 24]

<b>BARRIER VII Parameters</b>	<b>Units</b>	<b>Input Values</b>
<b><math>K_B</math> - Post Stiffness Along B (strong axis)</b>	kip/in. (kN/m)	2.60 (455.33)
<b><math>K_A</math> - Post Stiffness Along A (weak axis)</b>	kip/in. (kN/m)	2.60 (455.33)
<b><math>M_A</math> - Moment About A (strong axis)</b>	kip-in. (kN-m)	172.54 (19.49)
<b><math>M_B</math> - Moment About B (weak axis)</b>	kip-in. (kN-m)	61.90 (6.99)
<b><math>\delta_F</math> - Failure Displacement Along B</b>	in. (mm)	15 (381)
<b><math>\mu_k</math> - Kinetic Friction Coefficient</b>	Vehicle to Barrier	0.35

The BARRIER VII simulation was compared directly to full-scale crash test data to evaluate the barrier at an increased mounting height. A graphical comparison of the simulations for test no. MGSMRH-1 is shown in Figure 16. In the actual full-scale crash test, the right-front corner of the vehicle impacted the barrier. However, to generate a visual comparison with the models, sequential photos of the full-scale test were mirrored about the vertical axis, giving the indication of a left-front impact. It was assumed that an actual right-front wheel separation was identical to a virtual left-front wheel separation. BARRIER VII did an excellent job predicting the redirection of the 1100C vehicle at this top-rail height, with only minor discrepancies shown

in comparison to the full-scale test as the rail springs back after impact. The over-stiffness issue detailed in the baseline model was not found to be an issue at this height due to the reduced input parameters.

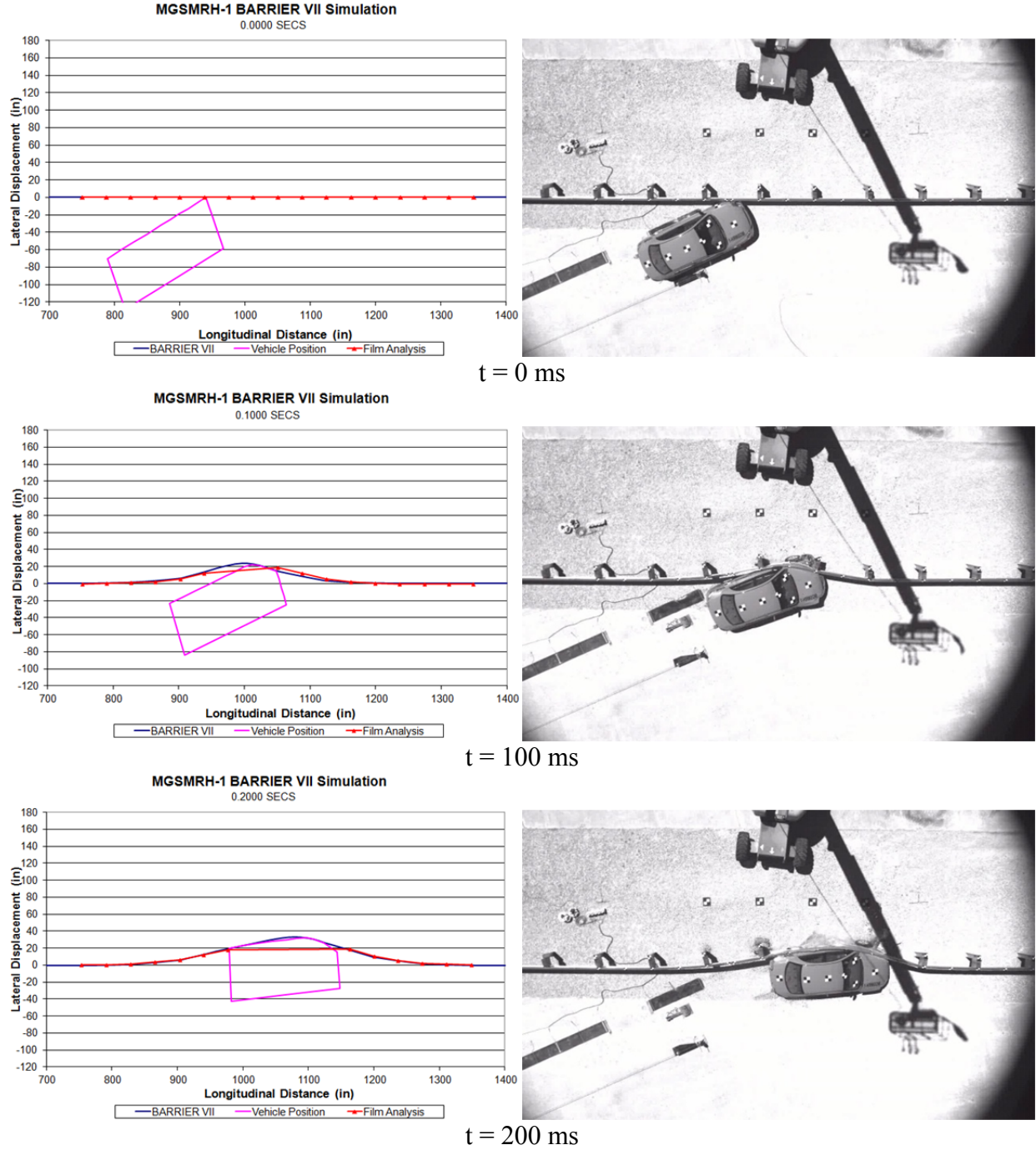


Figure 16. Sequential Figures from BARRIER VII and Test No. MGSMRH-1

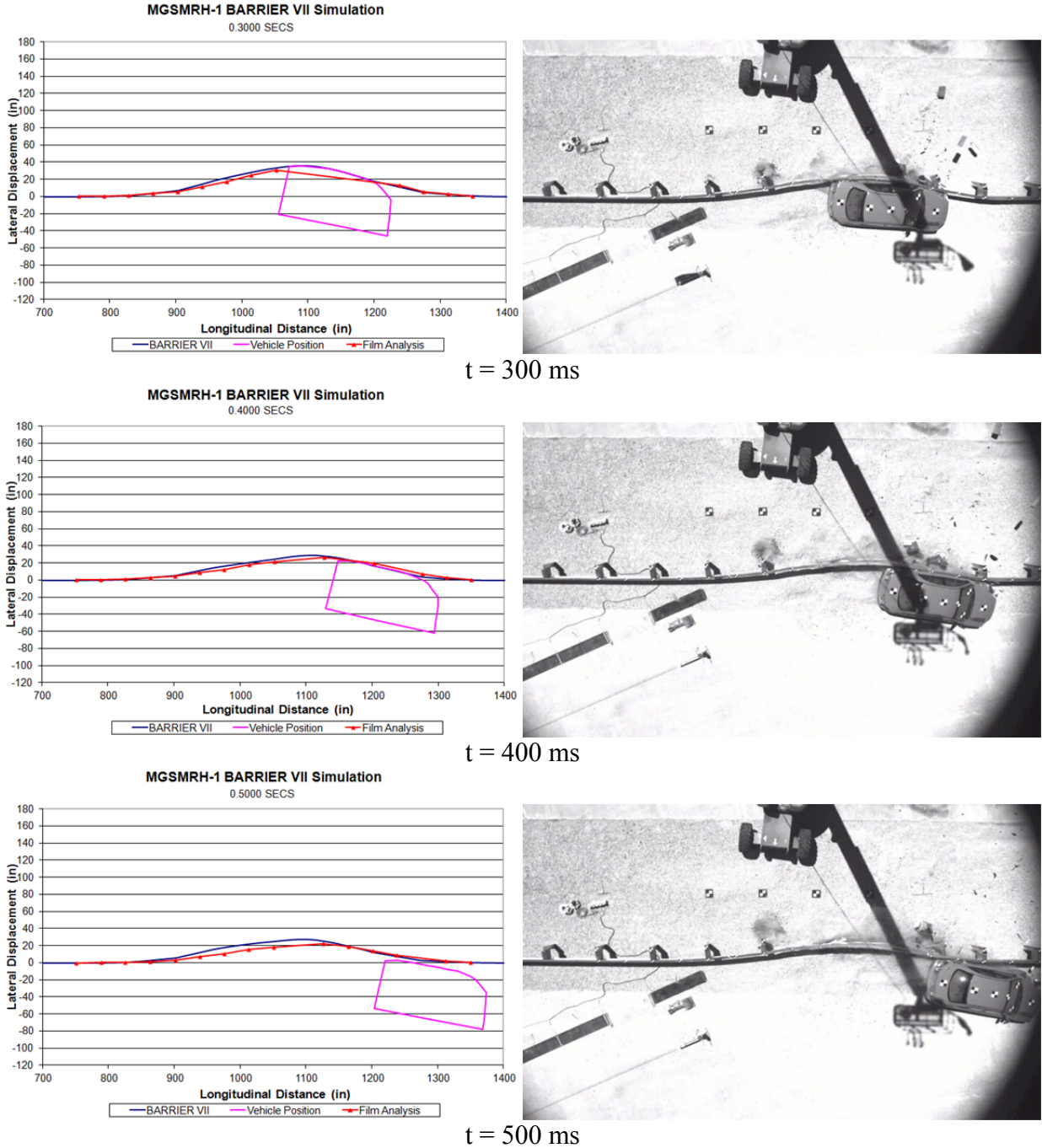


Figure 16. Sequential Figures from BARRIER VII and Test No. MGSMRH-1 (continued)

In general, LS-DYNA did a better job of predicting guardrail behavior than BARRIER VII. LS-DYNA has the added benefit of being able to simulate, and closely predict, vehicle behavior at exit. The full-scale crash test resulted in wheel snag near the vehicle exit from the

system, causing the vehicle to yaw towards the barrier rather than redirect away. LS-DYNA simulated this snag and yaw, whereas BARRIER VII predicted a smooth redirection away from the system at exit.

### **3.5.2 Comparison of Test Conditions and Simulation Results**

BARRIER VII calculated a number of useful parameters for determining the effectiveness of the guardrail to redirect a vehicle. Output data from BARRIER VII and data collected from test no. MGSMRH-1 are shown in Table 11.

BARRIER VII performed very well at estimating the parallel time and exit speed and angle for test no. MGSMRH-1. Use of BARRIER VII at this height was deemed acceptable and used to simulate a top-rail rail height of 36 in. (914 mm).

### **3.5.3 Development and Validation of the Test No. MGSMRH-2 Model**

A BARRIER VII model of test no. MGSMRH-2 was developed. The top rail height was increased to 36 in. for this system [9]. BARRIER VII and photos of the physical crash test were compared. The BARRIER VII input parameters are provided in Table 12.

The BARRIER VII simulation was compared directly to full-scale crash test data to evaluate the barrier at an increased mounting height. A graphical comparison of the simulations and physical test for test no. MGSMRH-2 is shown in Figure 17. In the actual full-scale crash test, the right-front corner of the vehicle impacted the barrier. However, to generate a visual comparison with the models, sequential photos of the full-scale test were mirrored about the vertical axis, giving the indication of a left-front impact. It was assumed that an actual right-front wheel separation was identical to a virtual left-front wheel separation.

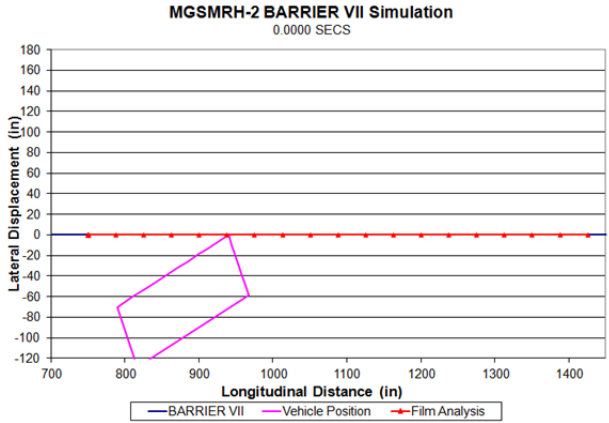


Table 11. Test and BARRIER VII Simulation Results

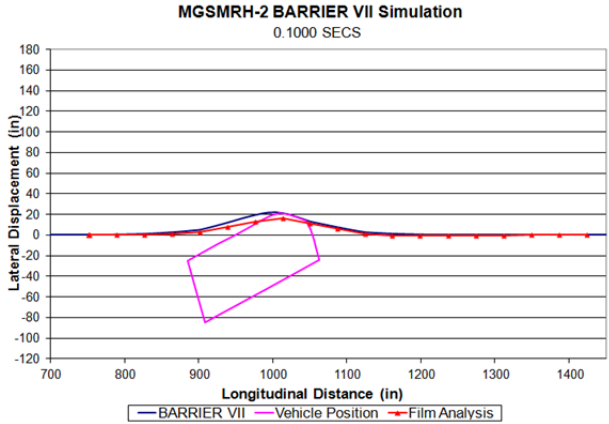
Evaluation Parameters	Units	Test Results	
		Test No. MGSMRH-1	B7 Simulation
Parallel Time	ms	236	239
Parallel Speed	mph (km/h)	43.8 (70.5)	42.5 (68.4)
Exit Angle	deg	-12.3	-11.1
Exit Speed	mph (km/h)	39.3 (63.2)	38.7 (62.3)
Dynamic Deflection	in. (mm)	-29.0 (-737)	-30.5 (-775)
Working Width	in. (mm)	49.4 (1255)	45.5 (1155)

Table 12. BARRIER VII Simulation Parameters for Test No. MGSMRH-2

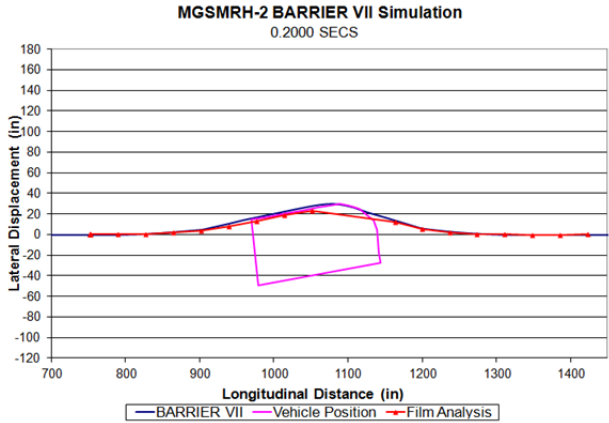
BARRIER VII Parameters	Units	Input Values
$K_B$ - Post Stiffness Along B (strong axis)	kip/in. (kN/m)	2.60 (455.33)
$K_A$ - Post Stiffness Along A (weak axis)	kip/in. (kN/m)	2.60 (455.33)
$M_A$ - Moment About A (strong axis)	kip-in. (kN-m)	172.54 (19.49)
$M_B$ - Moment About B (weak axis)	kip-in. (kN-m)	61.90 (6.99)
$\delta_F$ - Failure Displacement Along B	in. (mm)	15 (381)
$\mu_k$ - Kinetic Friction Coefficient	Vehicle to Barrier	0.35



t = 0 ms



t = 100 ms



t = 200 ms

Figure 17. Sequential Figures from BARRIER VII and Test No. MGSMRH-2

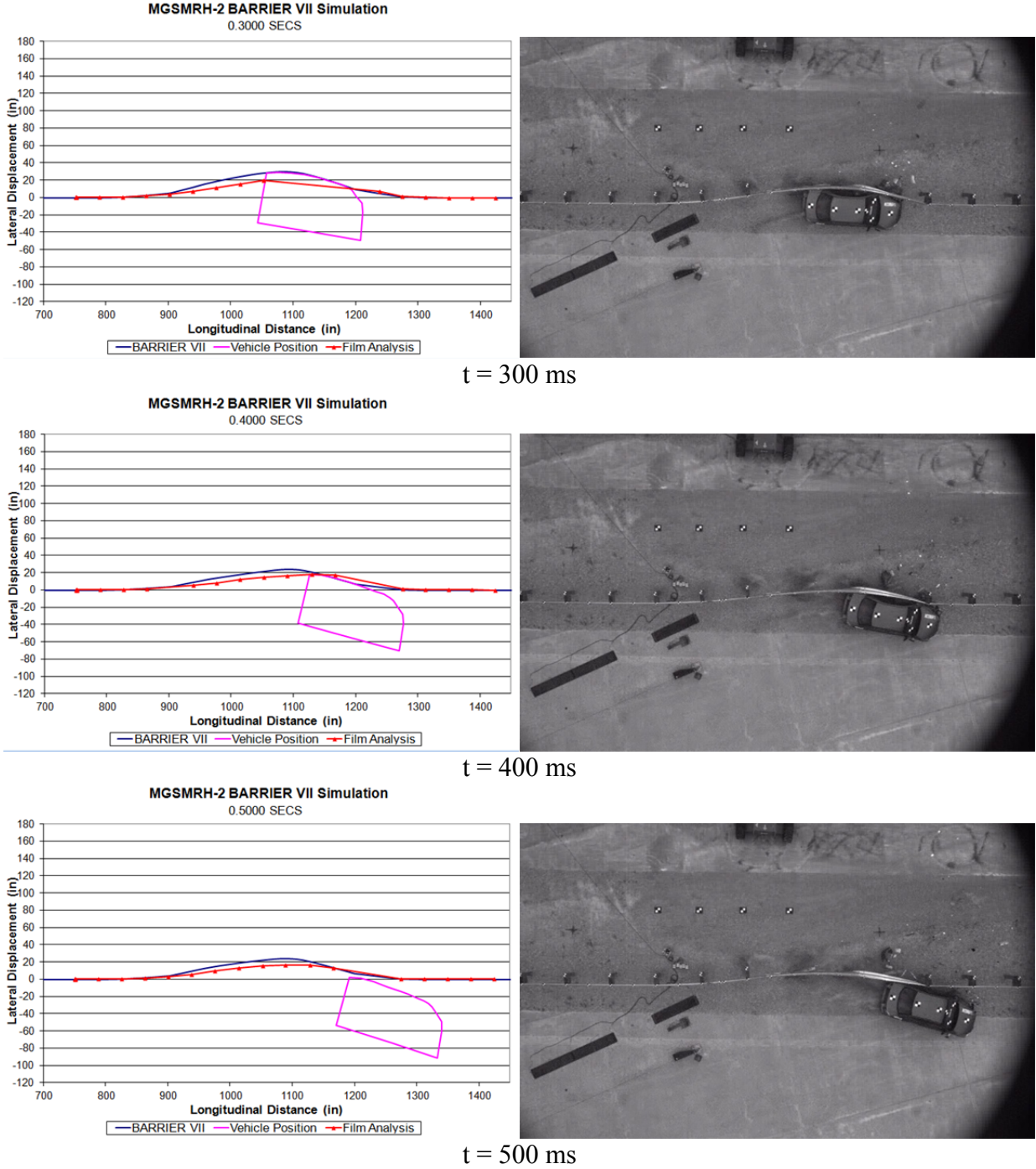


Figure 17. Sequential Figures from BARRIER VII and Test No. MGSMRH-2 (continued)

BARRIER VII adequately predicted the redirection of the 1100C vehicle at this top-rail height, with only minor discrepancies compared to the full-scale test, where the rail sprung back after impact. At this top-rail height, the rail deflected more in BARRIER VII than in the full-scale test. This was due to the fact that the car was beginning to underride slightly more than in previous simulations. This BARRIER VII simulation still gave reasonably accurate results, which can assist in evaluating maximum rail heights. As a 2-D program, BARRIER VII cannot predict the propensity for underride, which was necessary to properly evaluate barrier height. At any reasonable top-rail height prescribed in BARRIER VII, the car will always impact the barrier and will never underride the system. For this reason, the maximum height evaluations at higher top-rail heights had limited benefits with this program. However, they did show that the decreased post embedment depths still provided adequate containment forces to redirect the vehicle if underride was not an issue.

#### **3.5.4 Comparison of Test Conditions and Simulation Results**

BARRIER VII calculated many useful parameters for determining the effectiveness of guardrail at redirecting a vehicle. Output data from BARRIER VII and data collected from test no. MGSMRH-1 are shown in Table 13. BARRIER VII was shown to perform very well in calculating the parallel criterion for test no. MGSMRH-2. However, exit angles were significantly different due to the inability of BARRIER VII to predict snag or underride.

While BARRIER VII showed good redirection effectiveness for the 36-in. (914-mm) MGS barrier, the program's effectiveness was minimal at these increased heights due to its inability to predict underride. The decreased embedment depths of the posts did not sufficiently decrease the resistive force capabilities of the system at this top-rail height for 1100C cars. The vehicle did not pull the barrier free until the top-rail height reached 40 in. (1016 mm), at which point massive rail deflections occurred. The redirection of a small car at a top-rail height of 40

in. (1016 mm) was highly unlikely because of the geometry of standard 1100C passenger vehicles.

Table 13. Test and BARRIER VII Simulation Results

Evaluation Parameters	Units	Test Results	
		Test No. MGSMRH-2	B7 Simulation
Parallel Time	ms	262	243
Parallel Speed	mph (km/h)	41.1 (66.1)	41.6 (66.9)
Exit Angle	deg	21.9	11.3
Exit Speed	mph (km/h)	36.2 (58.3)	37.8 (60.9)
Dynamic Deflection	in. (mm)	23.5 (597)	30.2 (768)
Working Width	in. (mm)	40.5 (1029)	43.0 (1091)

### 3.6 Discussion

Although BARRIER VII is a 2-D simulation program, it performed remarkably well in comparison with the more robust LS-DYNA. LS-DYNA did perform better in the prediction of exit angles and dynamic rail deflections, but it was difficult to conclude that LS-DYNA was far better at simulating vehicle impacts at standard top-rail heights. LS-DYNA has far better visualization abilities, making it easier to interpret the results of the simulation. It was also able to predict the yaw of the vehicle into the barrier due to wheel snag – a critical part of this simulation that significantly affected some results. However, BARRIER VII made reasonably accurate predictions of the barrier shape, especially when the limitations of the 2-D program were recognized, and it was far less expensive to use.

This analysis showed that in some cases BARRIER VII performed well in predictive capabilities for parameters such as post failure, anchor displacement, and pocketing [24]. These are three critical system parameters that affect barrier performance. The inability to predict vehicle underride, vehicle suspension failure, or vehicle occupant compartment damage limited the effectiveness of BARRIER VII. The program did provide a good basis for comparison and verification for LS-DYNA where full-scale crash test data were limited. A baseline expectation of maximum barrier height could not be determined using the predictive capabilities of BARRIER VII. The lack of its ability to simulate underride did not provide enough data to make a valid conclusion on maximum rail height for small cars.

Therefore, it was determined that LS-DYNA simulations were the best method for determining a maximum guardrail height with respect to underride. However, the LS-DYNA simulation used in the study described in this chapter was less effective than BARRIER VII in some regards. Therefore, the LS-DYNA MGS model was replaced with a newer version of the model that was being developed in parallel with this study. In the new model, the anchors were updated to match the physically tested components to more accurately represent the full-scale test design [24]. This updated LS-DYNA model was used in all subsequent analyses described herein.

## **4 MODELING AND SIMULATION**

### **4.1 Introduction**

Finite element modeling can be an extremely useful tool in evaluating roadside hardware. An accurate model can be used in place of expensive physical testing to evaluate potential design changes. A finite element model of the MGS was used and altered to evaluate the potential for systems with increased top-rail heights to effectively redirect small cars and to adequately contain pickup trucks. Full-scale vehicle crash test data were used to validate the finite element model results.

### **4.2 Midwest Guardrail System Model**

An improved, second generation MGS LS-DYNA model was developed by researchers at the MwRSF. Goals of the new model were to: (1) improve end anchorage design to better match full-scale system construction and results; (2) refine the system mesh for improved barrier deflection performance; and (3) improve vehicle-to-barrier interaction and results. This new model improved performance in simulating full-scale vehicle crash tests [25]. An abbreviated list of guardrail model parts and the associated LS-DYNA modeling parameters is shown in Table 14. A comparison of the physical barrier system and the finite element model of the simulated end anchorage and overall barrier system is shown in Figures 18 and 19.

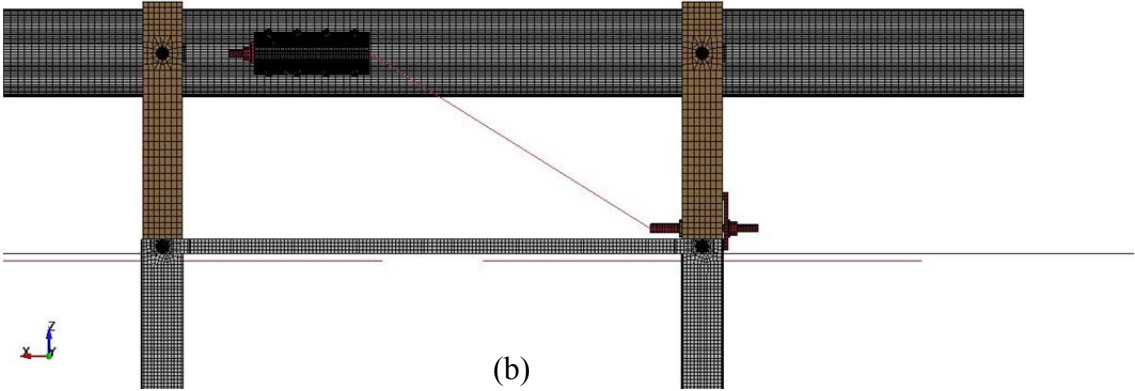
Table 14. Summary of MGS Model Part Properties

<b>Part Name</b>	<b>Element Type</b>	<b>Element Formulation</b>	<b>Material Type</b>	<b>Material Formulation</b>
Anchor Cable	Beam	Belytschko-Schwer, Resultant Beam	6x19 3/4" Wire Rope	Moment, Curvature Beam
Anchor Post Bolt	Solid	Constant Stress Solid Element	ASTM A36	Rigid
Anchor Post Bolt Heads	Shell	Belytschko-Tsay	ASTM A36	Rigid
Anchor Post Washers	Solid	Constant Stress Solid Element	ASTM A36	Rigid
BCT Anchor Post	Solid	Fully Integrated, S/R	Wood	Plastic Kinematic
Bearing Plate	Solid	Constant Stress Solid Element	ASTM A36	Rigid
Blockout	Solid	Fully Integrated, S/R	Wood	Elastic
Blockout Bolts	Shell	Belytschko-Tsay	ASTM A36	Rigid
Bolt Springs	Discrete	DRO=Translational Spring/Damper	ASTM A36	Spring, Non-Linear Elastic
Ground-Line Strut	Shell	Belytschko-Tsay	ASTM A36	Piecewise, Linear Plastic
Post Soil Tubes	Shell	Belytschko-Tsay	Equivalent Soil	Rigid
Soil Springs	Discrete	DRO=Translational Spring/Damper	Equivalent Soil	Spring, General Non-Linear
W-beam Guardrail Section	Shell	Fully Integrated, Shell Element	12 Ga. Galvanized Steel	Piecewise, Linear Plastic
W6x9 Post	Shell	Fully Integrated, Shell Element	ASTM A992 Gr. 50	Piecewise, Linear Plastic





(a)

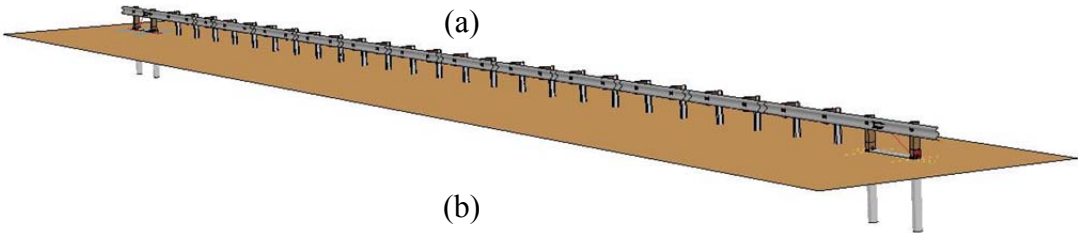


(b)

Figure 18. (a) Actual End Anchorage and (b) Finite Element Model



(a)



(b)

Figure 19. (a) Actual Overall System and (b) Simulation Model

#### **4.2.1 Increased Mounting Height Modeling**

A standard 31-in. (787-mm) rail height system was originally developed. Then, it was necessary to increase the top rail height to 32, 34, 36, and 37 in. (813, 864, 914, and 940 mm).

This change was completed by the following methods:

- Translating the W6x9 (W152x13.4) system posts in the z-direction to decrease post embedment;
- Translating corrugated rail and mounting hardware vertically to align with increased height of the W6x9 (W152x13.4) posts;
- Scaling the W6x9 (W152x13.4) post soil tubes vertically to align the base of the soil tube with the bottom of the post;
- Scaling the BCT anchor post elements between the rail mounting hole and the ground-line hole vertically to align the mounting holes with the rail; and
- Re-aligning the upstream and downstream anchor cables with the rail mounting and ground-line mounting locations.

Each of these processes was performed for each rail mounting height to create five different MGS models with rail heights of 31, 32, 34, 36, and 37 in. (787, 813, 864, 914, and 940 mm). The corresponding post embedment depths became 40, 39, 37, 35, and 34 in. (1016, 991, 940, 889, and 864 mm), respectively.

#### **4.2.2 Anchor Geometry Effects at Increased Mounting Height**

Due to the increased rail mounting height, the end anchorage geometry was subsequently changed, which required that the BCT anchor posts be scaled vertically for each system height to line up the rail mounting hole geometry.

Scaling of the BCT posts increased the aspect ratio of the elements in the affected area with a maximum aspect ratio of 1.654 for the 37-in. (940-mm)top- rail height. This scaling was

deemed minor. All elements were scaled uniformly and this aspect ratio was not deemed unsafe. The scaled 34-, 36-, and 37-in. (864-, 914-, and 940-mm) mounting height BCT posts were compared to the 32-in. (813-mm) BCT post in Figure 20. Scaling the BCT posts in this manner allowed the total number of elements in the posts to remain constant.

Changing the rail mounting height altered the geometry of the cable anchorages. A comparison of these cable geometry changes is shown in Figure 21. The rail increased in height and the angle the cable created with the ground-line strut increased. The angle of the cable increased from an angle of 28.84 degrees at a 31-in. (787-mm) top-rail height to 35.13 degrees at a 37-in. (940-mm) top-rail height, roughly increasing by a degree for every 1 in. (25.4 mm). Similarly, the higher top-rail height increased the length of the end anchorage cable. The increased angle coupled with the increased cable length had the potential to alter the impact force in the anchorage system.

## **4.3 Vehicle Models**

### **4.3.1 Geo Metro Vehicle Model**

Several vehicle models were used for the purpose of validating and simulating increased mounting height guardrail systems. Primarily, for underride studies, a Geo Metro vehicle model was used as the impacting vehicle. The Geo Metro vehicle model (820C), originally created by the National Crash Analysis Center (NCAC), was improved upon and obtained from Politecnico di Milano, Italy. This model was later modified by MwRSF personnel for use in roadside safety applications. The Geo model is shown in Figure 22.

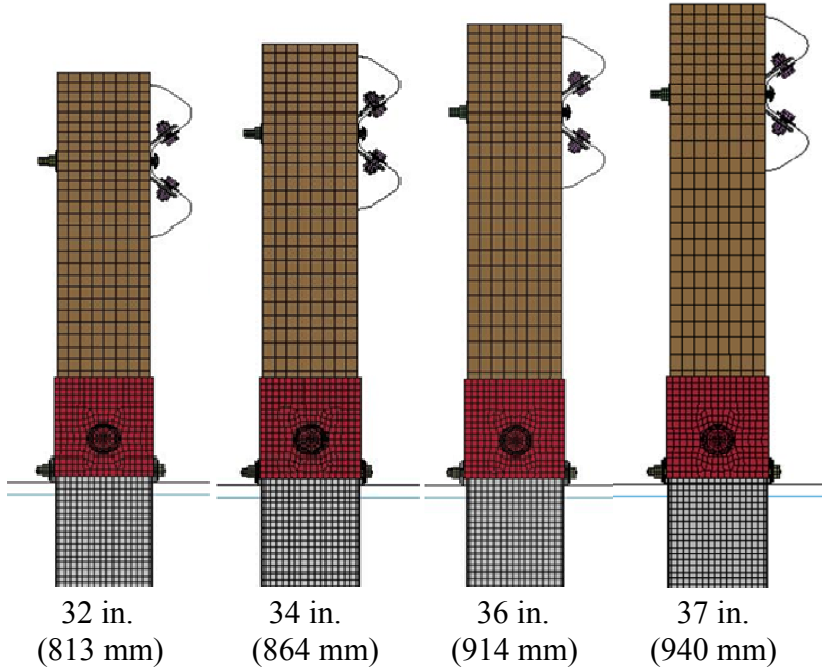


Figure 20. Post Scaling

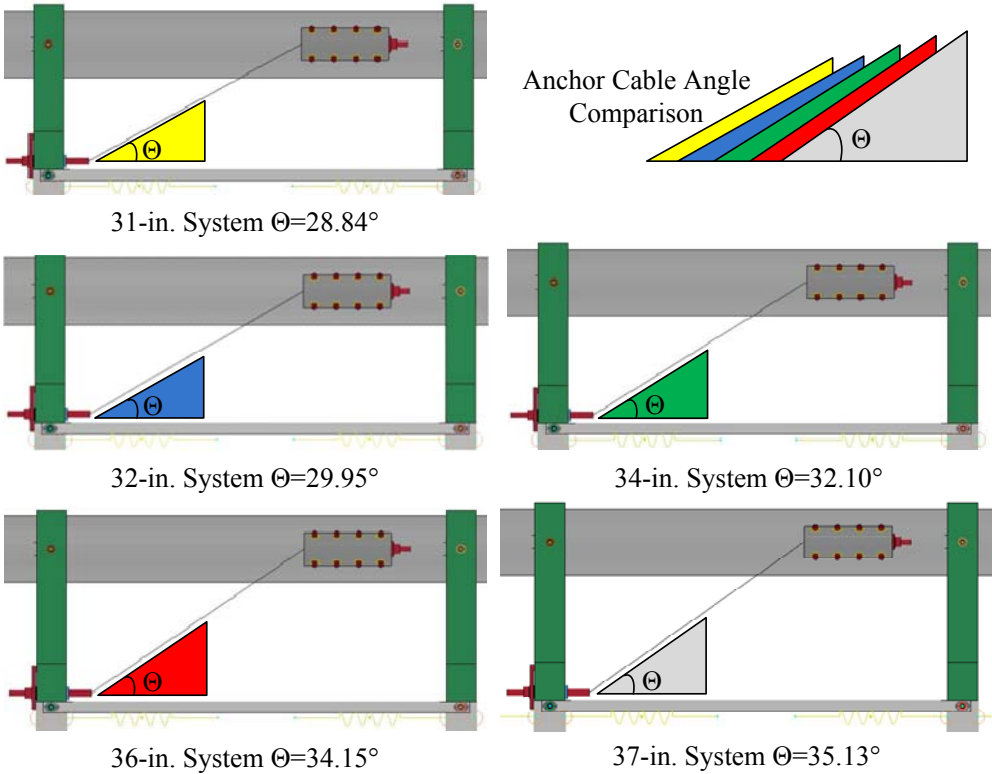


Figure 21. Anchor Cable Geometry Changes

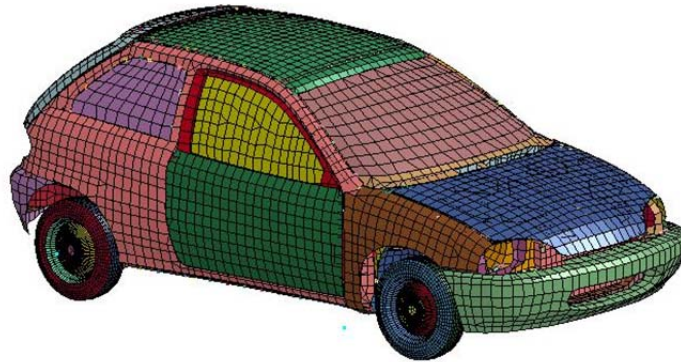


Figure 22. Geo Metro Vehicle Model

#### **4.3.2 Dodge Neon Vehicle Model**

Additionally, in order to study vehicle front-end geometry effects on the effectiveness of the system to redirect small cars, a Dodge Neon vehicle model (1100C) was used as the impacting vehicle. The Dodge Neon vehicle model was originally created by the NCAC and later modified by MwRSF personnel for use in roadside safety applications. The Dodge Neon vehicle model is shown in Figure 23.

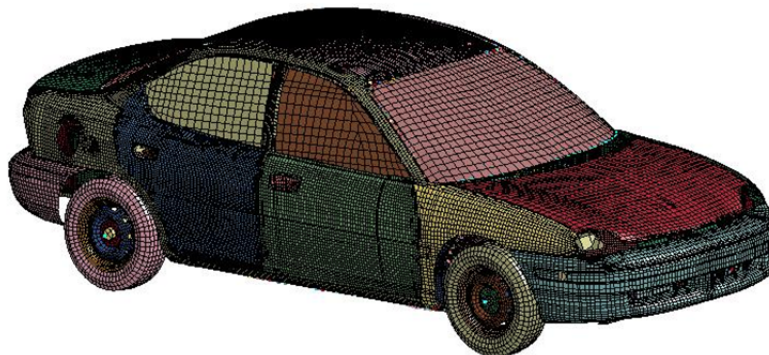


Figure 23. Dodge Neon Vehicle Model

#### **4.3.3 Chevrolet Silverado Vehicle Model**

Finally, to analyze anchor displacements and forces as well as override effects when the MGS was placed on approach slopes, a Chevrolet Silverado vehicle model (2270P) was used as the impacting vehicle. The Silverado vehicle model was originally created by the NCAC and

later modified by MwRSF personnel for use in roadside safety applications. The Silverado vehicle model is shown in Figure 24.



Figure 24. Chevrolet Silverado Vehicle Model

#### **4.4 Modeling Issues**

In the course of creating and validating a model using LS-DYNA, multiple simulation issues and model creation problems occurred which required careful consideration and tuning in order to provide the best representation of physical results. This section documents the issues encountered in generating the models for use in determining the maximum guardrail height. Problems encountered included scale factor issues, contact issues, and blockout failure criterion refinement.

##### **4.4.1 Surface Contact Scale Factors**

The penalty stiffness was adjusted to scale the stiffness of each interacting pair of masses (segments) separated by springs (penalty stiffness) to an optimum level so that the system remained stable with minimal penetration. Penalty stiffness, in essence, added massless springs that depended on segment mass for stability [26, 27]. Since the segment mass was already considered in element time-step calculations, there was no way to ensure stability with any added

penalty stiffness, so the stiffness was scaled back to a small fraction of the calculated stability limit. Initially, penetrated nodes were not moved during initialization; rather, the initial penetration for each segment pair was stored and subtracted from the current penetration before calculating penalty forces [26, 27]. The disadvantage of this method was that some parts may penetrate too much. In this case, where a great deal of sliding occurred as one segment of the vehicle fender slid along the rail, the vehicle fender penetrated a little deeper each time it passed from one segment to another because it entered the new segment from the side. At this point, the penetrated nodes became "trapped" behind the rail and a sort of induced snagging occurred where the fender caught and rotated the car.

#### **4.4.1.1 Simulation at 34-in. (864-mm) Rail Height**

At a contact scale factor of 1.0, the 34-in. (864-mm) MGS simulation errored out after 200 ms; the scale factors on the slave penalty stiffness (SFS) were changed to 0.5 from a default value of 1.0. This provided a stable simulation which was able to run to completion. Good similarity was exhibited up to 200 ms, as shown in Figure 25. Therefore, the change to SFS did not significantly alter the simulation results at this height; however, at a 36-in. (914-mm) rail height, significant differences were shown.

SFS was set in the \*CONTACT card and scaled the SLSFAC parameter, which was set in the \*CONTROL\_CONTACT card. The SLSFAC for all simulations was set to 0.1. Thus, an SFS set to 0.5 and 1.0, as used here, created an overall scale factor of 0.05 and 0.1, respectively.

#### **4.4.1.2 Simulation at 36-in. (914-mm) Rail Height**

Using a contact scale factor of 1.0, in the 36-in. (914-mm) MGS model allowed the simulation to run to completion, but the vehicle showed significant snagging and incurred major occupant compartment damage. This simulation was not deemed realistic due to the major vehicle twisting throughout the occupant compartment. Similar to the 34-in. (864-mm) simulation, the contact

scale factor was reduced to 0.5 and the simulation was re-run. A comparison between the contact scale factors is shown in Figure 26 for the 36-in. (914-mm) systems.

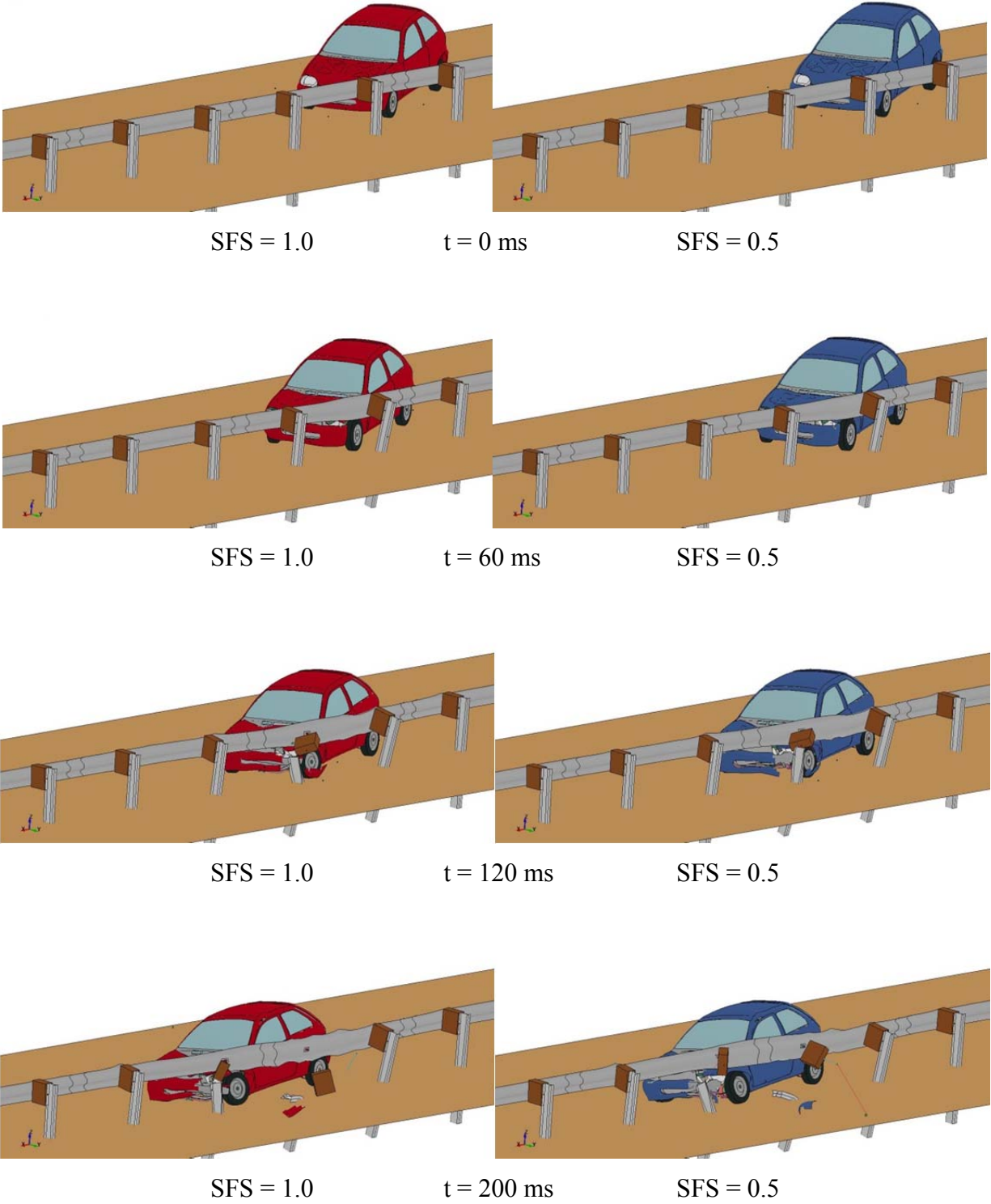


Figure 25. Comparison of 820C impact with SFS=1.0 and 0.5 at 34 in. (864 mm)



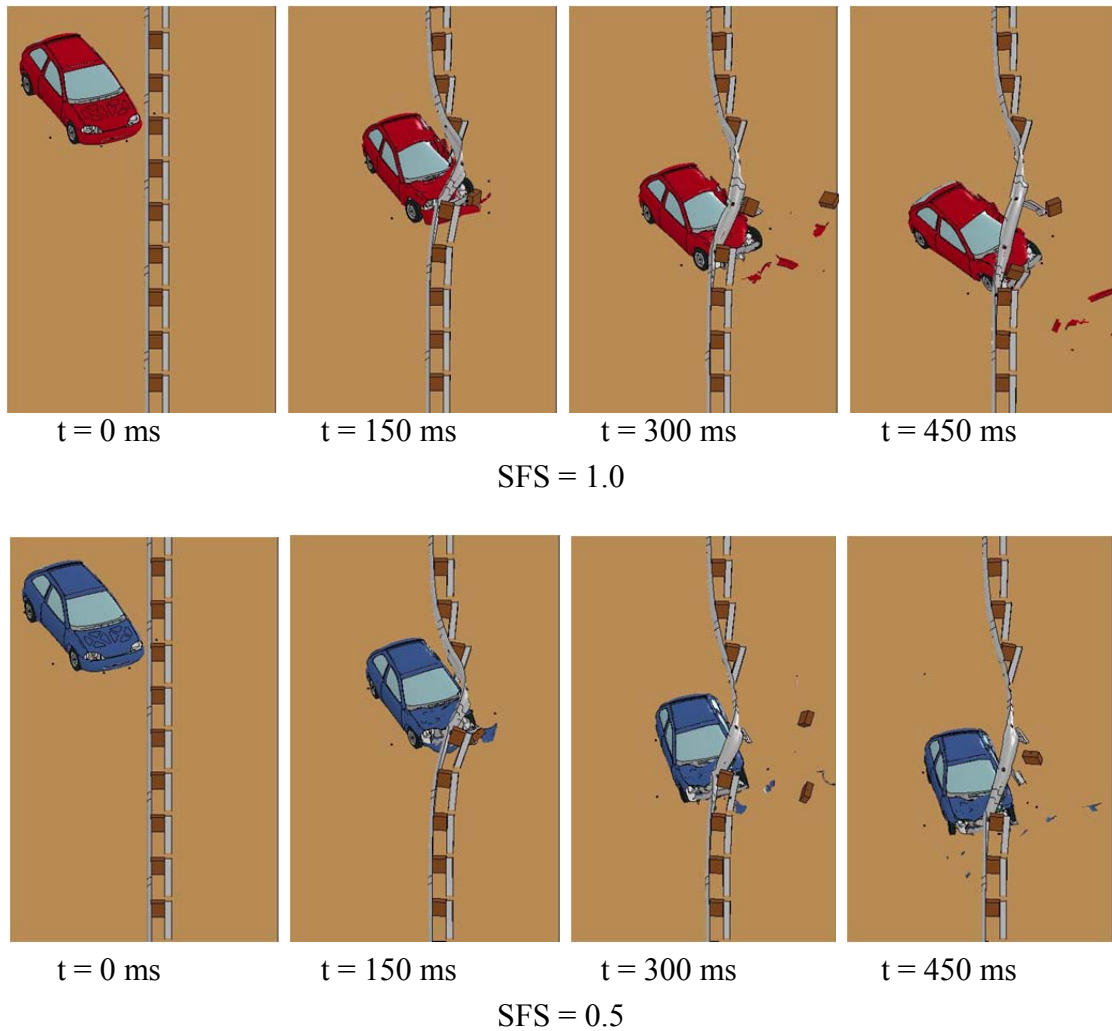


Figure 26. Comparison of 820C impact with SFS=1.0 and 0.5 at 36 in. (914 mm)

The perceived realism of decreasing the contact scale factor in the 36-in. (914-mm) simulations and the instabilities shown at SFS = 1.0 induced the decision to use SFS = 0.5. This scale factor was used in all simulations.

#### 4.4.2 Contact Formulation

From the LS-DYNA Theory Manual, the contact formulation was applied in \*CONTACT cards by setting SOFT = 0, 1, or 2 [26]. In this study, only SOFT=0 or 2 was used.

#### 4.4.2.1 SOFT=0

The SOFT = 0 formulation is a nodal-based contact and is the default setting [26,27]. For SOFT = 0, contact formulation of the surface timestep is proportional to  $\sqrt{\frac{m}{k}}$ , where m is essentially the mass attached to the contact "spring" and k is the contact spring stiffness, which is a function of the material bulk modulus and element size. The simplest way to increase the surface timestep is to reduce the contact stiffness by reducing SFS and the scale factor on the master penalty stiffness (SFM) on card 3 of \*CONTACT. SFM is used for two-way contacts such as \*CONTACT\_AUTOMATIC\_SURFACE\_TO\_SURFACE, which was used for the vehicle-to-rail contacts in all simulations.

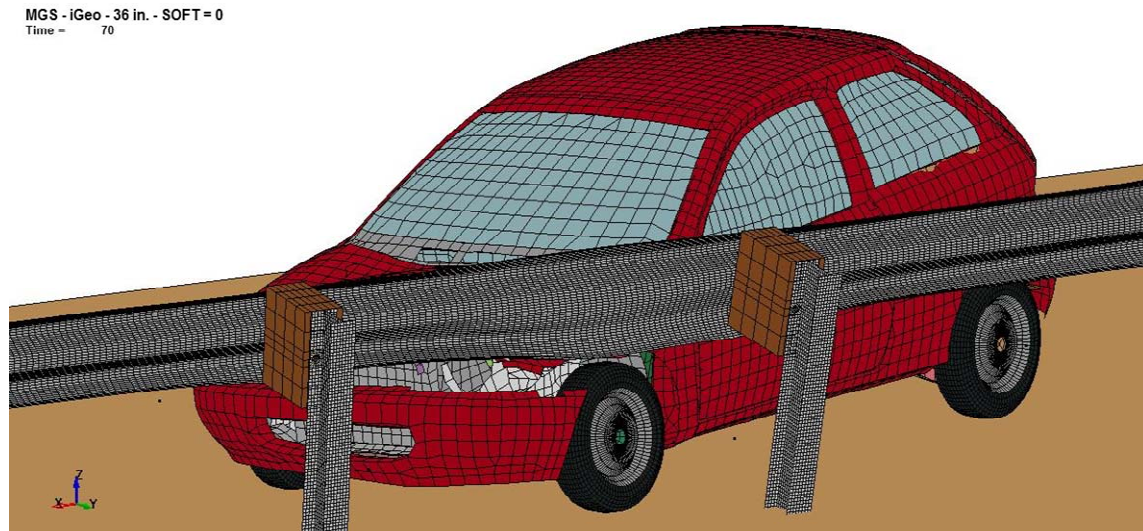
#### 4.4.2.2 SOFT=2

The contact formulation SOFT = 2 is segment based and is a general purpose shell and solid element penalty-type contact algorithm. Contact detection between segments prevents penetration of undetected nodes, which can happen with SOFT = 0 when nodes slip behind and between segments at edges and corners. For SOFT = 2, the contact stiffness is calculated based on the actual timestep. The contact timestep reported in the d3hsp file is not meaningful for SOFT = 2 contact. Initial penetrations exhibited by SOFT = 0 and SOFT = 1 are not eliminated by the use of SOFT = 2; Instead, they become a baseline from which added penetration is measured and from which contact forces are calculated.

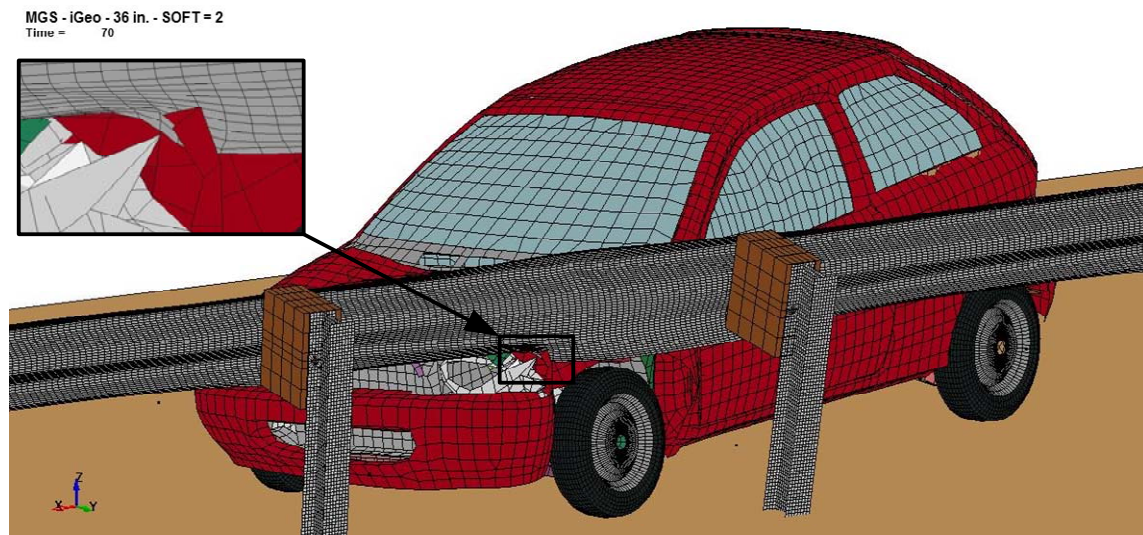
#### 4.4.2.3 Graphical Comparison of Cases

Contact with SOFT = 2 was expected to give the best results because segment-based contact is generally better at detecting edge-to-edge contact, which exists between the edges of the W-beam rail and many of the vehicle parts. However, setting SOFT = 2 trapped nodes behind the rail and allowed for induced mesh tangling, whereas setting SOFT = 0 had none of these

effects, as shown in Figure 27. Therefore,  $SOFT = 0$  was used for all simulations used in drawing conclusions with respect to maximum guardrail height.



SOFT = 0 at t = 70 ms



SOFT = 2 at t = 70 ms

Figure 27. Contact Formulation Differences

#### 4.4.3 Blockout Bolt Failure Deflection

The MGS is built with wood blockouts placed between the rail and the posts. During experimental tests, blockouts in the impact zone have been shown to split or be ejected intact

away from the system. The failure of these components may affect the dynamic deflection of the rail and, eventually, the vehicle kinematics. When considering the proper contact between the vehicle and the blockouts, a high failure mode caused an unrealistic snagging of the front bumper into this component of the barrier, whereas a low failure mode caused the rail-blockout-post connection to release outside of the impact zone.

Long bolts, used to attach blockouts to posts, were modeled using Belytschko-Tsay rigid shell elements (for the bolt surface, head, and nut) tensioned with discrete nonlinear elastic spring beam elements with nodes constrained to the bolt ends. The discrete beam elements were prescribed a failure deflection to simulate bolt failure. The optimal prescribed failure deflection defined in the section discrete card for the blockout bolts was 0.02 in. (0.5 mm) and positive for tension. This provided good blockout behavior with both the small car and pickup truck and compared well to full-scale vehicle crash test results.

Two primary modes of blockout and blockout bolt failure were shown: (1) the blockout bolt sheared and (2) the blockout bolt bent and the blockout ruptured. These failure modes are shown in Figure 28. Modeling of wood fracture in LS-DYNA is still a gross approximation, but is reasonably accurate in several applications. However, engineering judgment is still necessary when using these results.

Rather than attempt to model any wood fracture of the blockout, the blockout bolt springs were prescribed a failure deflection (FD). This provided a reasonable facsimile of the overall blockout failure and ejection of the blockout from the guardrail system. A comparison of the full-scale crash test blockouts post-test and the simulation are shown in Figure 29.



Figure 28. Blockout Bolt Failure Modes



Figure 29. Blockout and Bolt from Test No. MGSMRH-1 and Simulation

An analysis of the blockout bolt failure was done to ensure realistic rail-blockout-post release in the impact region. This blockout bolt failure criterion eventually affected the anchorage behavior. The blockout bolt displacement was parametrically studied to find a reasonable failure deflection criterion using anchorage displacements and a rail-blockout-post release comparison.

#### 4.4.3.1 Failure Deflection = 0.3

The displacement of the top center of anchor post nos. 1 and 29, of the 36-in. (914-mm) top-rail height system from an impact with the 820C vehicle using a failure deflection of 0.01 in. (0.3 mm) is shown in Figure 30. As expected, the upstream anchor displaced significantly more than the downstream anchor with a peak displacement of roughly 2.6 in. (67 mm) and 2 in. (52 mm), respectively.

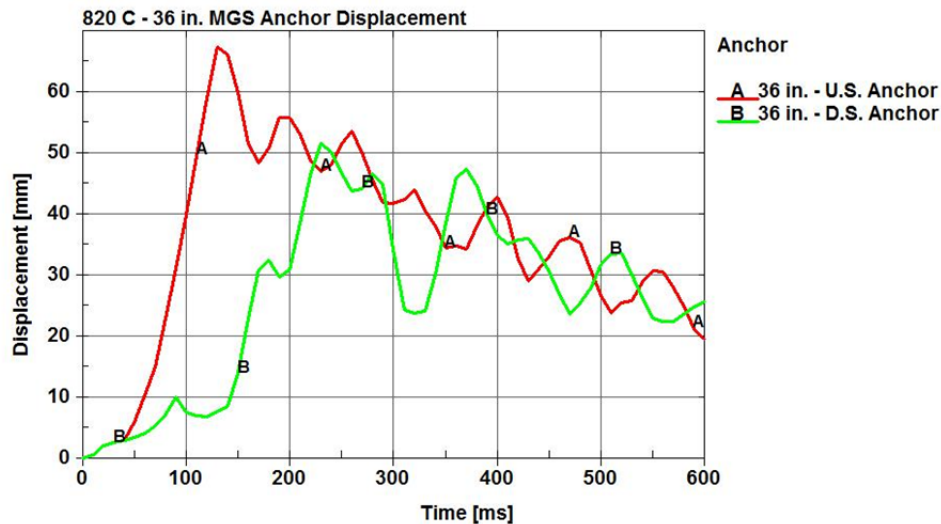


Figure 30. Anchor Displacement for 820C with FD=0.3

Initially, these anchor displacements seemed reasonable. However, as the rail height increased, an increased moment would result in slightly higher anchor deflections. However, the degree of anchor displacements shown here was similar to the anchor deflection in the simulation of the 2270P pickup truck impacting the same system. The increased loading of the larger vehicle should cause higher displacements than the small car.

#### 4.4.3.2 Failure Deflection = 0.5

Anchor displacements of the system with a failure deflection of the blockout bolt set to 0.02 in. (0.5 mm) provided lower, and seemingly much more reasonable, anchor displacements, as shown in Figure 31.

It was determined that at a failure deflection of 0.01 in. (0.3 mm) the rail detached from the posts downstream of the impact zone. This detachment caused a greater pulling force on the anchorages, accounting for the increased displacement and for the high oscillations of the displacement. This did not occur, nor is likely to occur, in full-scale vehicle crash testing.

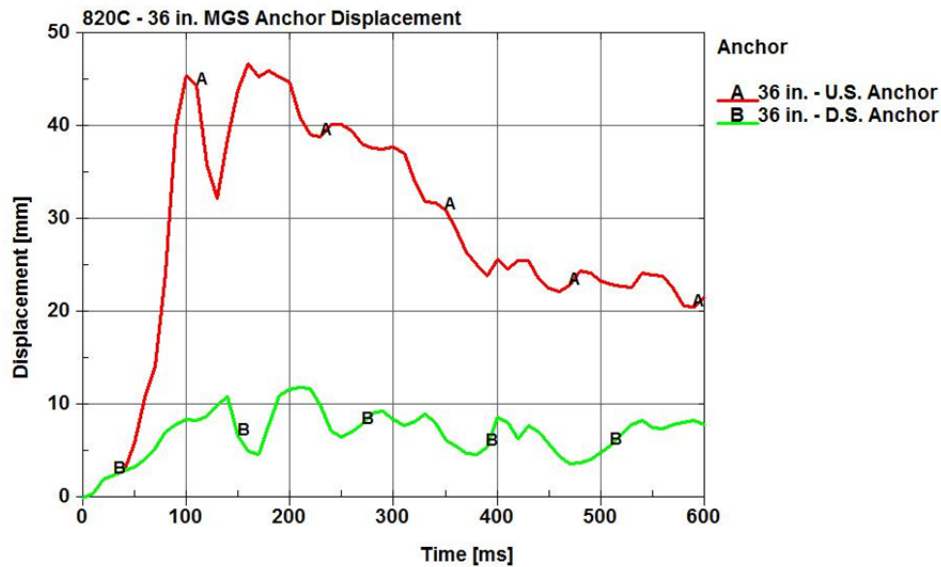


Figure 31. Anchor Displacement for 820C with FD=0.5

#### 4.4.3.3 Failure Deflection= 0.75

At a failure deflection of 0.03 in. (0.75 mm) and a top-rail height of 36 in. (914 mm) the blockouts did not disengage as desired, causing the car to snag on the blockout of a bent-over post, stopping the car and sending the car into a yaw rotation about the blockout. This again was very unlikely since the blockout should fail. The stiffer blockout bolts held the blockouts to the posts throughout the impact event, thus preventing vehicle-post interaction as observed in full-scale crash tests. While not an issue at the standard mounting height, this was a critical issue at increased W-Beam guardrail mounting heights. Higher deflections prevented blockout detachment from the posts in the desired conditions. Failure was defined to simulate blockout failures shown in physical tests from wood splitting and/or bolt failure.

### 4.4.3.4 Graphical Comparison of Failure Deflections

A failure deflection of 0.02 in. (0.5 mm) provided adequate blackout detachment without allowing the car's redirection to be influenced by snagging on the blackout. A comparison of the altered failure deflections at a top-rail height of 36 in. (914 mm) and SFS set to 0.5 is shown in Figure 32.

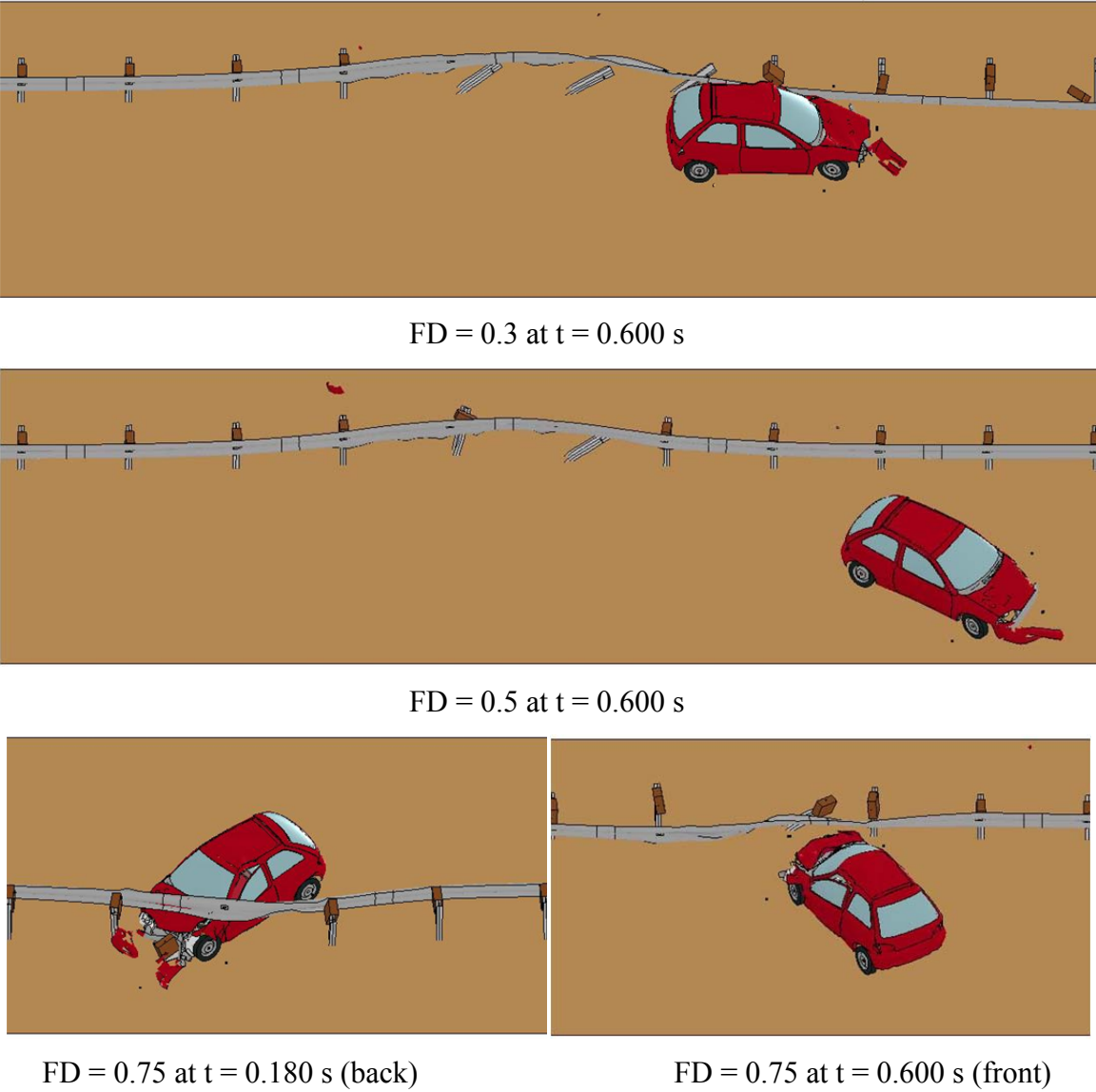


Figure 32. Blockout Bolt Failure Deflection Comparison



A failure deflection of 0.02 in. (0.5 mm) was the most reasonable, provided the best results, and most closely simulated full-scale tests. In comparison,  $FD = 0.3$  allowed the rail to detach from the blockouts downstream of impact; and  $FD = 0.75$  completely stopped the car and the rail did not detach from the post.

#### **4.5 Modeling Instabilities of 1100C (Neon) Vehicle Model**

Simulations using the 1100C (Neon) vehicle encountered significant issues with run completion and errors due to failed shell elements along the front bumper cover. The model became unstable and would error out. Additionally, when the bumper cover was taken out of the contact definition, further element failures along the fender of the vehicle would cause additional errors. The exact source of the errors in this simulation was unknown, but this model has exhibited instabilities in a variety of simulations. It is recommended that the current Toyota Yaris 1100C model being produced by NCAC be used to simulate impacts at the raised mounting heights when a usable version is available.

The simulations using the Neon model became unstable at roughly 140 ms. At this point, vehicle underride and whether or not the vehicle would satisfy test standards can be determined. The partial results were compared to the 820C simulations in Chapter 7. Furthermore, as shown in Section 7.2, the front-end geometry of the 820C Geo more closely matched that of the Kia Rio that was used in test nos. MGSMRH-1 and MGSMRH-2. For these reasons, it was determined that the Geo model was acceptable for use in examining maximum rail height and for comparing to full-scale crash tests.

#### **4.6 Summary of Parameters**

The 820C Geo models used in these studies were modified for use in roadside safety applications by researchers at the MwRSF [28]. Self-contact between the Geo Metro model parts was defined using a single-surface contact inclusive of the vehicle parts. Contact between the car

and barrier was defined using an automatic single surface contact. Additionally, the scale factor, SFS, was defined as 0.5 to prevent vehicle-barrier part penetration and subsequent simulation failure and was used to scale the SLSFAC. The SLSFAC for these models was set to 0.1; thus an SFS set to 0.5 created an overall contact scale factor of 0.05. The SOFT parameter of the contact card was set to zero. This prescribed a nodal contact penalty formulation and helped to provide the best representation of full-scale crash data. In order to provide good guardrail-blockout connection performance and behavior, a failure deflection of 0.02 in. (0.5 mm) was defined for the blockout bolt. These parameters are summarized in Table 15.

Table 15. Summary of 820C - Barrier Model

<b>Parameter</b>	<b>Input</b>
<b>Contact between Geo Metro Model Parts</b>	Single Surface
<b>Contact between Car and Barrier</b>	Automatic Single Surface
<b>SFS</b>	0.5
<b>SLSFAC</b>	0.1
<b>Overall Contact Scab Factor</b>	0.05
<b>SOFT</b>	0
<b>FD, in. (mm)</b>	0.02 (0.5)

## 5 BASELINE SIMULATION AT 32-IN. (813-MM) RAIL HEIGHT

### 5.1 Introduction

Simulations of the standard height MGS were performed to provide a basis for understanding of the 820C vehicle redirection behavior. Validation of the results was done with comparisons to the full-scale vehicle crash test no. NPG-1 [2, 12]. The MwRSF has generally tested small cars (1100C and 820C) at a nominal top-rail height of 32 in. (813 mm) to examine the potential for vehicle underride and snagging. This height is currently designated as the acceptable upper limit for the MGS system.

### 5.2 Simulation at 32-in. (813-mm) Rail Height

Test no. NPG-1 was performed June 29, 2001 with an 820C small car at a targeted impact angle of 20 degrees and speed of 62.1 mph (100 km/h). Impact was to occur 57½ in. (1461 mm) upstream from the center of the splice between post nos. 14 and 15. Complete targeted and tested criteria for test no. NPG-1 are shown in Table 16 along with the simulation parameters. These impact conditions met NCHRP Report No. 350 crash test standards [1].

Table 16. Test No. NPG-1 and Simulation Conditions

MGS at 32-in. (813-mm) Top-Rail Height	Units	Impact Conditions		
		NPG-1		LS-DYNA Simulation
		Target (without dummy)	Actual (with dummy)	
Weight	lb (kg)	1808 (820)	1956 (887)	1982 (899)
Impact Speed	mph (km/h)	62.1 (100)	63.9 (102.9)	62.1 (100)
Impact Angle	deg	20	20.0	20

Simulations were performed at this top rail height to verify and validate the model prior to examining increased rail mounting heights. Simulations were carried out using the 820C (Geo) vehicle model.

### **5.3 Comparison of Test Conditions and Simulation Results**

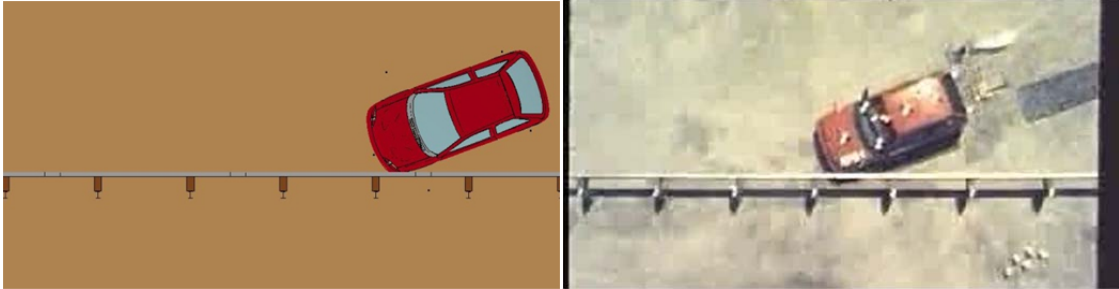
Excellent correlation between the simulation and the full-scale vehicle crash test no. NPG-1 was demonstrated, as shown in Figure 33. The visual assessment along with a numerical comparison between the simulation and the full-scale vehicle crash test provided verification for use of this model with increased rail mounting height simulations.

A complete verification of the model was carried out using the procedures for verification and validation of computer simulations used for roadside safety applications per NCHRP Report No. W179 [29]. The simulation satisfied the standardized criteria. The full verification report can be found in Appendix E.

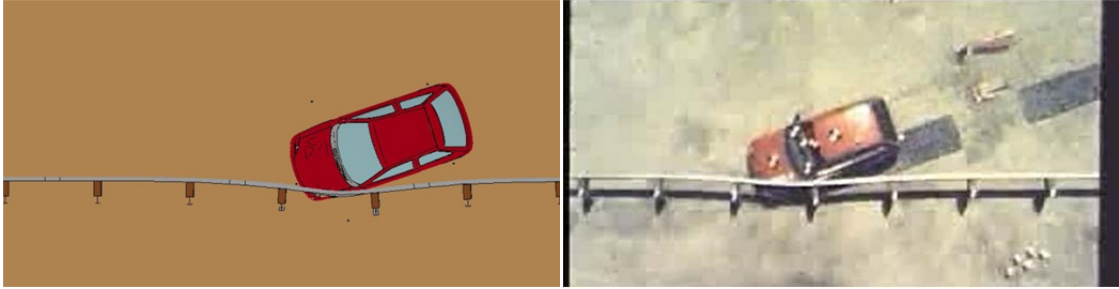
General comparisons between the simulation results and the crash test results are shown in Table 17. Maximum deflection, parallel time and parallel velocity compared very well between the simulation and the full-scale test which aided in validating the model and encouraged its use for increased heights.

#### **5.3.1 Anchor Displacement**

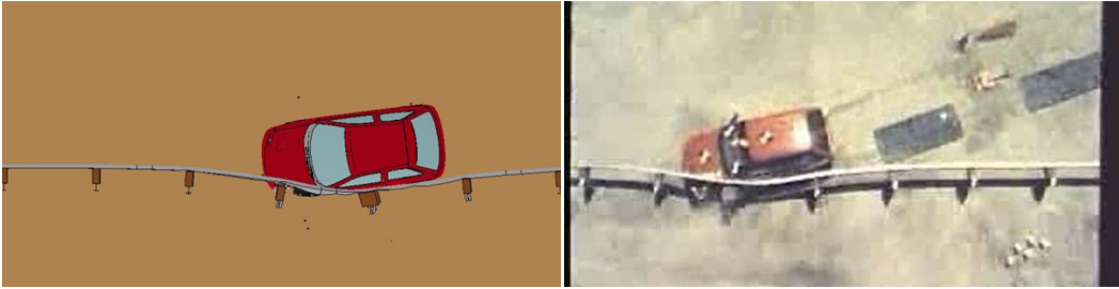
System anchor displacement was of particular interest for all vehicle impacts. While anchor movement was more pronounced with 2270P impacts, the anchor displacement involving the 820C vehicle was also examined. The simulated displacements of the top center of the anchors, post nos. 1 and 29, of the 32-in. (813-mm) system from an impact with the 820C vehicle is shown in Figure 34. As expected, the upstream anchor displaced significantly more than the downstream anchor with a peak displacement of about 1.10 in. (28 mm) and 0.51 in. (13 mm), respectively.



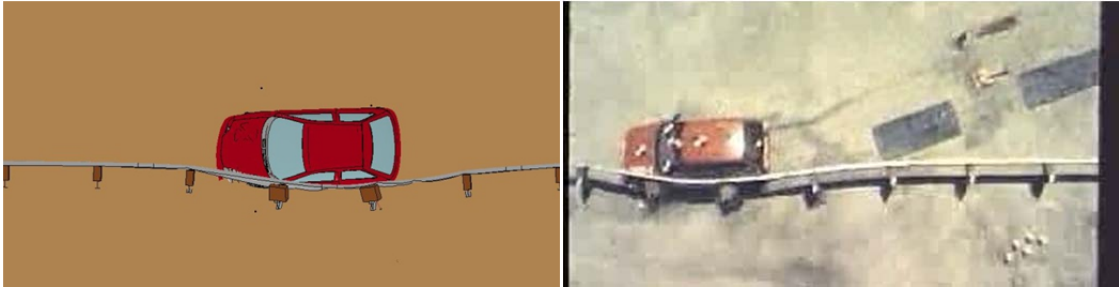
t = 0 ms



t = 60 ms



t = 160 ms



t = 200 ms

Figure 33. Sequential Figures from Simulation and Test No. NPG-1

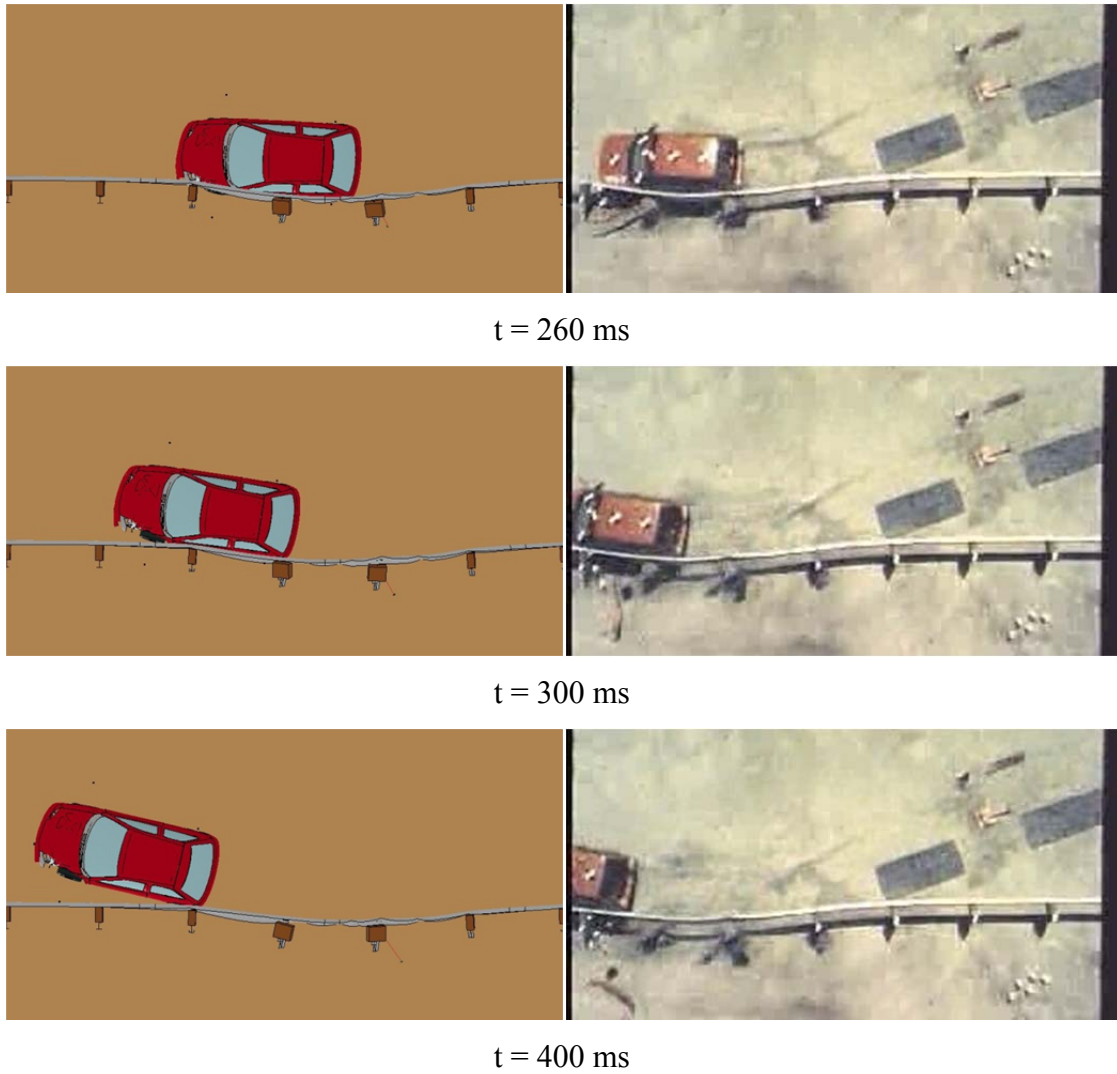


Figure 33. Sequential Figures from Simulation and Test No. NPG-1 (continued)

Table 17. Test No. NPG-1 and Simulation Results

MGS at 32 in. (813 mm) Top Rail Height	Units	Results	
		Test No. NPG-1	LS-DYNA Simulation
Max Deflection	in. (mm)	17.4 (443)	19.5 (496)
Vehicle Parallel Time	ms	201	220
Parallel Velocity	mph (km/h)	55.0 (88.5)	49.0 (78.8)

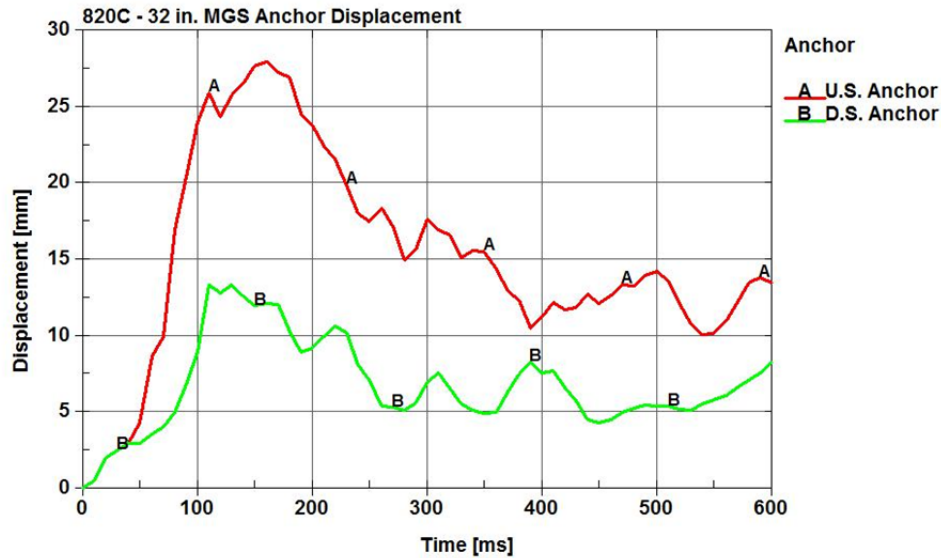


Figure 34. Anchor Displacement for 32-in. (813-mm) Top-Rail Height MGS

These anchor displacements were reasonable when compared to full-scale crash tests. While no overhead cameras were present on test no. NPG-1, some simple estimates can be made to determine a reasonable maximum displacement of the top of the anchor posts. Using a 2/3 embedment depth rotation point estimate for the upstream and downstream anchorages and soil gap measurements, an estimate can be formed from simple geometry to determine the maximum movement of the top of the anchor posts. From test no. NPG-1, there was an estimated 1/4-in. (6-mm) soil gap on the upstream and downstream anchors which would correspond to a 0.59-in. (15-mm) top-of-post displacement. This estimate corresponds well to the downstream anchorage. Although this was an estimate, it provides some validation that the anchor displacements were reasonably accurate.

### 5.3.2 Vehicle-Rail Interaction

Several parameters were examined to validate the simulation model with full-scale vehicle crash test data using test no. NPG-1 [12]. A time history of the full-scale test and the simulation is shown in Table 18.

Table 18. Event History of Test No. NPG-1 and Simulation

Event	Units	Test No. NPG-1	Simulation
Impact	ms	0	0
Post No. 14 (Post No. 12 for simulation) begins to deflect. Left front of car under rail.	ms	12	10
Post No. 15 (Post No. 13 for simulation) begins to visibly rotate back	ms	44	40
Post No. 16 (Post No. 14 for simulation) begins to visibly rotate back	ms	76	70
Car begins to roll away from rail	ms	78	74
Left front at Post No. 15 (Post No. 13 for simulation)	ms	148	90
Bumper cover begins to come off	ms	150	100
Blockout bolt on Post No. 15 (Post No. 13 for simulation) begins twisting and knocked loose from rail	ms	152	120
Maximum Dynamic Deflection Occurs	ms	131	150
Maximum Dynamic Deflection	in. (mm)	-17.4 (-442)	-19.5 (-496)
Car becomes parallel with system	ms	201	224
Parallel Velocity	mph (km/h)	47.8 (76.9)	49.0 (78.8)
Car out from under rail	ms	208	230
Left front is at Post No. 16 (Post No. 14 for simulation)	ms	236	175
Left front is at Post No. 17 (Post No. 15 for simulation)	ms	252	250
Car exits system	ms	450	410
Maximum Deflection at Exit	in. (mm)	-9.9 (-251)	-10.6 (-268)

The simulation showed that the vehicle did not reach parallel with the system as quickly as observed in the full-scale crash test. This difference was possibly due to the bumper cover failing sooner and subsequently allowing the car to pass behind and remain under the rail longer. This behavior kept the vehicle yawing into the system and increased the parallel time. Additionally, the exit time of the vehicle was 40 ms less in the simulation than in the full-scale test. Thus, some shifting and shortening of the series of events occurred.



### 5.3.3 Energy Balance

The energy balance analysis provided an indication of the energy distribution in the system. This energy balance will vary depending upon the barrier configuration, member properties, and time within a given impact simulation. The energy balance data of the 820C vehicle simulation at a 32-in. (813-mm) top-rail height is shown in Figure 35. The various energies will be described in Section 6.5.7.

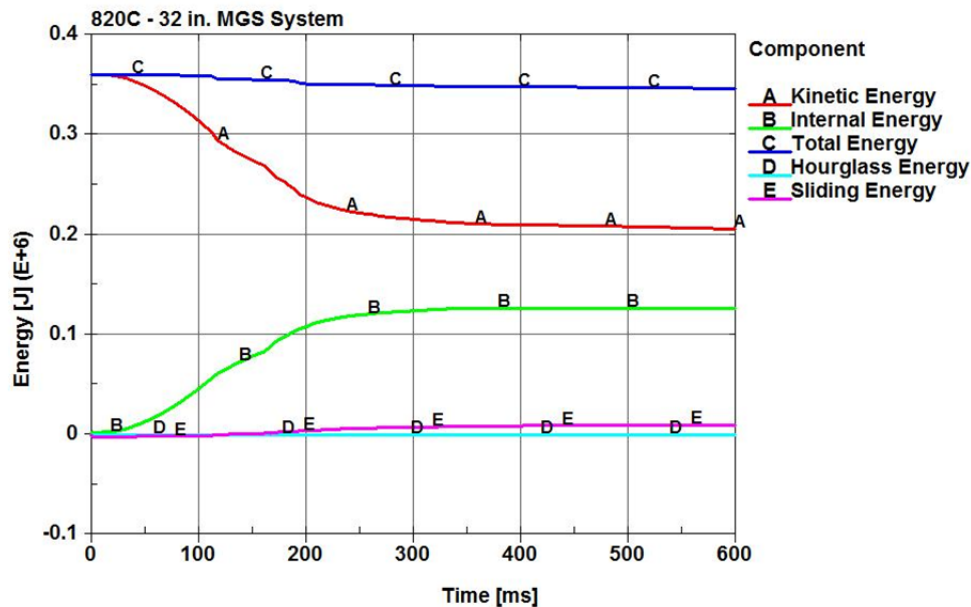


Figure 35. Energy Balance of 820C Vehicle Simulation

### 5.4 Discussion

The graphical assessment with overhead images from the full-scale vehicle crash test, along with a numerical comparison, provided verification for use of this model with increased rail mounting height simulations. Overall, it was shown that the finite element model was reasonably well verified by the procedures set forth in NCHRP Report No. W179 [29]. The visual validation and verification provided confidence that the barrier model was capable of accurately predicting the ability of increased rail-height MGS systems to safely redirect vehicles.

## **6 MAXIMUM SAFE GUARDRAIL HEIGHT EVALUATION WITH LS-DYNA**

### **6.1 Introduction**

Two relevant full-scale vehicle crash tests have been performed at increased rail mounting heights. In 2011, the MwRSF published a report that examined maximum height parameters for the MGS [9]. Two tests were performed on 175-ft (53.3-m) long systems with an 1100C small car at top-rail mounting heights above a 32-in. (813-mm) nominal mounting height. Test no. MGSMRH-1 was performed on the MGS with a 34-in. (864-mm) nominal top-rail mounting height, and test no. MGSMRH-2 had a 36-in. (914-mm) nominal top-rail mounting height. Both tests passed according to MASH standards. An LS-DYNA simulation study was undertaken to determine how much farther the MGS rail height could be safely raised. First, simulations were run to validate the vehicle-to-barrier interactions. Then, interpolation of the top-rail height was undertaken to determine the minimum safe guardrail mounting height.

### **6.2 Simulation at 34-in. (864-mm) Rail Height**

A top-rail mounting height of 34 in. (864 mm) was used to examine underride and redirection effectiveness with an 820C vehicle. An increased impact angle from 20 degrees to 25 degrees was made to account for the increased impact severity from the NCHRP Report No. 350 standards to that of MASH standards. Though there was no designation for an 820C vehicle in MASH, this made the simulation analysis slightly more comparable to test no. MGSMRH-1. The front-end geometry of the 820C vehicle more closely matched that of the Kia Rio used in the full-scale test with the MGS at a 34-in. (864-mm) nominal top-rail height. Primarily, the cowl height of the 820C (Geo) small car model more closely matched that of the crash-tested vehicle. However, the flatter hood of the Neon model was shown to underride the guardrail system, whereas the Kia Rio did not when tested at the same rail heights.

Sequential images of the 820C impacting the MGS system with a 34-in. (864-mm) nominal top-rail height are compared to test no. MGSMRH-1 in Figures 36 and 37. Note that the simulation images have been mirrored for better comparison with the full-scale test. Good correlation was shown in the reaction of the front of the vehicle as it impacted the rail. Slightly more penetration occurred in the full-scale vehicle crash test due to the increased mass of the larger vehicle. The resulting load caused the posts in the impact zone to bend to the ground, and for the vehicle to exit later in the full-scale test than was shown in the simulation.

As mentioned, front-end geometry was a primary area of concern and in this case was shown to be a contributor to how the vehicle reacted to the increased rail height. As the front, impacting corner of the vehicle pushed into the lower corrugation of the W-beam, the rail detached from the blockouts. As this occurred, the rail pushed up and back. The front corner of the vehicle remained in the W-beam valley as the rail was pushed up and back causing the vehicle to roll away from the system. The valley of the W-beam rode along the hood-line of the vehicle and caught at the lower portion of the A-pillar. As the W-beam valley rode along the hood-line, the rail did not ride farther up the A-pillar or intrude into the occupant compartment. In a certain range, based on the hood and front-end geometry, the guardrail valley will fold around the hood corner up to the cowl line, causing the car to roll back. If the guardrail was mounted too high in comparison to the cowl height and outside of this range, the front of the car will underide the barrier instead of redirect away from it.

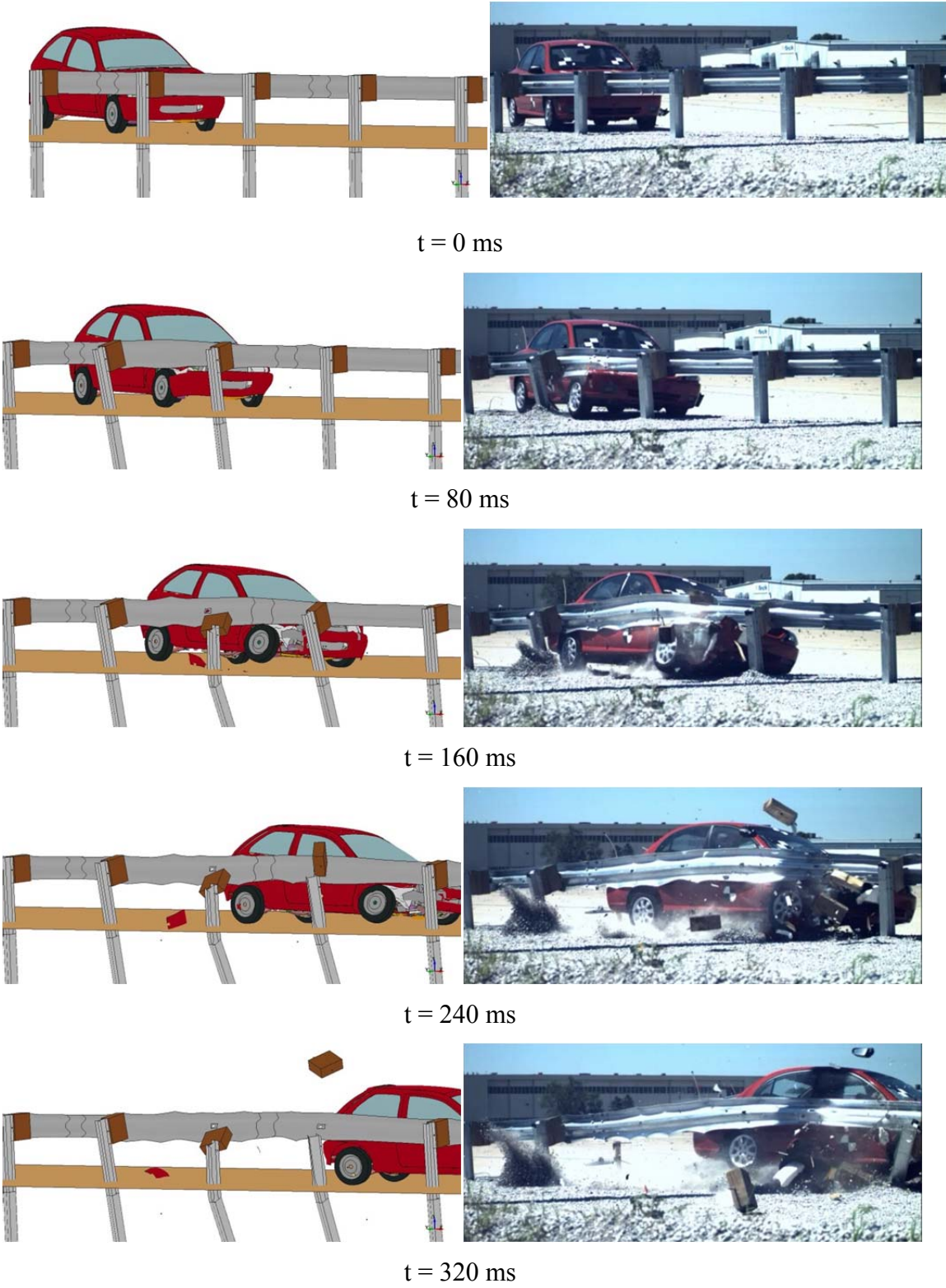


Figure 36. Backside Sequential Figures from Simulation and Test No. MGSMRH-1

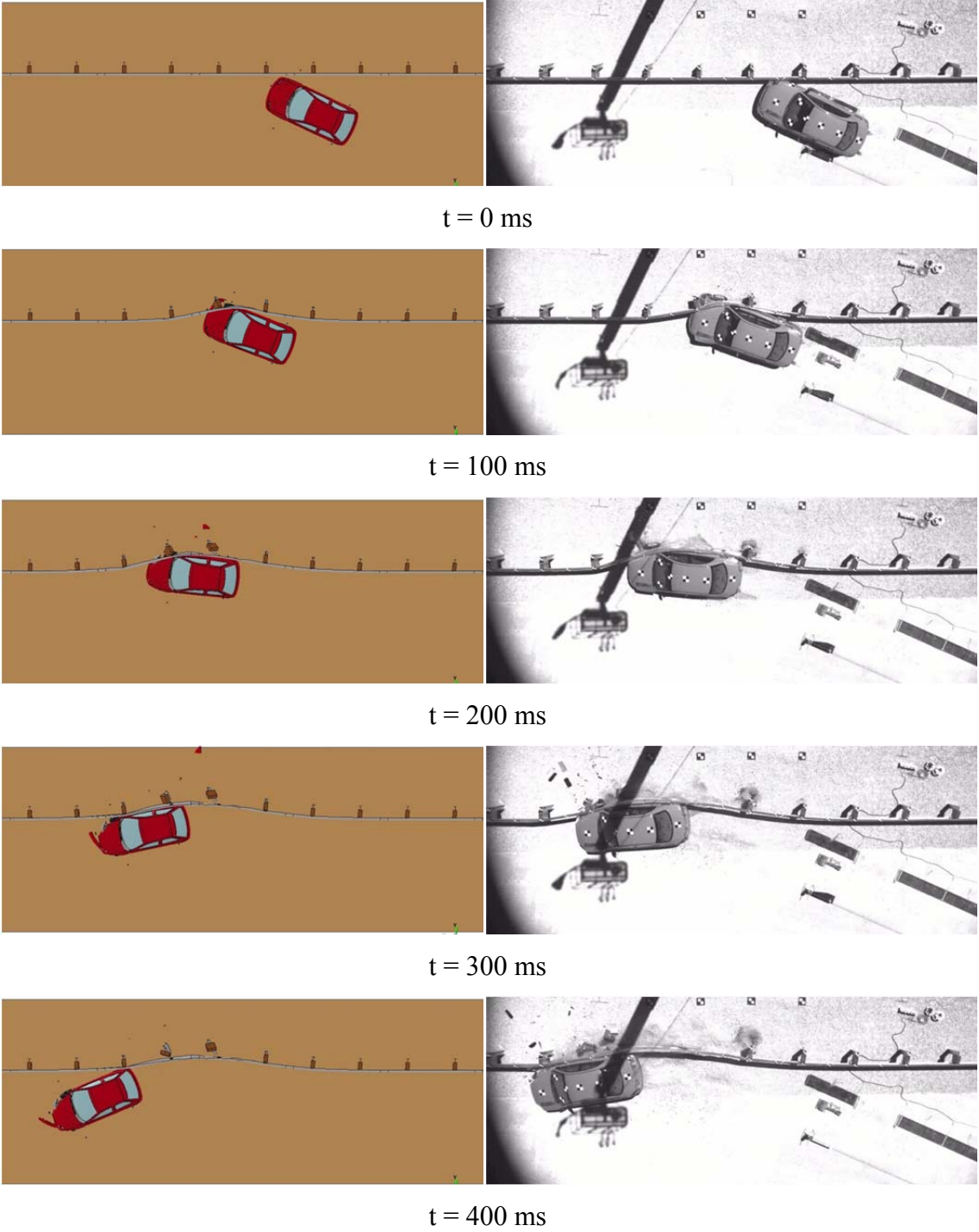


Figure 37. Overhead Sequential Figures from Simulation and Test No. MGSMRH-1

### **6.3 Simulation at 36-in. (914-mm) Rail Height**

A simulation at a 36-in. (914-mm) top-rail mounting height was performed with an 820C vehicle. The increased rail height was used to further examine its effects on vehicle redirection and safety. The results of this simulation were compared to full-scale vehicle crash test no. MGSMRH-2. The impact speed and angle were 62.1 mph (100 km/h) and 25 degrees. Time sequential images of the impact are shown in Figures 38 and 39. Again, the similarity of the front-end geometry of the Geo Metro vehicle and the Kia Rio used in test no. MGSMRH-2 made the simulation and test results comparable.

Much like the 34-in. (864-mm) top-rail height simulation, good correlation was shown in how the vehicle pushed the rail up and back, thus causing the car to roll away from the barrier. This caused the rail to slide along the hood corner up to the cowl line and smoothly redirect the vehicle.

### **6.4 Simulation at 37-in. (940-mm) Rail Height**

Again, using an 820C vehicle, a simulation was run at a 37-in. (940-mm) nominal top-rail height to examine underride and guardrail redirection effectiveness. The impact speed and angle were 62.1 mph (100 km/h) and 25 degrees. Time sequential images of the small car impacting the 37-in. (940-mm) top-rail height system are shown in Figure 40. Severe underride of the system occurred at this mounting height, and failure to redirect the vehicle was obvious. The 820C vehicle passed under the barrier causing the rail to deform the A-pillar and intrude into the occupant compartment, creating clear occupant risk and ultimately a test failure at this height. No further analysis was necessary, and this height was deemed to be over the rail height performance limit for the MGS on flat terrain.

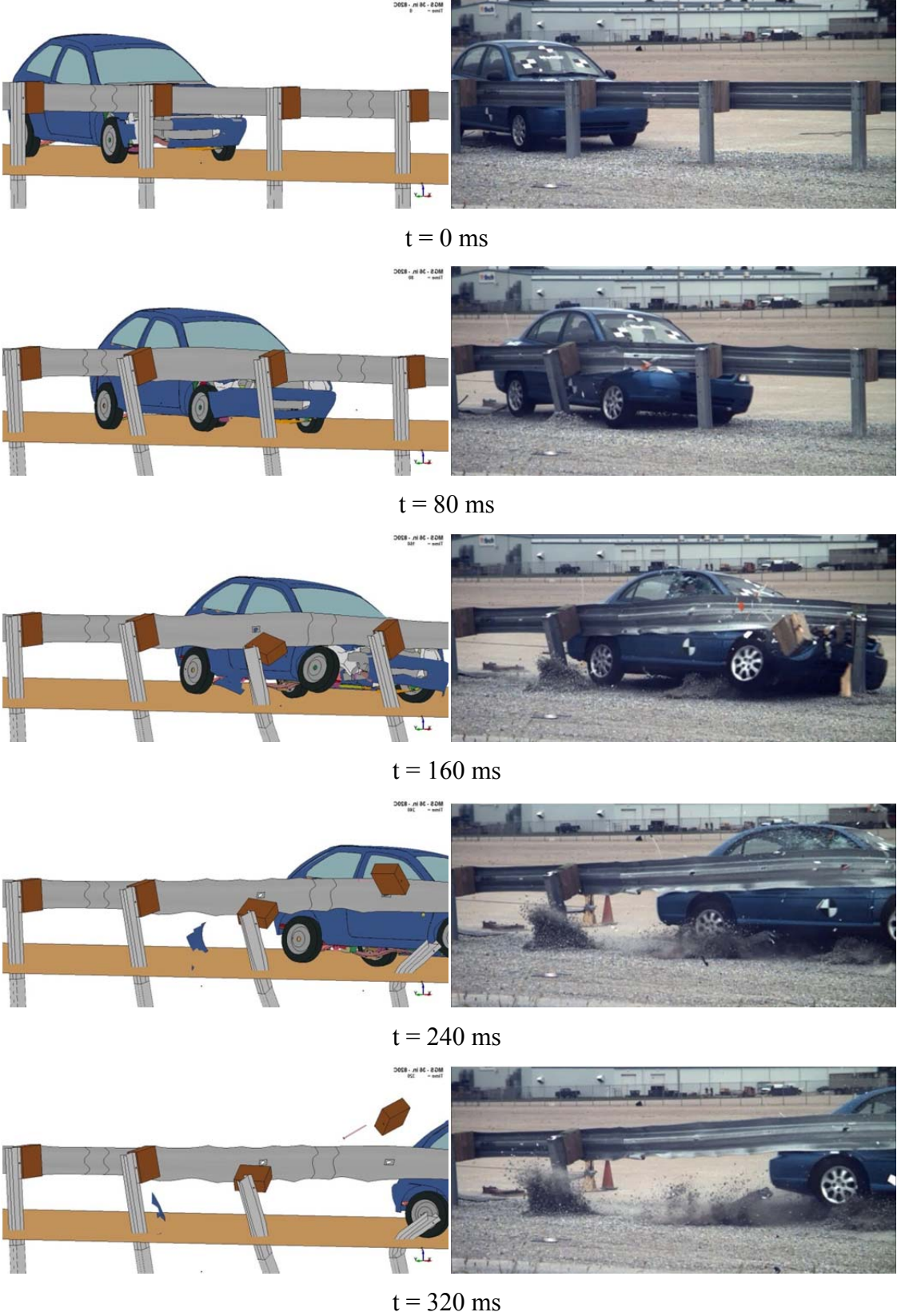


Figure 38. Back Side Sequential Figures from Simulation and Test No. MGSMRH-2

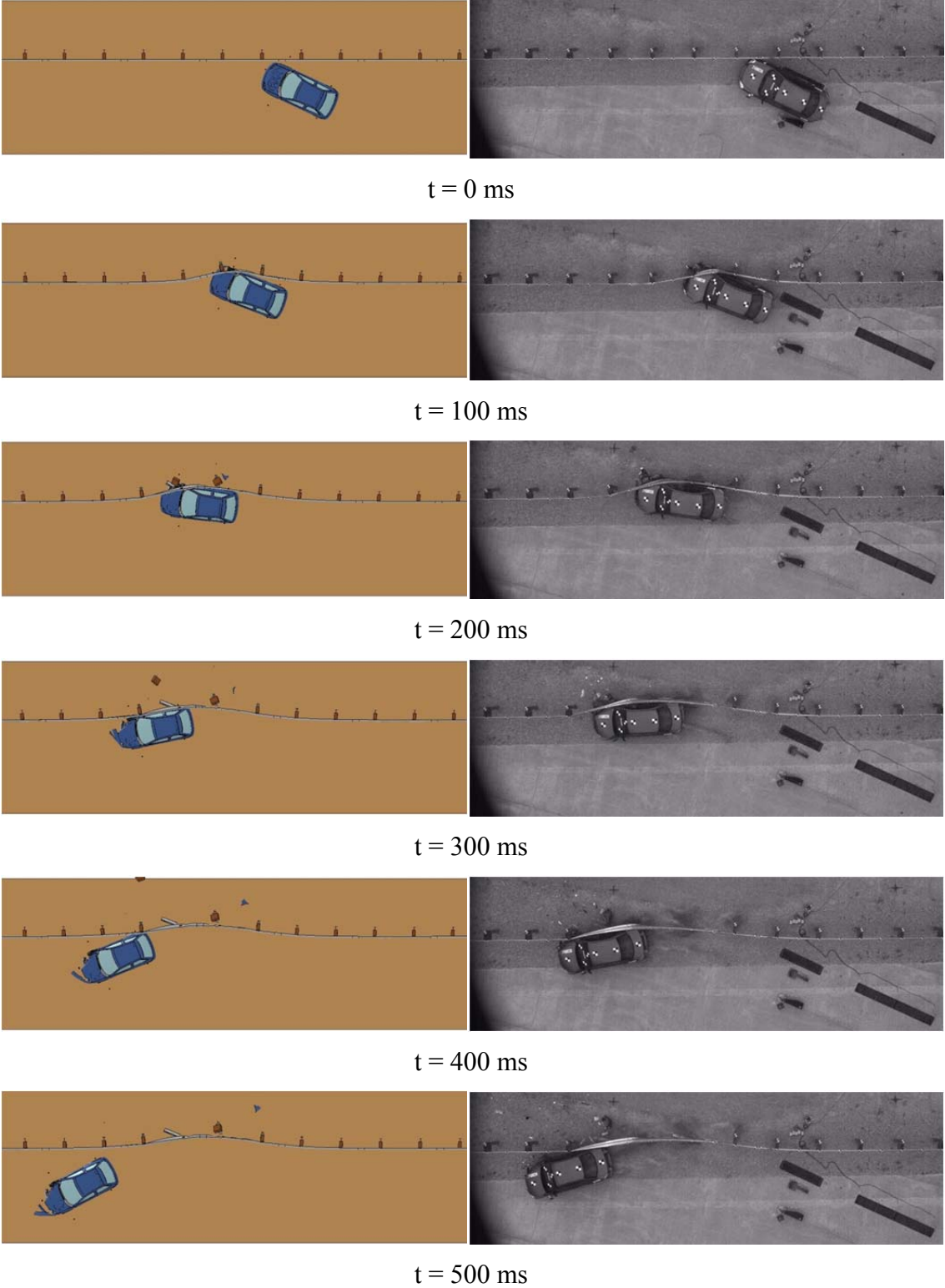
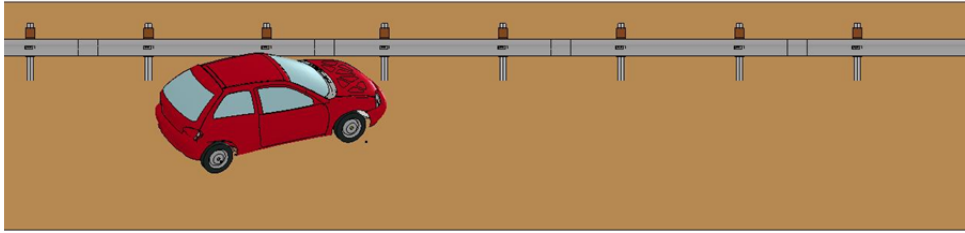
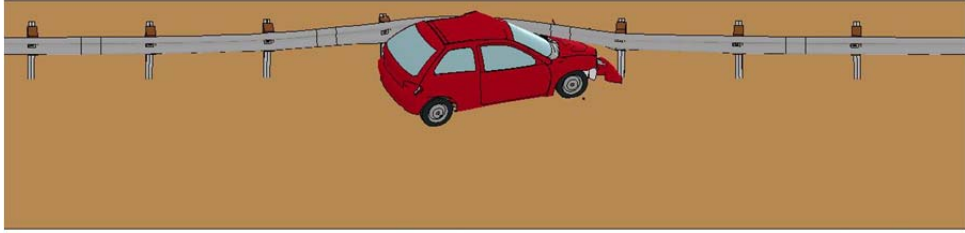


Figure 39. Overhead Sequential Figures from Simulation and Test No. MGSMRH-2

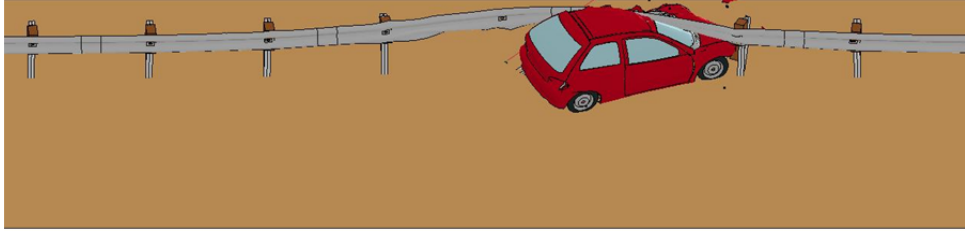




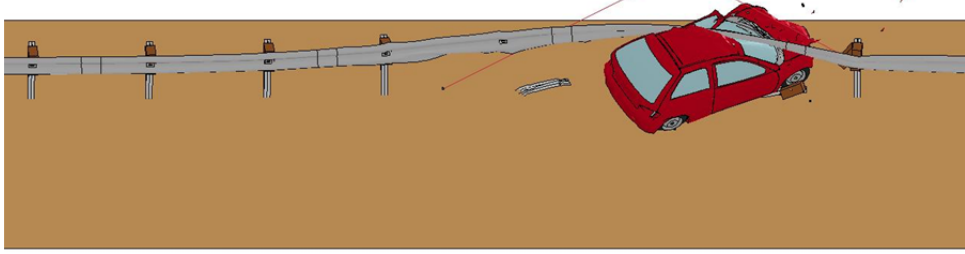
t = 0 ms



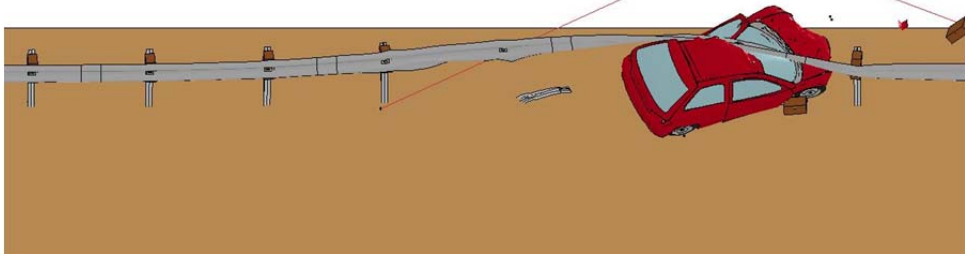
t = 150 ms



t = 300 ms



t = 450 ms



t = 600 ms

Figure 40. Sequential Figures from 37-in. (940-mm) Top-Rail Height Simulation

## **6.5 Comparison of Test Conditions and Simulation Results**

The simulations with the 820C vehicle at varying top-rail mounting heights were compared to understand and analyze the differences in a variety of parameters, as shown in Table 19. The 32-in. (813-mm) top-rail height simulation compared very well to test no. NPG-1 in all available parameters.

The underride distance was found by measuring the deepest penetration of the front impact corner of the vehicle and the maximum rail deflection. The rail deflection was subtracted from the vehicle corner penetration distance to yield an underride distance for comparison in this study. Consequently, the working width of the system increased due to the increased propensity for underride at increased heights.

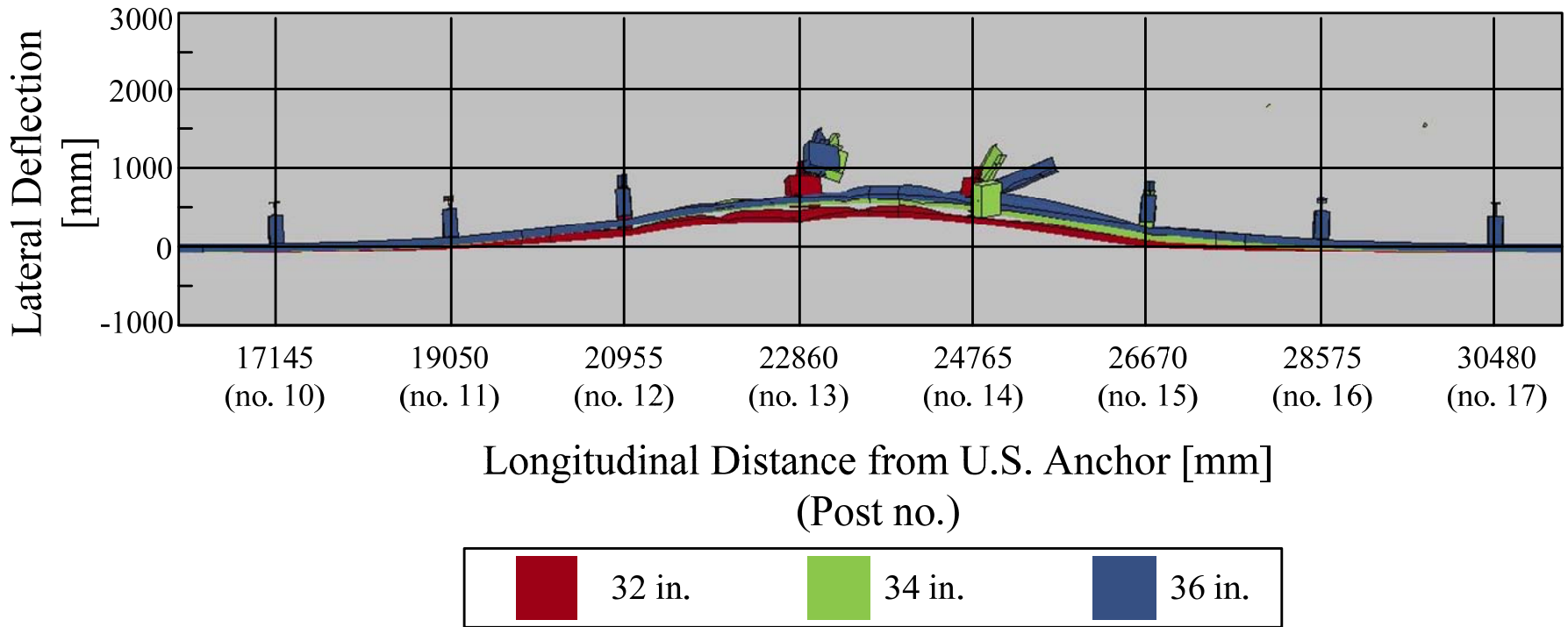
### **6.5.1 Rail Deflection Analysis**

A comparison of test nos. MGSMRH-1 and MGSMRH-2 was necessary based on the geometric similarities of the as-tested and simulated vehicle front-ends. An anomaly was shown in test no. MGSMRH-2: the increased rail height resulted in lower dynamic rail deflection and a decreased working width. The cause of this decreased rail deflection was unclear. The simulations showed that an increased propensity for underride exhibited by the higher rail was accompanied by greater rail deflection, as shown in Figure 41. It would be expected that full-scale vehicle crash tests would exhibit the same characteristics.

Table 19. Test and Simulation Conditions and Results Comparison

Evaluation Parameters	Units	Physical Test Conditions and Results			Simulation Conditions and Results			
		Test No. NPG-1	Test No. MGSMRH -1	Test No. MGSMRH -2	32-in. Simulation	34-in. Simulation	36-in. Simulation	37-in. Simulation
<b>Top Rail Height</b>	in. (mm)	32 (813)	34 (864)	36 (914)	32 (813)	34 (864)	36 (914)	37 (940)
<b>Tested Vehicle Mass</b>	lb (kg)	1956 (887)	2599 (1179)	2584 (1172)	1982 (899)	1982 (899)	1982 (899)	1982 (899)
<b>Impact Velocity</b>	mph (km/h)	63.9 (102.9)	60.8 (97.8)	62.1 (99.9)	62.1 (100)	62.1 (100)	62.1 (100)	62.1 (100)
<b>Tested Impact Angle</b>	deg	18.7	24.97	25.6	20	25	25	25
<b>Parallel Time</b>	ms	201	230	262	224	234	237	n/a
<b>Parallel Velocity</b>	mph (km/h)	47.8 (76.9)	43.7 (70.4)	41.1 (66.1)	49.0 (78.8)	46.1 (74.2)	46.3 (74.5)	n/a
<b>Dynamic Rail Deflection</b>	in. (mm)	-17.4 (-442)	-29.0 (-737)	-23.5 (-597)	-19.5 (-496)	-29.7 (-755)	-31.5 (-800)	-28.5 (-723)
<b>Working Width</b>	in. (mm)	40.3 (1023)	49.4 (1255)	40.5 (1029)	43.1 (1095)	50.8 (1290)	52.5 (1334)	73.7 (1872)
<b>Working Width Indicator</b>	-	Post	Hood Corner	Hood Corner	Post	Post	Post	Hood Corner
<b>Exit Time</b>	ms	450	518	562	410	410	430	n/a
<b>Resultant Velocity at Exit</b>	mph (km/h)	-	39.3 (63.2)	36.2 (58.3)	47.2 (75.9)	45.6 (73.4)	45.7 (73.5)	n/a
<b>Exit Angle</b>	deg	-10.3	-12.34	-21.85	-14.5	-22.9	-23.7	n/a
<b>Max Roll</b>	deg	-2.69	-11.4	-11.1	-2.5	5.56	7.16	n/a
<b>Max Pitch</b>	deg	0.6	-	-	1.0	2.64	4.69	n/a
<b>Underride Distance</b>	in. (mm)	-	-	-	10.4 (263)	12.0 (304)	11.6 (295)	45.2 (1149)
<b>Pass/Fail</b>	-	Pass	Pass	Pass	Pass	Pass	Pass	Fail

### Rail Deflection Comparison at 600 ms



85

Figure 41. Simulated Rail Deflection Comparison at 600 ms for 820C Vehicle Impact

### 6.5.2 Lateral Velocity

The lateral and velocities were compared for the 820C vehicle impact at various rail heights. These plots provided a good basis for understanding the reaction of the vehicle throughout the impact. In general, as the impact angle was increased from 20 degrees, the 32-in. (813-mm) system, to 25 degrees, the 34- and 36-in. (864- and 914-mm) systems, the lateral velocity increased. The lateral velocity versus time for the increased rail height systems followed a very similar trend for each rail height, as shown in Figure 42.

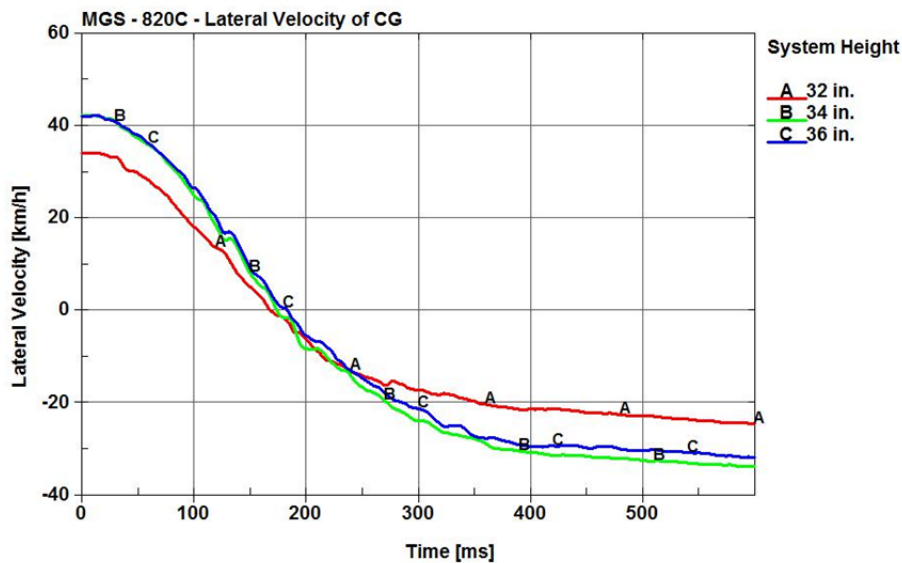


Figure 42. Comparison of Lateral CG Velocity of 820C Vehicle

### 6.5.3 Longitudinal Velocity

The increased impact angle resulted in lower longitudinal velocities throughout impact. However, the deceleration rate was slightly higher throughout impact causing more deceleration of the vehicle in the longitudinal direction. The longitudinal CG velocity versus time for all systems was consistent throughout impact, as shown in Figure 43.

Impacts into the 34- and 36-in. (864- and 914-mm) rail height systems followed similar trends due to the similar propensity for underride and wheel snag. The vehicle exhibited a similar

reaction at both heights with slightly more underride at a 36-in. (914-mm) top-rail height. As a result, the velocity throughout impact was similar for both the 34- and 36-in. (864- and 914-mm) top-rail heights, as shown in Figure 44.

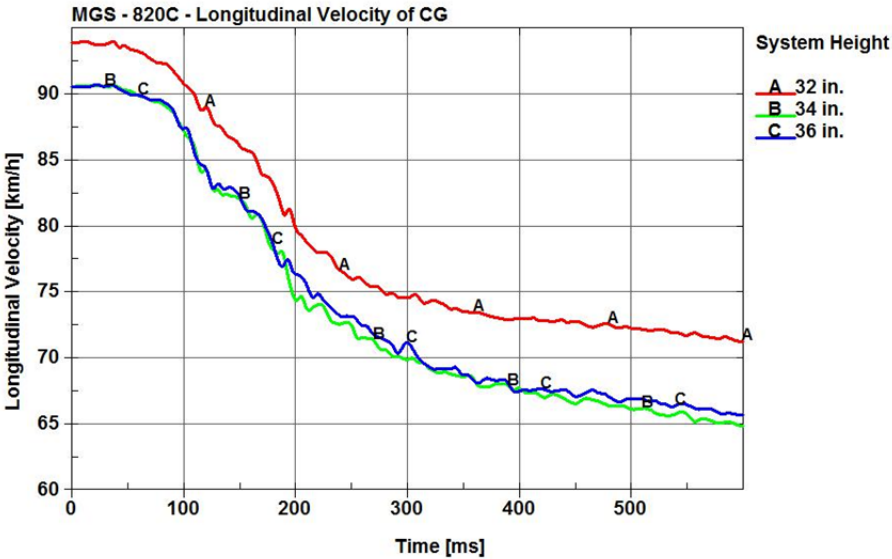


Figure 43. Comparison of Longitudinal CG Velocity of 820C Vehicle

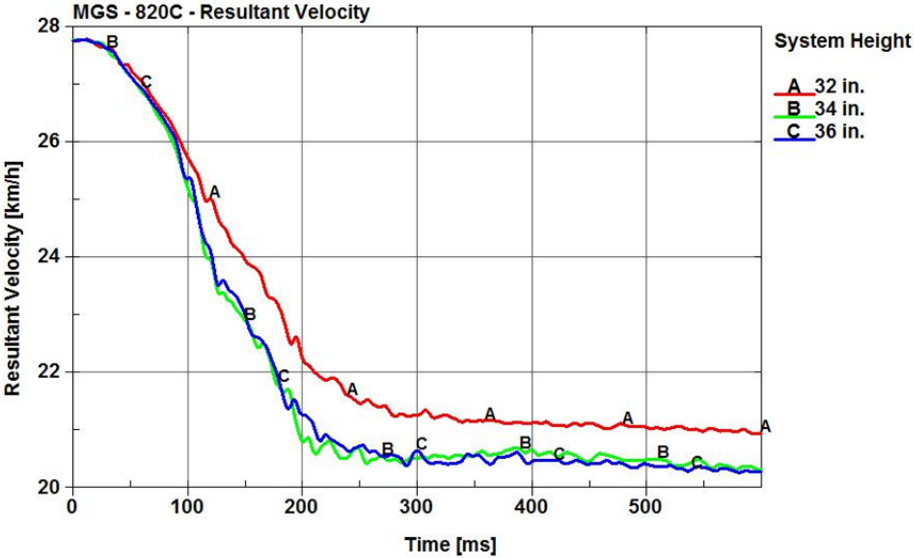


Figure 44. Comparison of Resultant CG Velocity of 820C

### 6.5.4 Yaw

Yaw rotation of the vehicle throughout impact gave further insight into the behavior of the vehicle and was a useful comparison tool, as shown in Figure 45. These angles were in relation to the barrier. Therefore, the vehicle started at a 20-degree impact angle for the 32-in. (813-mm) top-rail height simulation, and a 25-degree impact angle for the 34- and 36-in. (864- and 914-mm) top-rail height impacts. Again, the reactions of the vehicle from impact with the 34- and 36-in. (864- and 914-mm) top-rail height systems were very similar.

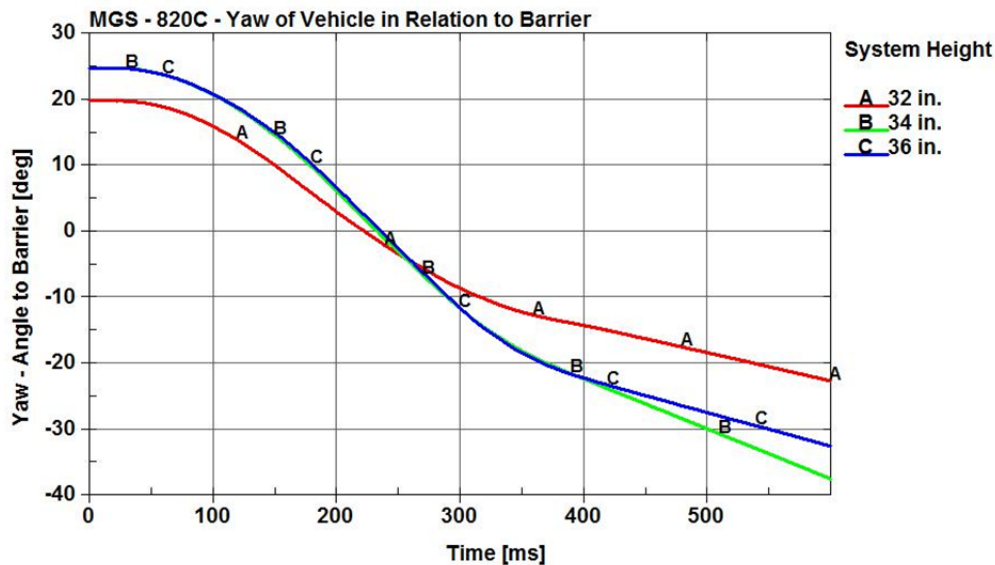


Figure 45. Yaw of 820C in Relation to Rail

### 6.5.5 Roll

One area that did differ between the simulations was the pitch and roll behavior of the cars. The roll of the vehicle increased according to the system height. At increased heights, the barrier caught the corner of the impacting hood of the vehicle, and as the rail deformed, the vehicle essentially rolled away from the barrier. Upon exit, the car rolled back to normal, overshot 0 degrees of roll, and rolled in the direction of the barrier. The deformed front-end of

the vehicle caused the vehicle to sit slightly askew of flat, at roughly a -2 degree roll angle, as shown in Figure 46.

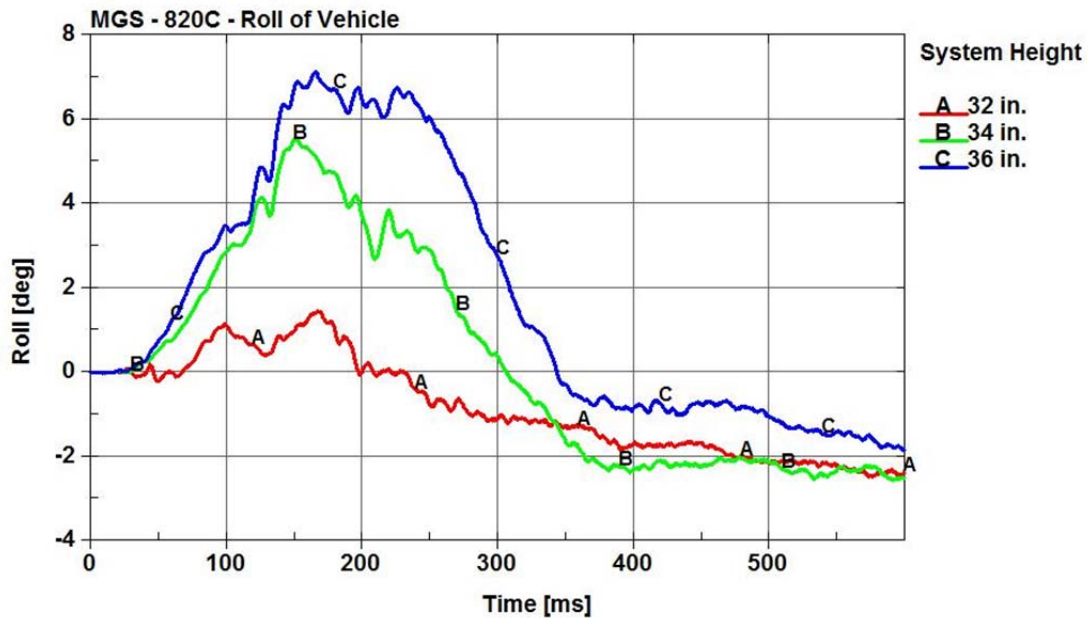


Figure 46. Roll of 820C

### 6.5.6 Pitch

As the car was redirecting, increased vehicle pitch occurred at increased rail heights, as shown in Figure 47. The increased roll angle showed that the redirection of the car was dependent on the deformation characteristics of the guardrail and its ability to essentially "bank" the car and redirect the vehicle away from the hazard. While this "banking" effect was a desirable characteristic that allowed for the use of increased rail height, it provided complications with vehicles of varying front-end geometries. A car with low hood height, such as that of sports cars, may likely allow unacceptable barrier underride. Higher car hood heights, such as those of crossovers and minivans, will easily redirect at the increased rail heights. A limit for every car exists at which point the guardrail is capable of causing this "banking" effect to redirect the vehicle.



A clearer picture of the vehicle redirection behavior at increased rail heights can now be developed. As the vehicle impacted the barrier, the following was shown to occur: (1) the front impacting corner of the vehicle crushed into the rail up to the cowl line of the car before the vehicle began to redirect; (2) the rail folded over the fender and hood up to the cowl, and the bottom of the rail rotated back and up; (3) the rotation of the rail forced the front-end of the car to roll away from the barrier and pulled the front impacting wheel off the ground, increasing pitch; and (4) once the lateral CG velocity reached zero and the car began to exit the system, the car slowly returned to level trajectory. Maximum roll occurred at roughly 170 ms across all simulations. This approximate time of maximum roll was shown from the front in Figure 48.

It should be noted, however, that the absolute value of both roll and pitch angles were all relatively small and posed no significant concern to overall vehicle behavior.

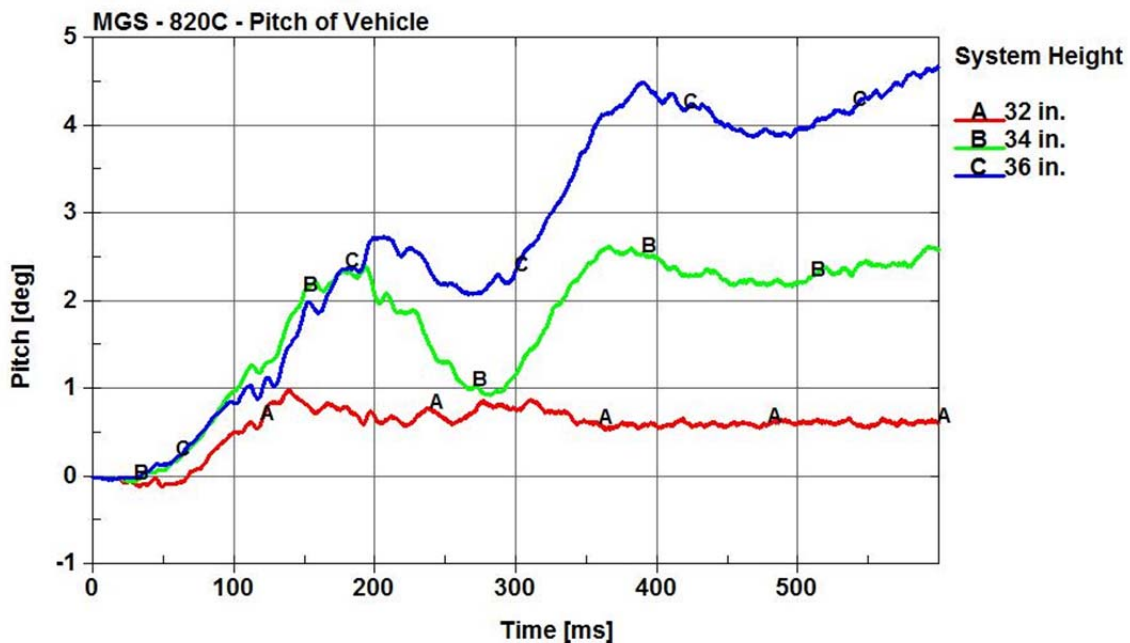
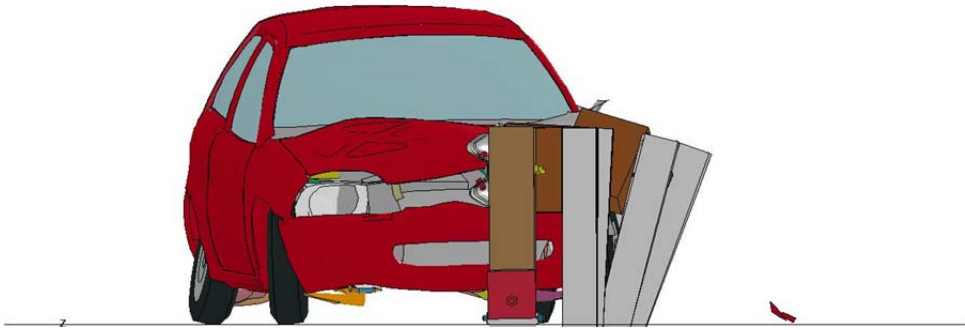
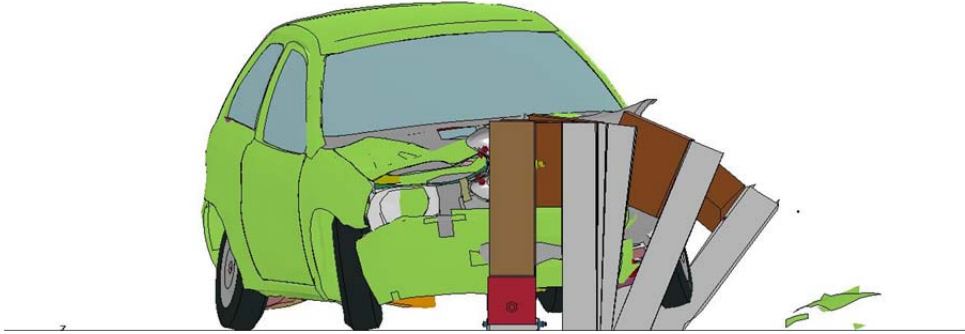


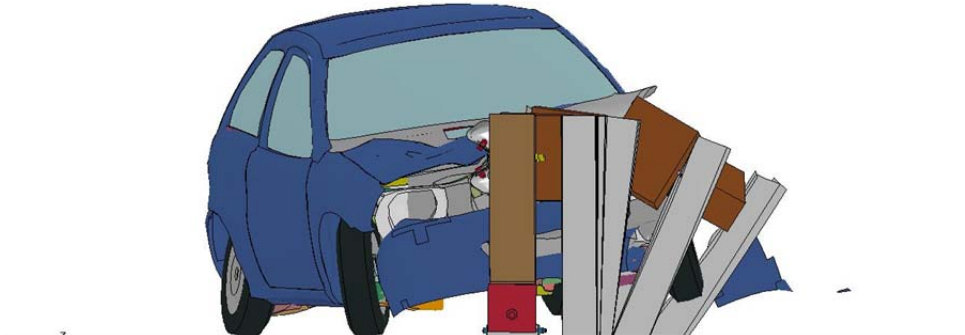
Figure 47. Pitch of 820C



32 in. (813 mm)



34 in. (864 mm)



36 in. (914 mm)

Figure 48. Roll Behavior of 820C Vehicle

### 6.5.7 Energy Balance

The energy balance analysis provided an indication of the energy distribution in the system. The energies examined included:

- *Kinetic Energy*: energy due to motion;
- *Internal Energy*: energy needed to create the system including kinetic and potential energy;
- *Total Energy*: sum of energy in all forms in the system;
- *Hourglass Energy*: nonphysical, zero-energy modes of deformation that produced zero strain and no stress which occurred in under-integrated solid, shell, and thick shell elements [26]; and
- *Sliding Energy*: sum of slave, master, and frictional contact energy [26].

This energy balance varied depending on the barrier configuration, member properties, and time within a given impact simulation. The energy distribution was fairly consistent across simulation runs, as shown in Figure 49. The 32-in. (813-mm) top-rail height simulation showed a slightly lower internal energy peak and a slightly higher kinetic energy valley due to the decreased impact angle.

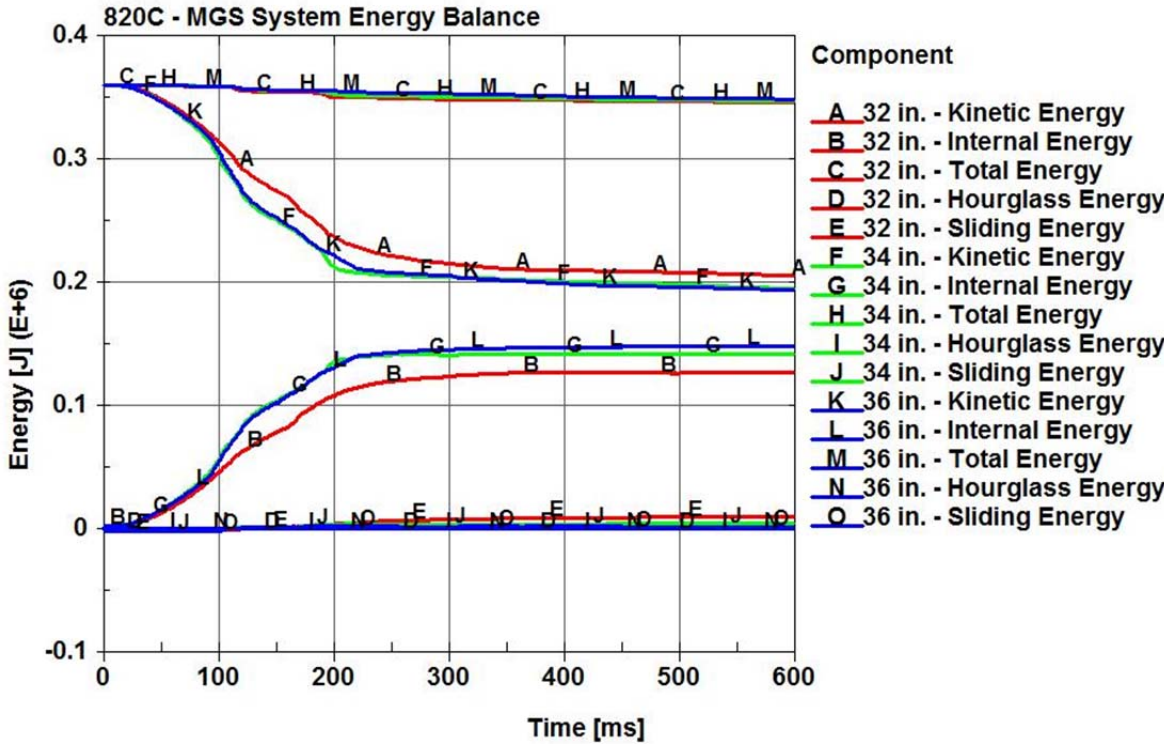


Figure 49. Energy Balance of 820C Vehicle Simulations

**6.6 Discussion**

Post snagging of the small car had previously been considered an issue as they underrode a system. These simulations showed that as the rail height was increased, a corresponding increase in underride did not occur. Rather, as the rail height was increased, to a certain degree, the car pitched up into the rail and rolled away from the system, thus preventing underride. The disconnection of the rail away from the blockouts as the vehicle came in contact with the lower corrugation of the W-beam caused the bottom of the rail to push up and out. This action rotated the W-beam. As it rotated, the corner of the vehicle hood counteracted this rotation by rolling away from the system. For the 820C vehicle model, the maximum safe guardrail mounting height was 36 in. (914 mm). The extent to which the guardrail can be raised and still show safe redirection of the vehicle was dependent on the front-end geometry of the vehicle. Furthermore, where post snagging occurred, no adverse behavior of the vehicle was observed.

## 7 ANALYSIS OF GEOMETRY AND RAIL HEIGHT EFFECTS

### 7.1 Vehicle-to-Rail Geometry Effects

As the rail height was increased, the relationship between the bumper height of the test vehicles and the rail changed, as shown in Figure 50. At a 32-in. (813-mm) top-rail mounting height, the windshield cowl of both the 820C and 1100C vehicles were above the top of the rail. As the height was increased to 34 in. (864 mm), the 820C model cowl was slightly above the top of the rail, whereas the 1100C model cowl was slightly below. At a 36-in. (914-mm) top-rail height, the front corner of the 820C model was higher than the bottom corrugation of the W-beam, whereas the corner of the 1100C model was slightly below.

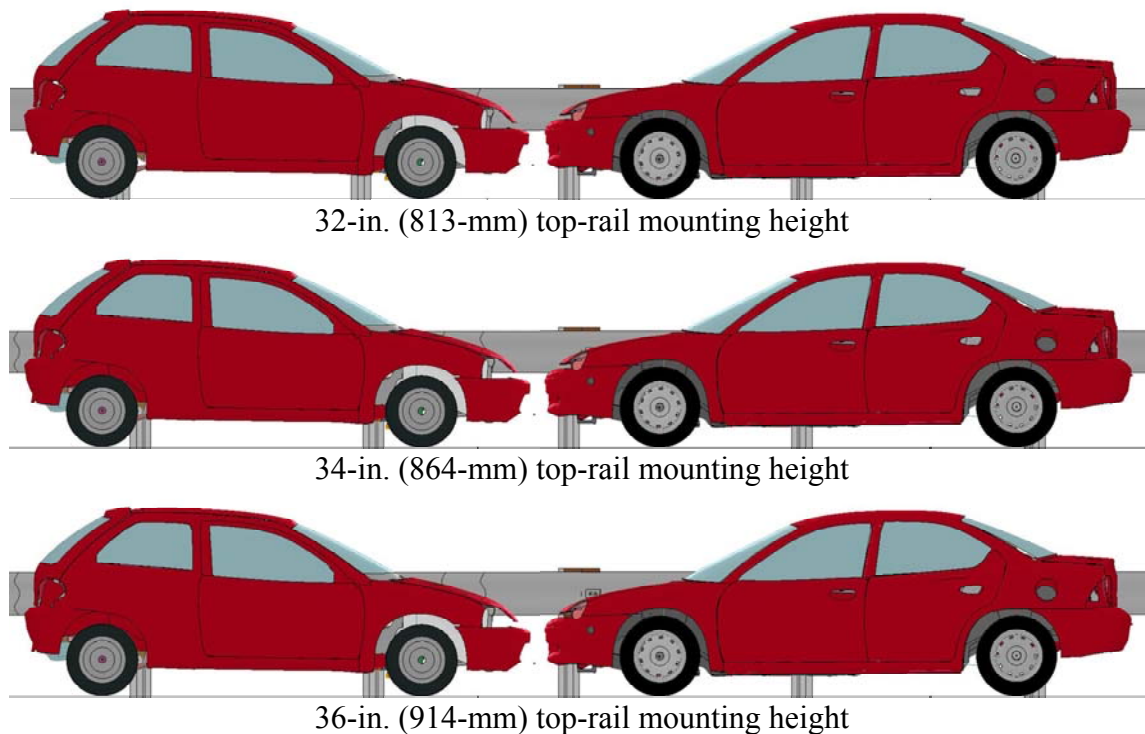


Figure 50. Vehicle-to-Rail Geometry - 820C and 1100C Profiles

The differing cowl heights had the potential to affect the success and failure of a simulation and full-scale crash test. The ability of the W-beam guardrail to contain the small car

relied on two factors: (1) the bottom W-beam corrugation had to be lower than the fender corner so as not to allow for severe underride and (2) the top W-beam corrugation had to be lower than the cowl so as not to cause severe A-pillar damage.

Although errors occurred in the Neon simulations, they were valid up to approximately 140 ms and were still very useful to examine the projection of the hood under and behind the system. In TL-3 full-scale tests, an 1100C vehicle could pass with a cowl height above 34 in. (864 mm) at top-rail mounting heights of 36 in. (914 mm). The difference in cowl heights between the Neon and the Geo Metro accounted for the difference in the failure heights for the two models. The Geo Metro was 1.2 in. (30 mm) taller at the cowl than the Neon and subsequently passed at a top-rail mounting height 1 in. (25 mm) higher than the Neon. A comparison of the Neon and Geo Metro models' hood corner projection into and under the system at varying rail heights is shown in Figures 51 and 52, respectively. At 130 ms, the vehicles began to redirect and/or the hood corner was extending under and behind the system. The Neon began to underride at a 36-in. (914-mm) top-rail mounting height, whereas the Geo Metro was being redirected at this height but underrode at a 37-in. (940-mm) top-rail height.

The underride exhibited by the Neon at a 36-in. (914-mm) top-rail height and Geo Metro at a 37-in. (940-mm) top-rail height caused severe occupant compartment deformation and would likely result in a test failure. Although the failure of the Neon simulation at a 36-in. (914-mm) top-rail height was a concern, an analysis in the following section of the front-end geometry of the Neon and recent model year vehicles alleviated these concerns.

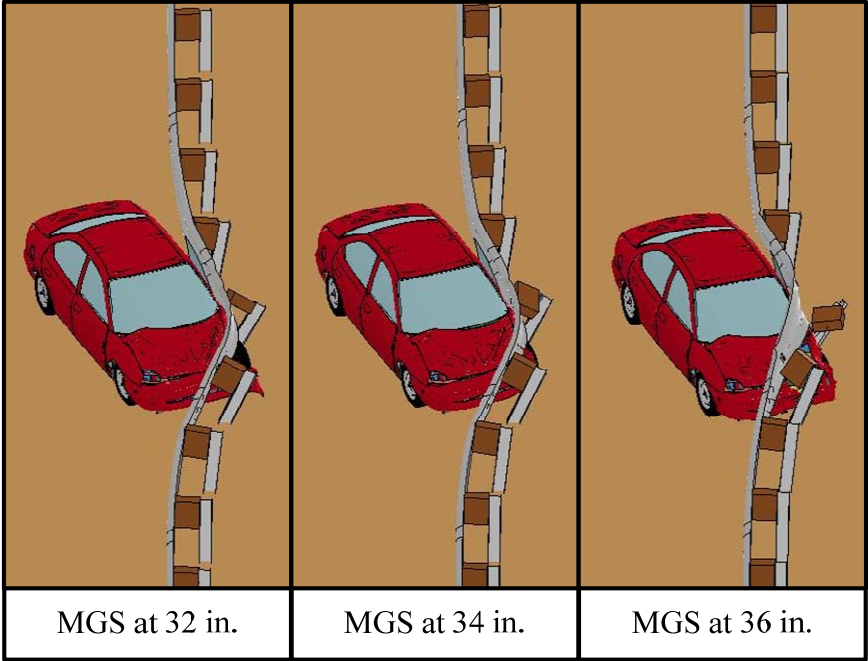


Figure 51. 1100C Neon Underride Comparison at 130 ms

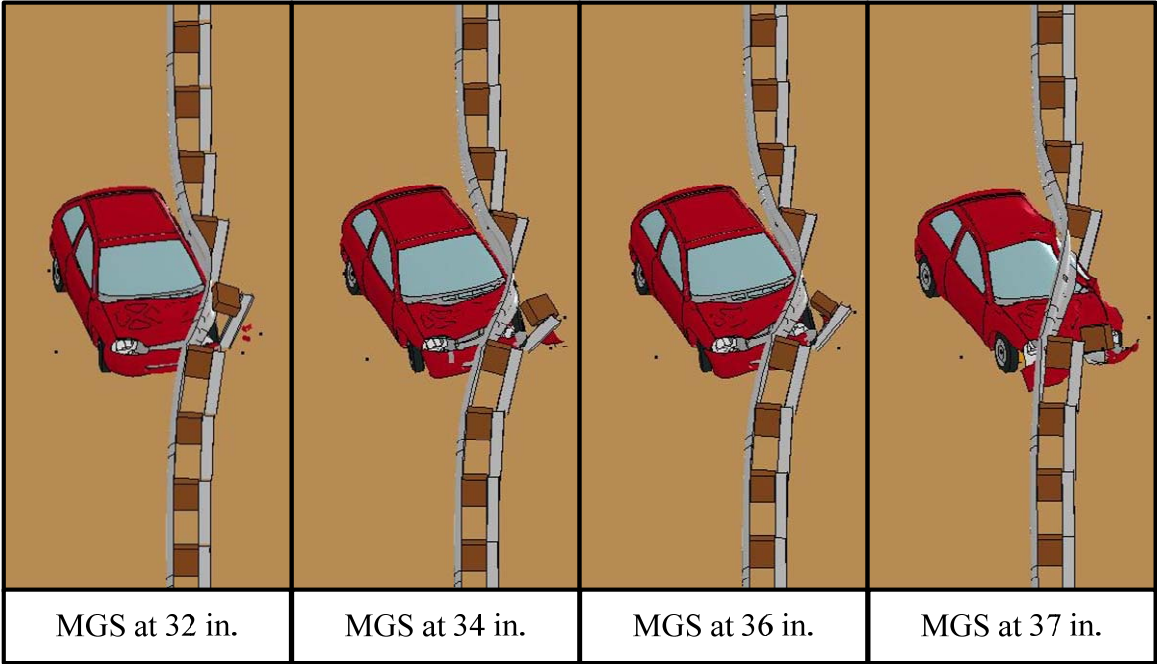


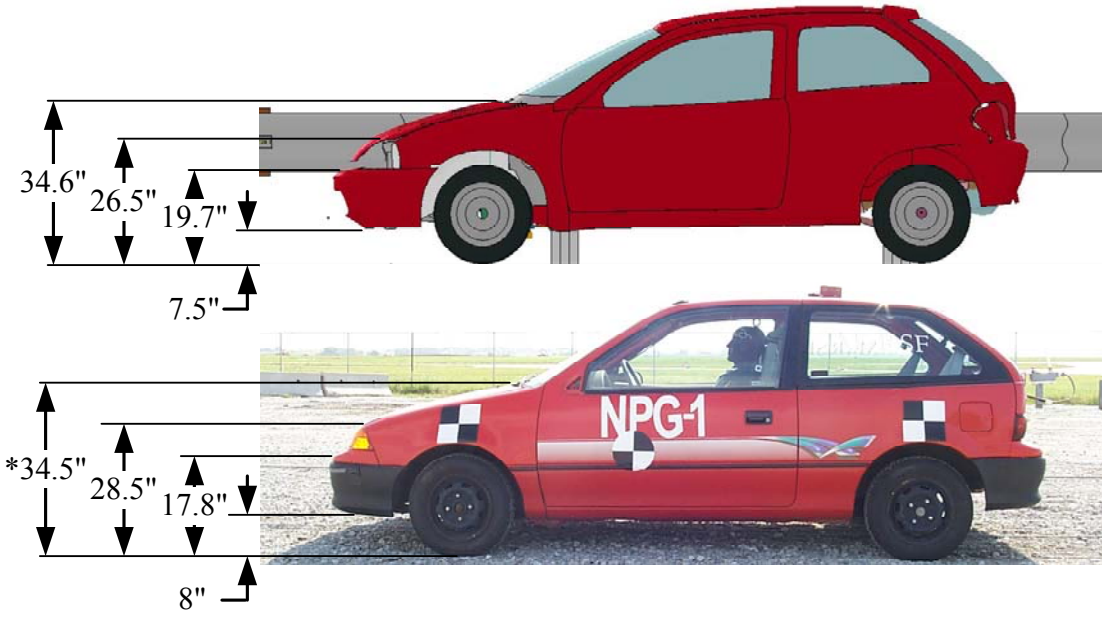
Figure 52. 820C Geo Metro Underride Comparison at 130 ms

## 7.2 Front-End Geometry Comparison

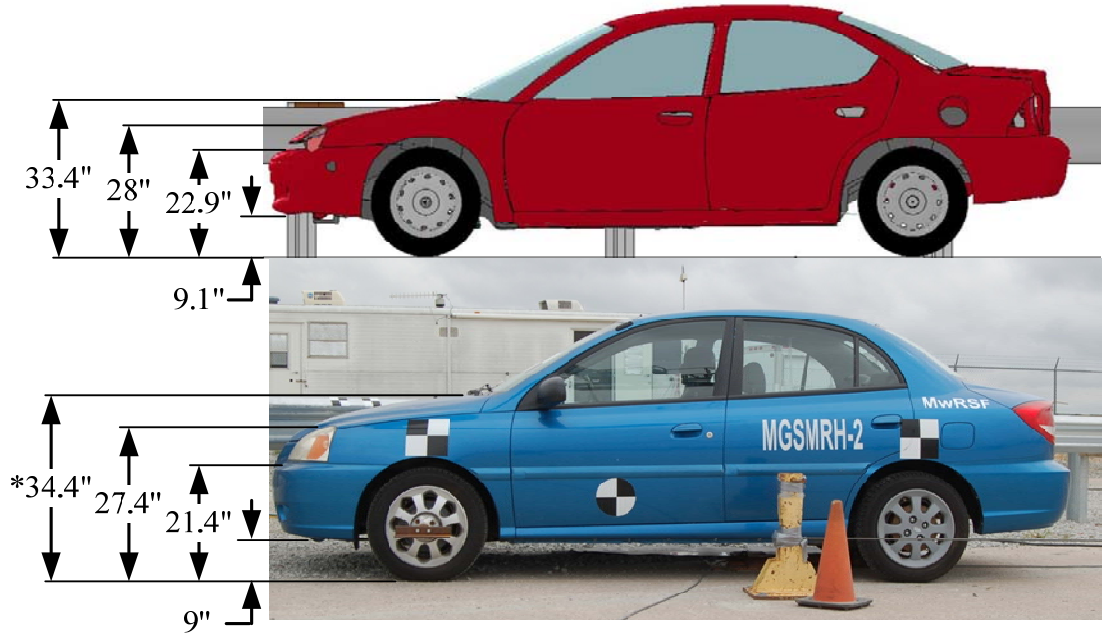
A better understanding of the geometry of current model year vehicles was needed to make relevant recommendations regarding rail heights for cars. A 36-in. (914-mm) top-rail height was passable according to MASH standards for the vehicles tested and simulated with the front-end geometry shown in Figure 53, but it may not be passable for all 1100C test vehicles. Vehicle cowl heights below that of the tested Kia Rio and simulated Geo Metro would be of concern due to the propensity for underride exhibited by the Neon model.

A survey of current model year vehicles was conducted. The front-end geometry of recent model year vehicles was measured to find those with the lowest front-end geometry profile. Vehicles with low front-end geometry were at risk for underride at increased rail heights. However, in recent years, vehicle front-end geometry has been progressing towards a more raked, wedge-shaped hood profile with an increased "beltline" and cowl height, as shown in Table 20. This suggested that the vehicles tested and simulated are at the low end of cowl heights and front-end geometry and may be considered a worst or near-worst case scenario. The lowest cowl geometry found was still higher than the tested and simulated vehicles with a range varying from 36 in. (914 mm) to 39.75 in. (1,010 mm). Therefore, the recommendations made with the vehicles tested and simulated are valid across the majority of new small cars in production and for sale in the U.S. today.





820C Simulation Model and Test No. NPG-1 test vehicle



1100C Simulation Model and Test No. MGSMRH-2 test vehicle

\*Top of hood measurements were not in the field book and were taken from similar vehicles

Figure 53. Simulation Model Vehicle and Test Vehicle Dimension Comparison

Table 20. Recent Model Year Vehicle Front-End Geometry Profiles

Model Year	Make	Model	a		b		c		d	
			in.	mm	in.	mm	in.	mm	in.	mm
2012	Chevrolet	Cobalt	36	914	27	686	21	533	8	203
2012	Honda	Insight	36.5	927	26.5	673	21.5	546	8	203
2011	Kia	Rio	36.5	927	28	711	23	584	8.5	216
2012	Honda	Civic	37.25	946	27.5	699	20.5	521	9	229
2012	Hyundai	Accent	37.5	953	29	737	23	584	6.75	171
2012	Ford	Fusion	37.75	959	30.25	768	20.5	521	9	229
2012	Chevrolet	Cruze	38	965	30	762	24.5	622	6.75	171
2012	Honda	Accord	38	965	28.5	724	21.5	546	8	203
2012	Nissan	Altima	38	965	29	737	23	584	8	203
2012	Ford	Focus	38.25	972	28.5	724	23.5	597	7.75	197
2012	Mazda	3	38.25	972	29	737	21	533	7.75	197
2010	Volkswagen	Jetta	38.25	972	27	686	21	533	8.5	216
2012	Ford	Fiesta	38.5	978	28.25	718	23	584	8	203
2012	Honda	Fit	38.5	978	26	660	20.5	521	7.5	191
2012	Hyundai	Elantra	38.5	978	29.25	743	23.5	597	8	203
2012	Nissan	Sentra	38.75	984	28.25	718	22.5	572	8	203
2012	Subaru	Legacy	38.75	984	28.5	724	22	559	9	229
2012	Toyota	Corolla	38.75	984	31	787	21.75	552	9	229
2012	Chrysler	200	39	991	28	711	23	584	8	203
2012	Toyota	Yaris	39.25	997	31.5	800	21	533	7.5	191
2011	Chevrolet	Aveo	39.5	1003	28	711	22	559	8	203
2012	Chevrolet	Sonic	39.5	1003	32	813	25.5	648	7	178
2012	Dodge	Avenger	39.5	1003	32	813	23	584	9.5	241
2012	Nissan	Versa	39.5	1003	29	737	20.5	521	7	178
2013	Hyundai	Sonata	39.75	1010	29.75	756	21.5	546	7	178
2012	Nissan	Maxima	39.75	1010	29	737	23	584	8	203
2012	Toyota	Prius	39.75	1010	32	813	22	559	8.5	216

## **8 ANCHORAGE AND RAIL DEFLECTION ANALYSIS**

### **8.1 Purpose of 2270P Pickup Truck Analysis**

Raising the rail height benefitted large-vehicle impacts because a higher rail placed the barrier closer to the center of gravity and theoretically provided better redirection properties. This can result in increased barrier performance by reducing the potential for rollover or barrier override. A concern with this increased rail height was anchorage performance. No full-scale crash tests have been performed with 2270P pickup trucks on W-beam barriers with top-rail mounting heights over 31 in. (787 mm). For this reason, simulations were performed at varying mounting heights to compare anchor forces, anchor deflections, and overall system rail deflections using the 2270P pickup model.

A complete verification of the model was carried out using the procedures for verification and validation of computer simulations used for roadside safety applications per NCHRP Report No. W179 [29]. The simulation satisfied the standardized criteria. The full verification report can be found in Appendix F.

### **8.2 Anchorage Force Analysis**

Comparison of the upstream anchor was of primary concern since it underwent greater deflection and higher forces during impacts as found in previous full-scale vehicle crash tests. A comparison of the anchor cable cross section force with truck impacts at post no. 12 is shown in Figure 54. The higher top-rail mounting heights provided some differences in anchor cable force but were generally in the same range. This suggested that the higher rail height, and subsequently changed cable geometry, may not significantly affect the performance of the barrier anchorage in regard to large trucks. A limiting effect may be induced by the end anchorage ground-line strut which prevented a significant increase in anchor cable forces.

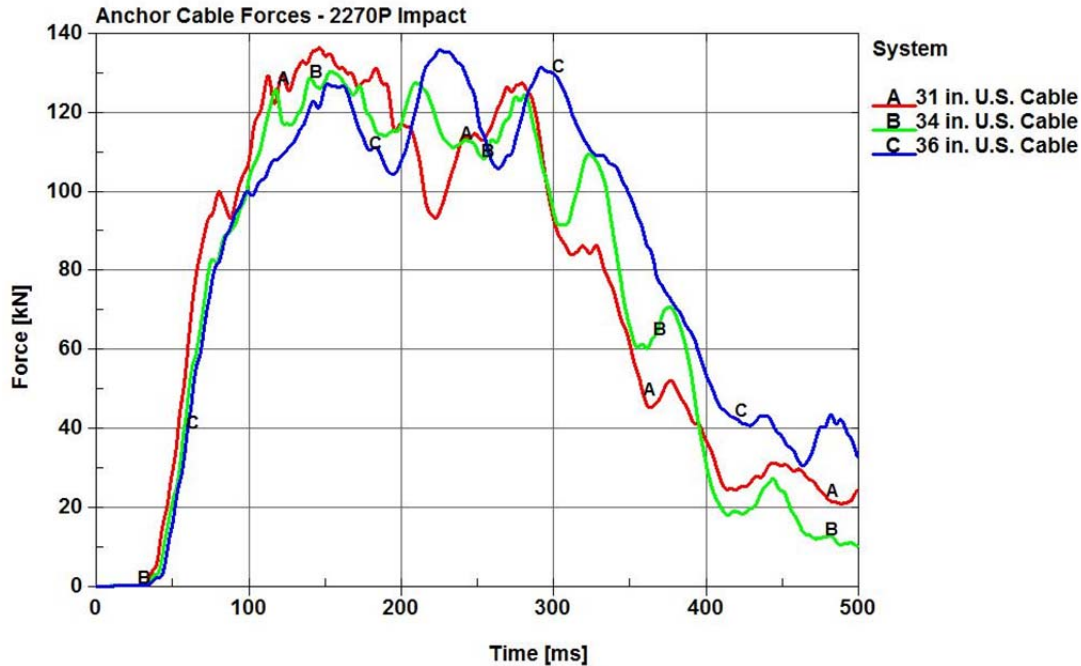


Figure 54. US Anchor Cable Cross Section Forces

Similarly, the downstream anchorages did not show large differences in the cross sectional force, as shown in Figure 55. The upstream cable anchorage showed a slight decrease in the initial peak cable force at increased rail mounting heights. This was followed by a slightly higher force as the vehicle reached parallel with the system and exited the system. The downstream anchorage displayed an inverse trend of decreased initial peak cable force followed by a higher sustained force throughout the impact and as the vehicle exited the system. This was due to the impact location being nearer to the upstream end of the system. As the vehicle moved through the impact zone, it moved closer to the downstream end anchorage, and an increased force was imparted to that anchorage.

In addition, the forces through the cross-sections of the rail after post no. 1, before post no. 2, and after post no. 2 were similar across all three impact heights at each individual location along the rail. These cross-sections locations are shown in Figure 56. However, loads at the three locations were not similar to one another. This was expected as the rail impact force did not

significantly change and the hardware connections and the rail materials did not change. Additionally, the anchor cable absorbed a majority of the force before it reached the section after post no. 1. Minor increases in rail force were expected only due to the increase in load placed on the rail from the increased system deflection.

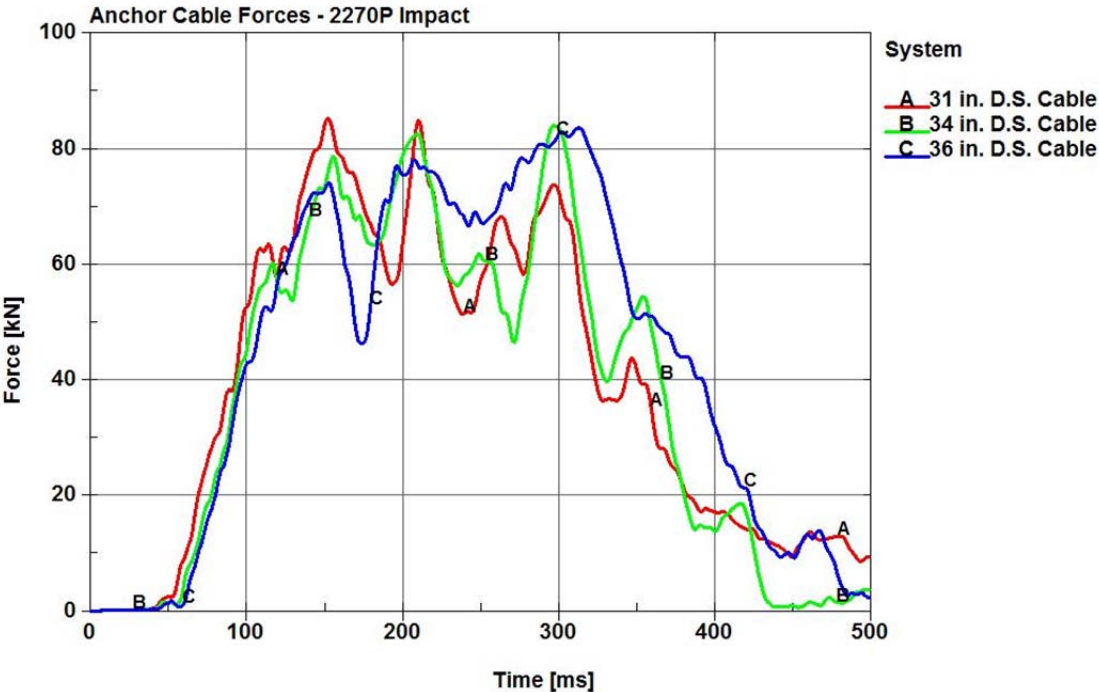


Figure 55. Downstream Anchor Cable Cross Section Forces

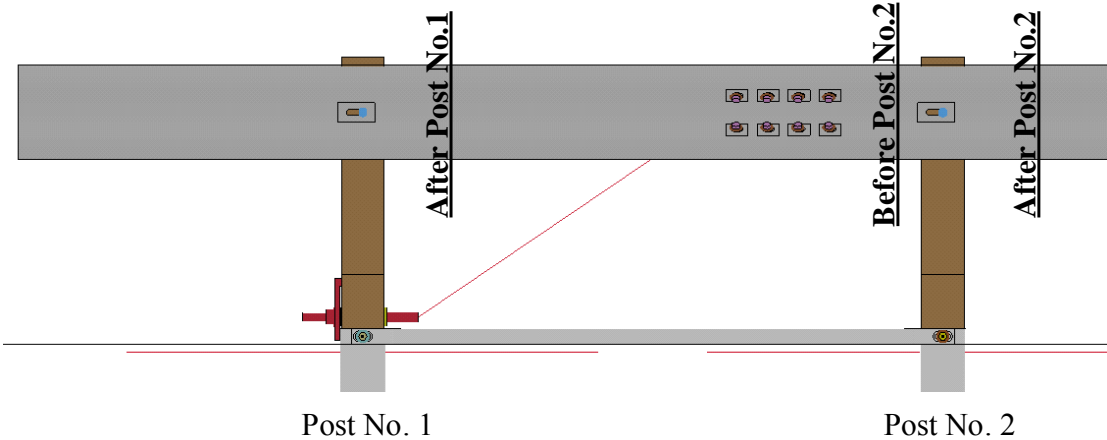


Figure 56. Upstream Anchor Cross-Sections

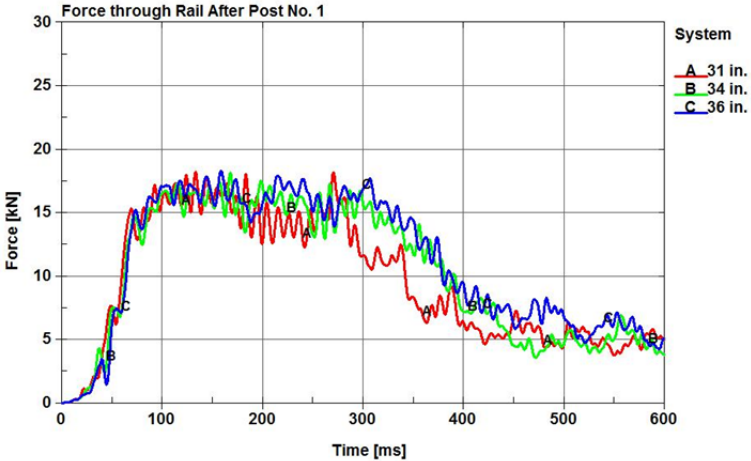
The load along the rail was transferred from the rail through the anchor cable and ultimately to the ground. This was evidenced by the relatively higher loads before and after post no. 2 and through the anchor cable as compared to the force through the rail after post no. 1. The forces through the rail cross-sections after post no. 1, before post no. 2, and after post no. 2, are shown in Figure 57.

The similarities in force were attributed to the relationship between the rail center and the height of the truck center of gravity, which was 28.5 in. (724 mm). At a 31-in. (787-mm) top-rail mounting height, the center of the rail was at 24 7/8 in. (632 mm), below the truck CG height. This meant that more force was being exerted on the top corrugation of the rail, subsequently introducing roll into the system and torque in the rail about its length. Additionally, reduced rail height meant more wheel contact area with the lower corrugation, generating the higher initial peak force as a slight torque was applied to the rail, flexing the anchorage cable.

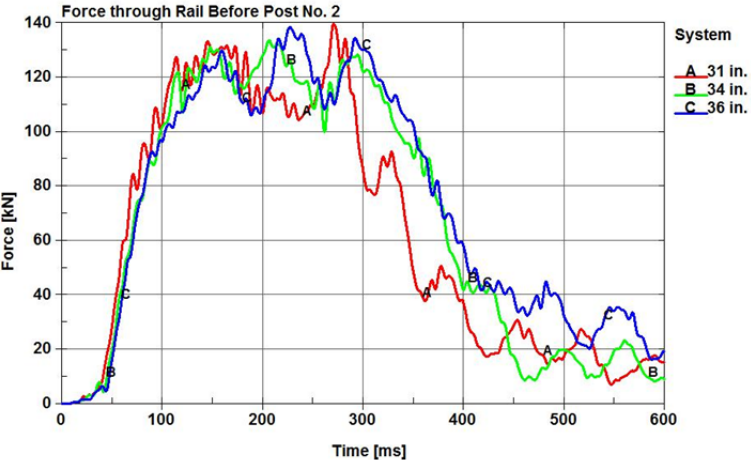
As the rail height increased to 34 in. (864 mm), the CG was near the rail center causing a similar force to be exerted in both the top and bottom corrugations, resulting in a more stable, level vehicle response. At this height, the apparent cable force peak was slightly lower but maintained a slightly higher force throughout the simulation as energy was being absorbed more evenly across the rail. The initial decrease in peak force was attributed to the decreased contact area between the tire and lower rail corrugation, which reduced the kinetic energy transfer from the stiffer suspension and wheel components by replacing that contact space with the relatively softer fender components. As the vehicle came farther into contact with the rail, this effect was reduced and the force increased.

When the rail height was raised to 36 in. (914 mm), the CG of the vehicle was slightly below the rail center. This generated a higher force along the bottom corrugation, causing it to fold under and result in some wheel underride as the truck tire passed behind the back side of the

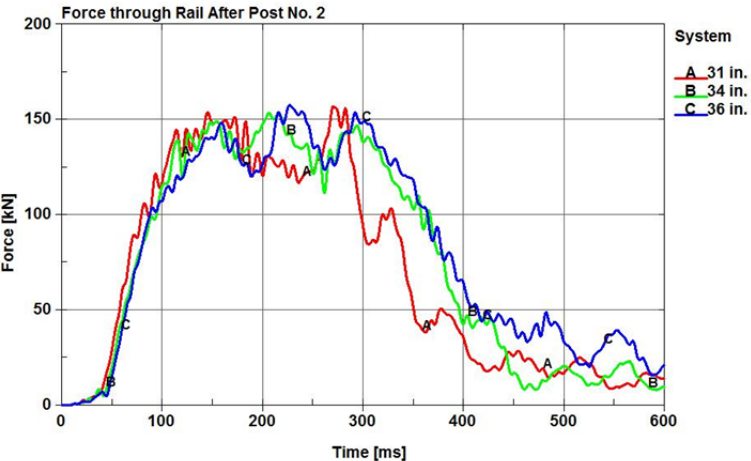
rail. Once behind the rail, the tire was trapped and subsequently, the truck pitched down when suspension failure was not prescribed to the pickup truck.



Force through Rail After Post No. 1



Force through Rail Before Post No. 2



Force through Rail After Post No. 2

Figure 57. Force through Rail from a 2270P Impact



### 8.3 Anchorage Displacement Analysis

The displacement of the top center of anchor post nos. 1 and 29 for the 31-, 34-, and 36-in. (787-, 864-, 914-mm) systems from an impact with the 2270P pickup truck is shown in Figures 58 and 59.

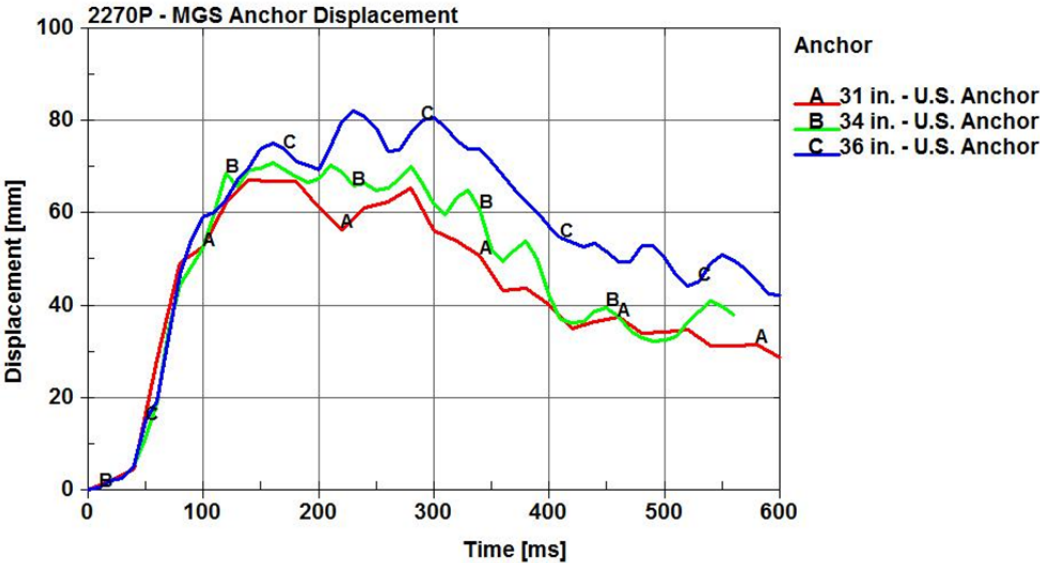


Figure 58. Upstream Anchor Displacement (2270P Pickup Truck)

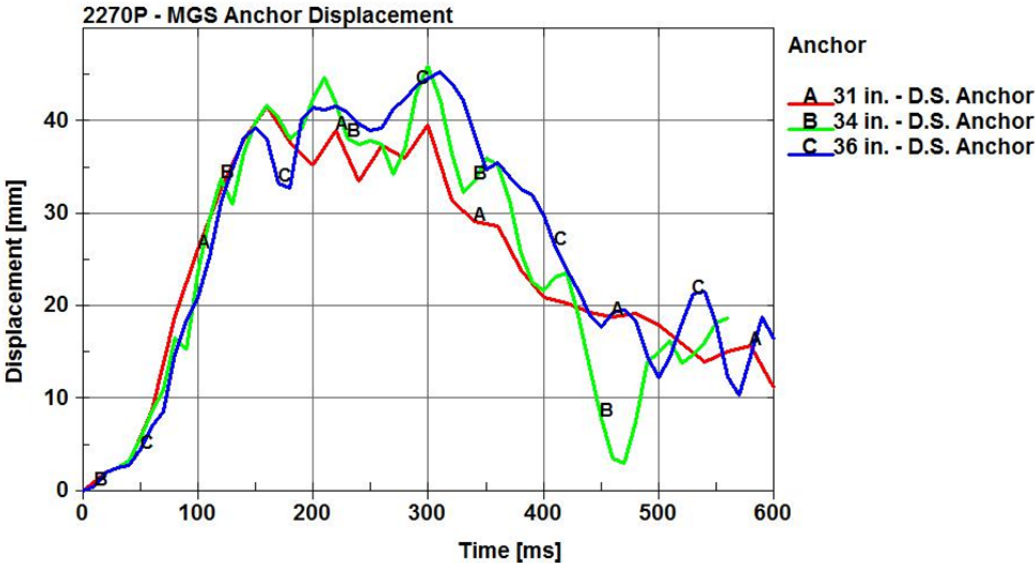


Figure 59. Downstream Anchor Displacement (2270P Pickup Truck)

As expected, the upstream anchor displaced significantly more than the downstream anchor, and the peak displacement increased as the rail mounting height increased. The increased displacement was expected due to the increased height of the system and elongated moment arm applied to the anchor posts. The maximum deflections occurred at a 36-in. (914-mm) top-rail height. The maximum deflections of the upstream and downstream anchors were 3.2 in. (81 mm) and 1.8 in. (46 mm), respectively.

#### **8.4 Impact Variations Due to Suspension Failure**

During the rail height analysis, it was noted that different vehicle reactions occurred from an impact with the 31- and 34-in. (787- and 864-mm) top-rail heights as compared to an impact with a 36-in. (914-mm) top-rail height. While the impacts on systems of 34 in. (864 mm) or less produced similar body roll reactions, the 36-in. (914-mm) top-rail height system caused the 2270P pickup truck wheel to ride under the rail. Once under the rail, the truck was pulled toward the system. Subsequently, snagging occurred, pulling the vehicle further into the rail. Prescribing suspension failure to the model created better vehicle behavior and prevented this snagging. The initial and parallel states, without suspension failure prescribed, of the 2270P pickup truck next to 31-, 34-, and 36-in. (787-, 864-, 914-mm) rail height systems are shown in Figure 60.

The 31- and 34-in. (787- and 864-mm) top-rail height systems adequately redirected the 2270P pickup truck. However, at a 36-in. (914-mm) top-rail height, the left-front wheel was trapped behind the rail, as mentioned. This resulted in wheel snag upon exit and hindered the effective redirection of the truck. Prescribed suspension failure of the left-front wheel led to different results, as shown in Figure 61. Suspension failure did little to change the response of the 31- and 34-in. (787- and 864-mm) top-rail height systems.

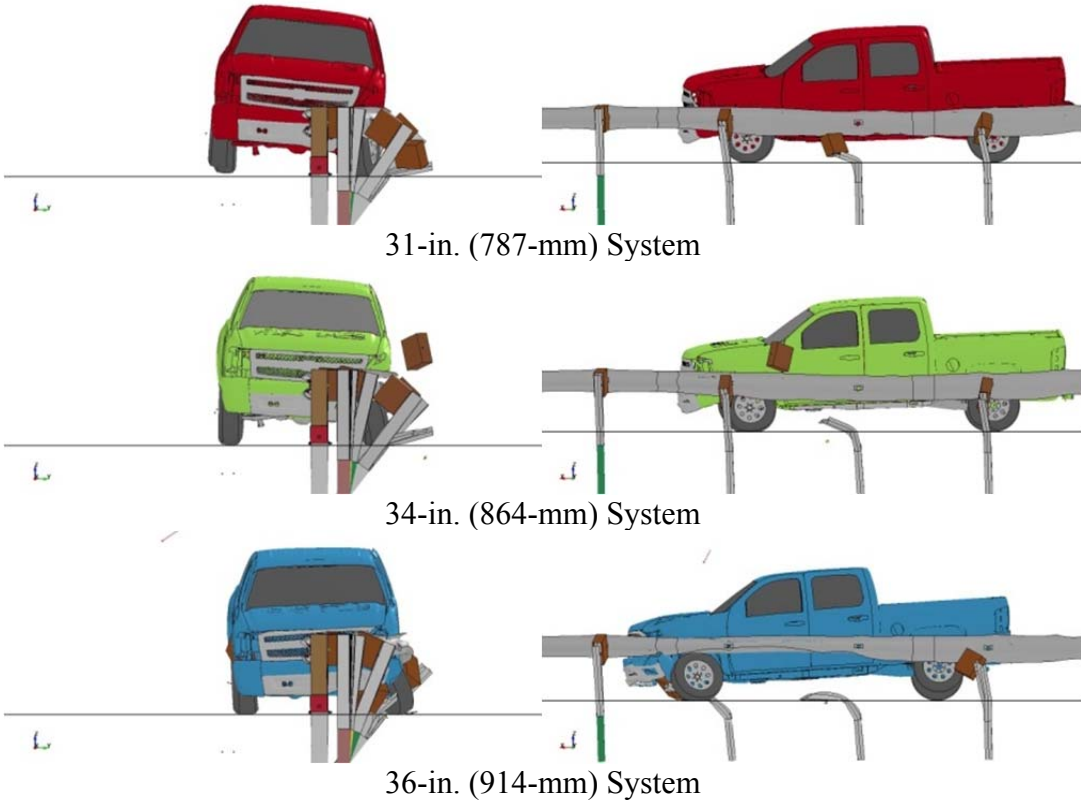


Figure 60. 2270P Pickup Truck Impact without Prescribed Suspension Failure

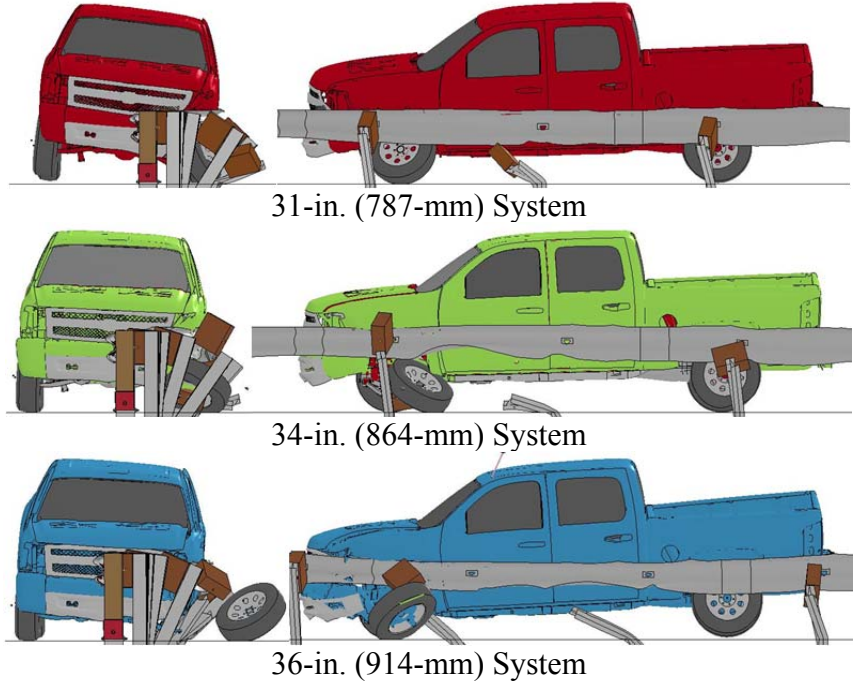


Figure 61. Prescribed Suspension Failure Impact Variations

The small differences in the simulations with suspension failure for the 31-in. (787-mm) tall system were noted while selecting a model for the simulation [25]. However, the increased barrier height and suspension failure allowed the left-front tire to become disengaged from the truck after passing behind the rail. This caused the left-front corner of the truck to drop down and lean into the barrier, which also allowed smoother redirection of the truck since the wheel did not snag on the posts. Full-scale tests showed that suspension failure and wheel disengagement were likely to occur in a high percentage of vehicle crash tests. Therefore, the suspension failure shown was a more likely scenario. Aside from the improved vehicle redirection of the suspension failure, significant differences were not shown in any of the parameters of interest in relation to the anchorage displacements and forces.

### **8.5 Comparison of Test Conditions and Simulation Results**

The simulations with the 2270P at varying top-rail mounting heights were compared to understand and analyze the differences in a variety of parameters, as shown in Table 21. Prescribed suspension failure did not significantly affect major redirection parameters with the exception of vehicle roll, which was expected. Suspension failure did provide improved vehicle behavior. At higher rail heights, the wheel snagged on posts and caused yawing of the vehicle toward the barrier, as indicated by the exit angle at 36-in. (914-mm) top-rail heights. As the rail height increased, corresponding and consistent increases in rail deflections were shown. However, the working width decreased slightly due to the angle at which posts were impacted and folded to the ground. At a 36-in. (914-mm) top-rail height, post rotation increased slightly in the impact zone, post nos. 11 through 18, which decreased the working width. In all cases the posts were the working width indicators.

Table 21. Comparison of Test Conditions and Simulation Results

Evaluation Parameters	Units	Test No. 2214MG-2	Simulation Conditions and Results					
			31-in. Simulation	31-in. Simulation	34-in. Simulation	34-in. Simulation	36-in. Simulation	36-in. Simulation
<b>Suspension Failure?</b>	(Y/N)	Y	N	Y	N	Y	N	Y
<b>Top Rail Height</b>	in. (mm)	31 (787)	31 (787)	31 (787)	34 (864)	34 (864)	36 (914)	36 (914)
<b>Tested Vehicle Mass</b>	lb (kg)	5000 (2268)	5004 (2270)	5004 (2270)	5004 (2270)	5004 (2270)	5004 (2270)	5004 (2270)
<b>Impact Velocity</b>	mph (km/h)	62.9 (101.2)	62.1 (100)	62.1 (100)	62.1 (100)	62.1 (100)	62.1 (100)	62.1 (100)
<b>Tested Impact Angle</b>	deg	25.49	25	25	25	25	25	25
<b>Parallel Time</b>	ms	282	262	260	270	266	316	310
<b>Parallel Velocity</b>	mph (km/h)	45.2 (72.8)	47.4 (76.3)	48.3 (77.8)	47.4 (76.3)	48.1 (77.4)	43.1 (69.4)	47.2 (76.0)
<b>Dynamic Rail Deflection</b>	in. (mm)	43.9 (-1114)	39.6 (-1005)	38.9 (-987)	44.8 (-1137)	43.4 (-1103)	47.8 (-1214)	46.9 (-1191)
<b>Working Width</b>	in. (mm)	48.6 (1234)	58.0 (1472)	57.7 (1465)	58.1 (1475)	60.4 (1533)	59.4 (1509)	60.8 (1545)
<b>Working Width Indicator</b>	-	Post	Post	Post	Post	Post	Post	Post
<b>Exit Time</b>	ms	718	620	620	660	660	-	-
<b>Resultant Velocity at Exit</b>	mph (km/h)	40.6 (65.4)	44.7 (72.0)	44.7 (72.0)	44.5 (71.6)	45.7 (73.6)	33.3 (53.6*)	43.6 (70.2*)
<b>Exit Angle</b>	deg	-13.5	-15.5	-16.2	-15.0	-16.0	-1.6*	-2.8*
<b>Max Roll</b>	deg	-4.08	-5.5	-10.2	-1.8	-4.0	2.6	-4.1
<b>Max Pitch</b>	deg	-1.8	-2.4	-1.9	-1.6	-2.2	3.2	-2.0
<b>Pass/Fail</b>	-	Pass	Pass	Pass	Pass	Pass	Pass	Pass

\*Truck did not exit system in simulation, value is end of simulation.

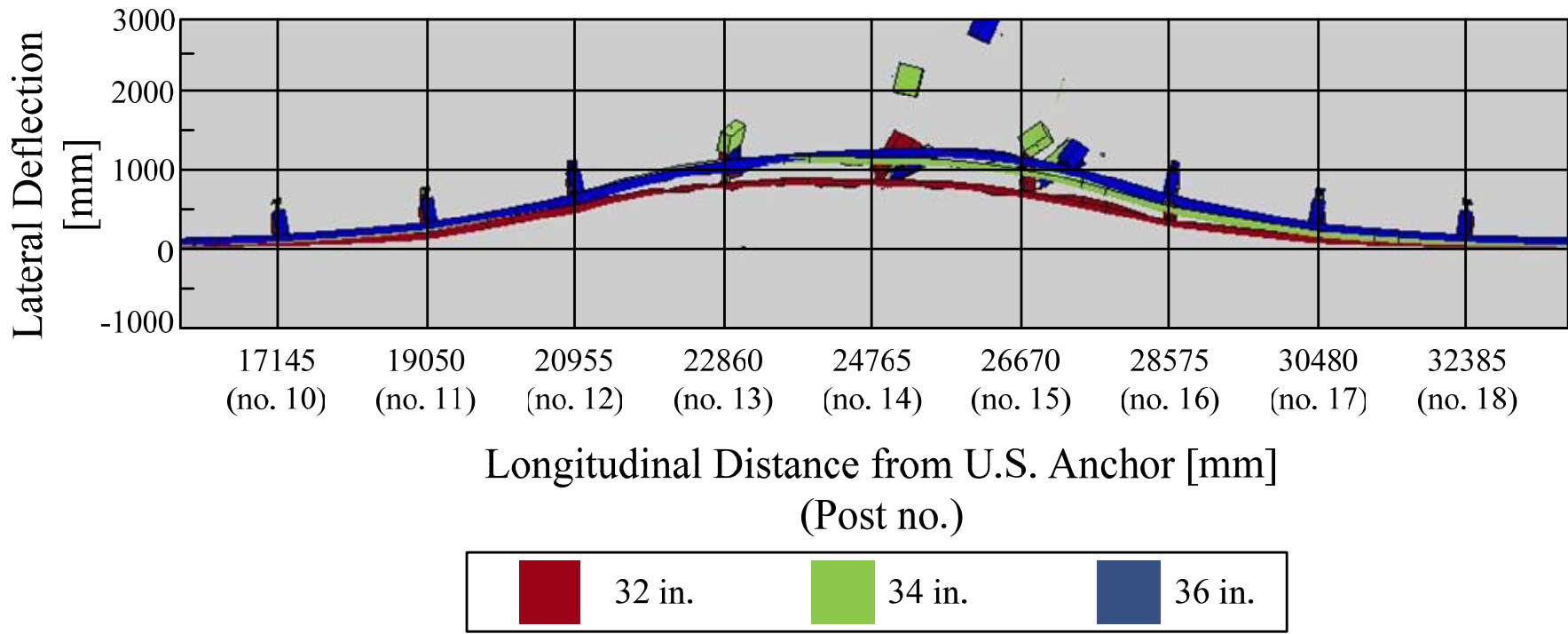
A concern with increased rail heights was the potential for increased rail deflection due to decreased post embedment depth and resulting decreased resistance. An overhead view of a post on impact on the 31-, 34-, and 36-in. (787-, 864-, and 914-mm) top-rail height MGS systems is shown in Figure 62. While there were differences in rail deflection between the three rail heights, the decreased post stiffness and increased rail deflection were not sufficient to cause failure.

## **8.6 Discussion**

For 2270P vehicle impacts, the increase in rail deflection and anchorage displacement with decreased post embedment depth and raised rail height was not severe enough to warrant concern with the taller MGS systems in the field. In design and use, due to the increased rail deflection, the working width of the system would also increase. Proper placement and lateral offsets should be adjusted accordingly to ensure that traffic is guarded from the fixed objects for which these barrier systems are designed to shield.

The minor increase in anchor displacement at increased rail heights relative to standard height systems led to two possible conclusions: (1) the model did not accurately predict the system anchor displacement or (2) there was a limiting factor of the anchor that prevented larger deflection, such as the ground-line strut. Due to the validation procedures undertaken for these models and their ability to accurately predict many other aspects of the impacts, the former seems less likely. It was believed that the latter may be a more apt conclusion. Due to the geometry of the anchor, the ground-line strut, and the anchor cable, there was a limiting factor that prevented the anchor posts from displacing to a much greater degree, though there was decreased lateral resistance from the system posts. As the force of impact displaced the anchor, the coupling of the two anchor posts caused a moderate displacement increase of the farthest upstream anchor post and a larger increase in displacement of the second anchor post, post no. 2, as shown in Figure 63.

### Rail Deflection Comparison at 600 ms



112

Figure 62. Simulated Rail Deflection Comparison at 600 ms for 2270P Pickup Truck Impact

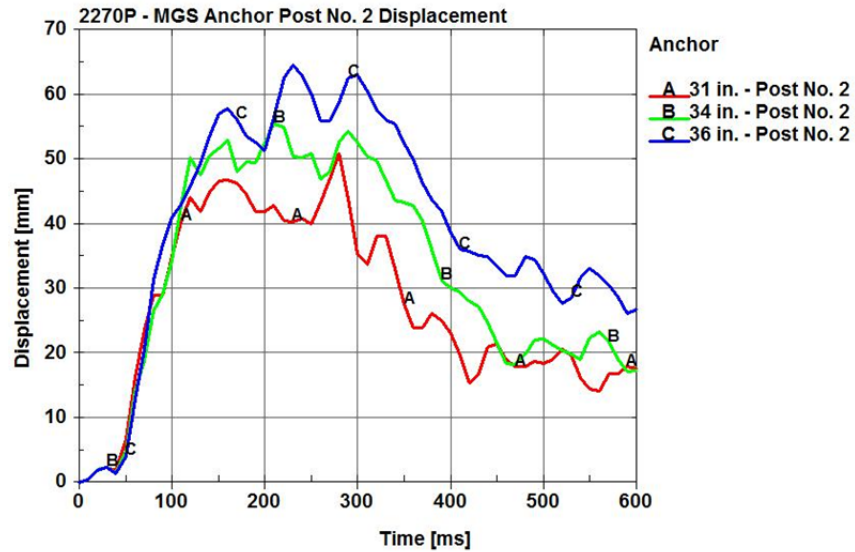


Figure 63. Anchor Post No. 2 Displacement

This showed that force was transferred to post no. 2 at a greater rate as rail height was increased and post embedment was decreased. However, for the systems simulated, deflections were not large enough to cause post failure or to limit the effectiveness of the system.

Modeling of soil and wood post fracture in LS-DYNA is still a gross approximation. These approximations have been shown to be reasonably accurate in several applications; however, engineering judgment is still necessary when using these results.



## 9 CRITICAL HEIGHT WITH APPROACH SLOPES

### 9.1 Background on Approach Slopes

According to the recommendation in AASHTO's Roadside Design Guide (RDG), standard W-beam guardrails should not be installed in combination with approach slopes of 8:1 or steeper [30]. Due to these slope limitations, designers often must place guardrails near the edge of the shoulder, which often increases accident frequency with guardrail systems. The development of the MGS with increased mounting height and deeper blockouts has been shown in full-scale crash tests to provide sufficiently improved performance to permit placement on slopes of 8:1 [31, 32]. The advent of further increased MGS mounting height has the potential to improve light truck performance on slopes and still allow for proper redirection of small cars on steeper slopes.

In previous research, an 8:1 approach slope was identified as a critical slope condition for pickup truck impacts at a guardrail offset of 5 ft (1.5 m) down from the slope break point to the front face of the MGS. Separate research has shown that on 6:1 approach slopes, a 2270P Silverado reached a maximum height above the ground at roughly 8.7 ft (2.7 m) from the slope break point when traversing a V-ditch [33]. At this point, the propensity for override was greatest; however, it was unlikely that a guardrail would be placed this far down a slope. The same research found that an 820C small car would reach its maximum suspension compression at a lateral distance of roughly 21.5 ft (6.6 m) to 25.4 ft (7.7 m) away from the slope break point [33]. Again, it was even more unlikely that a guardrail would be placed this far from the road edge.

In order to match previous crash test data and to use a lateral offset similar to the maximum truck trajectory height, a lateral offset distance of 5 ft (1.5 m) was deemed acceptable

to determine the effects of rail height on approach slopes. In addition, a lateral offset of 5 ft (1.5 m) was comparable for 8:1 and 6:1 approach slopes for both the small car and pickup truck, and it provided a reasonable lateral offset for barrier placement. Additionally, this lateral offset occurred prior to reaching the maximum trajectory height for an 820C vehicle.

Two full-scale vehicle crash tests were performed on the MGS system on approach slopes at a 31-in. (787-mm) top-rail mounting height. The first, test no. MGSAS-1, was with a ¾-ton pickup truck, impacting the system at a speed and angle of 62.4 mph (100.4 km/h) and 25.9 degrees, respectively, on an 8:1 approach slope and 5-ft (1.5-m) lateral offset [31, 32]. The second, test no. MGSAS-2, was performed using a small car, impacting the system with a speed and angle of 61.9 mph (99.6 km/h) and 21.6 degrees, respectively, on an 8:1 approach slope and 5-ft (1.5-m) lateral offset [31, 32]. Both tests were conducted, reported, and deemed acceptable in accordance with TL-3 requirements specified in the NCHRP Report No. 350, *Recommended Procedures for the Safety Performance Evaluation of Highway Features*.

## **9.2 Overview of Simulation Study**

An LS-DYNA simulation study was performed to examine the effects of the increased MGS mounting height on slopes in regard to small car redirection performance and specifically underride [7]. Current MASH standards utilize a 25-degree impact angle with small cars when testing for barrier performance to provide an increased impact severity. However, the NCHRP Report No. 350 indicated that standard impact angles of 20 degrees may be more severe at these increased heights. As the small car traverses the slope break and continues down the embankment to the barrier, the smaller angle of impact provides a greater distance of travel before striking the barrier and allows for the suspension to compress more, thus effectively lowering the frontal geometry of the car. This decreased front-end height may provide unacceptable impact conditions and redirection properties.

Simulations were performed on both 8:1 and 6:1 approach slopes with top rail mounting heights of 31, 34, and 36 in. (787, 864, and 914 mm) with test impact angles of both 20 and 25 degrees in order to determine a failure limit. Typically, an MGS rail height of 32 in. (813 mm) is used to test and evaluate small cars; however, the research performed by the MwRSF used a 31-in. (787-mm) rail height, so LS-DYNA simulations were also performed to validate the model at this height.

### **9.3 Underride on 8:1 Approach Slope with 820C**

#### **9.3.1 Simulation at 31-in. (787-mm) Rail Height**

Using test no. MGSAS-2 as a baseline and reference, crash test simulations were performed to find a failure condition for the small car with respect to underride and barrier height. An initial simulation was performed using the NCHRP Report No. 350 target impact conditions of test no. MGSAS-2, which had a 5-ft (1.5-m) offset measured from the beginning of the approach slope to the front of the blockout. The speed and angle of the impact were 62.1 mph (100 km/h) and 20.0 degrees, respectively. A time sequential of test no. MGSAS-2 in comparison with the simulation results is shown in Figure 64, which provided visual validation of the model. Note that the simulation images have been mirrored for best comparison with the full-scale test images.

A complete verification of the model was carried out using the procedures for verification and validation of computer simulations used for roadside safety applications per NCHRP Report No. W179 [29]. The simulation satisfied the standardized criteria. The full verification report can be found in Appendix G.

The simulation showed excellent correlation to test no. MGSAS-2 in vehicle behavior, post rotation, and blockout behavior, providing good validation for the model. The full-scale crash test did exhibit some yawing toward the barrier at exit which was not present in the

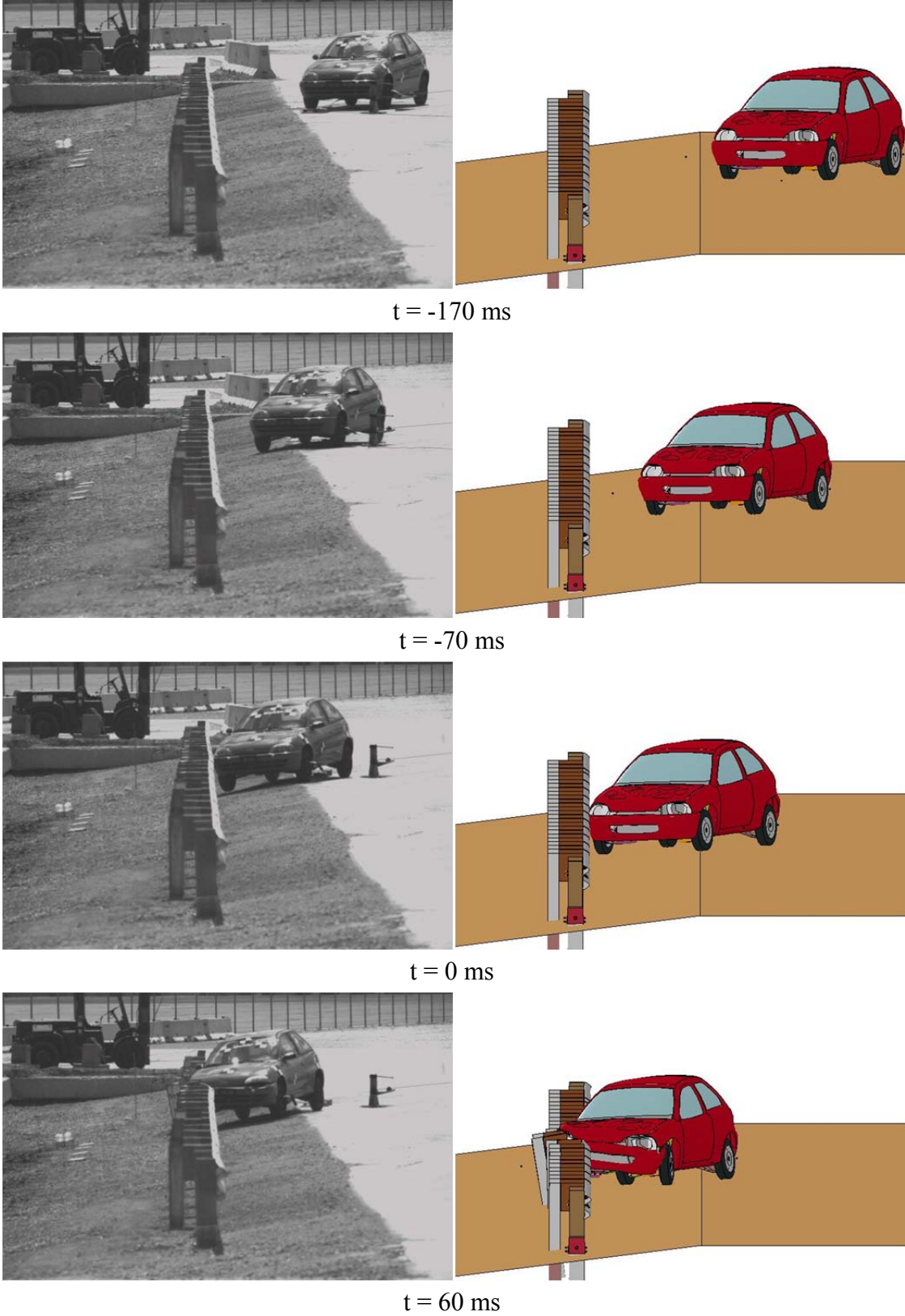
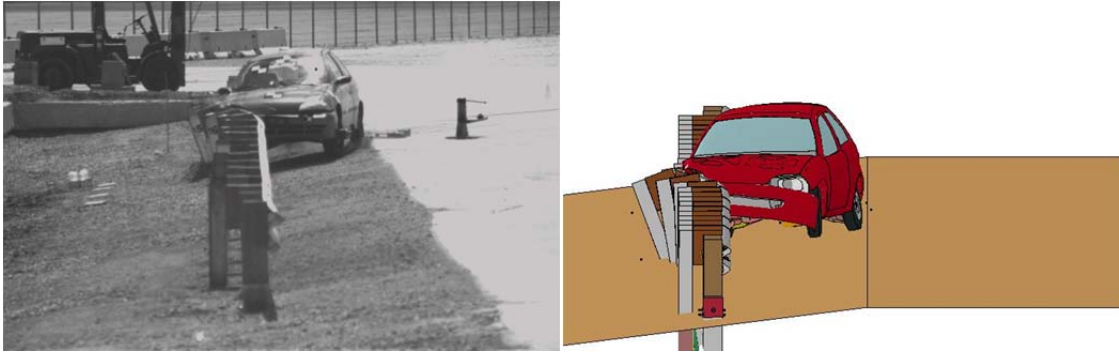
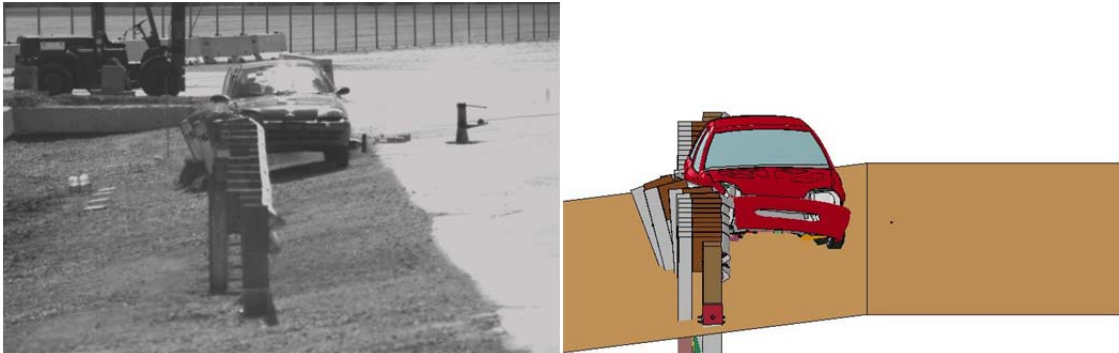


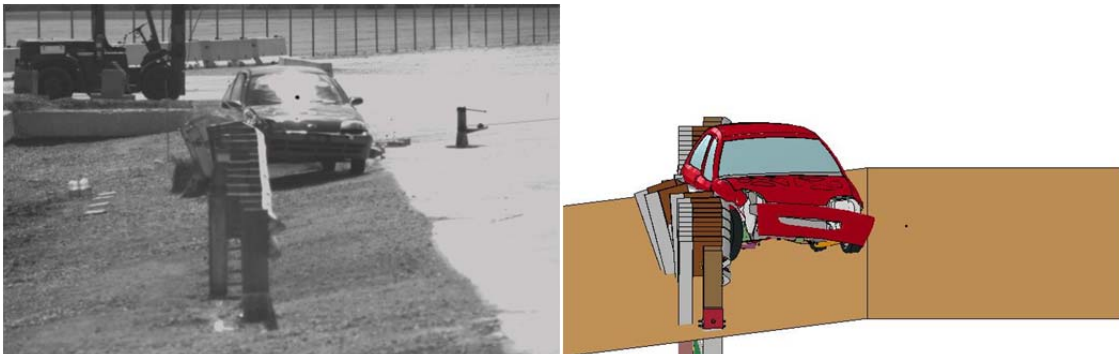
Figure 64. Time Sequential of Test No. MGSAS-2 and Simulation



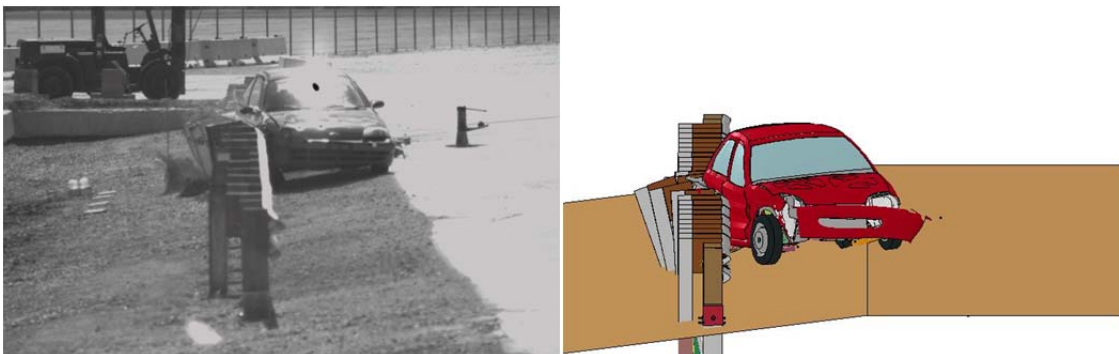
t = 120 ms



t = 180 ms



t = 240 ms



t = 300 ms

Figure 64. Time Sequential of Test No. MGSAS-2 and Simulation (continued)

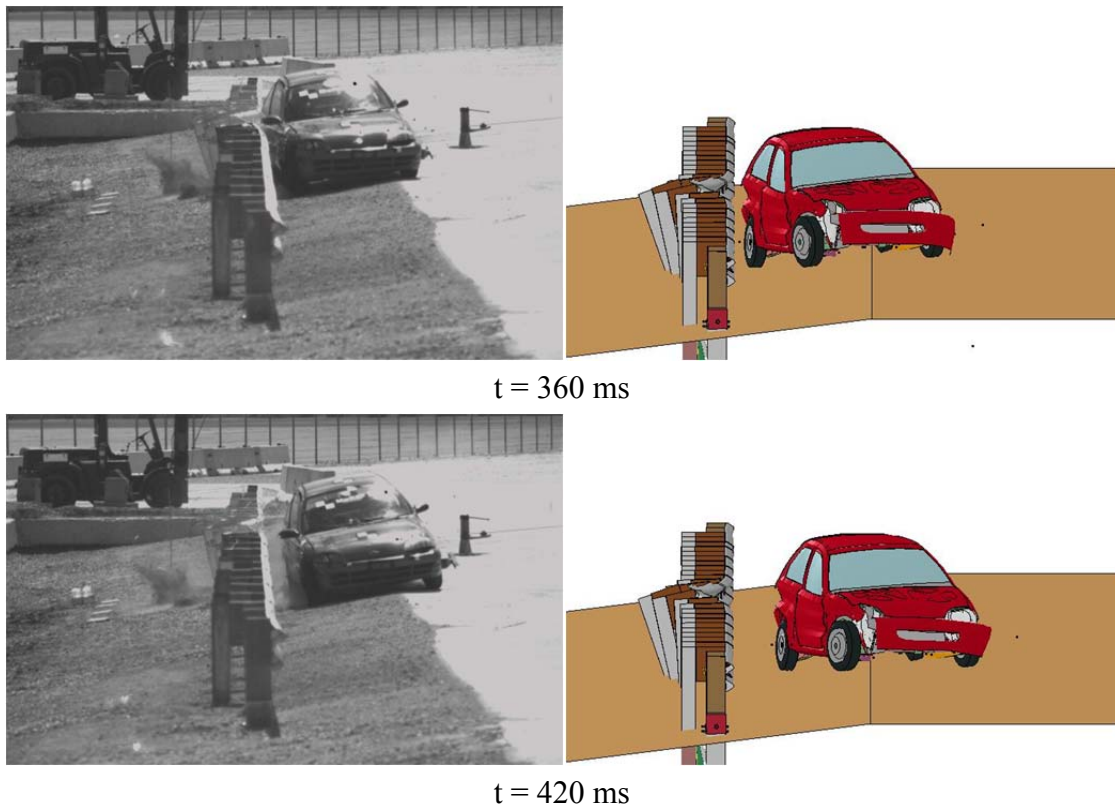


Figure 64. Time Sequential of Test No. MGSAS-2 and Simulation (continued)

simulation. However, this behavior was deemed acceptable for future use of this model as it would not affect the acceptability of the test. The primary difference came from suspension modeling differences, where the wheels in the simulation to steered away from the barrier whereas the wheels in the full-scale crash test steered toward the barrier.

### 9.3.2 Simulation at 34-in. (864-mm) Rail Height

Using the validated test no. MGSAS-2 baseline simulation, crash test simulations were performed to find a failure condition for the small car with respect to underride for each barrier height. Two additional respective heights were used based on previous research on acceptable maximum rail height. The NCHRP Report No. 350 standard impact speed and angle of 62.1 mph (100 km/h) and 20.0 degrees were used. In addition, an impact angle of 25 degrees was investigated per AASHTO MASH standards. Front-end geometry was a primary factor in

redirection effectiveness at increased rail heights. Specifically, the cowl height had a significant effect on the redirection behavior of the vehicle. A time sequential comparison of the 20-degree and 25-degree impact angles on the 8:1 approach slope at a 34-in. (864-mm) top-rail height is shown in Figure 65.

Differing impact angles on a slope can change the vehicle's suspension reaction when impacting a barrier based on the available distance the car has to traverse the slope. Differences between the 20-degree and 25-degree trajectories were noted as the vehicle traversed the approach slope at the 34-in. (864-mm) top-rail height. However, these differences did not contribute to significant differences in the redirection effectiveness, and both simulations exhibited characteristics that would be acceptable per NCHRP Report No. 350 and MASH standards.

### **9.3.3 Simulation at 36-in. (914-mm) Rail Height**

At a further increased rail height, the effects of the decreased impact angle on the slope were noticeable. The decreased impact angle allowed for greater body roll down the slope causing suspension compression and the potential for the nose of the vehicle to penetrate under the barrier, form a wedge, and push the rail up the hood and into the A-pillar. Simulations at increased rail heights showed that the cowl height was an important parameter regarding a vehicle's ability to be redirected. As the vehicle impacted the barrier, the fender near the front bumper was crushed back toward the occupant compartment until reaching the cowl. The cowl, which was much stiffer with support from the firewall, windshield and door frame, provided enough resistance to the barrier to safely redirect the vehicle. The benefit of this increased stiffness was diminished if the rail rode up and over the fender, allowing the rail to come into contact with the A-pillar. An impact angle of 25 degrees caused the vehicle's velocity vector to remain more lateral than at 20 degrees, which kept the bumper further in the air. At a 20-degree

impact angle, the vehicle was allowed to travel more vertically downward, effectively dropping the bumper, compressing the suspension, and allowing for underride of the system. This was shown in the sequential images of a 20- and 25-degree impact angle at a 36-in. (914-mm) top-rail height in Figure 66.

At a 20-degree impact angle, the vehicle rode along the barrier just after impact, the front of the car dropped much farther than observed for the vehicle impacting at 25 degrees. This caused the effect mentioned previously, in which the guardrail rode up over the hood, subsequently crushing the A-pillar and causing unacceptable occupant compartment damage, as shown in Figure 67.

At approximately 370 ms, the rail rode over the hood corner, slid up to the A-pillar, and crushed the occupant compartment. While redirection was shown, the occupant compartment damage as a result of this underride would render this test a failure, which was a function of how the vehicle traversed the slope, as shown in Figure 68.

At a 20-degree impact angle, the vehicle traveled 175.4 in. (4,455 mm) across the slope before impacting the barrier, whereas at a 25-degree impact angle the vehicle traveled 142 in. (3,607 mm) across the slope before impact. This 20-degree trajectory added an additional 33 in. (848 mm) to the path length and allowed the vehicle to roll down the slope, which dropped the front bumper and allowed the vehicle to underride, as shown in Figure 69.

The trajectory of the 25-degree impact vector kept the nose of the car more level with the road plane than the 20-degree impact vector. This resulted in a more sustained level redirection. At 20 degrees, the car rolled more downward at impact and throughout the simulation, causing the nose to drop and the rail to override the hood, as mentioned previously.



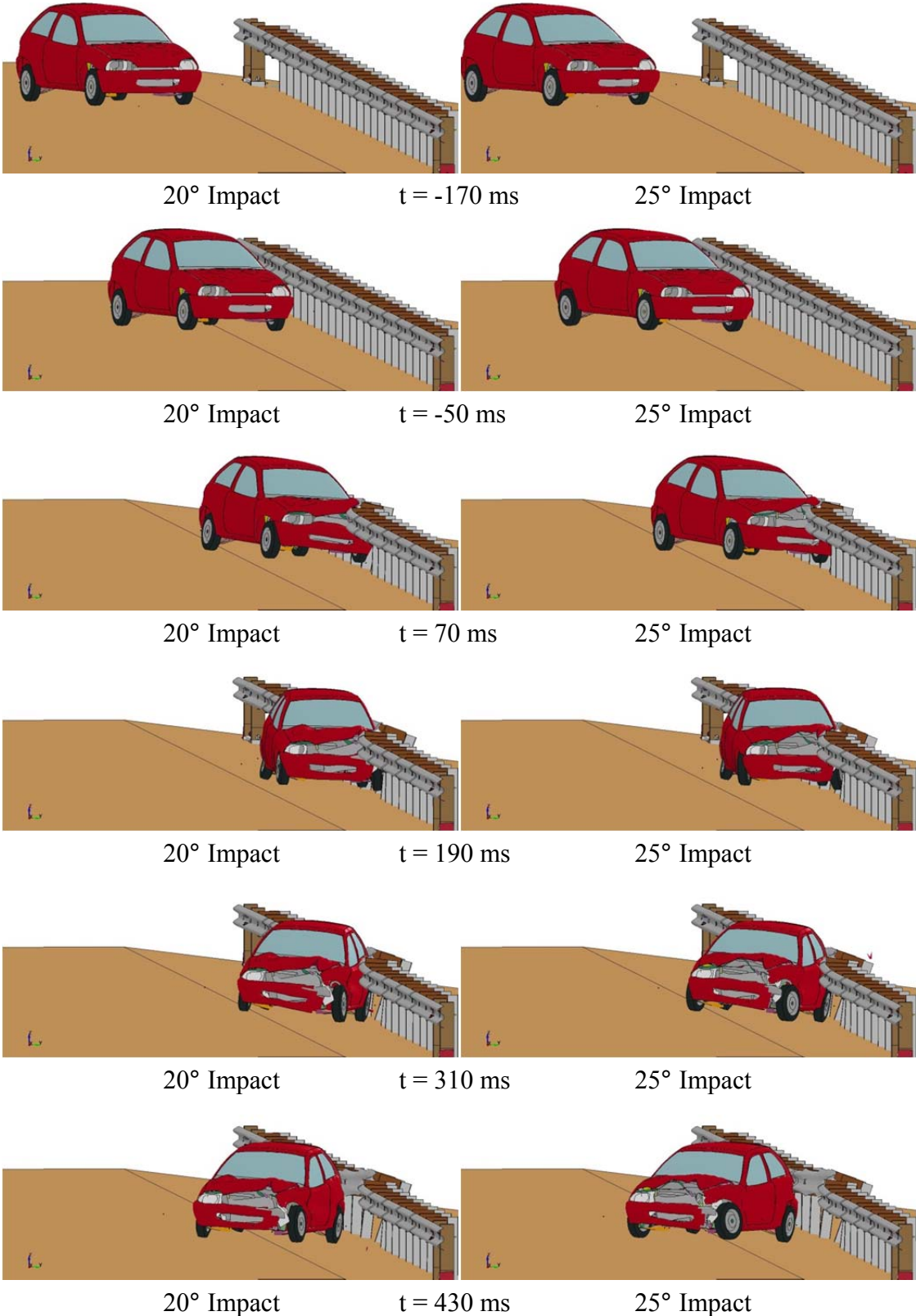


Figure 65. Sequential of 20- and 25-degree Impacts at 34-in. (864-mm) Top-Rail Height

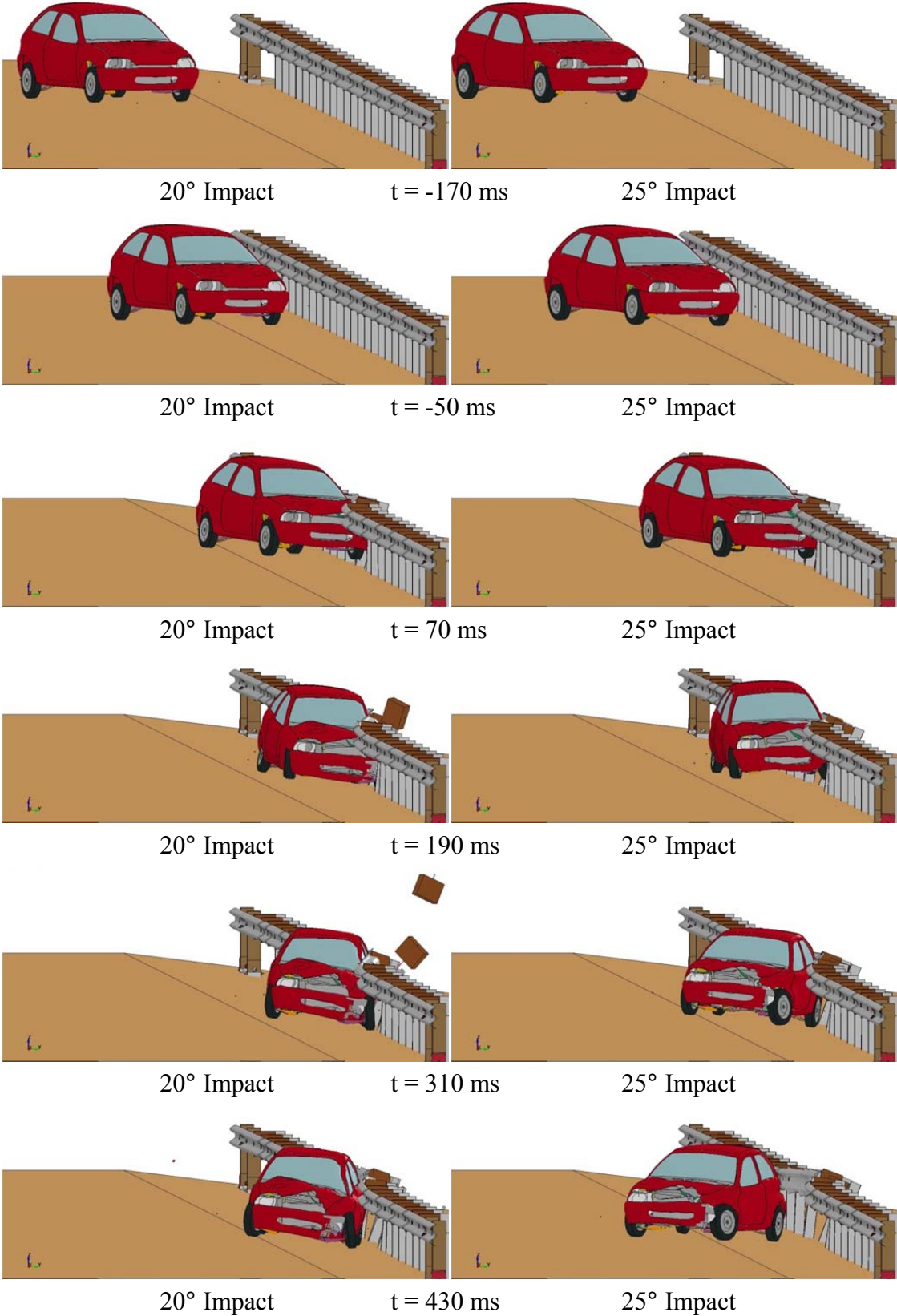


Figure 66. Sequential of 20- and 25-degree Impacts at 36-in. (914-mm) Top-Rail Height

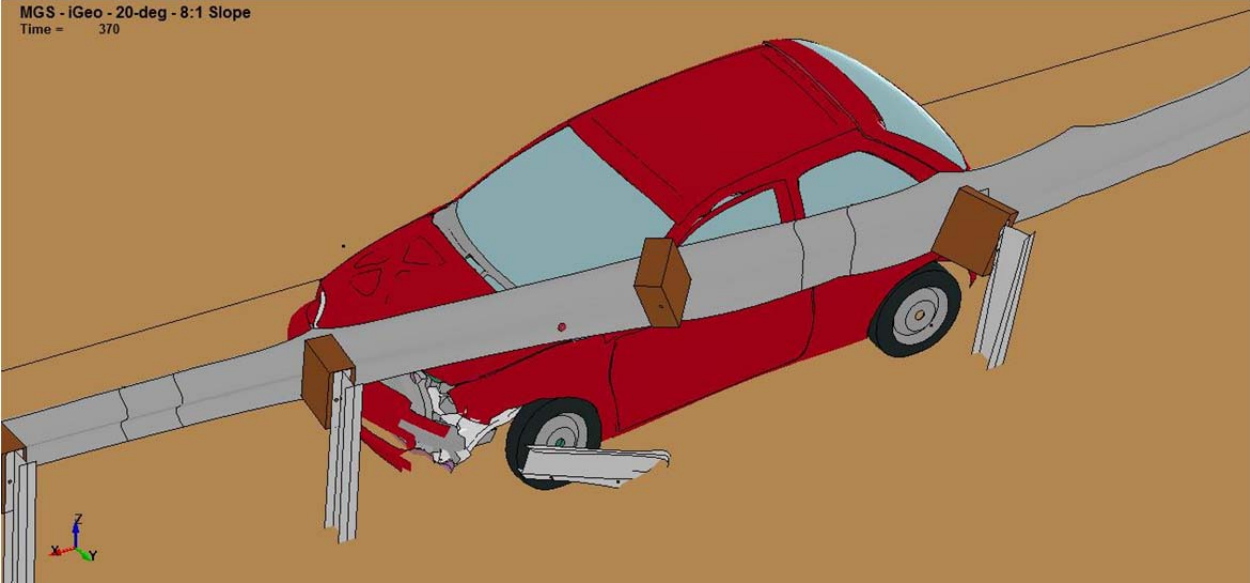


Figure 67. Crushing of A-Pillar

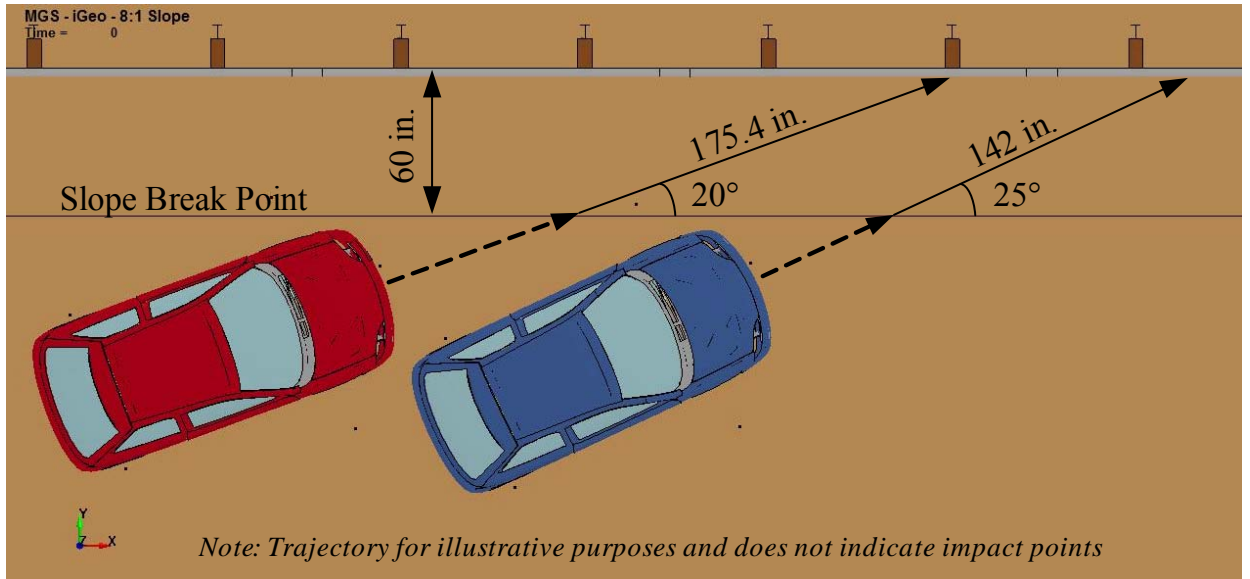


Figure 68. Vehicle Trajectory Across Approach Slope

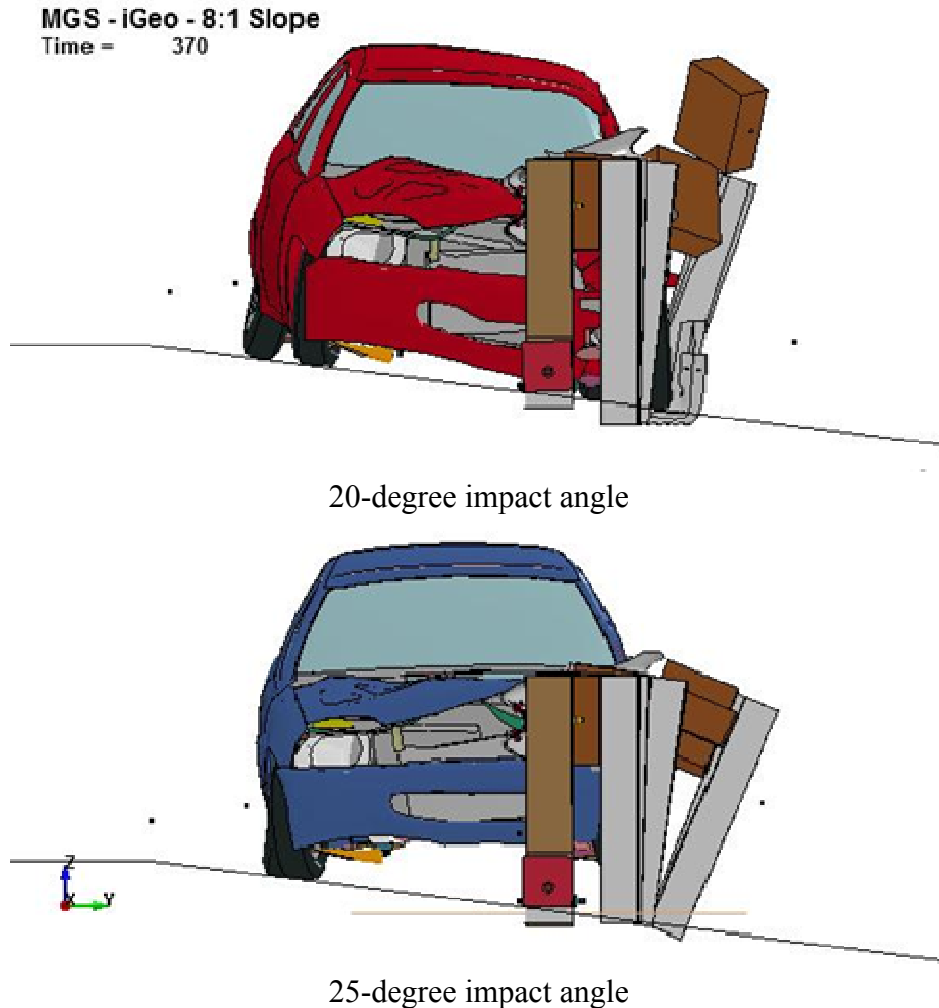


Figure 69. Vehicle Underride at 36 in. (914 mm)

### 9.3.4 Comparison of Test Conditions and Simulation Results

Comparison of the six simulations and test no. MGSAS-2 were done as a validation for the original model and to provide a more complete understanding of the effects of each simulation.

It was clear that the simulation of the MGSAS-2 did a very good job predicting the test results. Furthermore, as the rail height was increased, the vehicle underrode the system. The underride distance was calculated from the simulations using the left-front corner as a reference point. This point was tracked throughout the impact, and the distance the vehicle traveled

laterally into the barrier was found. Then, the dynamic deflection of the rail was subtracted, giving an estimate of the total distance the car underrode the barrier. All evaluation parameters and simulation results are shown in Table 22.

Table 22. Simulation Results for 820C Vehicle on 8:1 Approach Slope

Evaluation Parameters		Test No. MGSAS-2	Simulation Conditions and Results					
			31-in. Simulation	31-in. Simulation	34-in. Simulation	34-in. Simulation	36-in. Simulation	36-in. Simulation
<b>Tested Impact Angle</b>	deg	21.63	20	25	20	25	20	25
<b>Top Rail Height</b>	in. (mm)	31 (787)	31 (787)	31 (787)	34 (864)	34 (864)	36 (914)	36 (914)
<b>Tested Vehicle Mass</b>	lb (kg)	2011 (912)	1982 (899)	1982 (899)	1982 (899)	1982 (899)	1982 (899)	1982 (899)
<b>Impact Velocity</b>	mph (km/h)	61.9 (99.62)	62.1 (100)	62.1 (100)	62.1 (100)	62.1 (100)	62.1 (100)	62.1 (100)
<b>Barrier Offset on Slope</b>	in. (mm)	60 (1524)	60 (1524)	60 (1524)	60 (1524)	60 (1524)	60 (1524)	60 (1524)
<b>Parallel Time</b>	ms	156	145	153	160	173	224	174
<b>Parallel Velocity</b>	mph (km/h)	52.6 (84.7)	55.2 (88.9)	54.1 (87.1)	51.6 (83.5)	52.2 (84.0)	47.6 (76.6)	52.3 (84.1)
<b>Dynamic Rail Deflection</b>	in. (mm)	-25.0 (-635)	-20.0 (-509)	-21.4 (-543)	-19.7 (-501)	-23.1 (-586)	-24.1 (-612)	-24.4 (-621)
<b>Working Width</b>	in. (mm)	46.5 (1182)	41.1 (1044)	42.4 (1078)	40.8 (1036)	44.1 (1121)	45.2 (1147)	45.5 (1156)
<b>Working Width Indicator</b>	-	Post	Post	Post	Post	Post	Post	Post
<b>Exit Time</b>	ms	372	300	320	390	380	500	380
<b>Resultant Velocity at Exit</b>	mph (km/h)	51.5 (82.9)	53.7 (86.4)	53.0 (85.3)	47.4 (76.3)	51.0 (82.0)	38.8 (62.4)	51.0 (82.1)
<b>Underride Distance</b>	in. (mm)	0 (0)	0 (0)	0 (0)	5.6 (141)	5.9 (149)	8.4 (214)	8.5 (217)
<b>Exit Angle</b>	deg	-8.23	-12.4	-12.1	-14.5	-18.1	-6.45	-17.55
<b>Pass/Fail</b>	-	Pass	Pass	Pass	Pass	Pass	Fail	Pass

It was interesting to note that the increased impact angle did not cause much increased underride. Instead, rail deflection increased. The underride was still very much associated with the vehicle front-end geometry in relation to the rail. At a 36-in. (914-mm) top-rail height, the 25-degree impact angle increased the rail deflection and the underride distance by a great margin over the 20-degree impact angle. The increased rail deflection over the 34-in. (864-mm) system was systematic and due to decreased embedment depth and decreased post stiffness. At a 25-degree impact angle, the vehicle maintained a more level trajectory throughout the impact. This kept the bumper of the vehicle higher off the ground up to parallel, which prevented the rail from riding over the hood and into the A-pillar.

Parallel velocities consistently decreased across the simulations aside from the 20-degree, 36-in. (914-mm) top-rail height simulation, which ultimately was deemed to be unacceptable. The underride exhibited by this impact caused increased rail contact and slowed the vehicle more than simulations in which safe redirection was shown. Similarly exit velocities were consistently decreasing across simulation runs.

Exit vectors were higher than shown by the full-scale crash test. This was due to the steering mechanism differences and subsequent wheel reaction differences previously noted. As shown by the baseline simulation, the wheels tended to turn away from the barrier in the simulations rather than into the barrier, as exhibited by test no. MGSAS-2.

#### **9.4 Underride on 6:1 Approach Slope with 820C**

Good barrier performance was shown for small cars in 8:1 approach slope simulations. This suggested that the MGS may be safely used on steeper slopes. Previous simulations performed by researchers at the MwRSF have shown that the pickup truck will override the MGS system at the standard mounting height when placed on 6:1 approach slopes [31, 32]. For this reason the MGS was limited to placement on 8:1 or flatter approach slopes. An MGS that

would be allowed on steeper slopes using an increased rail height would provide more flexibility to highway engineers and designers.

Two impact angles, 20 and 25 degrees, were again chosen to examine the effects of increased barrier height and steeper approach slopes. For comparison, barrier heights of 31, 34, and 36 in. (787, 864, and 914 mm) were again used, and the front face of the MGS was placed 5 ft (1.5 m) away from the slope break point. It should be noted that, due to the increased slope with the same lateral offset, the barrier was effectively placed 2.5 in. (64 mm) lower than a similarly offset barrier on an 8:1 approach slope. The trajectory of the vehicle as it traversed the slope break point and lost contact with the ground was similar in both approach slope cases.

#### **9.4.1 Simulation at 31-in. (787-mm) Rail Height**

At a rail height of 31 in. (787 mm) and a 5-ft (1.5-m) lateral offset on a 6:1 approach slope, the vehicle was smoothly redirected, and no adverse observable conditions were present that would affect the MGS's effectiveness in redirecting an 820C small car. However, prior research has shown that pickup trucks impacting a 31-in. (787-mm) system on 6:1 approach slopes will override the system, thus rendering it unusable in practice [31, 32]. A sequential of the system redirecting the small car is shown in Figure 70.

It was clear that the increased slope and the additional 2.5 in. (64 mm) of rail drop caused the vehicle to impact the rail at a lower position on the bumper. This condition caused the car to roll more laterally over the barrier. This was the same reason that light trucks have failed at this rail height on a 6:1 approach slope.

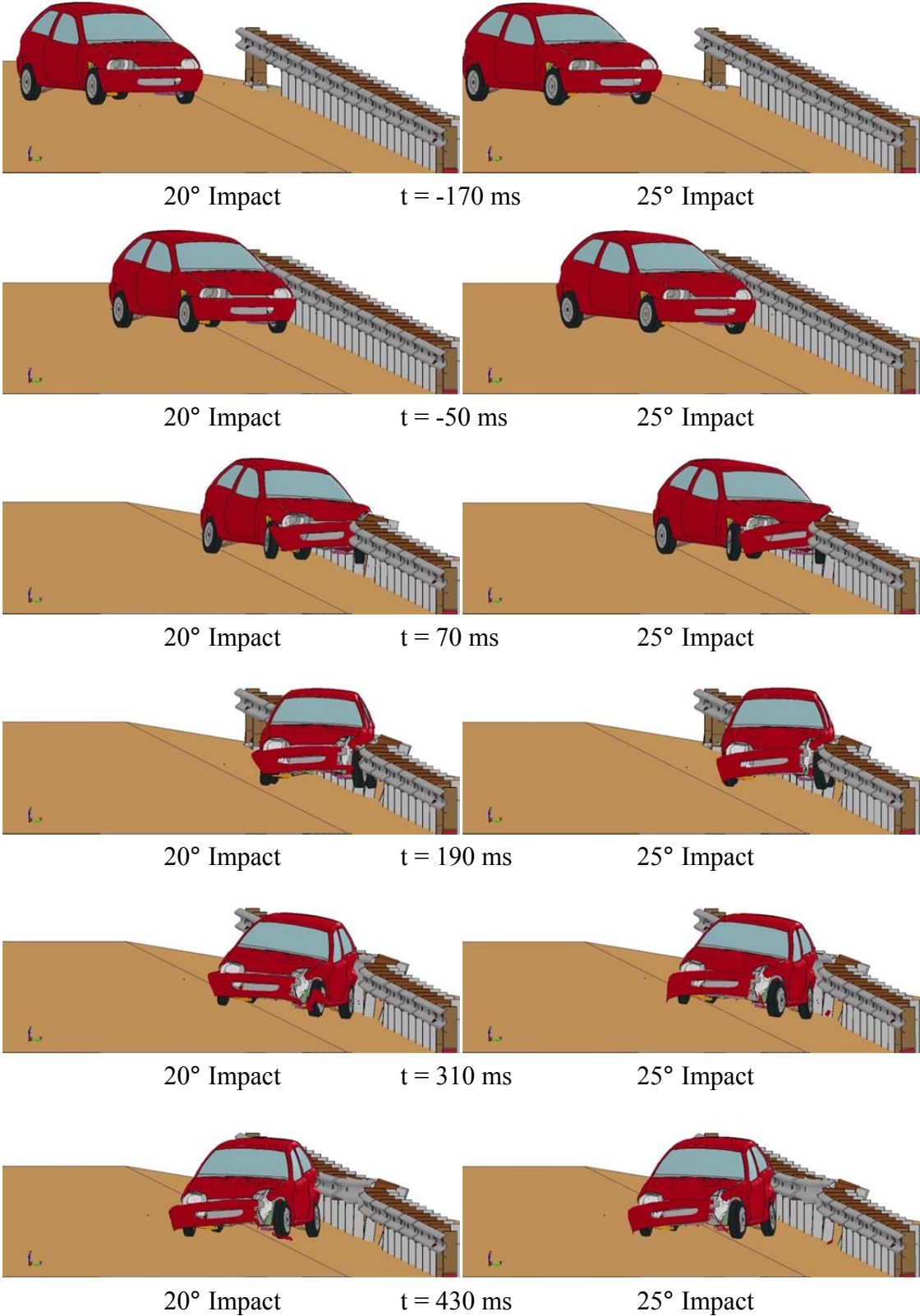


Figure 70. Sequential of 20- and 25-degree Impacts at 31-in. (787-mm) Top-Rail Height



#### **9.4.2 Simulation at 34-in. (864-mm) Rail Height**

At a rail height of 34 in. (864 mm) and a 5-ft (1.5-m) lateral offset on a 6:1 approach slope, the small car again was smoothly redirected, and no adverse observable conditions were present that would affect the MGS's ability to redirect an 820C small car. A sequential of the system redirecting the small car is shown in Figure 71.

Again, due to the increased slope and constant offset, as compared to the 8:1 approach slopes previously discussed, the rail was essentially placed 2.5 in. (64 mm) lower in relation to the road. This made the top of the 34-in. (864-mm) rail on a 6:1 approach slope effectively the same height in relation to the level roadway as a 31.5-in. (800-mm) rail on an 8:1 approach slope, making it very comparable to the 31-in. (787-mm) height tested on the 8:1 approach slope. Visually and numerically, the results are very comparable.

#### **9.4.3 Simulation at 36-in. (914-mm) Rail Height**

At a rail height of 36 in. (914 mm) with a 5-ft (1.5-m) lateral offset on a 6:1 approach slope, the small car was smoothly redirected, and no adverse observable conditions were present that would affect the MGS's ability to redirect an 820C small car. A sequential of the system redirecting the small car is shown in Figure 72.

Much like the discussion of the 34-in. (864-mm) system on a 6:1 approach slope, the increased slope and constant lateral offset made the top of the 36-in. (914-mm) system analogous to a 33.5-in. (851-mm) system on an 8:1 approach slope in relation to the level roadway, making it very comparable to the 34-in. (864-mm) height tested on the 8:1 approach slope. Due to this relationship, it was expected that underride would be shown at this height, which was indeed the case. At an impact angle of 25 degrees, the vehicle underrode a distance of approximately 4.7 in. (120 mm). Underride was not shown on the 20-degree system, leading to the understanding that this height was the maximum height before underride would begin.

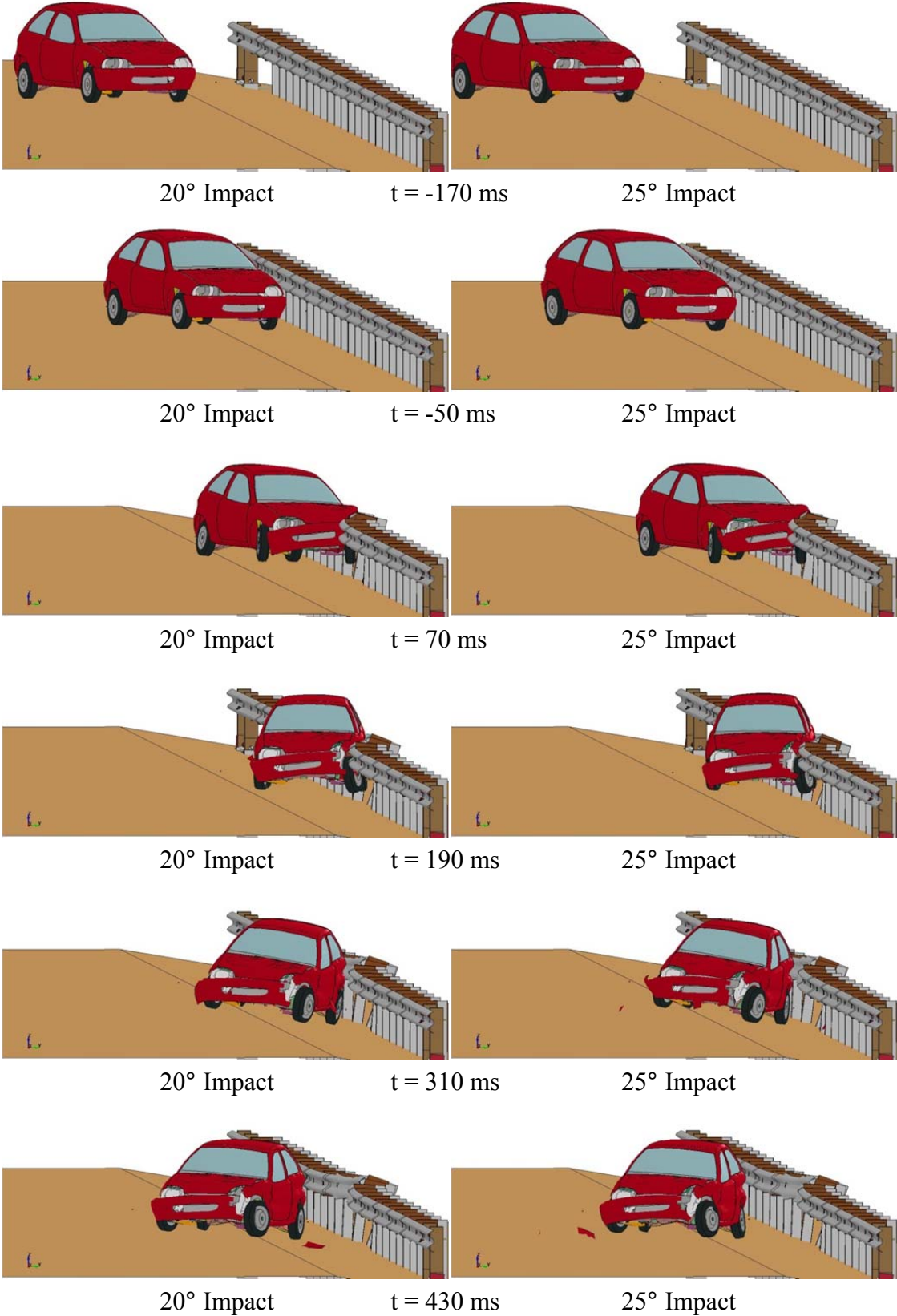


Figure 71. Sequential of 20- and 25-degree Impacts at 34-in. (864-mm) Top-Rail Height

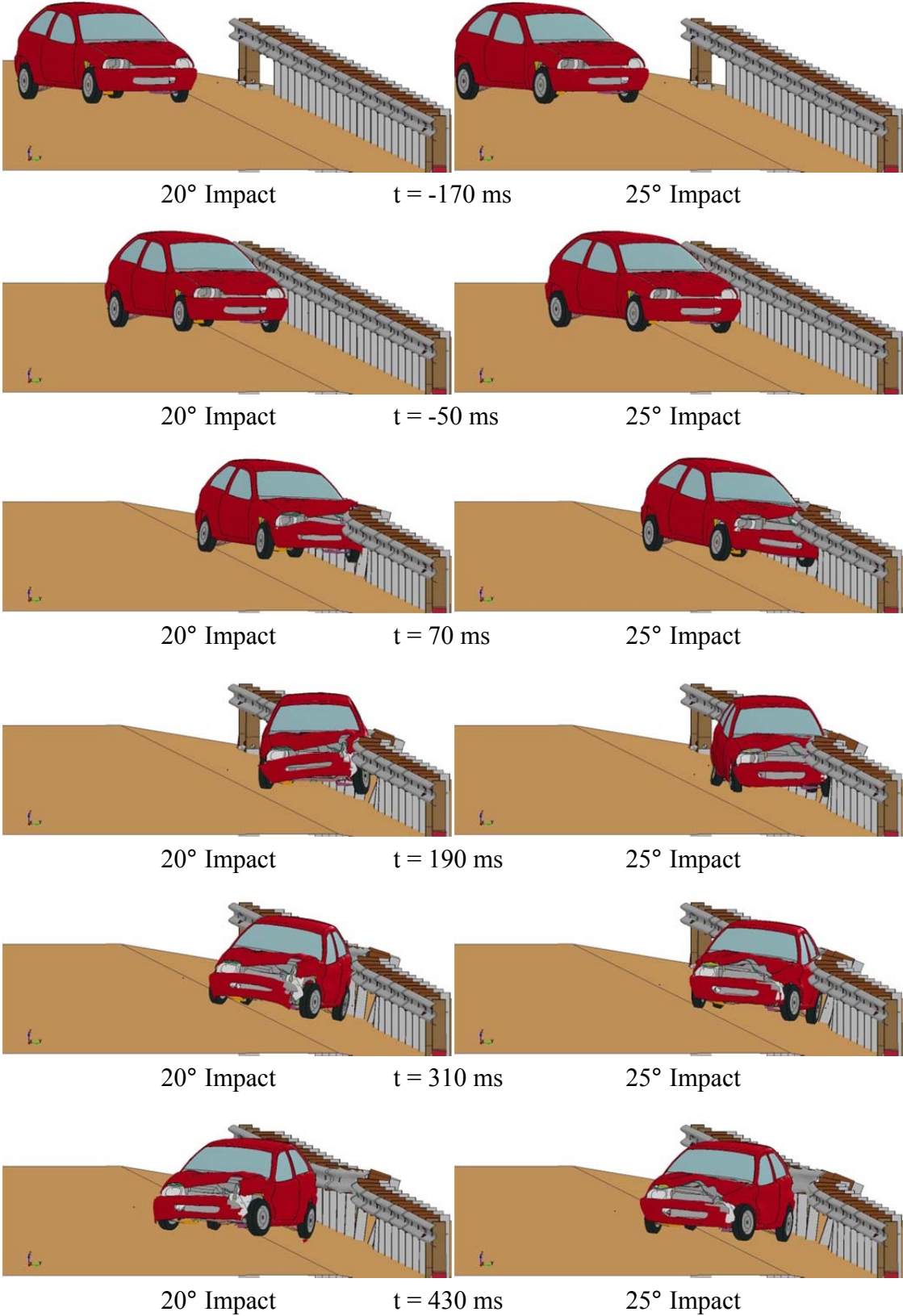


Figure 72. Sequential of 20- and 25-degree Impacts at 36-in. (914-mm) Top-Rail Height

The increased lateral velocity of a 25-degree impact angle over a 20-degree impact angle caused increased impact severity. However, this increased angle caused the car to rotate an additional 5 degrees to become parallel with the system, resulting in additional deceleration before the vehicle became parallel, as shown across all tests in Table 23. The additional deceleration at this height was just enough to allow the vehicle to drop vertically downward and slide under the barrier.

#### **9.4.4 Comparison of Test Conditions and Simulation Results**

A comparison of the six simulations was performed to provide a more complete understanding of the results of each simulation. The evaluation parameters and their results are shown in Table 23.

The vehicle did not underride the system as much as shown on an 8:1 approach slope. As mentioned, the vehicle trajectory was based on velocity and angle, and the trajectories shown are the same for each test. Thus, the vehicle impacted the rail at a different relative height. From Tables 22 and 23, underride occurred when the top of the rail was at a relative 26-in. (660-mm) vertical height above the road grade at a 5-ft (1.5-m) lateral offset. This concept is shown in Figure 73.

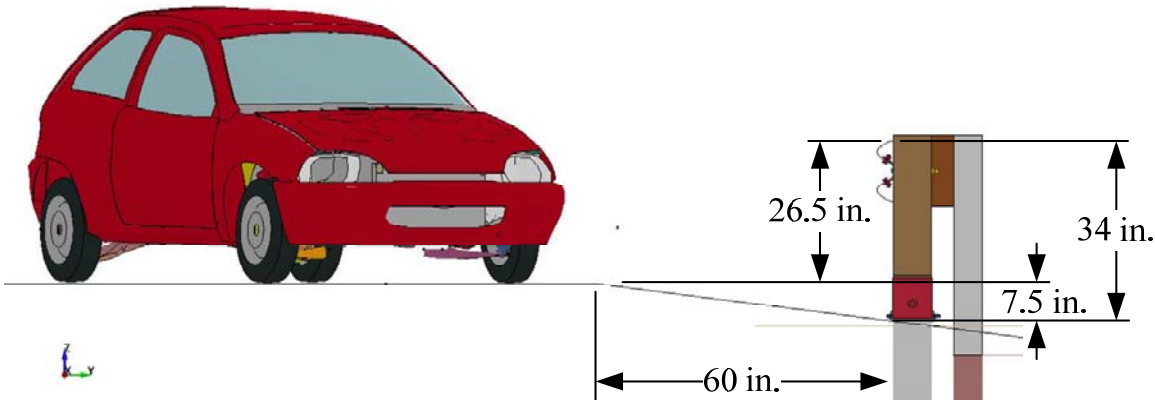
Although the rails were positioned at different top-rail mounting heights in relation to the slope, the top of the rail was at a similar distance above the flat roadway in both cases. In this range of heights on these slopes, it is analogous to compare the MGS at 36 in. (914 mm) on a 6:1 approach slope to the MGS at 34 in. (864 mm) on an 8:1 approach slope. Due to this fact, it was likely that an 820C small car traveling at an impact speed of 62.1 mph (100 km/h) would likely pass at rail heights up to 38 in. (965 mm) on this slope. However, it is undesired to increase the rail to this height because underride occurred on flat ground at 37 in. (940 mm). Further,

decreased impact angles or decreased speeds could allow the vehicle's trajectory to more closely follow the slope and override the MGS system.

Table 23. Simulation Results for 820C Vehicle on 6:1 Approach Slope

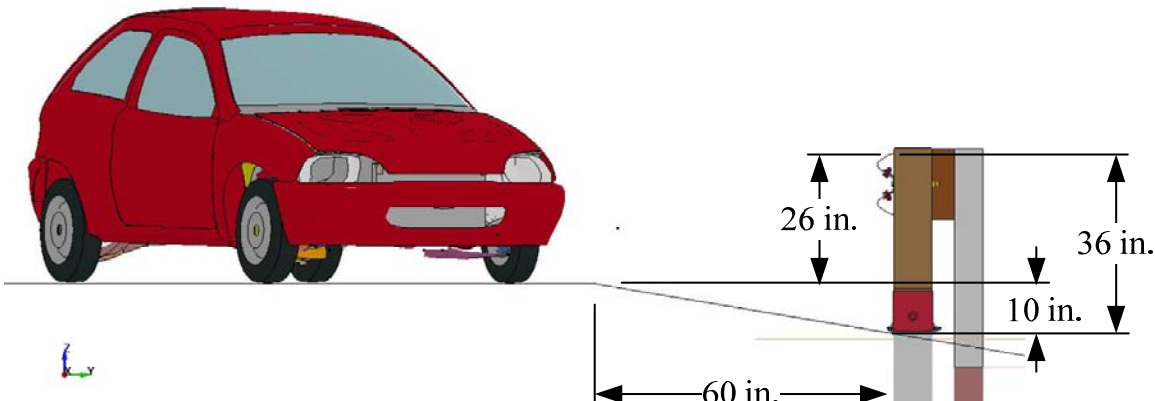
Evaluation Parameters	Units	Test Conditions and Results					
		31-in. Simulation	31-in. Simulation	34-in. Simulation	34-in. Simulation	36-in. Simulation	36-in. Simulation
<b>Tested Impact Angle</b>	deg	20	25	20	25	20	25
<b>Top Rail Height</b>	in. (mm)	31 (787)	31 (787)	34 (864)	34 (864)	36 (914)	36 (914)
<b>Tested Vehicle Mass</b>	lb (kg)	1982 (899)	1982 (899)	1982 (899)	1982 (899)	1982 (899)	1982 (899)
<b>Impact Velocity</b>	mph (km/h)	62.1 (100)	62.1 (100)	62.1 (100)	62.1 (100)	62.1 (100)	62.1 (100)
<b>Barrier Offset on Slope</b>	in. (mm)	60 (1524)	60 (1524)	60 (1524)	60 (1524)	60 (1524)	60 (1524)
<b>Parallel Time</b>	ms	143	147	147	151	152	174
<b>Parallel Velocity</b>	mph (km/h)	55.1 (88.7)	53.9 (86.8)	55.2 (88.9)	54.4 (87.6)	55.1 (88.7)	52.4 (84.4)
<b>Dynamic Rail Deflection</b>	in. (mm)	-19.4 (-492)	-20.8 (-528)	-21.2 (-539)	-22.5 (-571)	-22.5 (-572)	-22.8 (-578)
<b>Working Width</b>	in. (mm)	40.4 (1027)	41.9 (1063)	42.3 (1074)	43.5 (1106)	43.6 (1107)	43.8 (1113)
<b>Working Width Indicator</b>	-	Post	Post	Post	Post	Post	Post
<b>Exit Time</b>	ms	300	300	300	300	310	370
<b>Resultant Velocity at Exit</b>	mph (km/h)	53.9 (86.8)	52.8 (85.0)	55.1 (88.6)	54.0 (86.9)	54.6 (87.8)	50.8 (81.7)
<b>Underride Distance</b>	in. (mm)	0 (0)	0 (0)	0 (0)	0 (0)	0 (0)	4.7 (120)
<b>Exit Angle</b>	deg	-13.03	-12.96	-12.98	-12.49	-13.26	-14.2
<b>Pass/Fail</b>	-	Pass	Pass	Pass	Pass	Pass	Pass

MGS - iGeo - 25-deg - 8:1 Slope  
Time = 0



MGS at 34 in. (864 mm) on 8:1 Approach Slope

MGS-36 - iGeo - 25-deg - 6:1 Slope  
Time = 0



MGS at 36 in. (914 mm) on 6:1 Approach Slope

Figure 73. MGS on Approach Slope in Relation to Road Grade

**9.5 Override on 6:1 Approach Slope with 2270P at 5-ft (1.5-m) Offset**

By increasing the rail height to prevent pickup truck override, the usable range of the MGS would expand to include 6:1 fill slopes. Although the increased rail height provided stable and smooth redirection for the 820C vehicle, it was necessary to also simulate the same MGS system with a 2270P pickup truck to examine the potential for override and vehicular instabilities during redirection.

Suspension failure has been shown to provide stability in full-scale crash tests as the front-end of the pickup truck drops toward the ground. Differences between the simulation model and full-scale crash test vehicle suspension systems, as well as LS-DYNA model simplifications, caused the pickup truck suspension model to not exhibit the same failure as shown in full-scale tests. For this reason, two models were run - one without prescribed suspension failure and one with prescribed suspension failure just prior to the time of the highest joint forces.

#### **9.5.1 Simulation at 31-in. (787-mm) Rail Height**

On a 6:1 fill slope, previous simulations have shown that a 31-in. (787-mm) top-rail height was inadequate to contain a 2000P vehicle [31, 32]. Thus, it was fully expected that a 2270P vehicle would also not be contained by a 31-in. (787-mm) tall rail. This was true with and without suspension failure. Both simulations had instabilities roughly 240 ms after impact, causing the simulation to error out. However, at the point of simulation termination, override was already exhibited, indicating that the test would fail. Without suspension failure, the truck rolled over the barrier. In contrast, the truck was overrode the barrier when suspension failure was prescribed, as shown in Figure 74.

Suspension failure allowed for the truck to slide up and over the rail, as shown more closely in Figure 75. This vehicle override tendency also increased the risk of the vehicle to strike any fixed objects located behind the barrier.

Clear system failure and unacceptable vehicle behavior was apparent for a 2270P vehicle impacting into a 31-in. (787-mm) tall MGS barrier placed on a 6:1 fill slope. As mentioned, an increased rail height of 36-in. (914-mm) may allow the MGS to be placed on 6:1 fill slopes while safely containing both pickup trucks and small cars.

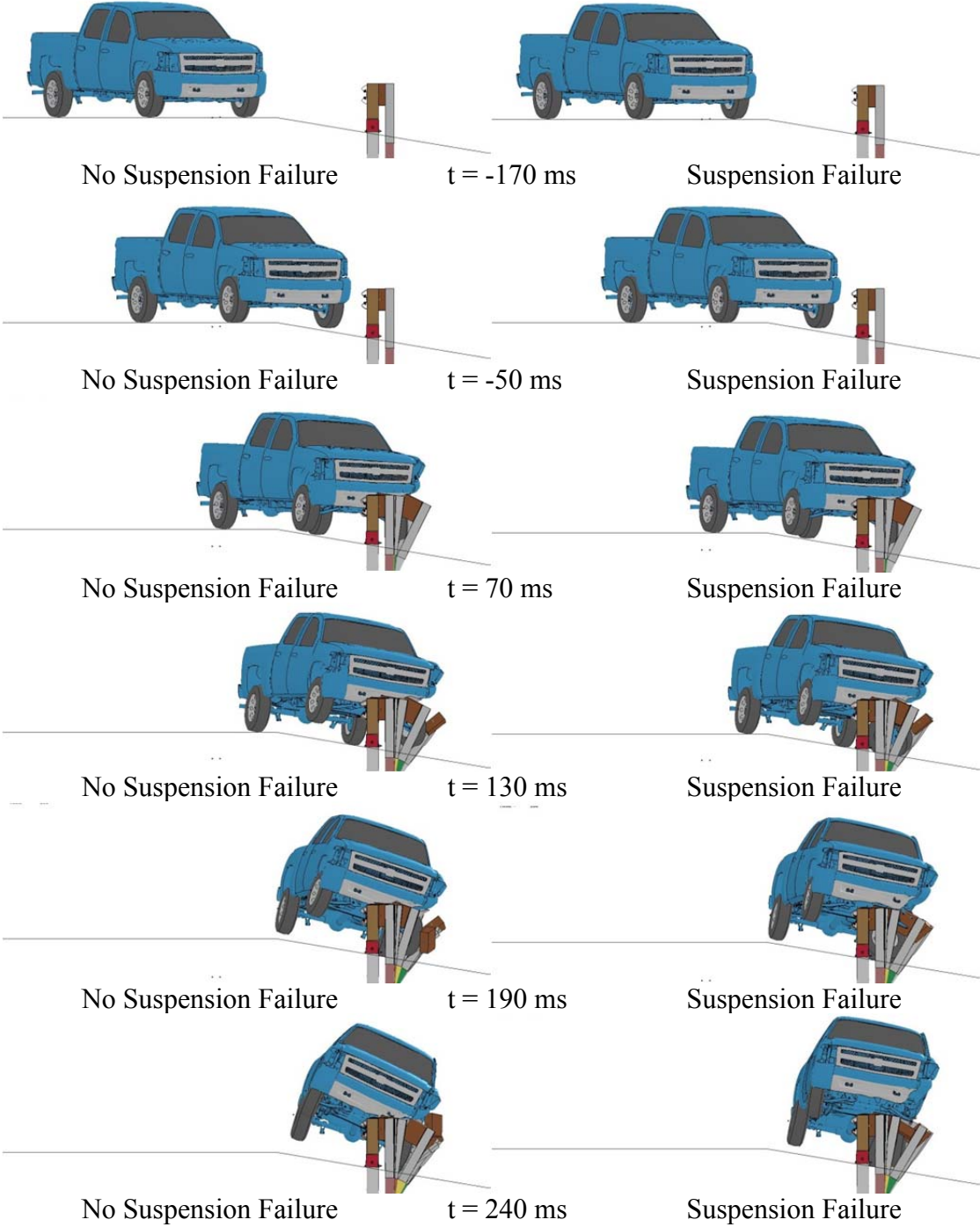


Figure 74. 2270P Simulation at 31-in. (787-mm) Top-Rail Height on 6:1 Approach Slope



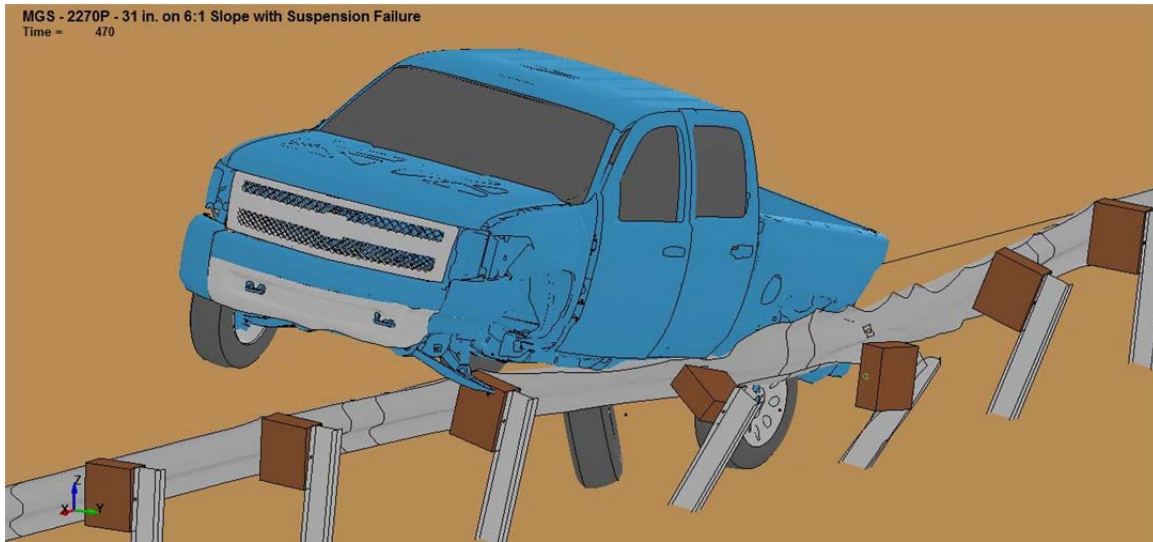


Figure 75. 2270P Override at 31-in. (787-mm) Rail Height on 6:1 Approach Slope

### **9.5.2 Simulation at 34-in. (864-mm) Top-Rail Height**

At a 34-in. (864-mm) top-rail height, the pickup truck was safely contained and redirected in the simulations. The pickup truck experienced moderate roll and pitch angles, which were within acceptable limits, as shown in Figure 76. In many full-scale crash tests, it has been shown that suspension failure may help to stabilize the trajectory of the pickup truck and prevent rollover. In these simulations, suspension failure may result in more severe consequences. Furthermore, these simulations appeared to marginally meet the required evaluation criteria pertaining to vehicle stability upon redirection.

### **9.5.3 Simulation at 36-in. (914-mm) Top-Rail Height**

Simulations at a 36-in. (914-mm) top-rail height on a 6:1 fill slope showed acceptable vehicle containment and redirection for cases with and without suspension failure. The 36-in. (914-mm) rail height kept the pickup truck closer to the ground than for the 31-in. (787-mm) or 34-in. (864-mm) rail heights, thus maintaining a more level redirection trajectory, lower pitch, and lower roll throughout the impact event.

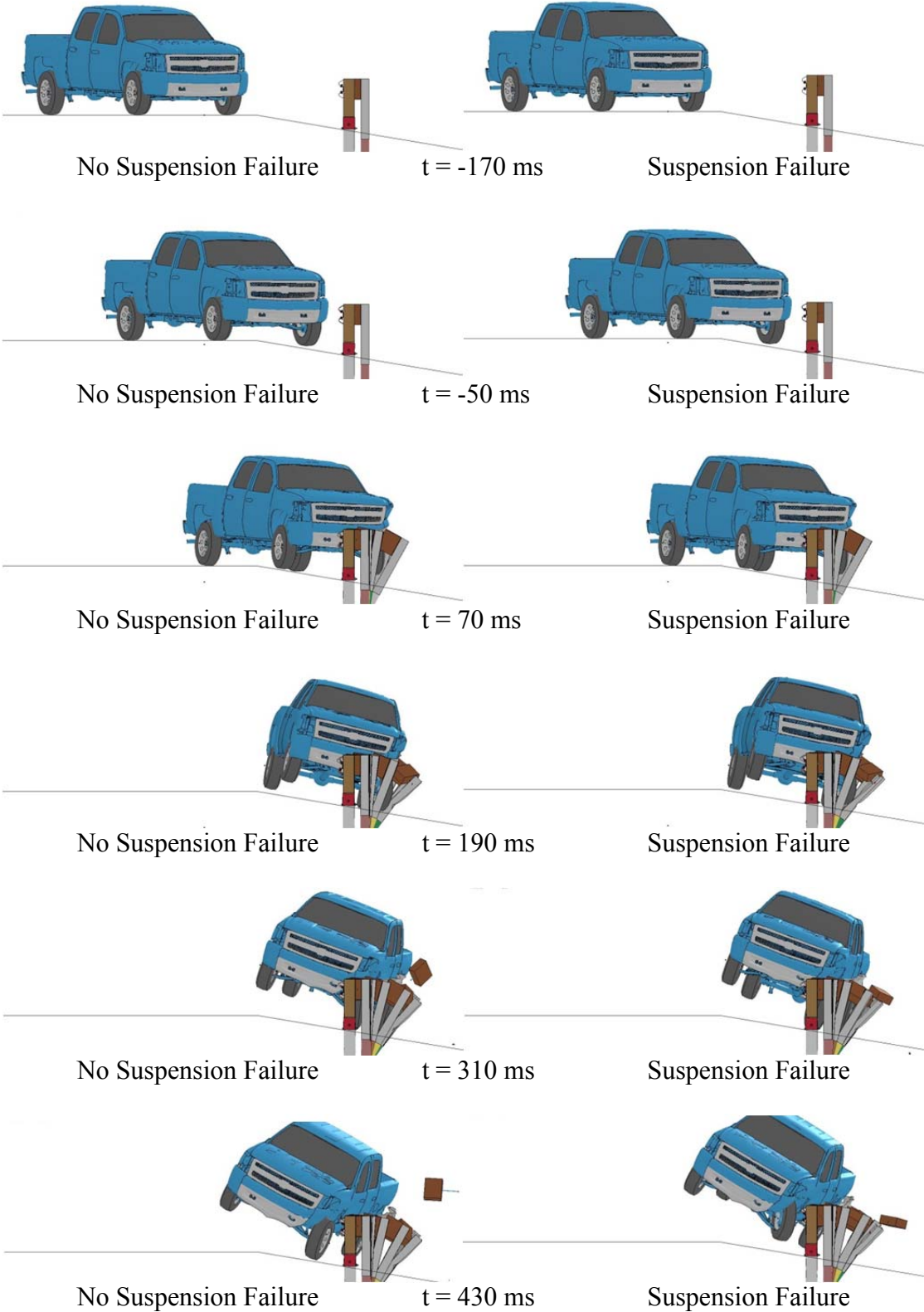


Figure 76. 2270P Simulation at 34-in. (864-mm) Top-Rail Height on 6:1 Approach Slope

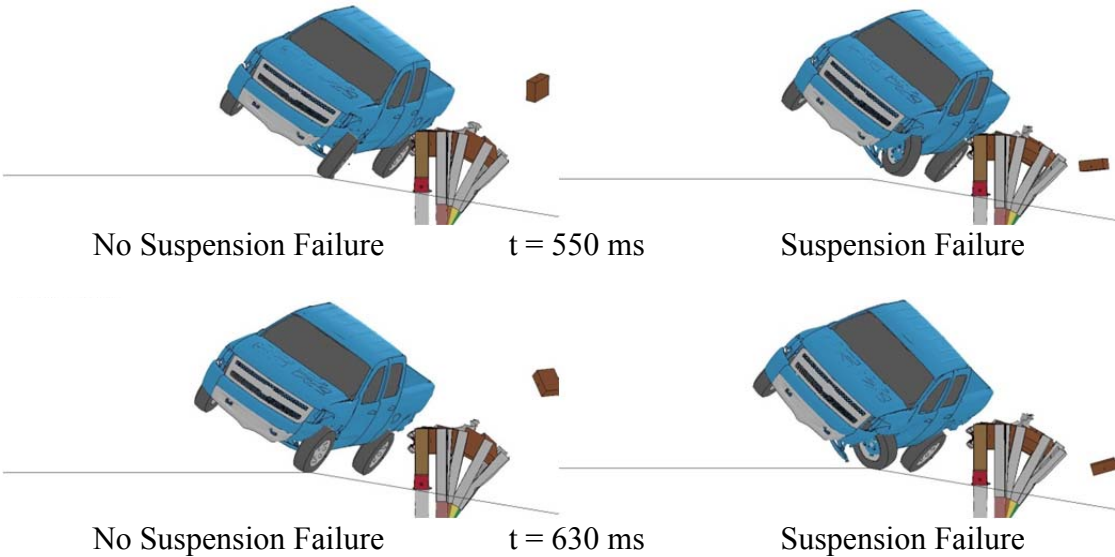


Figure 76. 2270P Simulation at 34-in. (864-mm) Top-Rail Height on 6:1 Approach Slope (continued)

With suspension failure prescribed, the wheel became detached and pushed up into the undercarriage at roughly 290 ms after impact, as shown in Figure 77. Simplifications of the tire model did not allow for tire deflation, which could be attributed to the degree of simulation pitch. The pickup truck landed on the inflated tire which pushed the truck upward and airborne. Physically, this behavior was highly unlikely as the tire would deflate.

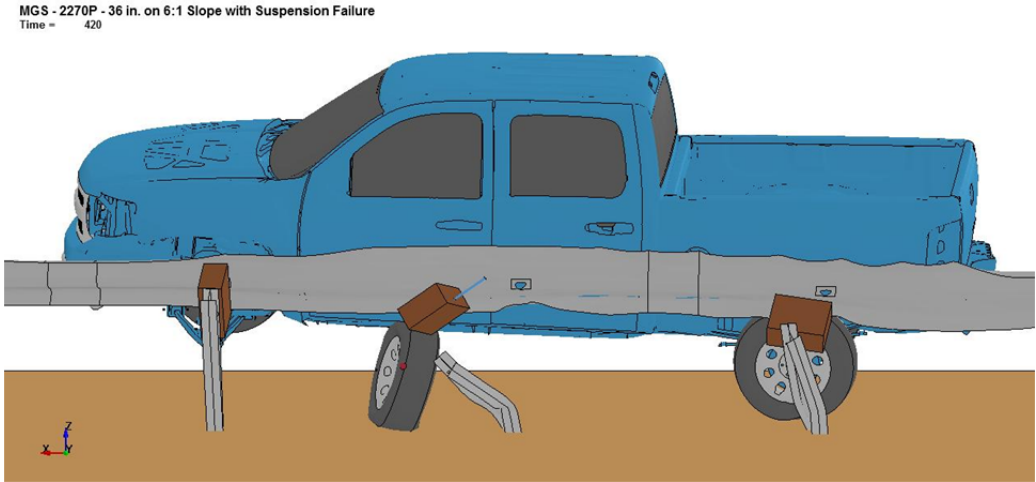


Figure 77. Wheel Contacting Undercarriage of Truck

Although the truck rolled into the barrier, it remained upright throughout the impact event. These simulations would suggest that at a 5-ft (1.5-m) lateral offset and at a 36-in. (914-mm) nominal top-rail mounting height, the 2270P vehicle would be safely redirected, as shown in Figure 78. 2270P Simulation at 36-in. (914-mm) Top-Rail Height on 6:1 Approach Slope

. In addition, due to the clear failure at the 31-in. (787-mm) top-rail mounting height and the clear success at the 36-in. (914-mm) top-rail mounting height, a minimum nominal top rail mounting height of 33.5 in. (851-mm) was recommended.

It was clear from these simulations that increased rail heights may allow the MGS to be installed on steeper slopes and still safely accommodate 2270P vehicles.

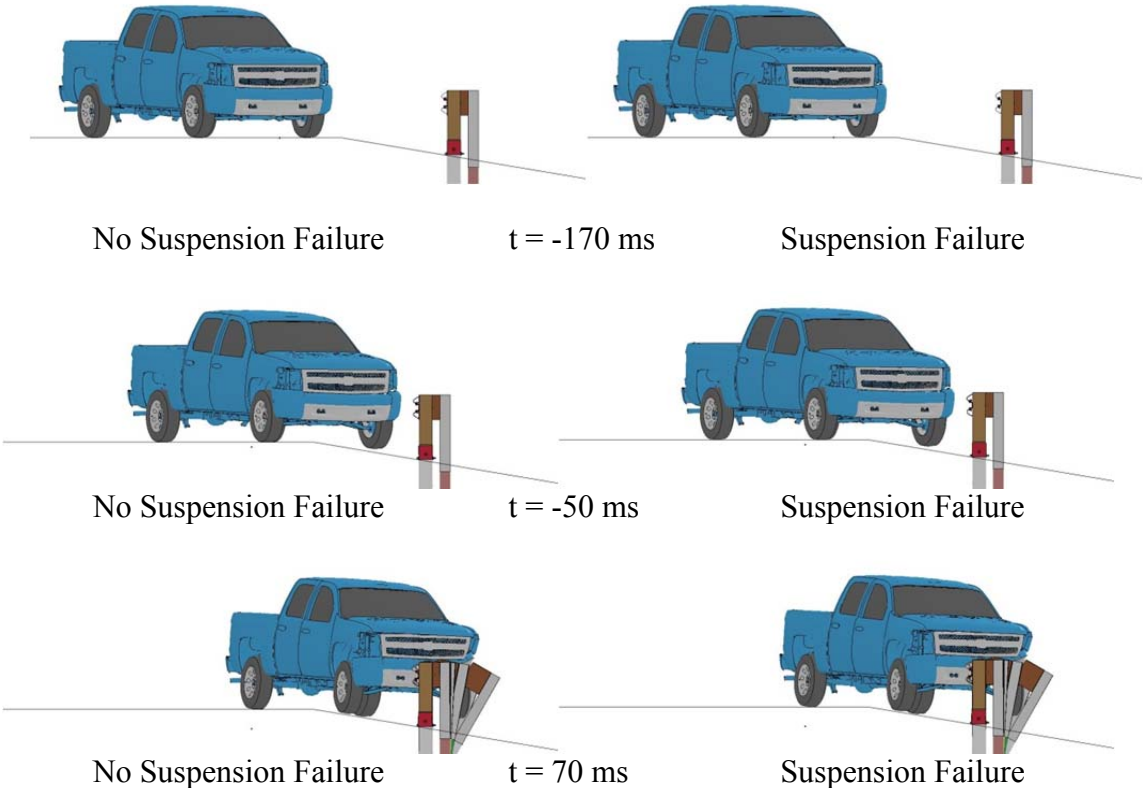


Figure 78. 2270P Simulation at 36-in. (914-mm) Top-Rail Height on 6:1 Approach Slope

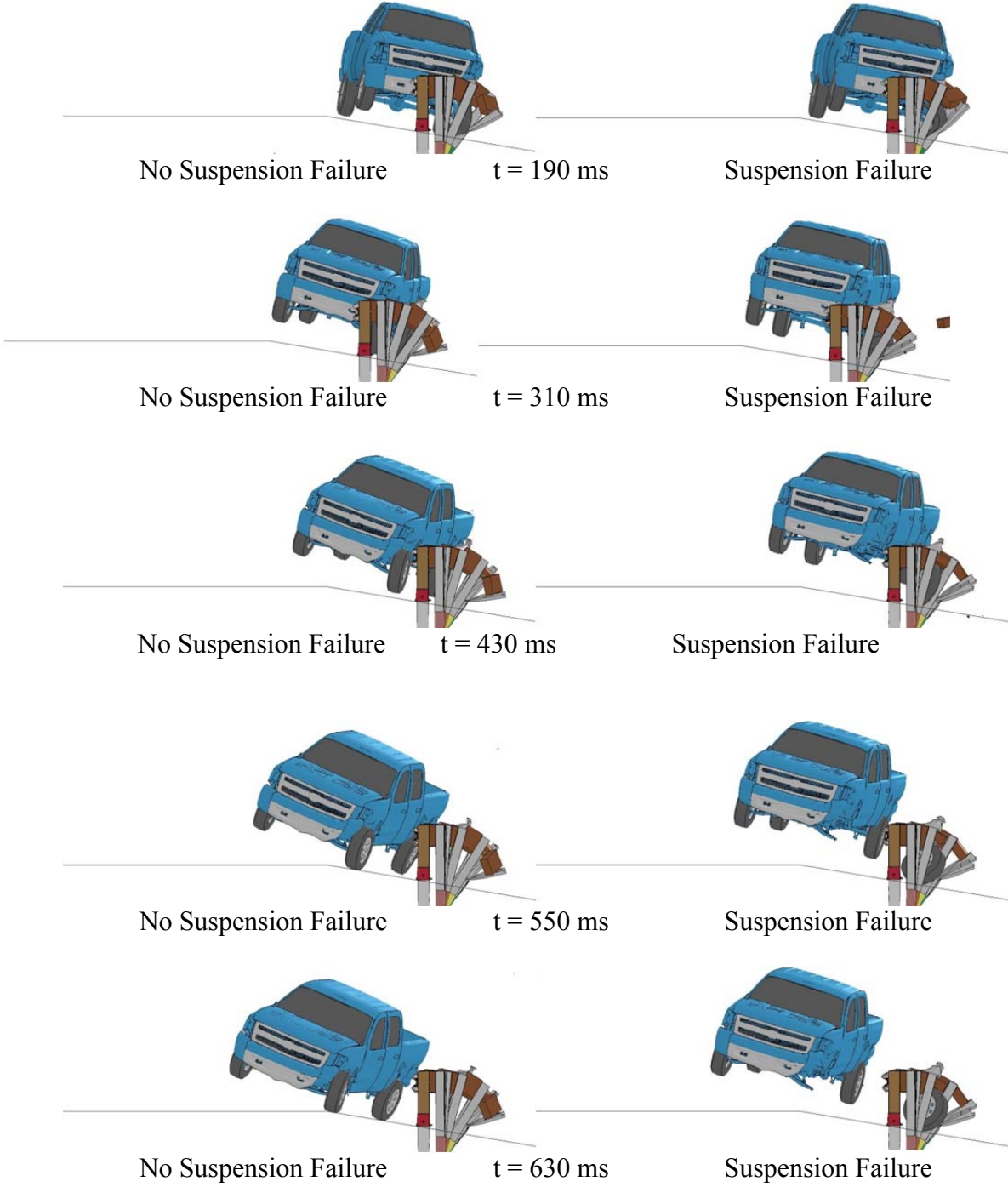


Figure 78. 2270P Simulation at 36-in. (914-mm) Top-Rail Height on 6:1 Approach Slope (continued)

### **9.5.1 Comparison of Test Conditions and Simulation Results**

Simulations were compared to garner a clear picture of the vehicle reaction and the barrier effectiveness at the varying rail heights on a 6:1 fill slope. The simulation results are shown in Table 24. Several results from the 31-in. (787-mm) top-rail height MGS simulations were not documented due to the failure of the system.

The increased roll angle observed in the 34-in. (864-mm) top-rail height simulation, from 33.6 to 42.7 degrees, was due to the nature of the suspension failure. The detached wheel allowed the vehicle body to roll more upon exit because there was no left-front wheel to come down on as it exited the system.

In the 36-in. (914-mm) top-rail height simulation, the vehicle reacted differently. Since the rail was higher and caught the pickup truck closer to the CG, it kept the truck more level throughout the impact event and reduced the magnitude of roll observed in the 34-in. (864-mm) top-rail height simulation. When suspension failure was prescribed, the roll motion was decreased from 23.6 to 15.6 degrees. As the wheel came in contact with the undercarriage, it caused the entire truck to vault and become airborne, increasing pitch. Despite this, all of the evaluation criteria were deemed acceptable. In all cases, except the 31-in (787-mm) top-rail height simulations, the truck returned to the ground in a level position during redirection after exit. This suggested that the vehicle would not roll over in these scenarios.

Table 24. Simulation Results for 2270P Vehicle on 6:1 Approach Slope

Evaluation Parameters	Units	Simulation Conditions and Results					
		31-in. Simulation	31-in. Simulation	34-in. Simulation	34-in. Simulation	36-in. Simulation	36-in. Simulation
<b>Suspension Failure Prescribed?</b>	(Y/N)	N	Y	N	Y	N	Y
<b>Top Rail Height</b>	in. (mm)	31 (787)	31 (787)	34 (864)	34 (864)	36 (914)	36 (914)
<b>Tested Vehicle Mass</b>	lb (kg)	5004 (2270)	5004 (2270)	5004 (2270)	5004 (2270)	5004 (2270)	5004 (2270)
<b>Impact Velocity</b>	mph (km/h)	62.1 (100)	62.1 (100)	62.1 (100)	62.1 (100)	62.1 (100)	62.1 (100)
<b>Tested Impact Angle</b>	deg	25	25	25	25	25	25
<b>Barrier Offset on Slope</b>	in. (mm)	60 (1524)	60 (1524)	60 (1524)	60 (1524)	60 (1524)	60 (1524)
<b>Parallel Time</b>	ms	-	-	264	267	264	265
<b>Parallel Velocity</b>	mph (km/h)	-	-	48.7 (78.3)	48.4 (77.9)	49.2 (79.1)	49.4 (79.5)
<b>Dynamic Rail Deflection</b>	in. (mm)	-40.7 (-1033*)	-37.3 (-947*)	-44.1 (-1121)	-44.7 (-1135)	-46.7 (-1185)	-46.8 (-1189)
<b>Working Width</b>	in. (mm)	n/a	n/a	57.7 (1466)	58.0 (1473)	63.2 (1606)	61.8 (1570)
<b>Working Width Indicator</b>	-	Post	Post	Post	Post	Post	Post
<b>Exit Time</b>	ms	-	-	620	670	670	640
<b>Resultant Velocity at Exit</b>	mph (km/h)	-	-	45.7 (73.5)	45.9 (73.8)	45.5 (73.2)	46.7 (75.1)
<b>Exit Angle</b>	deg	-	-	-14.9	-15.7	-15.42	-10.1
<b>Max Roll</b>	deg	23.5	10.9	33.6	42.7	23.6	15.6
<b>Max Pitch</b>	deg	11.3	14.1	6.8	7.2	5.8	6.9
<b>Pass/Fail</b>	-	Fail	Fail	Pass	Pass	Pass	Pass

\*Simulation did not complete, value is max of run

## **9.6 Override on 6:1 Approach Slope with 2270P at 9-ft (2.7-m) Offset**

Prior research involving simulated vehicle trajectories in V-ditches revealed that a lateral offset distance of 9 ft (2.7 m) may provide an override condition for the 2270P vehicle [33]. This lateral offset was determined by tracking bumper height in relation to the slope level, where the bumper reached a maximum vertical position above the slope. The maximum bumper height trajectory was shown at roughly a 9-ft (2.7-m) rail offset away from the slope break point, providing the worst-case condition for the impact event. Although the increased rail height provided stable and smooth redirection for the 2270P vehicle at a 5-ft (1.5-m) lateral offset, it was necessary to also simulate the same MGS system at this worst-case scenario, a 9-ft (2.7-m) rail offset.

Suspension failure provided stability in full-scale crash tests because the front-end of the pickup truck dropped to the ground. Differences between the vehicle suspension systems in the simulation model and full-scale crash test, as well as LS-DYNA model simplifications, caused the simulated truck suspension model to not exhibit the same failure as shown in full-scale tests. For this reason, two models were run - one without prescribed suspension failure and one with prescribed suspension failure just prior to the time of the highest joint forces.

### **9.6.1 Simulation at 36-in. (914-mm) Rail Height**

Simulations at a 36-in. (914-mm) top-rail height on a 6:1 fill slope showed acceptable vehicle containment and redirection for cases with and without suspension failure. The 36-in. (914-mm) rail height kept the truck closer to the ground than observed for the 31-in. (787-mm) or 34-in. (864-mm) top-rail heights at 5-ft (1.5-m) lateral offsets, thus maintaining a more level redirection trajectory, lower pitch, and lower roll throughout the impact event.



Although the truck rolled into the barrier, it remained upright throughout the impact event. These simulations would suggest that at a 9-ft (2.7-m) lateral offset and at a 36-in. (914-mm) nominal top-rail mounting height, the 2270P vehicle would be safely redirected as shown in Figure 79.

It was clear from these simulations that increased rail height may allow for the MGS to safely accommodate 2270P vehicles when installed on steeper approach slopes at this lateral rail offset. In these simulations, the impacting wheel did not tumble underneath the vehicle when suspension failure was prescribed, and thus the increased pitching shown at the 5-ft (1.5-m) lateral offset was not apparent in the simulation using a 9-ft (2.7-m) lateral offset.

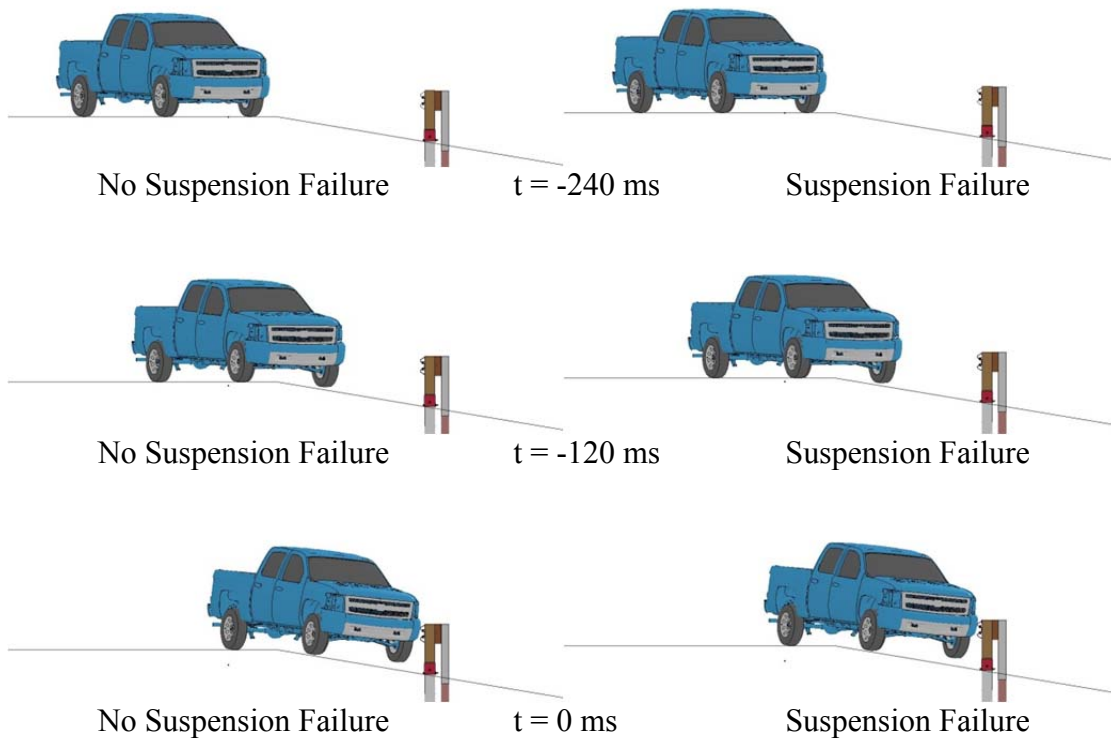


Figure 79. 2270P Vehicle Simulation at 36-in. (914-mm) Top-Rail Height and 9-ft (2.7-m) Offset on 6:1 Approach Slope

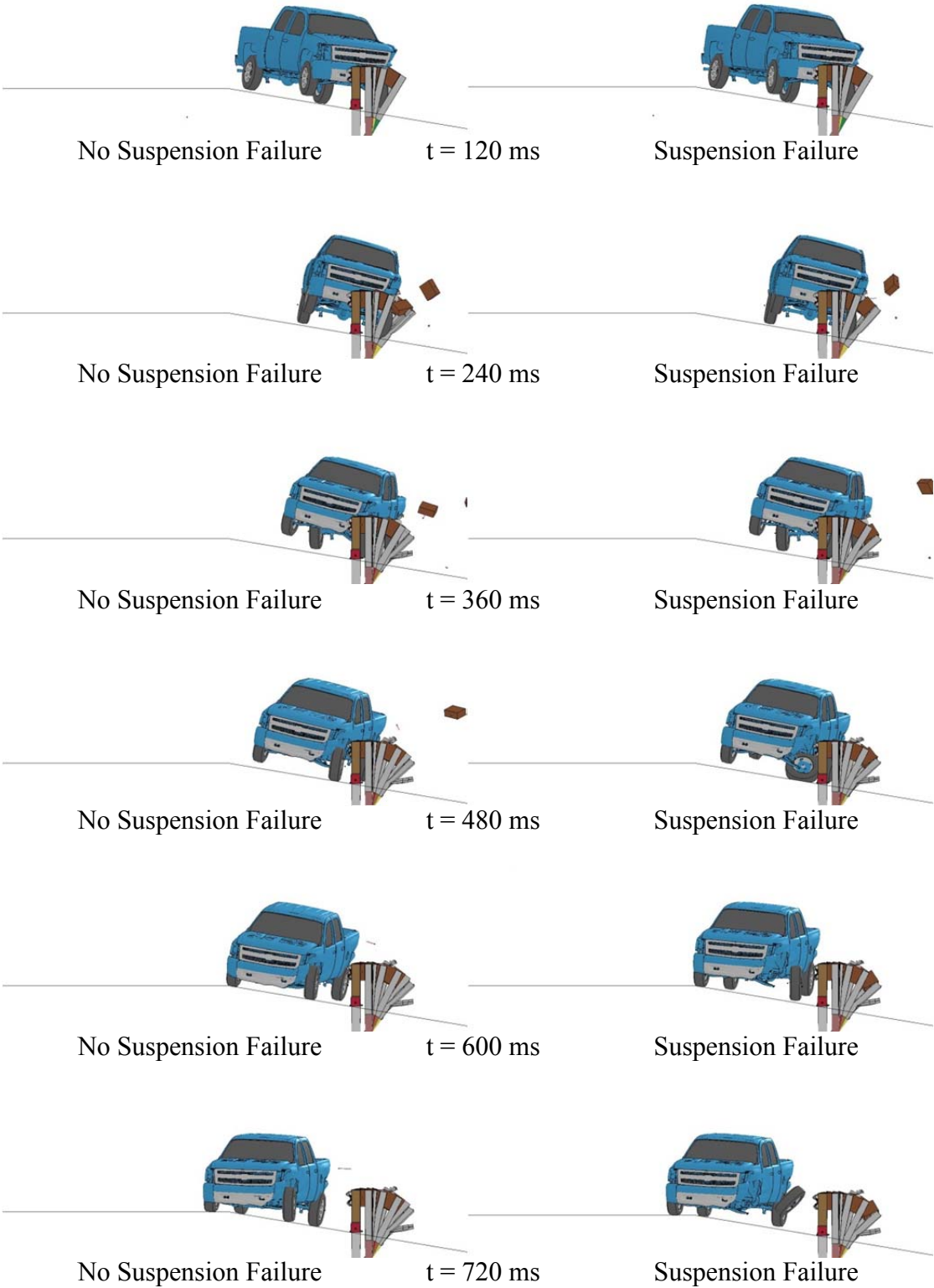


Figure 79. 2270P Vehicle Simulation at 36-in. (914-mm) Top-Rail Height and 9-ft (2.7-m) Offset on 6:1 Approach Slope (continued)

### **9.6.1 Comparison of Test Conditions and Simulation Results**

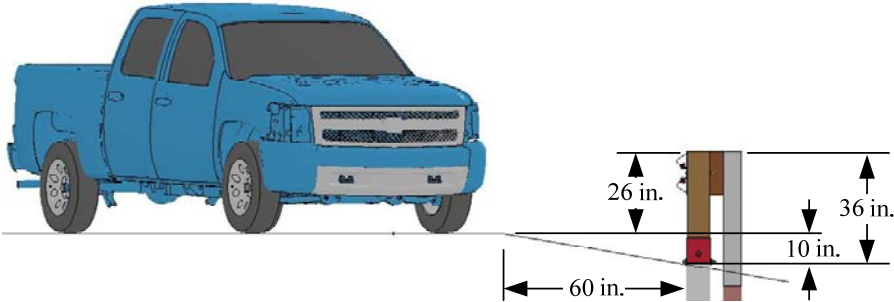
Simulations were compared to garner a clear picture of the vehicle reaction and the barrier's effectiveness at the 36-in. (914-mm) top-rail heights on a 6:1 fill slope at a 9-ft (2.7-m) lateral rail offset. The simulation results are shown in Table 25.

In the 36-in. (914-mm) top-rail height simulation at the 9-ft (2.7-m) lateral offset, the MGS guardrail system was able to redirect the truck better than observed at the 5-ft (1.5-m) lateral offset. As the truck traversed the slope, a higher roll rate occurred prior to the bumper contacting the rail. This roll motion allowed a better alignment of the pickup truck with the barrier instead of the trajectory taking the vehicle over the rail. All of the evaluation criteria were deemed acceptable. This suggested that the vehicle would not roll over in these scenarios, and that this test would pass in accordance with all applicable safety standards.

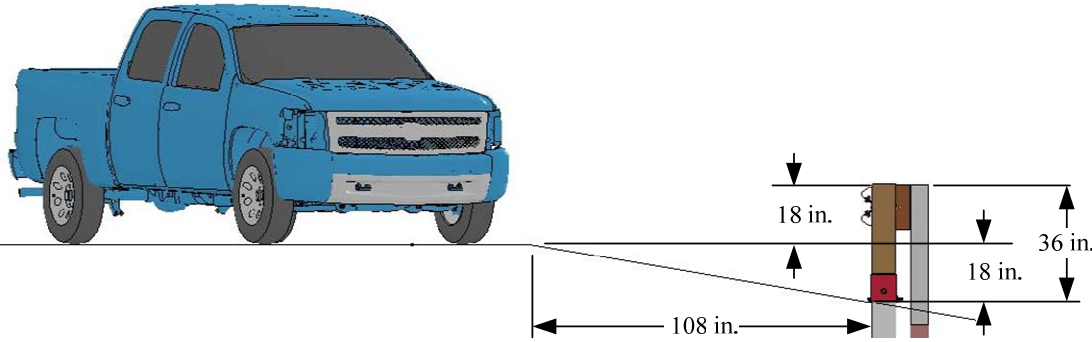
The vehicle does not override the system as severely at a 5-ft (1.5-m) lateral offset. Therefore, the vehicle impacted the rail at a different relative height. However, the increased rail offset allowed for additional roll of the pickup truck down the slope before impact, as shown in Figure 80. This also allowed for additional gravitational effects from the greater distance allotted in the trajectory between the slope break point and impact with the MGS, helping to align the truck better with the rail before impact. In addition, this caused the velocity vector of the vehicle CG to travel into the barrier versus over the barrier at this height, creating improved redirection behavior. Additionally, at this rail height, the impacting wheel did not snag on the guardrail posts as much as observed for the 5-ft (1.5-m) lateral rail offset. This prevented further pitching and rolling of the vehicle into and over the barrier.

Table 25. Simulation Results for 2270P Vehicle on 6:1 Approach Slope

Evaluation Parameters	Units	Simulation Conditions and Results	
		36-in. Simulation	36-in. Simulation
<b>Suspension Failure Prescribed?</b>	(Y/N)	N	Y
<b>Top Rail Height</b>	in. (mm)	36 (914)	36 (914)
<b>Tested Vehicle Mass</b>	lb (kg)	5004 (2270)	5004 (2270)
<b>Impact Velocity</b>	mph (km/h)	62.1 (100)	62.1 (100)
<b>Tested Impact Angle</b>	deg	25	25
<b>Barrier Offset on Slope</b>	in. (mm)	108 (2743)	108 (2743)
<b>Parallel Time</b>	ms	256	257
<b>Parallel Velocity</b>	mph (km/h)	49.0 (78.9)	48.9 (78.7)
<b>Dynamic Rail Deflection</b>	in. (mm)	-49.4 (-1254)	-49.3 (-1253)
<b>Working Width</b>	in. (mm)	56.3 (1429)	56.3 (1430)
<b>Working Width Indicator</b>	-	Post	Post
<b>Exit Time</b>	ms	600	560
<b>Resultant Velocity at Exit</b>	mph (km/h)	46.1 (74.2)	46.7 (75.1)
<b>Exit Angle</b>	deg	-11.4	-10.2
<b>Max Roll</b>	deg	-15.0	-13.7
<b>Max Pitch</b>	deg	-9.106	-8.5
<b>Pass/Fail</b>	-	Pass	Pass



MGS at 36 in. (914 mm) on 6:1 Approach Slope at 5-ft (1.5-m) Offset



MGS at 36 in. (914 mm) on 6:1 Approach Slope at 9-ft (2.7-m) Offset

Figure 80. MGS on Approach Slope in Relation to Road Grade

Although the rails were positioned at different top-rail mounting heights in relation to the slope, the top of the rail was shown to be at a similar distance above the flat roadway top in both cases. In this range of heights and on these slopes, it is analogous to compare the MGS at 36 in. (914 mm) on a 6:1 approach slope to the MGS at 34 in. (864 mm) on an 8:1 approach slope. Due to this fact, it was likely that an 820C small car traveling at an impact speed of 62.1 mph (100 km/h) would likely pass at rail heights up to 38 in. (965 mm) on this slope. However, it is undesired to increase the rail to this height because underride was shown to occur on flat ground at 37 in. (940 mm). Further, decreased impact angles or decreased speeds could allow the vehicle's trajectory to more closely follow the slope and underride the MGS system.

## **9.7 Discussion**

As with increased rail heights of the MGS on flat ground, an increased rail height also provided improved vehicle redirection for high CG vehicles impacting the MGS with steeper approach slopes. Furthermore, an increased rail height would also make it possible to safely place MGS systems at the slope break point of steeper embankments. At an approach slope of 6:1, the small car can be effectively redirected with rail heights of 31, 34, and 36 in. (787, 864, and 914 mm). Previous data suggested that 2000P pickup trucks would override a system on a 6:1 approach slope [31, 32]. This study showed, similarly, that a 2270P would override a 31-in. (787-mm) tall system on a 6:1 approach slope at a 5-ft (1.5-m) lateral offset. The effectiveness of the increased rail height provided the ability to locate the MGS on 6:1 approach slopes at the offset described. The MGS, with an increased rail height, was shown to safely redirect both small cars and large trucks at both 34- and 36-in. (864- and 914-mm) top-rail heights. However, full-scale crash tests are needed to confirm the simulation results and verify the safety performance of the MGS systems with varied height and placement on steeper approach slopes.

Out of the 31-, 34-, and 36-in. (787-, 813-, and 914-mm) tall MGS systems, it is most likely that a 36-in. (914-mm) tall MGS system would provide the greatest safety for use on 6:1 approach slopes at a lateral offset of 5 ft (1.5 m) for pickup trucks. Simulated vehicle trajectories for 820C small cars into a 6:1 V-ditch at a velocity of 62.1 mph (100 km/h) indicated that the front bumper will reach a minimum vertical offset above the embankment at a 25-ft (7.6-m) lateral distance from the slope break point [33]. At this point, the suspension compressed which lowered the front-end geometry of the car. This would indicate a worst case scenario for evaluating underride. However, this behavior occurred at a lateral offset that was well outside the practical distance a W-beam guardrail would normally be placed along a roadway.

Although this research indicated that the MGS would be safe in these conditions when installed on a 6:1 approach slope, it was not recommended that higher rail heights be pursued. A simulated 37-in. (940-mm) tall MGS system on flat ground induced severe underride, allowing an 820C small car to nearly pass under the rail and reach the windshield and A-pillar. This result was not acceptable when considering field implementation and construction tolerances. Additionally, these simulations were performed with impact speeds required by MASH and NCHRP Report No. 350. However, slower speeds at the same impact angles studied herein could allow the vehicles to travel farther down the slope without losing contact with the ground. This condition would keep the nose of the car down and potentially allow for vehicles to underride a taller MGS system.

On 6:1 approach slopes, good performance was shown at 36-in. (914-mm) top-rail heights. With consideration to vehicle trajectory over the embankment and small car and truck redirection, the minimum height would need to be raised over the standard recommended height. On this slope, it was recommended that the minimum rail height be raised to 33.5 in. (851 mm) and the maximum be 36 in. (914 mm).

Furthermore, the design of real roadsides is slightly different than the simulations performed in this study. The simulation used two intersecting planes that formed a perfect break point. In reality roadsides are far from this sort of uniformity. Typical embankments begin with a gravel shoulder with a small slope before increasing to the roadside slope. These differences may cause performance differences in physical systems and should be investigated before the findings of these simulations are implemented.

The simulations reported herein showed the potential for a modified MGS to be placed on steeper approach slopes by incorporating an increased rail height. However, full-scale vehicle crash tests must be performed to validate these simulations and further investigate the rail height effects on approach slopes. MASH impact safety standards require crash tests with both 1100C and 2270P vehicles under TL-3 conditions [3]. Two tests, one using each MASH required vehicle at a 36-in. (914-mm) rail height and 5-ft (1.5-m) lateral offset on a 6:1 approach slope, would be necessary to show that the MGS can be raised to improve effectiveness on steeper slopes. V-ditch research showed that a lateral offset distance of 9 ft (2.7 m) was the critical offset distance for the 2270P vehicle [33]. This was determined by tracking bumper height in relation to the slope level, where the bumper reached a maximum vertical position above the slope. In these simulations, the 9-ft (2.7-m) lateral rail offset was not accompanied by any further adverse redirection conditions at a 36-in. (914-mm) top-rail height than was exhibited at a 5-ft (1.5-m) lateral rail offset.



## **10 SUMMARY, CONCLUSIONS, AND RECOMMENDATIONS**

### **10.1 BARRIER VII**

The BARRIER VII analysis showed that in some cases the program performed well in comparison to LS-DYNA in predictive capabilities for parameters such as post failure, anchor displacement, and pocketing [24]. These were three critical system parameters that affect barrier performance. The inability to predict vehicle underride, vehicle suspension failure, or vehicle occupant compartment damage somewhat limited the usefulness of BARRIER VII. The program did provide a good basis for comparison and verification with LS-DYNA when full-scale data were limited. A baseline expectation of maximum barrier height could not be determined using the predictive capabilities of BARRIER VII. The lack of ability to simulate underride in BARRIER VII simulations did not provide enough data to make a valid conclusion on maximum rail height for small cars. Therefore, it was determined that LS-DYNA simulations were the best method for determining a maximum guardrail height with respect to underride. However, the LS-DYNA simulation compared in this study was shown to be less effective than BARRIER VII in some regards. This analysis led to the use of an updated LS-DYNA MGS model in which the entire mesh of the rail was refined. The anchors were updated to more closely match the physically tested components, which was shown on the whole to better represent full-scale test results.

### **10.2 Maximum Height Determination on Flat Ground**

This study set out to evaluate the maximum allowable rail mounting height for the MGS when impacted by a small passenger vehicle. Previously, two full-scale crash tests were run on the steel-post MGS with rail mounting heights of 34 in. (864 mm) and 36 in. (914 mm), respectively [9]. The barrier systems were 175 ft (53.3 m) long. Both of these tests passed in

accordance with MASH standards. An LS-DYNA simulation study was undertaken to evaluate a maximum allowable rail height. In addition, an LS-DYNA investigation and evaluation of the MGS with increased height and installed on approach slopes was performed to evaluate the allowable ranges of use.

Using the full-scale crash data from test no. MGSMRH-1, which was performed on the MGS with a top-rail mounting height of 34 in. (864 mm), an LS-DYNA model was created to simulate crash performance. The system incorporated 72-in. (1,829-mm) long, W6x9 (W152x13.4) steel posts with an embedment depth of 37 in. (940 mm). The full-scale test consisted of a 2,599-lb (1,179-kg) passenger car impacting the barrier system at a speed of 63.6 mph (102.4 km/h) and an angle of 25.0 degrees. During the test, the vehicle was smoothly redirected without any significant snagging or vehicle underride.

The current 1100C vehicle model provided by the NCAC, a Dodge Neon, had dissimilar front-end geometry to the as-tested vehicle. In the full-scale test a 2003 Kia Rio sedan was used which had an approximate 34.4-in. (874-mm) cowl height. The 1100C Dodge Neon model had a 33.4-in. (848-mm) cowl height. The 820C Geo Metro model had a cowl height of 34.6 in. (879 mm), which was more analogous to the as-tested vehicle geometry. This cowl height was a critical factor in determining the rail height at which the vehicle could be redirected. Thus the 820C vehicle model was used.

For the LS-DYNA barrier model, a 34-in. (864-mm) top-rail height was used in combination with 72-in. (1,829-mm) long, W6x9 (W152x13.4) steel posts with an embedment depth of 37 in. (940 mm). Longitudinal and lateral springs were used to simulate post-soil resistance. The simulations were performed with a 1,982-lb (899-kg) small car impacting the barrier system at a speed of 62.1 mph (100.0 km/h) and an angle of 25.0 degrees. For the LS-DYNA simulation, the vehicle was smoothly redirected without any significant snagging or

vehicle underride. The maximum simulated dynamic deflection was 29.7 in. (755 mm), while the working width of the system was 50.8 in. (1,290 mm). In comparison, in the actual full-scale crash test with a 2,599-lb (1,179-kg) passenger car, the maximum permanent set and dynamic deflections were found to be 18¼ in. (464 mm) and 29.0 in. (737 mm), respectively. The actual working width of the system was found to be 49.4 in. (1,255 mm).

At the 34-in. (864-mm) top-rail height, a simulation was also performed using a 2270P pickup truck model. The simulation consisted of a 5,004-lb (2270-kg) pickup truck impacting the barrier system at a speed of 62.1 mph (100.0 km/h) and an angle of 25.0 degrees. During the simulation, the pickup exhibited some minor snagging. Without prescribed suspension failure, the maximum dynamic deflection was 44.8 in. (1,137 mm), while the working width of the system was 58.1 in. (1,475 mm). With prescribed suspension failure, the maximum dynamic deflection was 43.4 in. (1,103 mm), while the working width of the system was 60.4 in. (1,533 mm). Both of the simulation results met all of the MASH safety requirements for test designation 3-11.

Using the full-scale crash data from test no. MGSMRH-2, which was performed on the MGS with a top-rail mounting height of 36 in. (914 mm), an LS-DYNA model was created to simulate crash performance. The system incorporated 72-in. (1,829-mm) long, W6x9 (W152x13.4) steel posts with an embedment depth of 35 in. (889 mm). The test consisted of a 2,583-lb (1,172-kg) passenger car impacting the barrier system at a speed of 64.1 mph (103.2 km/h) and an angle of 25.6 degrees. During the test, the vehicle was smoothly redirected without any significant snagging or vehicle underride.

For the LS-DYNA barrier model, a 36-in. (914-mm) top-rail height was used in combination with 72-in. (1,829-mm) long, W6x9 (W152x13.4) steel posts with an embedment depth of 35 in. (889 mm). The simulations were performed with a 1,982-lb (899-kg) passenger

car impacting the barrier system at a speed of 62.1 mph (100.0 km/h) and an angle of 25.0 degrees. During the simulation, the vehicle was smoothly redirected without any significant snagging or vehicle underride. The maximum dynamic deflection was 31.5 in. (799 mm), and the working width of the system was 52.5 in. (1,334 mm). In the actual full-scale crash test with a 2,599-lb (1,179-kg) passenger car, the maximum permanent set and dynamic deflections were 16<sup>3</sup>/<sub>4</sub> in. (425 mm) and 23.5 in. (597 mm), respectively. The working width of the system was 40.5 in. (1,029 mm).

At the 36-in. (914-mm) top-rail height, a simulation was performed using a 1100C Dodge Neon car model. The simulation consisted of a 2,425-lb (1100-kg) passenger car impacting the barrier system at a speed of 62.1 mph (100.0 km/h) and an angle of 25.0 degrees. This simulation was unstable past 200 ms. However, it was already shown at that time that the vehicle was underriding the system. Significant A-pillar damage was apparent, which would suggest failure per MASH safety requirements for test designation 3-10. This suggested that vehicle front-end geometry played a crucial role in the redirection capability of a guardrail system.

Additionally, at the 36-in. (914-mm) top-rail height, a simulation was performed using a 2270P pickup truck model. The simulation consisted of a 5,004-lb (2270-kg) pickup truck impacting the barrier system at a speed of 62.1 mph (100.0 km/h) and an angle of 25.0 degrees. During the simulation, the pickup exhibited some minor snagging but was redirected in a safe manner. Without prescribed suspension failure, the maximum dynamic deflection was 47.8 in. (1,214 mm), while the working width of the system was 59.4 in. (1,509 mm). With prescribed suspension failure, the maximum dynamic deflection was 46.9 in. (1,191 mm), while the working width of the system was 60.8 in. (1,545 mm). Both of the simulation results met all of the MASH safety requirements for test designation 3-11.

As part of this investigation, it was necessary to increase the simulated top-rail height to 37 in. (940 mm). The LS-DYNA barrier model was modified to include a 37-in. (940-mm) top-rail height with 72-in. (1,829-mm) long, W6x9 (W152x13.4) steel posts at an embedment depth of 34 in. (864 mm). The simulation consisted of a 1,982-lb (899-kg) passenger car impacting the barrier system at a speed of 62.1 mph (100.0 km/h) and an angle of 25.0 degrees. During the simulation, the vehicle severely underrode the system, causing significant A-pillar damage and intrusion into the occupant compartment. The results of the simulation failed to meet the MASH safety requirements for test designation 3-10.

### **10.3 Maximum Height Determination on Approach Slopes Summary**

An investigation and evaluation of the MGS with increased height and installed on approach slopes was performed to evaluate allowable ranges of use. Previously, two full-scale crash tests were run on the steel-post MGS with a top-rail mounting height of 31 in. (787 mm) at a 5-ft (1.5-m) lateral offset from the slope break point to the front of the system on an 8:1 approach slope. The barrier system was 175 ft (53.3 m) long. Test no. MGSAS-1 utilized a 2000P pickup truck, and test no. MGSAS-2 utilized an 820C small car. Both tests passed in accordance with the NCHRP Report No. 350 safety standards. An LS-DYNA simulation study was undertaken to examine the effects of increasing the rail height while increasing the slope.

Using the full-scale crash data from test no. MGSAS-2, an LS-DYNA model was created to simulate the aspects of this impact on the 8:1 approach slope. The system incorporated 72-in. (1,829-mm) long, W6x9 (W152x13.4) steel posts with an embedment depth of 40 in. (1016 mm). During the simulation, the vehicle was smoothly redirected without any significant snagging or vehicle underride and very accurately represented the results obtained from the full-scale crash test.

Subsequent simulations were performed to evaluate increased rail heights for the MGS on 8:1 and 6:1 approach slopes with varying impact angles. At 31-, 34- and 36-in. (787-, 864-, and 914-mm) top-rail heights, simulations were performed using both the 820C small car and the 2270P pickup truck model. Simulations were performed on 8:1 and 6:1 approach slopes at a 5-ft (1.5-m) lateral offset.

At 31- and 34-in. (787- and 864-mm) rail heights on 8:1 approach slopes, at both 20- and 25-degree impact angles, the small car was safely redirected. However, at a 36-in. top-rail height, the small car failed at an impact angle of 20 degrees and passed at a 25-degree angle. This result, although initially counterintuitive, made sense when considering that the small car had a greater distance to traverse the slope at lower angles. Therefore, as the car's trajectory over the slope was changed, the suspension compression observed at the lower impact angle created a lower front-end geometry, causing the car to slide under the rail. Damage to the A-pillar and intrusion into the occupant compartment occurred due to this underride. As a result, a top-rail height of 34 in. (864 mm) was deemed to be the maximum allowable height on an 8:1 approach slope.

On 6:1 approach slopes and at a 5-ft (1.5-m) lateral offset, the simulations showed acceptable results for the 820C vehicle at 31-, 34- and 36-in. (787-, 864-, and 914-mm) top-rail heights. On this steeper slope, the guardrail was effectively lowered by 2.5 in. (64 mm) in relation to the road grade. This drop made the 36-in. (914-mm) rail height with a 6:1 approach slope more comparable to the 34-in. (864-mm) rail height on an 8:1 approach slope. Due to this effect, the lower guardrail caused stability issues when simulated with the 2270P vehicle. The trajectory of the truck overrode the barrier at a 31-in. rail height on 6:1 approach slopes at a 5-ft (1.5-m) lateral offset. At a 34-in. (864-mm) top-rail height, a high degree of roll was observed, but it was deemed acceptable because the truck was recoverable. Vehicle behavior improved at a 36-in. (914-mm) top-rail height on the same slope as vehicle roll decreased and the probability of

vehicle recoverability increased. Due to the relationship between road grade and barrier height and its effect on vehicle-to-barrier impact location, it was determined that a 33.5-in. (851-mm) top-rail height was a critical minimum on 6:1 approach slopes with a 34-in. (864-mm) top-rail height being a practical minimum. The corresponding critical maximum rail height was 36 in. (914 mm). The MGS with a rail height above 36 in. (914 mm) could present issues when impacted by small cars at decreased impact angles or reduced speeds due to lower trajectories off the slope break point and greater vehicle drop prior to striking the barrier.

Prior research involving simulated vehicle trajectories in V-ditches revealed that a lateral offset of 9 ft (2.7 m) may provide a potential override condition for the 2270P vehicle [33]. This lateral offset was determined by tracking bumper height in relation to the slope, where the bumper reached a maximum vertical position above the slope. The 36-in. (914-mm) rail height system at a 9-ft (2.7-m) offset was not shown, in these simulations, to be accompanied by any further adverse conditions than was exhibited at a 5-ft (1.5-m) lateral rail offset.

#### **10.4 Discussion Summary**

Wheel snag did not pose a significant threat to the vehicle in test nos. MGSMRH-1 or MGSMRH-2 nor in the simulations at increased rail heights. The primary threat to occupant safety was underide of the MGS, resulting in A-pillar and occupant compartment damage. Given a high enough cowl height, the small car was safely redirected at a 36-in. (914-mm) rail height. Wheel snag occurred in several of the simulations when the right-front tire contacted the upstream edge of the front flange of a guardrail post. In all cases, after contact with the wheel, the post twisted and bent downstream and did not pose a threat to the vehicle.

Rail snag under the hood did not occur for either full-scale crash tests. For the 32-in. (813-mm) tall MGS simulation, the corner of the 1100C engine hood was located above the top corrugation of the rail. In full-scale vehicle crash test nos. MGSMRH-1 and MGSMRH-2, the

corner of the engine hood was located between the corrugations of the rail. As a result, the corner of the engine hood slid into the valley of the W-beam and crumpled, jarring the hood open. Vehicle underride only occurred when the corner of the engine hood was below the lower W-beam corrugation, as was the case at a 37-in. (940-mm) top-rail height.

For the LS-DYNA simulations, during redirection, the rail deflected upward as it released away from the posts and slid up the side of the vehicle. The vehicle contacted the detached posts and overrode them, which caused the vehicle to pitch upward and roll away from the barrier. As the vehicle rolled away from the barrier, the side of the vehicle that was in contact with the rail moved upward. As a consequence, the rail slid up the vehicle, contacted the base of the A-pillar, and remained at this level through the redirection. At this same time, the rail was applying a downward force on the vehicle which counteracted the vehicle roll. In all cases, pitch and roll angles were relatively low (less than 12 degrees).

Recent small car design has changed the front-end geometry of cars. A more "raked," aerodynamic, slanted hood and windshield profile design has dominated the market and increased both the front-corner engine hood and cowl heights. Recent car design changes may render these results obsolete, and rail height may no longer be less limited by vehicle geometry but rather limited by post-in-soil strength. The updated 1100C Toyota Yaris model that was introduced by NCAC may be better suited to predict vehicle-to-guardrail behavior of current model-year vehicles. A field study of current model-year vehicles showed that small car cowl heights have increased over the tested and simulated vehicle models. A cowl height increase of 3 to 6 in. (76 to 152 mm) was shown across many makes and models.



## 10.5 Guidelines

Due to recent small car design trends, previous full-scale vehicle crash testing, MASH and NCHRP Report No. 350 safety standards, and the simulations performed in these studies, the following conclusions and recommendations were made:

- i. There appears to be a considerable amount of upside tolerance for the rail height on the MASH-approved MGS. This was supported by both the high flare rate study and this maximum mounting height study.
- ii. Maximum top-rail mounting height for the MGS should not exceed 36 in. (940 mm) when placed on level terrain;
- iii. Vehicle front-end geometry, specifically the vehicle cowl height, was a critical factor in determining the susceptibility of a small car to underride a guardrail system;
- iv. The MGS may be suitable for use on 6:1 approach slopes with 5- and 9-ft (1.5- and 2.7-m) lateral offsets when mounted at a 36-in. (940-mm) top rail height;
- v. Improved performance of the MGS could be shown on 8:1 approach slopes when the system was mounted at a 34-in. (864-mm) rail height; and
- vi. For compliance with MASH TL-3 standards, full-scale vehicle crash tests should be performed, as outlined in Table 26.

## 10.6 Future Research

Current MASH FHWA approval for the MGS consists of a nominal 31-in. (787-mm) top-rail mounting height. The crash tests reported herein indicate that there exists a considerable factor of safety applicable to barrier height. However, a taller MGS was not ready for MASH approval as more research must be performed on the system.

Table 26. Recommended MASH Testing for Longitudinal Barriers

Test No.	Vehicle Type	Impact Speed	Impact Angle	Impact Location	Recommended	Comment
		mph (km/h)	deg		(Y/N)	
System: Midwest Guardrail System (MGS) Length: 175-ft (53.3-m); Nominal Top Rail Height: 36-in. (914-mm); Terrain: Level						
3-10	1100C	62.1 (100)	25	Post No. 12	N	Test No. MGSMRH-2 has been performed and passed successfully.
3-11	2270P	62.1 (100)	25	Post No. 12	Y	Needed to verify acceptable system resistance to loading with decreased post embedment depth.
System: Midwest Guardrail System (MGS) Length: 175-ft (53.3-m); Nominal Top Rail Height: 36-in. (914-mm); Terrain: 6:1 Approach Slope at 5-ft (1.5-m) lateral offset						
3-10	1100C	62.1 (100)	25	Post No. 12	N	A 20-deg impact angle shown to be more critical at increased rail height.
3-10 (mod.)	1100C	62.1 (100)	20	Post No. 12	Y	Needed to examine susceptibility of small car to underride system at increased mounting heights on approach slopes.
3-11	2270P	62.1 (100)	25	Post No. 12	Y	Needed to verify acceptable system resistance to loading with decreased post embedment depth, and to examine susceptibility of truck to override system.
System: Midwest Guardrail System (MGS) Length: 175-ft (53.3-m); Nominal Top Rail Height: 36-in. (914-mm); Terrain: 6:1 Approach Slope at 9-ft (2.7-m) lateral offset						
3-10	1100C	62.1 (100)	25	Post No. 12	N	Test at 5-ft (1.5-m) lateral offset more critical.
3-10 (mod.)	1100C	62.1 (100)	20	Post No. 12	Y	Vehicle trajectory presents unknown behavior and potential underride issues at this offset.
3-11	2270P	62.1 (100)	25	Post No. 12	Y	Vehicle trajectory in the air presents unknown behavior.

At a minimum, full-scale vehicle crash testing should be performed on the MGS at a 36-in. (914-mm) top-rail height:

- i. with a 2270P pickup truck; and
- ii. on transitions to and from a 31-in. (787-mm) rail to examine potential “wedging” of the small car.

For practical usage, full-scale vehicle crash testing should be performed on the MGS at a 36-in. (914-mm) top-rail height with:

- i. end terminals; and
- ii. transitions to other systems (e.g., thrie-beam and concrete barriers).

For extended usage, full-scale vehicle crash testing should be performed on the MGS at a 36-in. (914-mm) top-rail height with no blockouts.

These full-scale vehicle crash tests should be supported with LS-DYNA simulations, including the use of the new NCAC 1100C Toyota Yaris model.

For use on approach slopes, two full-scale tests should be performed at a 36-in. (914-mm) top-rail height on a 6:1 approach slope at a 5-ft (1.5-m) lateral rail offset with:

- i. the 2270P pickup truck at a 25-degree impact angle; and
- ii. the 1100C small car at a 20-degree impact angle.

Furthermore, verification of and improvements to the existing post-soil model used in LS-DYNA should be pursued. Physical bogie testing should be performed with decreased post embedment to verify and fine tune the post-soil model. Alternate soil modeling techniques, such as Arbitrary-Lagrangian Eulerian (ALE) methods, may prove better at simulating soil in these models.

## 11 REFERENCES

1. Ross, H.E., Sicking, D.L., Zimmer, R.A., and Michie, J.D., *Recommended Procedures for the Safety Performance Evaluation of Highway Features*, National Cooperative Research Program (NCHRP) Report No. 350, Transportation Research Board, Washington, D.C., 1993.
2. Polivka, K.A., Faller, R.K., Sicking, D.L., Reid, J.D., Rohde, J.R., Holloway, J.C., Bielenberg, R.W., and Kuipers, B.D., *Development of the Midwest Guardrail System (MGS) for Standard and Reduced Post Spacing and in Combination with Curbs*, Final Report to the Midwest States' Regional Pooled Fund Program, Report No. TRP-03-139-04, Project No. SPR-3(017)-Years 10, 12-13, Midwest Roadside Safety Facility, University of Nebraska-Lincoln, September 1, 2004.
3. *Manual for Assessing Safety Hardware (MASH)*, American Association of State Highway and Transportation Officials (AASHTO), Washington, D.C., 2009.
4. Polivka, K.A., Faller, R.K., Sicking, D.L., Rohde, J.R., Bielenberg, B.W., and Reid, J.D., *Performance Evaluation of the Midwest Guardrail System - Update to NCHRP 350 Test No. 3-11 with 28" C.G. Height (2214MG-2)*, Final Report to the National Cooperative Highway Research Program (NCHRP), Transportation Research Board, Transportation Research Report No. TRP-03-171-06, Midwest Roadside Safety Facility, University of Nebraska-Lincoln, October 11, 2006.
5. Polivka, K.A., Faller, R.K., Sicking, D.L., Rohde, J.R., Bielenberg, R.W., and Reid, J.D., *Performance Evaluation of the Midwest Guardrail System – Update to NCHRP 350 Test No. 3-10 (2214MG-3)*, Final Report to the National Cooperative Highway Research Program (NCHRP), Transportation Research Report No. TRP-03-172-06, Project No. 22-14(2), Midwest Roadside Safety Facility, University of Nebraska-Lincoln, October 11, 2006.
6. Faller, R.K., Sicking, D.L., Bielenberg, R.W., Rohde, J.R., Polivka, K.A., and Reid, J.D., *Performance of Steel-Post, W-Beam Guardrail Systems*, Transportation Research Record 2025, TRB, National Research Council, Washington D.C., 2007, pp. 18-33.
7. Kuipers, B.D., Faller, R.K., and Reid, J.D., *Critical Flare Rates for W-beam Guardrail – Determining Maximum Capacity Using Computer Simulation*, Final Report to the National Cooperative Highway Research Program (NCHRP), Transportation Research Board, MwRSF Research Report No. TRP-03-157-04, NCHRP 17-20(3), Midwest Roadside Safety Facility, University of Nebraska-Lincoln, January 24, 2005.
8. Reid, J.D., Kuipers, B.D., Sicking, D.L., and Faller, R.K., *Impact performance of W-beam guardrail installed at various flare rates*. International Journal of Impact Engineering, Vol. 36, Issue 1, March 2009, pp. 476-485.
9. Stolle, C.J., Lechtenberg, K.A., Reid, J.D., Faller, R.K., Bielenberg, R.W., Rosenbaugh, S.K., Sicking, D.L., and Johnson, E.A., *Determination of the Maximum MGS Mounting Height – Phase I Crash Testing*, Final Report to the Midwest States Pooled Fund

Program, Report No. TRP-03-255-11, Midwest Roadside Safety Facility, University of Nebraska-Lincoln, March 9, 2012.

10. Hallquist, J.O. *LS-DYNA Keyword User's Manual*. Livermore, CA: Livermore Software Technology Corporation. 2007.
11. Polivka, K.A., Faller, R.K., Sicking, D.L., Rohde, J.R., Bielenberg, B.W., and Reid, J.D., *Performance Evaluation of the Midwest Guardrail System - Update to NCHRP 350 Test No. 3-11 with 28" C.G. Height (2214MG-1)*, Final Report to the National Cooperative Highway Research Program (NCHRP), Transportation Research Board, Transportation Research Report No. TRP-03-170-06, Midwest Roadside Safety Facility, University of Nebraska-Lincoln, October 10, 2006.
12. Sicking, D.L., Reid, J.D., and Rohde, J.R., *Development of the Midwest Guardrail System*, Transportation Research Record 1797, TRB, National Research Council, Washington, D.C., November 2002, pp. 44-52.
13. Baxter, J.R., *FHWA NCHRP Report No. 350 approval letter B-133 of Midwest Guardrail System (MGS)*, To R.K. Faller, Midwest Roadside Safety Facility, Lincoln, NE, March 1, 2005.
14. Stolle, C.S., Polivka, K.A., Reid, J.D., Faller, R.K., Sicking, D.L., Bielenberg, R.W., and Rohde, J.R., *Evaluation of Critical Flare Rates for the Midwest Guardrail System (MGS)*, Final Report to the Midwest States Pooled Fund Program, Report No. TRP-03-191-08, Project No. SPR-3(017)-Years 14-15, Midwest Roadside Safety Facility, University of Nebraska-Lincoln, July 15, 2008.
15. Rice, G.E., *FHWA NCHRP Report No. 350 approval letter CC-96 of SKT and FLEAT Terminals*, To A. Artar, Gregory Highway Products, Canton, OH, December 21, 2007.
16. Rice, G.E., *FHWA NCHRP Report No. 350 approval letter CC-100 of SRT-31 Terminal for MGS, T-31, and GMS*, To H. Ross, Texas Transportation Institute, August 30, 2007.
17. Baxter, J.R., *FHWA NCHRP Report No. 350 approval letter CC-88 of SKT, SKT-LITE, and FLEAT for MGS*, To K. Kothmann, Road Systems, Inc. Big Spring, TX, March 8, 2005.
18. Bielenberg, B.W., Faller, R.K., Holloway, J.C., Reid, J.D., Rohde, J.R., and Sicking, D.L., *Performance Evaluation of the FLEAT-MGS End Terminal –NCHRP 350 Test No. 3-34 (FLEAT-6)*, Final Report to Safety by Design Company, Report No. TRP-03-152-04, Midwest Roadside Safety Facility, University of Nebraska-Lincoln, June 29, 2004.
19. Bielenberg, B.W., Faller, R.K., Holloway, J.C., Reid, J.D., Rohde, J.R., and Sicking, D.L., *Performance Evaluation of the FLEAT-MGS End Terminal with Redesigned Breakaway Posts and End Anchorage –NCHRP 350 Test No. 3-30 (FLEAT-8)*, Final Report to Safety by Design, Inc., Report No. TRP-03-153-04, Midwest Roadside Safety Facility, University of Nebraska-Lincoln, June 30, 2004.

20. Baxter, J.R., *FHWA NCHRP Report No. 350 approval letter CC-94 of ET-Plus 31 Terminal for MGS*, To S.L. Brown, Trinity Highway Safety Products Division, September 2, 2005.
21. Polivka, K.A., Faller, R.K., Sicking, D.L., Rohde, J.R., Bielenberg, R.W., Reid, J.D., and Coon, B.A., *Performance Evaluation of the SKT-MGS Tangent End Terminal – Update to NCHRP 350 Test No. 3-34 (2214TT-1)*, Final Report to the National Cooperative Highway Research Program (NCHRP), Report No. TRP-03-176-06, Project No. 22-14(2), Midwest Roadside Safety Facility, University of Nebraska-Lincoln, Oct 12, 2006.
22. Ferdous, M.R., Abu-Odeh, A., Bligh, R.P., Jones, H.L., and Sheikh, N.M., *Performance Limit Analysis for Common Roadside and Median Barriers Using LS-DYNA*, International Journal of Crashworthiness, 16:6. 2011. 691-706.
23. Kuipers, B.D., *Identification of a Critical Flare Rate for W-Beam Guardrail in High-Speed Facilities Using Computer Simulation*. MS Thesis. University of Nebraska – Lincoln, Lincoln, NE. 2004. Print.
24. Julin, R.D., *Midwest Guardrail System BARRIER VII Analysis*, MwRSF Internal Report, Midwest Roadside Safety Facility, University of Nebraska-Lincoln, October 6, 2011.
25. Julin, R.D., *Midwest Guardrail System LS-DYNA Model Comparison*, MwRSF Internal Report, Midwest Roadside Safety Facility, University of Nebraska-Lincoln, October 6, 2011.
26. Hallquist, J.O. *LS-DYNA Theory Manual*. Livermore, CA: Livermore Software Technology Corporation. 2006.
27. LSTC Inc. "*SOFT Option*." *LS-DYNA Support*. 16 May 2003. Livermore Software. 7 May 2012. <http://www.dynasupport.com/howtos/contact/soft-option>
28. Mongiardini, M. and Reid, J.D., *Investigation of a Series of Relevant Phenomena for Modeling the Full-Scale Crash Test of a Small Vehicle with a Guardrail System*, International Journal of Computer Aided Engineering and Technology, 2012.
29. Mongiardini, M., Ray, M.H., Plaxico, C.A., Anghileri, M., *Procedures for Verification and Validation of Computer Simulations Used for Roadside Safety Applications*, Final Report to the National Cooperative Highway Research Program (NCHRP), NCHRP Report No. W179, Project No. 22-24, Worcester Polytechnic Institute, March, 2010.
30. AASHTO Roadside Design Guide (4th Edition). American Association of State Highway and Transportation Officials (AASHTO), 2011.
31. Johnson, E.A., Lechtenberg, K.A., Reid, J.D., Sicking, D.L., Faller, R.K., Bielenberg, R.W., and Rohde, J.R., *Approach Slope for Midwest Guardrail System*, Final Report to the Midwest States' Regional Pooled Fund Program, MwRSF Research Report No. TRP-03-188-08, Project No. SRP-3(017), Midwest Roadside Safety Facility, University of Nebraska-Lincoln, December 4, 2008.

32. Reid, John D. *Approach Slopes for Midwest Guardrail System*, Journal of Transportation Safety & Security, 1: 1. 2009. 32 - 45.
33. Mongiardini, M., Faller, R.K., Rosenbaugh, S.K. and Reid, J.D., *Test Matrices for Evaluating Cable Median Barriers Placed in V-Ditches*, Draft Report to the Midwest States' Regional Pooled Fund Program, MwRSF Research Report No. TRP-03-265-12, Project No. TPF-5(193), Midwest Roadside Safety Facility, University of Nebraska-Lincoln, April 2, 2012.

## **12 APPENDICES**



**Appendix A. - MGS 31-in. (787-mm) BARRIER VII Input Deck (2270P)**

```

MGS 175ft, 2270P at 31-in. System Height
225 2 1 1 253 6 2 0
0.0001 0.0001 2.000 2000 0 1.0 1
10 10 10 10 10 500 1
1 0.0 0.0
225 2100 0.0
1 225 223 1 9.375
1 225 0.40
225 224 223 222 221 220 219 218 217 216
215 214 213 212 211 210 209 208 207 206
205 204 203 202 201 200 199 198 197 196
195 194 193 192 191 190 189 188 187 186
185 184 183 182 181 180 179 178 177 176
175 174 173 172 171 170 169 168 167 166
165 164 163 162 161 160 159 158 157 156
155 154 153 152 151 150 149 148 147 146
145 144 143 142 141 140 139 138 137 136
135 134 133 132 131 130 129 128 127 126
125 124 123 122 121 120 119 118 117 116
115 114 113 112 111 110 109 108 107 106
105 104 103 102 101 100 99 98 97 96
95 94 93 92 91 90 89 88 87 86
85 84 83 82 81 80 79 78 77 76
75 74 73 72 71 70 69 68 67 66
65 64 63 62 61 60 59 58 57 56
55 54 53 52 51 50 49 48 47 46
45 44 43 42 41 40 39 38 37 36
35 34 33 32 31 30 29 28 27 26
25 24 23 22 21 20 19 18 17 16
15 14 13 12 11 10 9 8 7 6
5 4 3 2 1
100 1
1 2.29 1.99 9.375 30000.0 6.92 99.5 68.5 0.05 12-Gauge W-Beam
300 3
1 24.875 0.00 6.0 6.0 100.0 675.0 675.0 0.05 Simulated Strong
Anchor Post
100.0 100.0 15.0 15.0
2 24.875 0.00 3.0 3.0 100.0 150.0 225.00 0.05 Second BCT Post
50.0 50.0 15.0 15.0
3 24.875 0.0 3.00 2.60 54.0 61.90 164.18 0.05 W6x9 by 6' Long
Emb. 40" in H.E. 8 soil
15.0 25.0 15.0 15.0
1 1 2 224 1 101 0.0 0.0 0.0
225 1 301 0.0 0.0 0.0 0.0
226 9 302 0.0 0.0 0.0 0.0
227 17 251 8 303 0.0 0.0 0.0 0.0
252 217 302 0.0 0.0 0.0 0.0
253 225 301 0.0 0.0 0.0 0.0
5000.0 58310.0 20 6 4 0 1
1 0.055 0.12 6.00 17.0
2 0.057 0.15 7.00 18.0
3 0.062 0.18 10.00 12.0
4 0.110 0.35 12.00 6.0
5 0.35 0.45 6.00 5.0
6 1.45 1.50 15.00 1.0
1 102.50 15.875 1 12.0 1 1 0 0
2 102.50 27.875 1 12.0 1 1 0 0
3 102.50 39.000 2 12.0 1 1 0 0
4 88.75 39.000 2 12.0 1 1 0 0
5 76.75 39.000 2 12.0 1 1 0 0
6 64.75 39.000 2 12.0 1 1 0 0
7 52.75 39.000 2 12.0 1 1 0 0
8 40.75 39.000 2 12.0 1 1 0 0
9 28.75 39.000 2 12.0 1 1 0 0
10 16.75 39.000 2 12.0 1 1 0 0
11 -13.25 39.000 3 12.0 1 1 0 0
12 -33.25 39.000 3 12.0 1 1 0 0
13 -53.25 39.000 3 12.0 1 1 0 0
14 -73.25 39.000 3 12.0 1 1 0 0

```

15	-93.25	39.000	3	12.0	1	1	0	0
16	-125.35	39.000	4	12.0	1	1	0	0
17	-125.35	-39.000	4	12.0	0	0	0	0
18	102.50	-39.000	1	12.0	0	0	0	0
19	62.40	33.90	5	1.0	1	1	0	0
20	-77.85	33.90	6	1.0	1	1	0	0
1	62.40	33.90		0.0	608.			
2	62.40	-33.90		0.0	608.			
3	-77.85	33.90		0.0	492.			
4	-77.85	-33.90		0.0	492.			
25	0.0	0.0						
3	900.00	0.0	25.0	62.10		0.0	0.0	1.0

**Appendix B. - MGS 32-in. (813-mm) BARRIER VII Input Deck (1100C)**

```

MGS 175ft, 1100C at 32-in. System Height
225 2 1 1 253 6 2 0
0.0001 0.0001 2.000 2000 0 1.0 1
2 10 10 10 10 500 1
1 0.0 0.0
225 2100 0.0
1 225 223 1 9.375
1 225 0.30
225 224 223 222 221 220 219 218 217 216
215 214 213 212 211 210 209 208 207 206
205 204 203 202 201 200 199 198 197 196
195 194 193 192 191 190 189 188 187 186
185 184 183 182 181 180 179 178 177 176
175 174 173 172 171 170 169 168 167 166
165 164 163 162 161 160 159 158 157 156
155 154 153 152 151 150 149 148 147 146
145 144 143 142 141 140 139 138 137 136
135 134 133 132 131 130 129 128 127 126
125 124 123 122 121 120 119 118 117 116
115 114 113 112 111 110 109 108 107 106
105 104 103 102 101 100 99 98 97 96
95 94 93 92 91 90 89 88 87 86
85 84 83 82 81 80 79 78 77 76
75 74 73 72 71 70 69 68 67 66
65 64 63 62 61 60 59 58 57 56
55 54 53 52 51 50 49 48 47 46
45 44 43 42 41 40 39 38 37 36
35 34 33 32 31 30 29 28 27 26
25 24 23 22 21 20 19 18 17 16
15 14 13 12 11 10 9 8 7 6
5 4 3 2 1
100 1
1 2.29 1.99 9.375 30000.0 6.92 99.5 68.5 0.05 12-Gauge W-Beam
300 3
1 25.875 0.00 6.0 6.0 100.0 675.0 675.0 0.05 Simulated Strong
Anchor Post
100.0 100.0 15.0 15.0
2 25.875 0.00 3.0 3.0 100.0 150.0 225.00 0.05 Second BCT Post
50.0 50.0 15.0 15.0
3 25.875 0.0 3.00 2.60 54.0 61.90 142.05 0.05 W6x9 by 6' Long
Emb. 39" in H.E. 8 soil
15.0 25.0 15.0 15.0
1 1 2 224 1 101 0.0 0.0 0.0
225 1 301 0.0 0.0 0.0 0.0
226 9 302 0.0 0.0 0.0 0.0
227 17 251 8 303 0.0 0.0 0.0 0.0
252 217 302 0.0 0.0 0.0 0.0
253 225 301 0.0 0.0 0.0 0.0
2579.0 16264.9 20 1 4 0 1
1 0.033 0.150 4.5 13.0
1 75.750 -32.188 1 43.240 1 1 0 0
2 75.750 -21.458 1 10.729 1 1 0 0
3 75.750 -10.729 1 10.729 1 1 0 0
4 75.750 0.000 1 10.729 1 1 0 0
5 75.750 10.729 1 10.729 1 1 0 0
6 75.750 21.458 1 10.729 1 1 0 0
7 75.750 32.188 1 12.940 1 1 0 0
8 60.600 32.188 1 15.150 1 1 0 0
9 45.450 32.188 1 15.150 1 1 0 0
10 30.300 32.188 1 15.150 1 1 0 0
11 15.150 32.188 1 15.150 1 1 0 0
12 0.000 32.188 1 18.888 1 1 0 0
13 -22.625 32.188 1 22.625 1 1 0 0
14 -45.250 32.188 1 22.625 1 1 0 0
15 -67.875 32.188 1 22.625 1 1 0 0
16 -90.5 32.188 1 22.625 1 1 0 0
17 -90.500 -32.188 1 45.250 1 1 0 0
18 0.000 -32.188 1 45.250 1 1 0 0
19 38.5 27.813 1 1.000 1 1 0 0

```

20	38.5	-27.813	1	1.000	1	1	0	0
1	38.5	27.813		0.00	380.250			
2	38.5	-27.813		0.00	380.250			
3	-57.0	27.813		0.00	264.500			
4	-57.0	-27.813		0.00	264.500			
1	0.00	0.00						
7	950.00	0.0		25.0	62.10	0.0	0.0	1.0

**Appendix C. - MGS 34-in. (864-mm) BARRIER VII Input Deck (1100C)**

```

MGSMRH-1 175ft, 1100C at 34-in. System Height
225 2 1 1 253 6 2 0
0.0001 0.0001 2.000 2000 0 1.0 1
10 10 10 10 10 500 1
1 0.0 0.0
225 2100 0.0
1 225 223 1 9.375
1 225 0.35
225 224 223 222 221 220 219 218 217 216
215 214 213 212 211 210 209 208 207 206
205 204 203 202 201 200 199 198 197 196
195 194 193 192 191 190 189 188 187 186
185 184 183 182 181 180 179 178 177 176
175 174 173 172 171 170 169 168 167 166
165 164 163 162 161 160 159 158 157 156
155 154 153 152 151 150 149 148 147 146
145 144 143 142 141 140 139 138 137 136
135 134 133 132 131 130 129 128 127 126
125 124 123 122 121 120 119 118 117 116
115 114 113 112 111 110 109 108 107 106
105 104 103 102 101 100 99 98 97 96
95 94 93 92 91 90 89 88 87 86
85 84 83 82 81 80 79 78 77 76
75 74 73 72 71 70 69 68 67 66
65 64 63 62 61 60 59 58 57 56
55 54 53 52 51 50 49 48 47 46
45 44 43 42 41 40 39 38 37 36
35 34 33 32 31 30 29 28 27 26
25 24 23 22 21 20 19 18 17 16
15 14 13 12 11 10 9 8 7 6
5 4 3 2 1
100 1
1 2.29 1.99 9.375 30000.0 6.92 99.5 68.5 0.05 12-Gauge W-Beam
300 3
1 27.875 0.00 6.0 6.0 100.0 675.0 675.0 0.05 Simulated Strong
Anchor Post
100.0 100.0 15.0 15.0
2 27.875 0.00 3.0 3.0 100.0 150.0 225.00 0.05 Second BCT Post
50.0 50.0 15.0 15.0
3 27.875 0.0 2.60 2.60 54.0 61.90 160.98 0.05 W6x9 by 6' Long
Emb. 37" in H.E. 8 soil
15.0 25.0 15.0 15.0
1 1 2 224 1 101 0.0 0.0 0.0
225 1 301 0.0 0.0 0.0 0.0 0.0
226 9 302 0.0 0.0 0.0 0.0 0.0
227 17 251 8 303 0.0 0.0 0.0 0.0
252 217 302 0.0 0.0 0.0 0.0 0.0
253 225 301 0.0 0.0 0.0 0.0 0.0
2599.0 16264.9 20 1 4 0 1
1 0.030 0.150 4.5 13.0
1 75.750 -32.188 1 43.240 1 1 0 0
2 75.750 -21.458 1 10.729 1 1 0 0
3 75.750 -10.729 1 10.729 1 1 0 0
4 75.750 0.000 1 10.729 1 1 0 0
5 75.750 10.729 1 10.729 1 1 0 0
6 75.750 21.458 1 10.729 1 1 0 0
7 75.750 32.188 1 12.940 1 1 0 0
8 60.600 32.188 1 15.150 1 1 0 0
9 45.450 32.188 1 15.150 1 1 0 0
10 30.300 32.188 1 15.150 1 1 0 0
11 15.150 32.188 1 15.150 1 1 0 0
12 0.000 32.188 1 18.888 1 1 0 0
13 -22.625 32.188 1 22.625 1 1 0 0
14 -45.250 32.188 1 22.625 1 1 0 0
15 -67.875 32.188 1 22.625 1 1 0 0
16 -90.5 32.188 1 22.625 1 1 0 0
17 -90.500 -32.188 1 45.250 1 1 0 0
18 0.000 -32.188 1 45.250 1 1 0 0
19 38.5 27.813 1 1.000 1 1 0 0

```

20	38.5	-27.813	1	1.000	1	1	0	0
1	38.5	27.813		0.00	380.250			
2	38.5	-27.813		0.00	380.250			
3	-57.0	27.813		0.00	264.500			
4	-57.0	-27.813		0.00	264.500			
1	0.00	0.00						
7	940.00	0.0		25.0	62.10	0.0	0.0	1.0

**Appendix D. - MGS 36-in. (914-mm) BARRIER VII Input Deck (1100C)**

```

MGSMRH-2 175ft, 1100C at 36-in. System Height
225 2 1 1 253 6 2 0
0.0001 0.0001 2.000 2000 0 1.0 1
10 10 10 10 10 500 1
1 0.0 0.0
225 2100 0.0
1 225 223 1 9.375
1 225 0.35
225 224 223 222 221 220 219 218 217 216
215 214 213 212 211 210 209 208 207 206
205 204 203 202 201 200 199 198 197 196
195 194 193 192 191 190 189 188 187 186
185 184 183 182 181 180 179 178 177 176
175 174 173 172 171 170 169 168 167 166
165 164 163 162 161 160 159 158 157 156
155 154 153 152 151 150 149 148 147 146
145 144 143 142 141 140 139 138 137 136
135 134 133 132 131 130 129 128 127 126
125 124 123 122 121 120 119 118 117 116
115 114 113 112 111 110 109 108 107 106
105 104 103 102 101 100 99 98 97 96
95 94 93 92 91 90 89 88 87 86
85 84 83 82 81 80 79 78 77 76
75 74 73 72 71 70 69 68 67 66
65 64 63 62 61 60 59 58 57 56
55 54 53 52 51 50 49 48 47 46
45 44 43 42 41 40 39 38 37 36
35 34 33 32 31 30 29 28 27 26
25 24 23 22 21 20 19 18 17 16
15 14 13 12 11 10 9 8 7 6
5 4 3 2 1
100 1
1 2.29 1.99 9.375 30000.0 6.92 99.5 68.5 0.05 12-Gauge W-Beam
300 3
1 29.875 0.00 6.0 6.0 100.0 675.0 675.0 0.05 Simulated Strong
Anchor Post
100.0 100.0 15.0 15.0
2 29.875 0.00 3.0 3.0 100.0 150.0 225.00 0.05 Second BCT Post
50.0 50.0 15.0 15.0
3 29.875 0.0 3.00 2.60 54.0 61.90 172.53 0.05 W6x9 by 6' Long
Emb. 35" in H.E. 8 soil
15.0 25.0 15.0 15.0
1 1 2 224 1 101 0.0 0.0 0.0
225 1 301 0.0 0.0 0.0 0.0
226 9 302 0.0 0.0 0.0 0.0
227 17 251 8 303 0.0 0.0 0.0 0.0
252 217 302 0.0 0.0 0.0 0.0
253 225 301 0.0 0.0 0.0 0.0
2583.0 16264.9 20 1 4 0 1
1 0.030 0.150 4.5 13.0
1 75.750 -32.188 1 43.240 1 1 0 0
2 75.750 -21.458 1 10.729 1 1 0 0
3 75.750 -10.729 1 10.729 1 1 0 0
4 75.750 0.000 1 10.729 1 1 0 0
5 75.750 10.729 1 10.729 1 1 0 0
6 75.750 21.458 1 10.729 1 1 0 0
7 75.750 32.188 1 12.940 1 1 0 0
8 60.600 32.188 1 15.150 1 1 0 0
9 45.450 32.188 1 15.150 1 1 0 0
10 30.300 32.188 1 15.150 1 1 0 0
11 15.150 32.188 1 15.150 1 1 0 0
12 0.000 32.188 1 18.888 1 1 0 0
13 -22.625 32.188 1 22.625 1 1 0 0
14 -45.250 32.188 1 22.625 1 1 0 0
15 -67.875 32.188 1 22.625 1 1 0 0
16 -90.5 32.188 1 22.625 1 1 0 0
17 -90.500 -32.188 1 45.250 1 1 0 0
18 0.000 -32.188 1 45.250 1 1 0 0

```

19	38.5	27.813	1	1.000	1	1	0	0
20	38.5	-27.813	1	1.000	1	1	0	0
1	38.5	27.813		0.00	380.250			
2	38.5	-27.813		0.00	380.250			
3	-57.0	27.813		0.00	264.500			
4	-57.0	-27.813		0.00	264.500			
1	0.00	0.00						
7	940.00	0.0	25.0	62.10		0.0	0.0	1.0



**Appendix E. - Validation for Small Car Striking a 32-in. MGS**

VALIDATION/VERIFICATION REPORT  
FOR

A Report 350 820C Small Car  
(Report 350 or MASH or EN1317 Vehicle Type)

Striking a 32-in. tall Midwest Guardrail System  
(roadside hardware type and name)

Report Date: 5/29/2012

Type of Report (check one)

- Verification (known numerical solution compared to new numerical solution) or  
 Validation (full-scale crash test compared to a numerical solution).

General Information	Known Solution	Analysis Solution
Performing Organization	MwRSF	MwRSF/Julin
Test/Run Number:	NPG-1	NPG-1 SIM-2012 01
Vehicle:	1994 Geo Metro	MwRSF modified Geo (NCAC/Politecnico di Milano 820C)
Impact Conditions		
Vehicle Mass:	887 kg	899 kg
Speed:	102.9 km/h	100 km/h
Angle:	18.7 degrees	20 degrees
Impact Point:	Upstream of post no. 14	Upstream of post no. 12

**Composite Validation/Verification Score**

List the Report 350/MASH or EN1317 Test Number		3-10
Part I	Did all solution verification criteria in Table E-1 pass?	Yes
Part II	Do all the time history evaluation scores from Table E-2 result in a satisfactory comparison (i.e., the comparison passes the criterion)? If all the values in Table E-2 did not pass, did the weighted procedure shown in Table E-3 result in an acceptable comparison. If all the criteria in Table E-2 pass, enter "yes." If all the criteria in Table E-2 did not pass but Table E-3 resulted in a passing score, enter "yes."	Yes
Part III	All the criteria in Table E-4 (Test-PIRT) passed?	Yes
	Are the results of Steps I through III all affirmative (i.e., YES)? If all three steps result in a "YES" answer, the comparison can be considered validated or verified. If one of the steps results in a negative response, the result cannot be considered validated or verified.	Yes

The analysis solution (check one)  is  is NOT verified/validated against the known solution.

**PART I: BASIC INFORMATION**

These forms may be used for validation or verification of roadside hardware crash tests. If the known solution is a full-scale crash test (i.e., physical experiment) which is being compared to a numerical solution (e.g., LSDYNA analysis) then the procedure is a validation exercise. If the known solution is a numerical solution (e.g., a prior finite element model using a different program or earlier version of the software) then the procedure is a verification exercise. This form can also be used to verify the repeatability of crash tests by comparing two full-scale crash test experiments. Provide the following basic information for the validation/verification comparison:

- 1. What type of roadside hardware is being evaluated (check one)?
  - Longitudinal barrier or transition
  - Terminal or crash cushion
  - Breakaway support or work zone traffic control device
  - Truck-mounted attenuator
  - Other hardware: \_\_\_\_\_
  
- 2. What test guidelines were used to perform the full-scale crash test (check one)?
  - NCHRP Report No. 350
  - MASH
  - EN1317
  - Other: \_\_\_\_\_
  
- 3. Indicate the test level and number being evaluated (fill in the blank). 3-10
  
- 4. Indicate the vehicle type appropriate for the test level and number indicated in item 3 according to the testing guidelines indicated in item 2.

NCHRP Report No. 350/MASH

- 700C                       820C                       1100C
- 2000P                       2270P
- 8000S                       10000S
- 36000V
- 36000T

EN1317

- Car (900 kg)                       Car (1300 kg)                       Car (1500 kg)
- Rigid HGV (10 ton)                       Rigid HGV (16 ton)
- Rigid HGV (30 ton)
- Bus (13 ton)
- Articulated HGV (38 ton)

## PART II: ANALYSIS SOLUTION VERIFICATION

Using the results of the analysis solution, fill in the values for Table E-1. These values are indications of whether the analysis solution produced a numerically stable result and do not necessarily mean that the result is a good comparison to the known solution. The purpose of this table is to ensure that the numerical solution produces results that are numerically stable and conform to the conservation laws (e.g., energy, mass and momentum).

Table E-1. Analysis Solution Verification Table

Verification Evaluation Criteria	Change (%)	Pass?
<b>Total energy</b> of the analysis solution (i.e., kinetic, potential, contact, etc.) must not vary more than 10 percent from the beginning of the run to the end of the run.	3.97	Yes
<b>Hourglass Energy</b> of the analysis solution at the end of the run is less than <i>five percent</i> of the total <i>initial energy</i> at the <i>beginning</i> of the run.	0	Yes
<b>Hourglass Energy</b> of the analysis solution at the end of the run is less than <i>ten percent</i> of the total <i>internal energy</i> at the <i>end</i> of the run.	0	Yes
The part/material with the highest amount of hourglass energy at the end of the run is less than ten percent of the total internal energy of the part/material at the end of the run.	0	Yes
Mass added to the total model is less than five percent of the total model mass at the beginning of the run.	0.3	Yes
The part/material with the most mass added had less than 10 percent of its initial mass added.	2.1	Yes
The moving parts/materials in the model have less than five percent of mass added to the initial moving mass of the model.	0.3	Yes
There are no shooting nodes in the solution?	Yes	Yes
There are no solid elements with negative volumes?	Yes	Yes

The Analysis Solution (check one)  passes  does NOT pass all the criteria in Table E1-1  
 with  without exceptions as noted.

**PART III: TIME HISTORY EVALUATION TABLE**

Table E-2. Roadside Safety Validation Metrics Rating Table – Time History Comparisons

(single channel option)

Evaluation Criteria							Time interval [0 sec; 0.5 sec]					
O	<b>Sprague-Geers Metrics</b> List all the data channels being compared. Calculate the M and P metrics using RSVVP and enter the results. Values less than or equal to 40 are acceptable.						M	P	Pass?			
	<b>RSVVP Curve Preprocessing Options</b>											
		Filter Option	Sync. Option	Shift		Drift						
				True Curve	Test Curve	True Curve	Test Curve					
	X acceleration	CFC 180	Min. Area of Residuals	Y	N	Y	N	2.8	30.5	Yes		
	Y acceleration	CFC 180	Min. Area of Residuals	Y	N	Y	N	17.4	22.4	Yes		
	Z acceleration	CFC 180	Min. Area of Residuals	Y	N	Y	N	32.4	48.9	No		
	Roll rate	CFC 180	Min. Area of Residuals	Y	N	Y	N	37.9	37.9	Yes		
Pitch rate	CFC 180	Min. Area of Residuals	Y	N	Y	N	46.7	48.8	No			
Yaw rate	CFC 180	Min. Area of Residuals	Y	N	Y	N	0.2	8.6	Yes			
P	<b>ANOVA Metrics</b> List all the data channels being compared. Calculate the ANOVA metrics using RSVVP and enter the results. Both of the following criteria must be met: <ul style="list-style-type: none"> <li>The mean residual error must be less than five percent of the peak acceleration (<math>\bar{e} \leq 0.05 \cdot a_{Peak}</math>) and</li> <li>The standard deviation of the residuals must be less than 35 percent of the peak acceleration (<math>\sigma \leq 0.35 \cdot a_{Peak}</math>)</li> </ul>						Mean Residual	Standard Deviation of Residuals	Pass?			
	X acceleration/Peak									0.03	0.23	Yes
	Y acceleration/Peak									0.05	0.21	Yes
	Z acceleration/Peak									0.06	0.32	No
	Roll rate									0.04	0.35	Yes
	Pitch rate									0.08	0.44	No
	Yaw rate									0.05	0.12	Yes

The Analysis Solution (check one)  passes  does NOT pass all the criteria in Table E-2.

Table E-3. Roadside Safety Validation Metrics Rating Table – Time History Comparisons

(multi-channel option)

Evaluation Criteria (time interval [0 sec; 0.5 sec])				
Channels (Select which were used)				
<input checked="" type="checkbox"/> X Acceleration	<input checked="" type="checkbox"/> Y Acceleration	<input checked="" type="checkbox"/> Z Acceleration		
<input checked="" type="checkbox"/> Roll rate	<input checked="" type="checkbox"/> Pitch rate	<input checked="" type="checkbox"/> Yaw rate		
<b>Multi-Channel Weights</b>  <input checked="" type="checkbox"/> Area II method <input type="checkbox"/> Inertial method	<b>X Channel: 0.149209</b> <b>Y Channel: 0.269629</b> <b>Z Channel: 0.081161</b> <b>Yaw Channel: 0.464020</b> <b>Roll Channel: 0.016895</b> <b>Pitch Channel: 0.019084</b>			
O	<b>Sprague-Geer Metrics</b> Values less or equal to 40 are acceptable.	M	P	Pass?
		9.4	20.1	Yes
P	<b>ANOVA Metrics</b> Both of the following criteria must be met: <ul style="list-style-type: none"> <li>The mean residual error must be less than five percent of the peak acceleration (<math>\bar{e} \leq 0.05 \cdot a_{Peak}</math>)</li> <li>The standard deviation of the residuals must be less than 35 percent of the peak acceleration (<math>\sigma \leq 0.35 \cdot a_{Peak}</math>)</li> </ul>	Mean Residual	Standard Deviation of Residuals	Pass?
		0.02	0.19	Yes

The Analysis Solution (check one)  passes  does NOT pass all the criteria in Table E-3.

**PART IV: PHENOMENA IMPORTANCE RANKING TABLE**

Table E-4. Evaluation Criteria Test Applicability Table

Evaluation Factors	Evaluation Criteria			Applicable Tests	
Structural Adequacy	A	Test article should contain and redirect the vehicle; the vehicle should not penetrate, under-ride, or override the installation although controlled lateral deflection of the test article is acceptable.		10, 11, 12, 20, 21, 22, 35, 36, 37, 38	
	B	The test article should readily activate in a predictable manner by breaking away, fracturing or yielding.		60, 61, 70, 71, 80, 81	
	C	Acceptable test article performance may be by redirection, controlled penetration or controlled stopping of the vehicle.		30, 31,, 32, 33, 34, 39, 40, 41, 42, 43, 44, 50, 51, 52, 53	
Occupant Risk	D	Detached elements, fragments or other debris from the test article should not penetrate or show potential for penetrating the occupant compartment, or present an undue hazard to other traffic, pedestrians or personnel in a work zone.		All	
	E	Detached elements, fragments or other debris from the test article, or vehicular damage should not block the driver's vision or otherwise cause the driver to lose control of the vehicle. (Answer Yes or No)		70, 71	
	F	The vehicle should remain upright during and after the collision although moderate roll, pitching and yawing are acceptable.		All except those listed in criterion G	
	G	It is preferable, although not essential, that the vehicle remain upright during and after collision.		12, 22 (for test level 1 – 30, 31, 32, 33, 34, 35, 36, 37, 38, 39, 40, 41, 42, 43, 44)	
	H	Occupant impact velocities should satisfy the following:			10, 20, 30,31, 32, 33, 34, 36, 40, 41, 42, 43, 50, 51, 52, 53, 80, 81
		Occupant Impact Velocity Limits (m/s)			
		Component	Preferred	Maximum	
Longitudinal and Lateral	9	12	60, 61, 70, 71		
Longitudinal	3	5			
I	Occupant ridedown accelerations should satisfy the following:			10, 20, 30,31, 32, 33, 34, 36, 40, 41, 42, 43, 50, 51, 52, 53, 60, 61, 70, 71, 80, 81	
	Occupant Ridedown Acceleration Limits (g's)				
	Component	Preferred	Maximum		
Longitudinal and Lateral	15	20			
Vehicle Trajectory	L	The occupant impact velocity in the longitudinal direction should not exceed 40 ft/sec and the occupant ride-down acceleration in the longitudinal direction should not exceed 20 G's.		11,21, 35, 37, 38, 39	
	M	The exit angle from the test article preferable should be less than 60 percent of test impact angle, measured at the time of vehicle loss of contact with test device.		10, 11, 12, 20, 21, 22, 35, 36, 37, 38, 39	
	N	Vehicle trajectory behind the test article is acceptable.		30, 31, 32, 33, 34, 39, 42, 43, 44, 60, 61, 70, 71, 80, 81	

Table E-5. (a) Roadside Safety Phenomena Importance Ranking Table (Structural Adequacy)

		Evaluation Criteria	Known Result	Analysis Result	Difference Relative/ Absolute	Agree?	
Structural Adequacy	A	A1	Test article should contain and redirect the vehicle; the vehicle should not penetrate, under-ride, or override the installation although controlled lateral deflection of the test article is acceptable. (Answer Yes or No)	Yes	Yes	X	Yes
		A2	Maximum dynamic deflection: - Relative difference is less than 20 percent or - Absolute difference is less than 0.15 m	0.442 m	0.496 m	11.9% 0.054 m	Yes
		A3	Length of vehicle-barrier contact: - Relative difference is less than 20 percent or - Absolute difference is less than 2 m	450 ms	410 ms	8.9%	Yes
		A4	Number of broken or significantly bent posts is less than 20 percent.	2	2	0%	Yes
		A5	Did the rail element rupture or tear (Answer Yes or No)	No	No	X	Yes
		A6	Were there failures of connector elements (Answer Yes or No).	No	No	X	Yes
		A7	Was there significant snagging between the vehicle wheels and barrier elements (Answer Yes or No).	No	No	X	Yes
		A8	Was there significant snagging between vehicle body components and barrier elements (Answer Yes or No).	No	No	X	Yes

Table E-5. (b) Roadside Safety Phenomena Importance Ranking Table (Occupant Risk)

Evaluation Criteria			Known Result	Analysis Result	Difference Relative/Absolute	Agree ?		
Occupant Risk	D	Detached elements, fragments or other debris from the test article should not penetrate or show potential for penetrating the occupant compartment, or present an undue hazard to other traffic, pedestrians or personnel in a work zone. (Answer Pass or Fail)	Pass	Pass	X	Yes		
	F1	The vehicle should remain upright during and after the collision although moderate roll, pitching and yawing are acceptable. (Answer Pass or Fail)	Pass	Pass	X	Yes		
	F	F2	Maximum roll of the vehicle: - Relative difference is less than 20 percent or - Absolute difference is less than 5 degrees.	2.69°	2.5°	7.6% 0.19°	Yes	
		F3	Maximum pitch of the vehicle is: - Relative difference is less than 20 percent or - Absolute difference is less than 5 degrees.	0.6°	1.0°	66.6% 0.4°	Yes	
		F4	Maximum yaw of the vehicle is: - Relative difference is less than 20 percent or - Absolute difference is less than 5 degrees.	3.2°	2.55°	20% 0.65°	Yes	
			Occupant impact velocities: - Relative difference is less than 20 percent or - Absolute difference is less than 2 m/s.					
	L	L1	• Longitudinal OIV (m/s)	3.52	3.28	6.8% 0.24 m/s	Yes	
			• Lateral OIV (m/s)	5.68	4.74	16.5% 0.97 m/s	Yes	
			• THIV (m/s)	*N.R.	*N.R.			
		L2		Occupant accelerations: - Relative difference is less than 20 percent or - Absolute difference is less than 4 g's.				
			• Longitudinal ORA	6.13	6.3	0.17 g	Yes	
			• Lateral ORA	7.97	8.64	0.67 g	Yes	
			• PHD	*N.R.	*N.R.			
	• ASI	*N.R.	1.85					



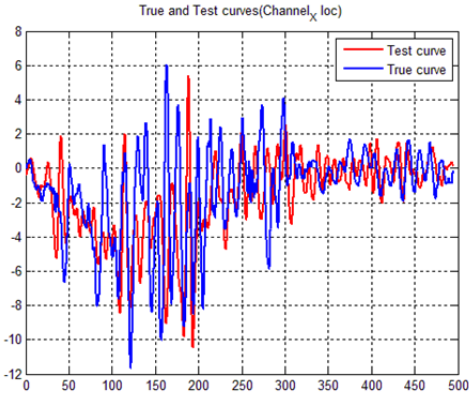
Table E-5. (c) Roadside Safety Phenomena Importance Ranking Table (Vehicle Trajectory)

		Evaluation Criteria	Known Result	Analysis Result	Difference Relative/Absolute	Agree?	
Vehicle Trajectory	M	M1	The exit angle from the test article preferable should be less than 60 percent of test impact angle, measured at the time of vehicle loss of contact with test device.	10.3° 55%	12.8° 73%	X	Yes
		M2	Exit angle at loss of contact: - Relative difference is less than 20 percent or - Absolute difference is less than 5 degrees.	10.3°	14.5°	28% 4.2°	Yes
		M3	Exit velocity at loss of contact: - Relative difference is less than 20 percent or - Absolute difference is less than 5 degrees.	*N.R.	75.9 km/h		
		M4	One or more vehicle tires failed or de-beaded during the collision event (Answer Yes or No).	Yes	*N.M.	X	

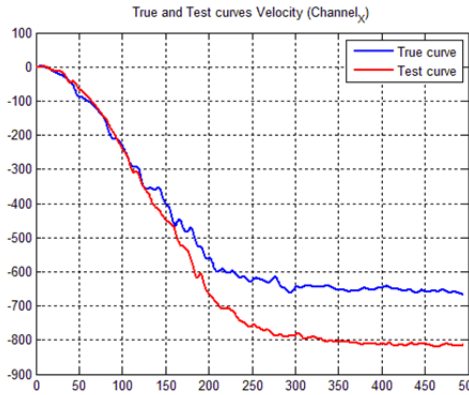
\*N.R. - Not Reported

\*N.M. - Not Modeled

The Analysis Solution (check one)  passes  does NOT pass all the criteria in Tables E-5a through E-5c  with exceptions as noted  without exceptions.

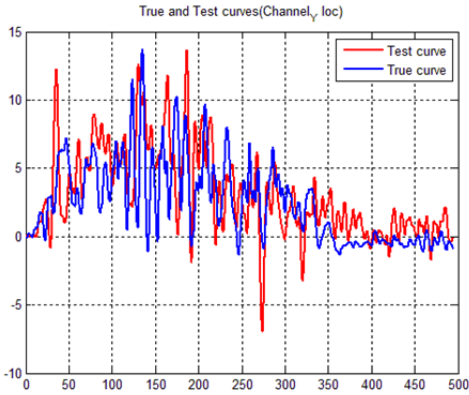


(a)

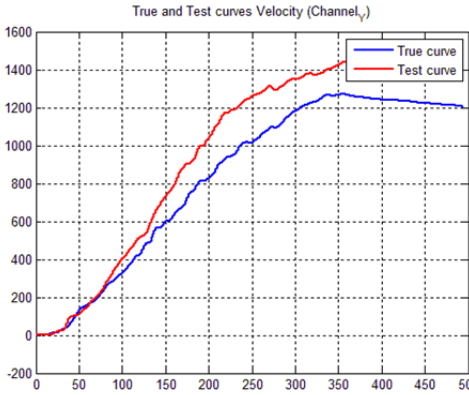


(b)

Figure E-1. X-Channel (a) acceleration-time history data used to compute metrics and (b) integration of acceleration-time history data

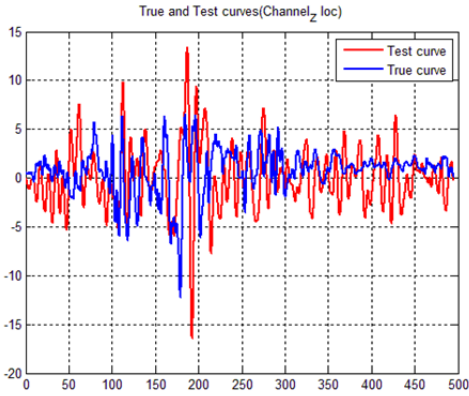


(a)

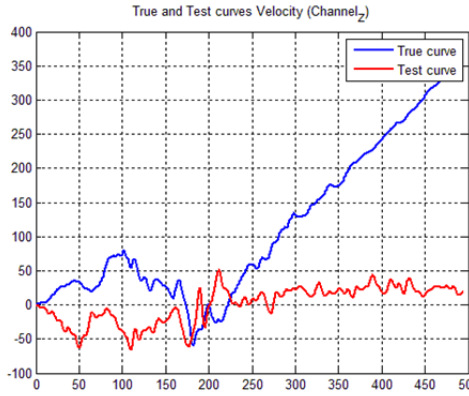


(b)

Figure E-2. Y-Channel (a) acceleration-time history data used to compute metrics and (b) integration of acceleration-time history data

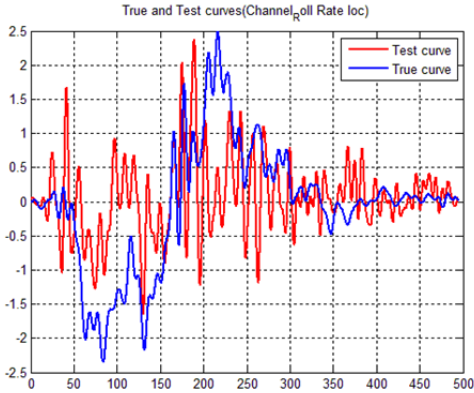


(a)

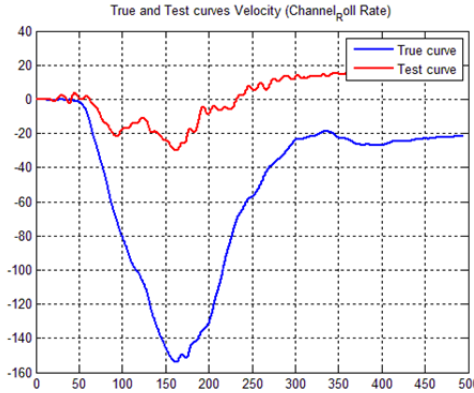


(b)

Figure E-3. Z-Channel (a) acceleration-time history data used to compute metrics and (b) integration of acceleration-time history data

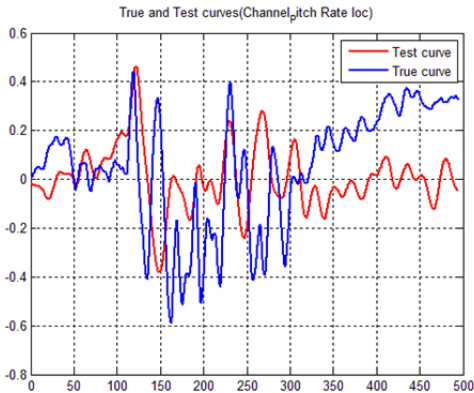


(a)

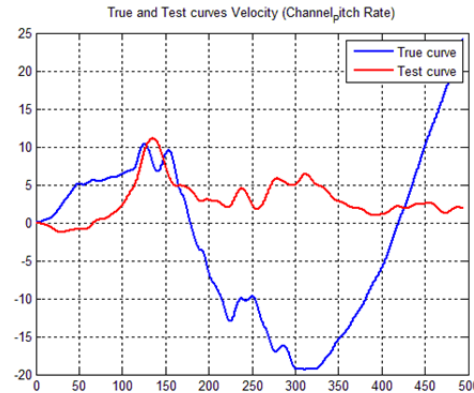


(b)

Figure E-4. Roll Channel (a) angular rate-time history data used to compute metrics and (b) integration of angular rate-time history data

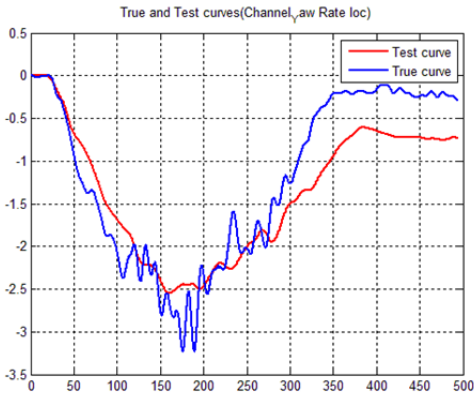


(a)

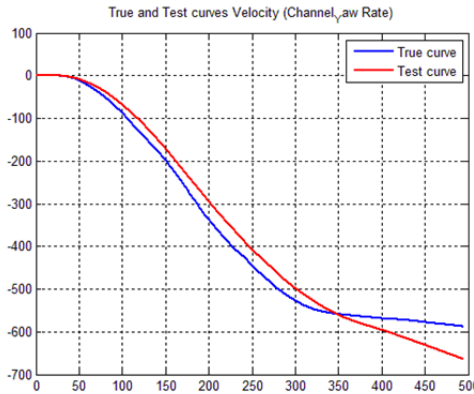


(b)

Figure E-5. Pitch Channel (a) angular rate-time history data used to compute metrics and (b) integration of angular rate-time history data



(a)



(b)

Figure E-6. Yaw Channel (a) angular rate-time history data used to compute metrics and (b) integration of angular rate-time history data

**Appendix F. - Validation for Pickup Truck Striking a 31-in. MGS**

VALIDATION/VERIFICATION REPORT  
FOR

A           **MASH 2270P Pickup Truck**            
(Report 350 or MASH or EN1317 Vehicle Type)

Striking a           **31-in. tall Midwest Guardrail System**            
(roadside hardware type and name)

Report Date:           **5/30/2012**          

Type of Report (check one)

- Verification (known numerical solution compared to new numerical solution) or  
 Validation (full-scale crash test compared to a numerical solution).

General Information	Known Solution	Analysis Solution
Performing Organization	MwRSF	MwRSF/Julin
Test/Run Number:	2214MG-2	2214MG-2 SIM-2012 SUSP
Vehicle:	2002 Dodge Ram	MwRSF modified Silverado (NCAC)
Impact Conditions		
Vehicle Mass:	2268 kg	2270 kg
Speed:	101.2 km/h	100 km/h
Angle:	25.5 degrees	25 degrees
Impact Point:	Upstream of post no. 12	Upstream of post no. 12

**Composite Validation/Verification Score**

List the Report 350/MASH or EN1317 Test Number		3-11
Part I	Did all solution verification criteria in Table F-1 pass?	Yes
Part II	Do all the time history evaluation scores from Table F-2 result in a satisfactory comparison (i.e., the comparison passes the criterion)? If all the values in Table F-2 did not pass, did the weighted procedure shown in Table F-3 result in an acceptable comparison. If all the criteria in Table F-2 pass, enter “yes.” If all the criteria in Table F-2 did not pass but Table F-3 resulted in a passing score, enter “yes.”	Yes
Part III	All the criteria in Table F-4 (Test-PIRT) passed?	Yes
	Are the results of Steps I through III all affirmative (i.e., YES)? If all three steps result in a “YES” answer, the comparison can be considered validated or verified. If one of the steps results in a negative response, the result cannot be considered validated or verified.	Yes

The analysis solution (check one)  is  is NOT verified/validated against the known solution.

**PART I: BASIC INFORMATION**

These forms may be used for validation or verification of roadside hardware crash tests. If the known solution is a full-scale crash test (i.e., physical experiment) which is being compared to a numerical solution (e.g., LSDYNA analysis) then the procedure is a validation exercise. If the known solution is a numerical solution (e.g., a prior finite element model using a different program or earlier version of the software) then the procedure is a verification exercise. This form can also be used to verify the repeatability of crash tests by comparing two full-scale crash test experiments. Provide the following basic information for the validation/verification comparison:

- 5. What type of roadside hardware is being evaluated (check one)?
  - Longitudinal barrier or transition
  - Terminal or crash cushion
  - Breakaway support or work zone traffic control device
  - Truck-mounted attenuator
  - Other hardware: \_\_\_\_\_
  
- 6. What test guidelines were used to perform the full-scale crash test (check one)?
  - NCHRP Report No. 350
  - MASH
  - EN1317
  - Other: \_\_\_\_\_
  
- 7. Indicate the test level and number being evaluated (fill in the blank). 3-11
  
- 8. Indicate the vehicle type appropriate for the test level and number indicated in item 3 according to the testing guidelines indicated in item 2.

NCHRP Report No. 350/MASH

- 700C                       820C                       1100C
- 2000P                       2270P
- 8000S                       10000S
- 36000V
- 36000T

EN1317

- Car (900 kg)                       Car (1300 kg)                       Car (1500 kg)
- Rigid HGV (10 ton)                       Rigid HGV (16 ton)
- Rigid HGV (30 ton)
- Bus (13 ton)
- Articulated HGV (38 ton)

**PART II: ANALYSIS SOLUTION VERIFICATION**

Using the results of the analysis solution, fill in the values for Table F-1. These values are indications of whether the analysis solution produced a numerically stable result and do not necessarily mean that the result is a good comparison to the known solution. The purpose of this table is to ensure that the numerical solution produces results that are numerically stable and conform to the conservation laws (e.g., energy, mass and momentum).

Table F-1. Analysis Solution Verification Table

Verification Evaluation Criteria	Change (%)	Pass?
<b>Total energy</b> of the analysis solution (i.e., kinetic, potential, contact, etc.) must not vary more than 10 percent from the beginning of the run to the end of the run.	5.2	Yes
<b>Hourglass Energy</b> of the analysis solution at the end of the run is less than <i>five percent</i> of the total <i>initial energy</i> at the <i>beginning</i> of the run.	1.5	Yes
<b>Hourglass Energy</b> of the analysis solution at the end of the run is less than <i>ten percent</i> of the total <i>internal energy</i> at the <i>end</i> of the run.	1.6	Yes
The part/material with the highest amount of hourglass energy at the end of the run is less than ten percent of the total internal energy of the part/material at the end of the run.	1.5	Yes
Mass added to the total model is less than five percent of the total model mass at the beginning of the run.	0.6	Yes
The part/material with the most mass added had less than 10 percent of its initial mass added.	1.2	Yes
The moving parts/materials in the model have less than five percent of mass added to the initial moving mass of the model.	0.6	Yes
There are no shooting nodes in the solution?	Yes	Yes
There are no solid elements with negative volumes?	Yes	Yes

The Analysis Solution (check one)  passes  does NOT pass all the criteria in Table E1-1  
 with  without exceptions as noted.

**PART III: TIME HISTORY EVALUATION TABLE**

Table F-2. Roadside Safety Validation Metrics Rating Table – Time History Comparisons

(single channel option)

Evaluation Criteria							Time interval [0 sec; 0.6 sec]						
O	<b>Sprague-Geers Metrics</b> List all the data channels being compared. Calculate the M and P metrics using RSVVP and enter the results. Values less than or equal to 40 are acceptable.						M	P	Pass?				
	<b>RSVVP Curve Preprocessing Options</b>												
		Filter Option	Sync. Option	Shift		Drift							
				True Curve	Test Curve	True Curve				Test Curve			
	X acceleration	CFC 180	Min. Area of Residuals	Y	N	Y				N	7.9	32.5	Yes
	Y acceleration	CFC 180	Min. Area of Residuals	Y	N	Y				N	21.7	19.5	Yes
	Z acceleration	CFC 180	Min. Area of Residuals	Y	N	Y				N	157.8	46.3	No
	Roll rate	CFC 180	Min. Area of Residuals	Y	N	Y				N	54.9	45.6	No
Pitch rate	CFC 180	Min. Area of Residuals	Y	N	Y	N	140.4	48.2	No				
Yaw rate	CFC 180	Min. Area of Residuals	Y	N	Y	N	6.6	7.3	Yes				
P	<b>ANOVA Metrics</b> List all the data channels being compared. Calculate the ANOVA metrics using RSVVP and enter the results. Both of the following criteria must be met: <ul style="list-style-type: none"> <li>The mean residual error must be less than five percent of the peak acceleration (<math>\bar{e} \leq 0.05 \cdot a_{Peak}</math>) and</li> <li>The standard deviation of the residuals must be less than 35 percent of the peak acceleration (<math>\sigma \leq 0.35 \cdot a_{Peak}</math>)</li> </ul>						Mean Residual	Standard Deviation of Residuals	Pass?				
	X acceleration/Peak									0.04	0.28	Yes	
	Y acceleration/Peak									0.05	0.31	Yes	
	Z acceleration/Peak									0.02	0.72	No	
	Roll rate									0.27	0.49	No	
	Pitch rate									0.08	0.81	No	
	Yaw rate									0.03	0.13	Yes	

The Analysis Solution (check one)  passes  does NOT pass all the criteria in Table F-2.

Table F-3. Roadside Safety Validation Metrics Rating Table – Time History Comparisons

(multi-channel option)

Evaluation Criteria (time interval [0 sec; 0.6 sec])																		
Channels (Select which were used)																		
<input checked="" type="checkbox"/> X Acceleration	<input checked="" type="checkbox"/> Y Acceleration	<input checked="" type="checkbox"/> Z Acceleration																
<input checked="" type="checkbox"/> Roll rate	<input checked="" type="checkbox"/> Pitch rate	<input checked="" type="checkbox"/> Yaw rate																
<b>Multi-Channel Weights</b>  <input checked="" type="checkbox"/> Area II method <input type="checkbox"/> Inertial method	<b>X Channel: 0.192377</b> <b>Y Channel: 0.296924</b> <b>Z Channel: 0.010698</b> <b>Yaw Channel: 0.433215</b> <b>Roll Channel: 0.032576</b> <b>Pitch Channel: 0.034208</b>	<table border="1"> <caption>Channel Weights Data</caption> <thead> <tr> <th>Channel</th> <th>Weight</th> </tr> </thead> <tbody> <tr> <td>X acc</td> <td>0.192377</td> </tr> <tr> <td>Y acc</td> <td>0.296924</td> </tr> <tr> <td>Z acc</td> <td>0.010698</td> </tr> <tr> <td>Yaw rate</td> <td>0.433215</td> </tr> <tr> <td>Roll rate</td> <td>0.032576</td> </tr> <tr> <td>Pitch rate</td> <td>0.034208</td> </tr> </tbody> </table>			Channel	Weight	X acc	0.192377	Y acc	0.296924	Z acc	0.010698	Yaw rate	0.433215	Roll rate	0.032576	Pitch rate	0.034208
Channel	Weight																	
X acc	0.192377																	
Y acc	0.296924																	
Z acc	0.010698																	
Yaw rate	0.433215																	
Roll rate	0.032576																	
Pitch rate	0.034208																	
O	<b>Sprague-Geer Metrics</b> Values less or equal to 40 are acceptable.	<b>M</b>	<b>P</b>	<b>Pass?</b>														
		19.1	18.8	Yes														
P	<b>ANOVA Metrics</b> Both of the following criteria must be met: <ul style="list-style-type: none"> <li>The mean residual error must be less than five percent of the peak acceleration (<math>\bar{e} \leq 0.05 \cdot a_{Peak}</math>)</li> <li>The standard deviation of the residuals must be less than 35 percent of the peak acceleration (<math>\sigma \leq 0.35 \cdot a_{Peak}</math>)</li> </ul>	<b>Mean Residual</b>	<b>Standard Deviation of Residuals</b>	<b>Pass?</b>														
		0.3	0.25	Yes														

The Analysis Solution (check one)  passes  does NOT pass all the criteria in Table F-3.



**PART IV: PHENOMENA IMPORTANCE RANKING TABLE**

Table F-4. Evaluation Criteria Test Applicability Table

Evaluation Factors	Evaluation Criteria			Applicable Tests	
Structural Adequacy	A	Test article should contain and redirect the vehicle; the vehicle should not penetrate, under-ride, or override the installation although controlled lateral deflection of the test article is acceptable.		10, 11, 12, 20, 21, 22, 35, 36, 37, 38	
	B	The test article should readily activate in a predictable manner by breaking away, fracturing or yielding.		60, 61, 70, 71, 80, 81	
	C	Acceptable test article performance may be by redirection, controlled penetration or controlled stopping of the vehicle.		30, 31,, 32, 33, 34, 39, 40, 41, 42, 43, 44, 50, 51, 52, 53	
Occupant Risk	D	Detached elements, fragments or other debris from the test article should not penetrate or show potential for penetrating the occupant compartment, or present an undue hazard to other traffic, pedestrians or personnel in a work zone.		All	
	E	Detached elements, fragments or other debris from the test article, or vehicular damage should not block the driver's vision or otherwise cause the driver to lose control of the vehicle. (Answer Yes or No)		70, 71	
	F	The vehicle should remain upright during and after the collision although moderate roll, pitching and yawing are acceptable.		All except those listed in criterion G	
	G	It is preferable, although not essential, that the vehicle remain upright during and after collision.		12, 22 (for test level 1 – 30, 31, 32, 33, 34, 35, 36, 37, 38, 39, 40, 41, 42, 43, 44)	
	H	Occupant impact velocities should satisfy the following:			10, 20, 30,31, 32, 33, 34, 36, 40, 41, 42, 43, 50, 51, 52, 53, 80, 81
		Occupant Impact Velocity Limits (m/s)			
		Component	Preferred	Maximum	
Longitudinal and Lateral	9	12	60, 61, 70, 71		
Longitudinal	3	5			
I	Occupant ridedown accelerations should satisfy the following:			10, 20, 30,31, 32, 33, 34, 36, 40, 41, 42, 43, 50, 51, 52, 53, 60, 61, 70, 71, 80, 81	
Occupant Ridedown Acceleration Limits (g's)					
Component	Preferred	Maximum			
Longitudinal and Lateral	15	20			
Vehicle Trajectory	L	The occupant impact velocity in the longitudinal direction should not exceed 40 ft/sec and the occupant ride-down acceleration in the longitudinal direction should not exceed 20 G's.		11,21, 35, 37, 38, 39	
	M	The exit angle from the test article preferable should be less than 60 percent of test impact angle, measured at the time of vehicle loss of contact with test device.		10, 11, 12, 20, 21, 22, 35, 36, 37, 38, 39	
	N	Vehicle trajectory behind the test article is acceptable.		30, 31, 32, 33, 34, 39, 42, 43, 44, 60, 61, 70, 71, 80, 81	

Table F-5. (a) Roadside Safety Phenomena Importance Ranking Table (Structural Adequacy)

		Evaluation Criteria	Known Result	Analysis Result	Difference Relative/ Absolute	Agree?	
Structural Adequacy	A	A1	Test article should contain and redirect the vehicle; the vehicle should not penetrate, under-ride, or override the installation although controlled lateral deflection of the test article is acceptable. (Answer Yes or No)	Yes	Yes	X	Yes
		A2	Maximum dynamic deflection: - Relative difference is less than 20 percent or - Absolute difference is less than 0.15 m	1.114 m	0.987 m	11.4% 0.127 m	Yes
		A3	Length of vehicle-barrier contact: - Relative difference is less than 20 percent or - Absolute difference is less than 2 m	718 ms	620 ms	13.6%	Yes
		A4	Number of broken or significantly bent posts is less than 20 percent.	3	3	0%	Yes
		A5	Did the rail element rupture or tear (Answer Yes or No)	No	No	X	Yes
		A6	Were there failures of connector elements (Answer Yes or No).	No	No	X	Yes
		A7	Was there significant snagging between the vehicle wheels and barrier elements (Answer Yes or No).	No	No	X	Yes
		A8	Was there significant snagging between vehicle body components and barrier elements (Answer Yes or No).	No	No	X	Yes

Table F-5. (b) Roadside Safety Phenomena Importance Ranking Table (Occupant Risk)

Evaluation Criteria			Known Result	Analysis Result	Difference Relative/ Absolute	Agree ?	
Occupant Risk	D	Detached elements, fragments or other debris from the test article should not penetrate or show potential for penetrating the occupant compartment, or present an undue hazard to other traffic, pedestrians or personnel in a work zone. (Answer Pass or Fail)	Pass	Pass	X	Yes	
	F1	The vehicle should remain upright during and after the collision although moderate roll, pitching and yawing are acceptable. (Answer Pass or Fail)	Pass	Pass	X	Yes	
	F	F2	Maximum roll of the vehicle: - Relative difference is less than 20 percent or - Absolute difference is less than 5 degrees.	4.08°	5.5°	25.8% 1.42°	Yes
		F3	Maximum pitch of the vehicle is: - Relative difference is less than 20 percent or - Absolute difference is less than 5 degrees.	-1.8°	-2.4°	33.3% 0.6°	Yes
		F4	Maximum yaw of the vehicle is: - Relative difference is less than 20 percent or - Absolute difference is less than 5 degrees.	-45.7°	-41.3°	9.6% 4.4°	Yes
			Occupant impact velocities: - Relative difference is less than 20 percent or - Absolute difference is less than 2 m/s.				
	L	L1	• Longitudinal OIV (m/s)	4.2	4.69	11.7% 0.49 m/s	Yes
			• Lateral OIV (m/s)	4.8	2.98	37.9% 1.82 m/s	Yes
			• THIV (m/s)	6.9	5.04	27% 1.86 m/s	Yes
		L2	Occupant accelerations: - Relative difference is less than 20 percent or - Absolute difference is less than 4 g's.				
		• Longitudinal ORA	8.2	5.01	3.19 g	Yes	
		• Lateral ORA	6.9	4.37	2.53 g	Yes	
		• PHD	10.8	9.7	1.1 g	Yes	
		• ASI	*N.R.	*N.R.			

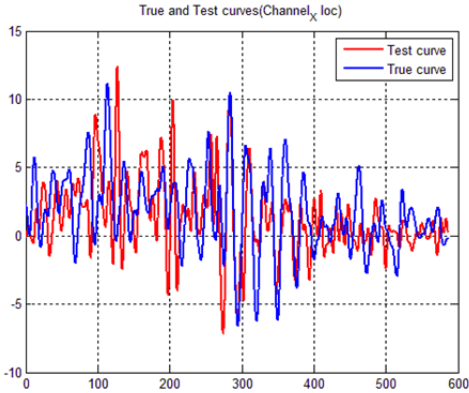
Table F-5. (c) Roadside Safety Phenomena Importance Ranking Table (Vehicle Trajectory)

Evaluation Criteria		Known Result	Analysis Result	Difference Relative/ Absolute	Agree?	
Vehicle Trajectory	M1	The exit angle from the test article preferable should be less than 60 percent of test impact angle, measured at the time of vehicle loss of contact with test device.	13.5° 54%	16.2° 62%	X	Yes
	M2	Exit angle at loss of contact: - Relative difference is less than 20 percent or - Absolute difference is less than 5 degrees.	13.5°	16.2°	20% 2.7°	Yes
	M3	Exit velocity at loss of contact: - Relative difference is less than 20 percent or - Absolute difference is less than 5 degrees.	40.6 km/h	44.7 km/h	10.1% 4.1 km/h	Yes
	M4	One or more vehicle tires failed or de-beaded during the collision event (Answer Yes or No).	Yes	Yes	X	Yes

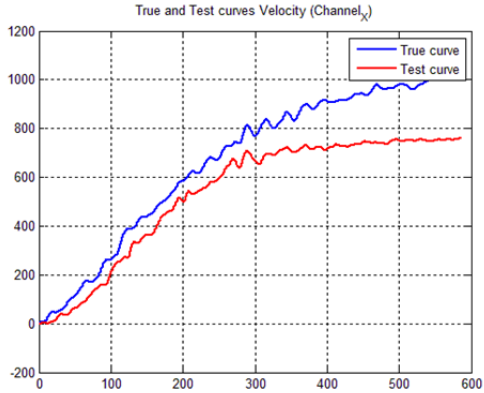
\*N.R. - Not Reported

\*N.M. - Not Modeled

The Analysis Solution (check one)  passes  does NOT pass all the criteria in Tables F-5a through F-5c  with exceptions as noted  without exceptions .

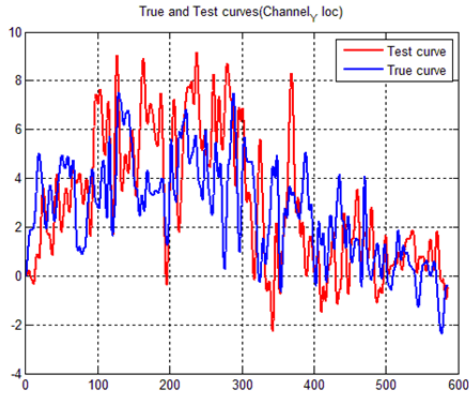


(a)

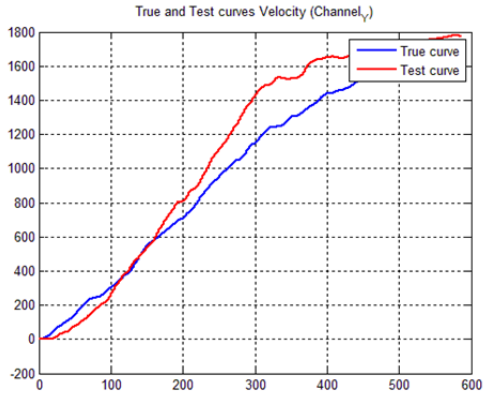


(b)

Figure F-1. X-Channel (a) acceleration-time history data used to compute metrics and (b) integration of acceleration-time history data

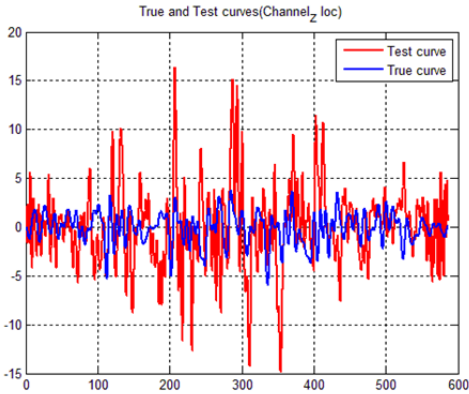


(a)

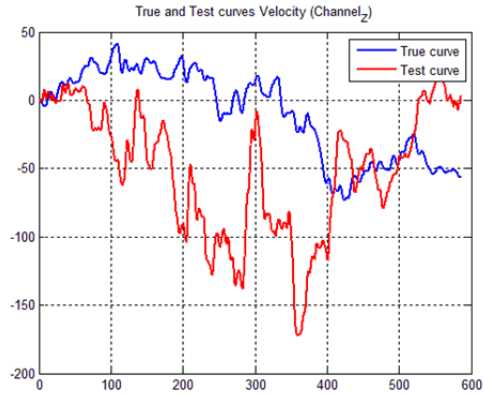


(b)

Figure F-2. Y-Channel (a) acceleration-time history data used to compute metrics and (b) integration of acceleration-time history data

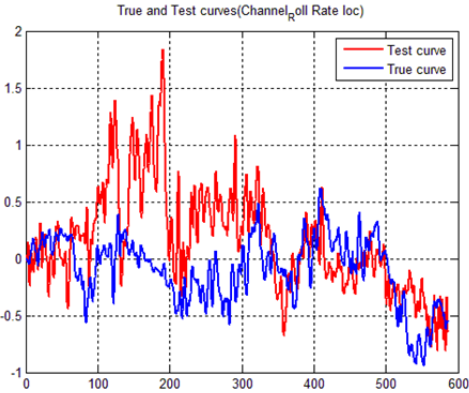


(a)

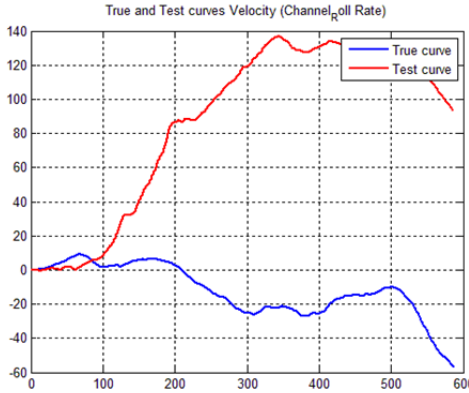


(b)

Figure F-3. Z-Channel (a) acceleration-time history data used to compute metrics and (b) integration of acceleration-time history data

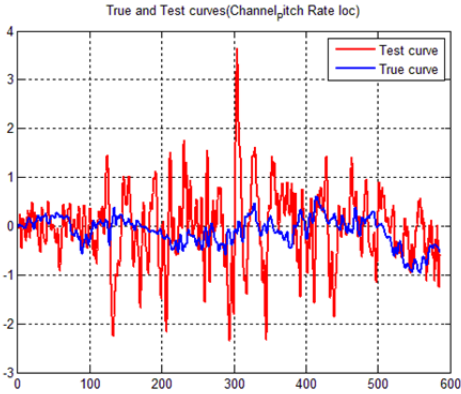


(a)

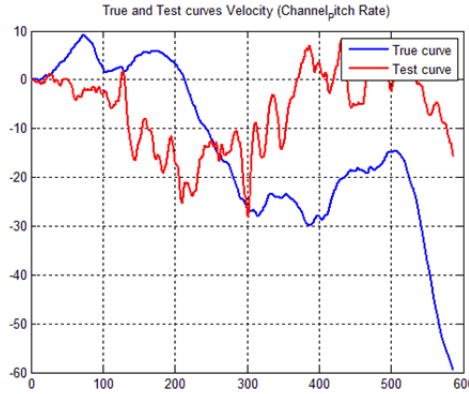


(b)

Figure F-4. Roll Channel (a) angular rate-time history data used to compute metrics and (b) integration of angular rate-time history data

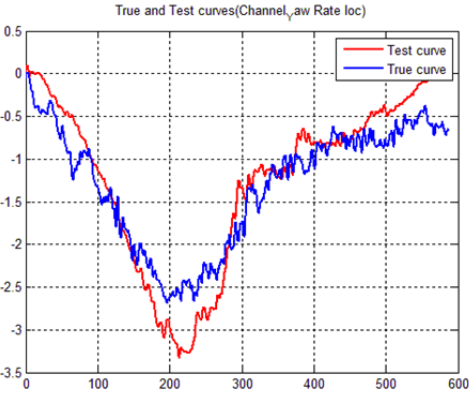


(a)

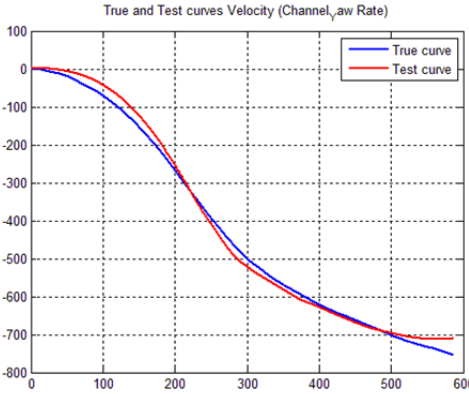


(b)

Figure F-5. Pitch Channel (a) angular rate-time history data used to compute metrics and (b) integration of angular rate-time history data



(a)



(b)

Figure F-6. Yaw Channel (a) angular rate-time history data used to compute metrics and (b) integration of angular rate-time history data

**Appendix G. - Validation for Small Car Striking a 31-in. MGS on Approach Slope**

VALIDATION/VERIFICATION REPORT  
FOR

A Report 350 820C Small Car  
(Report 350 or MASH or EN1317 Vehicle Type)

Striking a 31-in. tall Midwest Guardrail System on 8:1 Approach Slope  
(roadside hardware type and name)

Report Date: 5/31/2012

Type of Report (check one)

- Verification (known numerical solution compared to new numerical solution) or  
 Validation (full-scale crash test compared to a numerical solution).

General Information	Known Solution	Analysis Solution
Performing Organization	MwRSF	MwRSF/Julin
Test/Run Number:	MGSAS-2	MGSAS-2 SIM-2012_01
Vehicle:	2000 Geo Metro	MwRSF modified Geo (NCAC/Politecnico di Milano 820C)
<b>Impact Conditions</b>		
Vehicle Mass:	912 kg	899 kg
Speed:	99.62 km/h	100 km/h
Angle:	21.6 degrees	20 degrees
Impact Point:	Upstream of post no. 14	Upstream of post no. 14

**Composite Validation/Verification Score**

List the Report 350/MASH or EN1317 Test Number		3-10
Part I	Did all solution verification criteria in Table G-1 pass?	Yes
Part II	Do all the time history evaluation scores from Table G-2 result in a satisfactory comparison (i.e., the comparison passes the criterion)? If all the values in Table G-2 did not pass, did the weighted procedure shown in Table G-3 result in an acceptable comparison. If all the criteria in Table G-2 pass, enter "yes." If all the criteria in Table G-2 did not pass but Table G-3 resulted in a passing score, enter "yes."	Yes
Part III	All the criteria in Table G-4 (Test-PIRT) passed?	Yes
	Are the results of Steps I through III all affirmative (i.e., YES)? If all three steps result in a "YES" answer, the comparison can be considered validated or verified. If one of the steps results in a negative response, the result cannot be considered validated or verified.	Yes

The analysis solution (check one)  is  is NOT verified/validated against the known solution.

## PART I: BASIC INFORMATION

These forms may be used for validation or verification of roadside hardware crash tests. If the known solution is a full-scale crash test (i.e., physical experiment) which is being compared to a numerical solution (e.g., LSDYNA analysis) then the procedure is a validation exercise. If the known solution is a numerical solution (e.g., a prior finite element model using a different program or earlier version of the software) then the procedure is a verification exercise. This form can also be used to verify the repeatability of crash tests by comparing two full-scale crash test experiments. Provide the following basic information for the validation/verification comparison:

9. What type of roadside hardware is being evaluated (check one)?
- Longitudinal barrier or transition
  - Terminal or crash cushion
  - Breakaway support or work zone traffic control device
  - Truck-mounted attenuator
  - Other hardware: \_\_\_\_\_
10. What test guidelines were used to perform the full-scale crash test (check one)?
- NCHRP Report No. 350
  - MASH
  - EN1317
  - Other: \_\_\_\_\_
11. Indicate the test level and number being evaluated (fill in the blank). 3-10
12. Indicate the vehicle type appropriate for the test level and number indicated in item 3 according to the testing guidelines indicated in item 2.

### NCHRP Report No. 350/MASH

- |                                 |                                          |                                |
|---------------------------------|------------------------------------------|--------------------------------|
| <input type="checkbox"/> 700C   | <input checked="" type="checkbox"/> 820C | <input type="checkbox"/> 1100C |
| <input type="checkbox"/> 2000P  | <input type="checkbox"/> 2270P           |                                |
| <input type="checkbox"/> 8000S  | <input type="checkbox"/> 10000S          |                                |
| <input type="checkbox"/> 36000V |                                          |                                |
| <input type="checkbox"/> 36000T |                                          |                                |

### EN1317

- |                                                   |                                             |                                        |
|---------------------------------------------------|---------------------------------------------|----------------------------------------|
| <input type="checkbox"/> Car (900 kg)             | <input type="checkbox"/> Car (1300 kg)      | <input type="checkbox"/> Car (1500 kg) |
| <input type="checkbox"/> Rigid HGV (10 ton)       | <input type="checkbox"/> Rigid HGV (16 ton) |                                        |
| <input type="checkbox"/> Rigid HGV (30 ton)       |                                             |                                        |
| <input type="checkbox"/> Bus (13 ton)             |                                             |                                        |
| <input type="checkbox"/> Articulated HGV (38 ton) |                                             |                                        |



## PART II: ANALYSIS SOLUTION VERIFICATION

Using the results of the analysis solution, fill in the values for Table G-1. These values are indications of whether the analysis solution produced a numerically stable result and do not necessarily mean that the result is a good comparison to the known solution. The purpose of this table is to ensure that the numerical solution produces results that are numerically stable and conform to the conservation laws (e.g., energy, mass and momentum).

Table G-1. Analysis Solution Verification Table

Verification Evaluation Criteria	Change (%)	Pass?
<b>Total energy</b> of the analysis solution (i.e., kinetic, potential, contact, etc.) must not vary more than 10 percent from the beginning of the run to the end of the run.	1.96	Yes
<b>Hourglass Energy</b> of the analysis solution at the end of the run is less than <i>five percent</i> of the total <i>initial energy</i> at the <i>beginning</i> of the run.	0	Yes
<b>Hourglass Energy</b> of the analysis solution at the end of the run is less than <i>ten percent</i> of the total <i>internal energy</i> at the <i>end</i> of the run.	0	Yes
The part/material with the highest amount of hourglass energy at the end of the run is less than ten percent of the total internal energy of the part/material at the end of the run.	4.3	Yes
Mass added to the total model is less than five percent of the total model mass at the beginning of the run.	0.3	Yes
The part/material with the most mass added had less than 10 percent of its initial mass added.	0.9	Yes
The moving parts/materials in the model have less than five percent of mass added to the initial moving mass of the model.	0.3	Yes
There are no shooting nodes in the solution?	Yes	Yes
There are no solid elements with negative volumes?	Yes	Yes

The Analysis Solution (check one)  passes  does NOT pass all the criteria in Table E1-1  
 with  without exceptions as noted.

**PART III: TIME HISTORY EVALUATION TABLE**

Table G-2. Roadside Safety Validation Metrics Rating Table – Time History Comparisons

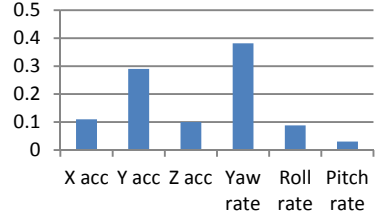
(single channel option)

Evaluation Criteria							Time interval [0 sec; 0.43 sec]						
O	<b>Sprague-Geers Metrics</b> List all the data channels being compared. Calculate the M and P metrics using RSVVP and enter the results. Values less than or equal to 40 are acceptable.						M	P	Pass?				
	<b>RSVVP Curve Preprocessing Options</b>												
		Filter Option	Sync. Option	Shift		Drift							
				True Curve	Test Curve	True Curve				Test Curve			
	X acceleration	CFC 180	Min. Area of Residuals	Y	N	Y				N	31.2	38.8	Yes
	Y acceleration	CFC 180	Min. Area of Residuals	Y	N	Y				N	36.9	25.6	Yes
	Z acceleration	CFC 180	Min. Area of Residuals	Y	N	Y				N	33.2	46	No
	Roll rate	CFC 180	Min. Area of Residuals	Y	N	Y				N	3.5	39.5	Yes
Pitch rate	CFC 180	Min. Area of Residuals	Y	N	Y	N	20.1	42.8	No				
Yaw rate	CFC 180	Min. Area of Residuals	Y	N	Y	N	12.9	10.8	Yes				
P	<b>ANOVA Metrics</b> List all the data channels being compared. Calculate the ANOVA metrics using RSVVP and enter the results. Both of the following criteria must be met: <ul style="list-style-type: none"> <li>The mean residual error must be less than five percent of the peak acceleration (<math>\bar{e} \leq 0.05 \cdot a_{Peak}</math>) and</li> <li>The standard deviation of the residuals must be less than 35 percent of the peak acceleration (<math>\sigma \leq 0.35 \cdot a_{Peak}</math>)</li> </ul>						Mean Residual	Standard Deviation of Residuals	Pass?				
	X acceleration/Peak									0.003	0.20	Yes	
	Y acceleration/Peak									0.07	0.28	No	
	Z acceleration/Peak									0.07	0.32	No	
	Roll rate									0.06	0.40	No	
	Pitch rate									0.06	0.31	No	
	Yaw rate									0.12	0.11	No	

The Analysis Solution (check one)  passes  does NOT pass all the criteria in Table G-2.

Table G-3. Roadside Safety Validation Metrics Rating Table – Time History Comparisons

(multi-channel option)

Evaluation Criteria (time interval [0 sec; 0.43 sec])				
Channels (Select which were used)				
<input checked="" type="checkbox"/> X Acceleration	<input checked="" type="checkbox"/> Y Acceleration	<input checked="" type="checkbox"/> Z Acceleration		
<input checked="" type="checkbox"/> Roll rate	<input checked="" type="checkbox"/> Pitch rate	<input checked="" type="checkbox"/> Yaw rate		
<b>Multi-Channel Weights</b>  <input checked="" type="checkbox"/> Area II method <input type="checkbox"/> Inertial method	<b>X Channel: 0.109794</b> <b>Y Channel: 0.290212</b> <b>Z Channel: 0.099994</b> <b>Yaw Channel: 0.381478</b> <b>Roll Channel: 0.088161</b> <b>Pitch Channel: 0.030361</b>			
O	<b>Sprague-Geer Metrics</b> Values less or equal to 40 are acceptable.		<b>M</b>	<b>P</b>
			23.3	25.2
P	<b>ANOVA Metrics</b> Both of the following criteria must be met: <ul style="list-style-type: none"> <li>The mean residual error must be less than five percent of the peak acceleration (<math>\bar{e} \leq 0.05 \cdot a_{Peak}</math>)</li> <li>The standard deviation of the residuals must be less than 35 percent of the peak acceleration (<math>\sigma \leq 0.35 \cdot a_{Peak}</math>)</li> </ul>		<b>Mean Residual</b>	<b>Standard Deviation of Residuals</b>
			0.05	0.22

The Analysis Solution (check one)  passes  does NOT pass all the criteria in Table G-3.

**PART IV: PHENOMENA IMPORTANCE RANKING TABLE**

Table G-4. Evaluation Criteria Test Applicability Table

Evaluation Factors	Evaluation Criteria			Applicable Tests	
Structural Adequacy	A	Test article should contain and redirect the vehicle; the vehicle should not penetrate, under-ride, or override the installation although controlled lateral deflection of the test article is acceptable.		10, 11, 12, 20, 21, 22, 35, 36, 37, 38	
	B	The test article should readily activate in a predictable manner by breaking away, fracturing or yielding.		60, 61, 70, 71, 80, 81	
	C	Acceptable test article performance may be by redirection, controlled penetration or controlled stopping of the vehicle.		30, 31,, 32, 33, 34, 39, 40, 41, 42, 43, 44, 50, 51, 52, 53	
Occupant Risk	D	Detached elements, fragments or other debris from the test article should not penetrate or show potential for penetrating the occupant compartment, or present an undue hazard to other traffic, pedestrians or personnel in a work zone.		All	
	E	Detached elements, fragments or other debris from the test article, or vehicular damage should not block the driver's vision or otherwise cause the driver to lose control of the vehicle. (Answer Yes or No)		70, 71	
	F	The vehicle should remain upright during and after the collision although moderate roll, pitching and yawing are acceptable.		All except those listed in criterion G	
	G	It is preferable, although not essential, that the vehicle remain upright during and after collision.		12, 22 (for test level 1 – 30, 31, 32, 33, 34, 35, 36, 37, 38, 39, 40, 41, 42, 43, 44)	
	H	Occupant impact velocities should satisfy the following:			10, 20, 30,31, 32, 33, 34, 36, 40, 41, 42, 43, 50, 51, 52, 53, 80, 81
		Occupant Impact Velocity Limits (m/s)			
		Component	Preferred	Maximum	
Longitudinal and Lateral	9	12	80, 81		
Longitudinal	3	5	60, 61, 70, 71		
I	Occupant ridedown accelerations should satisfy the following:			10, 20, 30,31, 32, 33, 34, 36, 40, 41, 42, 43, 50, 51, 52, 53, 60, 61, 70, 71, 80, 81	
	Occupant Ridedown Acceleration Limits (g's)				
	Component	Preferred	Maximum		
Longitudinal and Lateral	15	20			
Vehicle Trajectory	L	The occupant impact velocity in the longitudinal direction should not exceed 40 ft/sec and the occupant ride-down acceleration in the longitudinal direction should not exceed 20 G's.		11,21, 35, 37, 38, 39	
	M	The exit angle from the test article preferable should be less than 60 percent of test impact angle, measured at the time of vehicle loss of contact with test device.		10, 11, 12, 20, 21, 22, 35, 36, 37, 38, 39	
	N	Vehicle trajectory behind the test article is acceptable.		30, 31, 32, 33, 34, 39, 42, 43, 44, 60, 61, 70, 71, 80, 81	

Table G-5. (a) Roadside Safety Phenomena Importance Ranking Table (Structural Adequacy)

		Evaluation Criteria	Known Result	Analysis Result	Difference Relative/ Absolute	Agree?	
Structural Adequacy	A	A1	Test article should contain and redirect the vehicle; the vehicle should not penetrate, under-ride, or override the installation although controlled lateral deflection of the test article is acceptable. (Answer Yes or No)	Yes	Yes	X	Yes
		A2	Maximum dynamic deflection: - Relative difference is less than 20 percent or - Absolute difference is less than 0.15 m	0.635 m	0.509 m	19.8% 0.126 m	Yes
		A3	Length of vehicle-barrier contact: - Relative difference is less than 20 percent or - Absolute difference is less than 2 m	372 ms	300 ms	19.4%	Yes
		A4	Number of broken or significantly bent posts is less than 20 percent.	2	2	0%	Yes
		A5	Did the rail element rupture or tear (Answer Yes or No)	No	No	X	Yes
		A6	Were there failures of connector elements (Answer Yes or No).	No	No	X	Yes
		A7	Was there significant snagging between the vehicle wheels and barrier elements (Answer Yes or No).	No	No	X	Yes
		A8	Was there significant snagging between vehicle body components and barrier elements (Answer Yes or No).	No	No	X	Yes

Table G-5. (b) Roadside Safety Phenomena Importance Ranking Table (Occupant Risk)

Evaluation Criteria			Known Result	Analysis Result	Difference Relative/Absolute	Agree ?	
Occupant Risk	D	Detached elements, fragments or other debris from the test article should not penetrate or show potential for penetrating the occupant compartment, or present an undue hazard to other traffic, pedestrians or personnel in a work zone. (Answer Pass or Fail)	Pass	Pass	X	Yes	
	F1	The vehicle should remain upright during and after the collision although moderate roll, pitching and yawing are acceptable. (Answer Pass or Fail)	Pass	Pass	X	Yes	
	F	F2	Maximum roll of the vehicle: - Relative difference is less than 20 percent or - Absolute difference is less than 5 degrees.	11.3°	6.93°	38.7% 4.37°	Yes
		F3	Maximum pitch of the vehicle is: - Relative difference is less than 20 percent or - Absolute difference is less than 5 degrees.	3.2°	2.23°	30.3% 0.97°	Yes
		F4	Maximum yaw of the vehicle is: - Relative difference is less than 20 percent or - Absolute difference is less than 5 degrees.	28.6°	32.3°	12.9% 3.7°	Yes
	L	L1	Occupant impact velocities: - Relative difference is less than 20 percent or - Absolute difference is less than 2 m/s.				
			• Longitudinal OIV (m/s)	3.75	3.23	13.9% 0.52 m/s	Yes
			• Lateral OIV (m/s)	5.31	6.99	31.6% 1.68 m/s	Yes
			• THIV (m/s)	5.93	4.62	22.1% 1.31 m/s	Yes
		L2	Occupant accelerations: - Relative difference is less than 20 percent or - Absolute difference is less than 4 g's.				
			• Longitudinal ORA	4.03	4.81	0.78 g	Yes
			• Lateral ORA	9.65	7.61	2.04 g	Yes
	• PHD		9.68	12.56	2.88 g	Yes	
		• ASI	*N.R.	1.69			

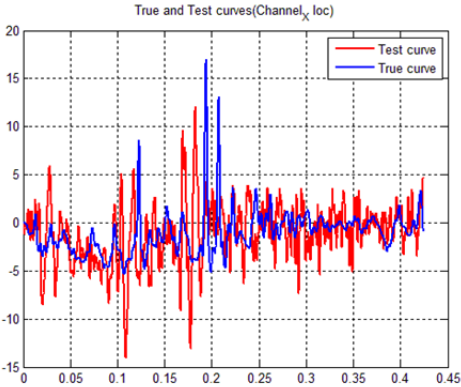
Table G-5. (c) Roadside Safety Phenomena Importance Ranking Table (Vehicle Trajectory)

Evaluation Criteria		Known Result	Analysis Result	Difference Relative/ Absolute	Agree?	
Vehicle Trajectory	M1	The exit angle from the test article preferable should be less than 60 percent of test impact angle, measured at the time of vehicle loss of contact with test device.	8.23° 41%	12.4° 62%	X	Yes
	M2	Exit angle at loss of contact: - Relative difference is less than 20 percent or - Absolute difference is less than 5 degrees.	8.23°	12.4°	51% 4.2°	Yes
	M3	Exit velocity at loss of contact: - Relative difference is less than 20 percent or - Absolute difference is less than 5 degrees.	51.5 km/h	53.7 km/h	4.3% 2.2 km/h	Yes
	M4	One or more vehicle tires failed or de-beaded during the collision event (Answer Yes or No).	Yes	N.M.*	X	

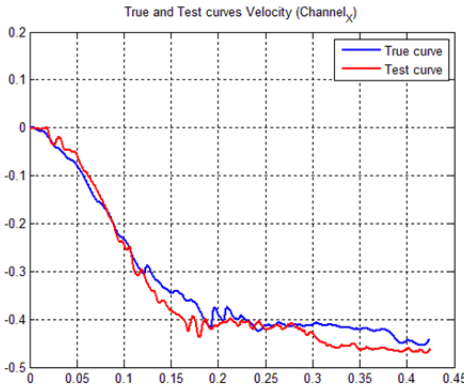
\*N.R. - Not Reported

\*N.M. - Not Modeled

The Analysis Solution (check one)  passes  does NOT pass all the criteria in Tables G-5a through G-5c  with exceptions as noted  without exceptions.

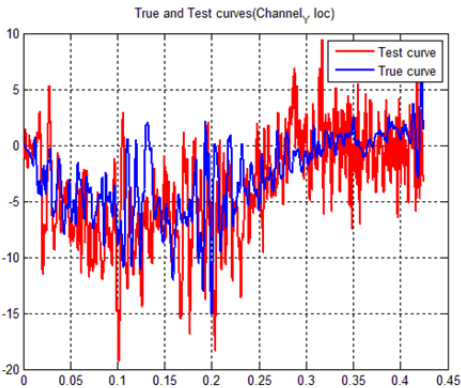


(a)

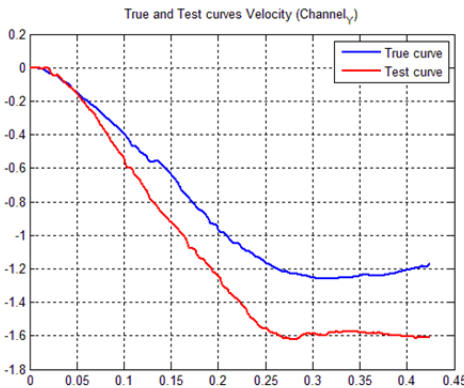


(b)

Figure G-1. X-Channel (a) acceleration-time history data used to compute metrics and (b) integration of acceleration-time history data

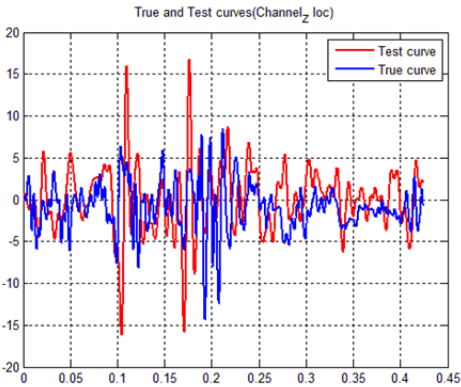


(a)

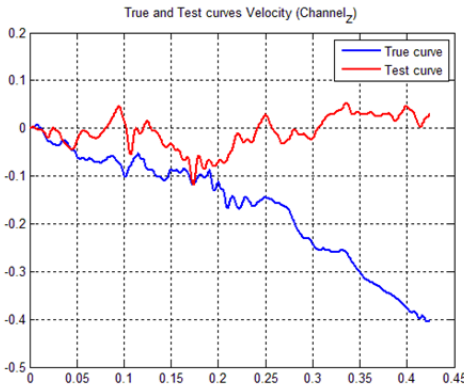


(b)

Figure G-2. Y-Channel (a) acceleration-time history data used to compute metrics and (b) integration of acceleration-time history data



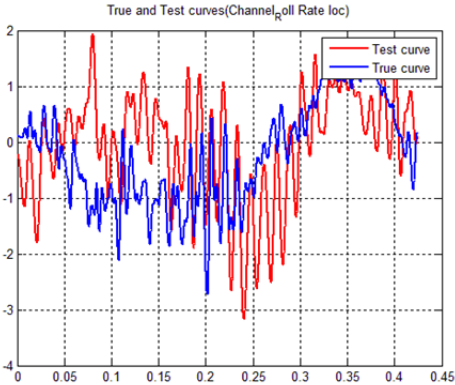
(a)



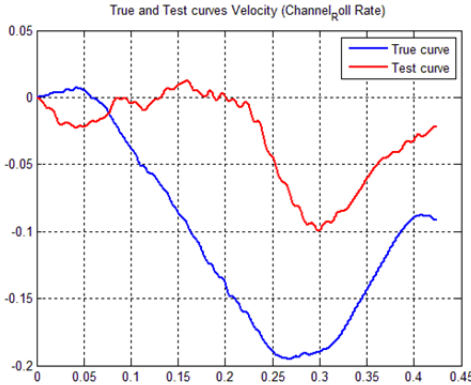
(b)

Figure G-3. Z-Channel (a) acceleration-time history data used to compute metrics and (b) integration of acceleration-time history data



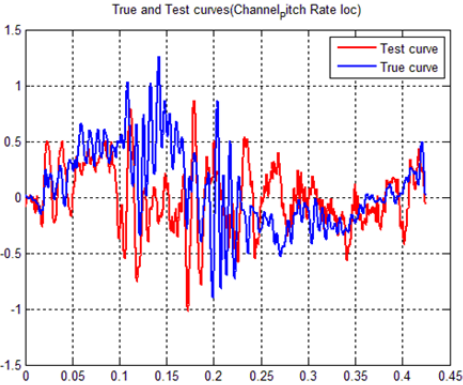


(a)

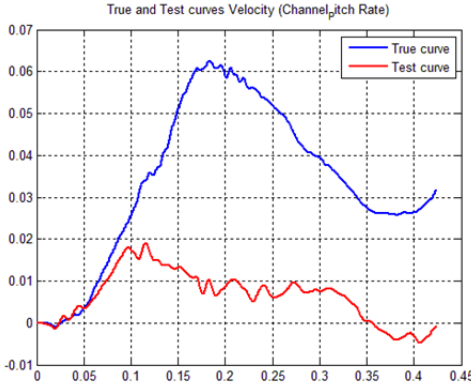


(b)

Figure G-4. Roll Channel (a) angular rate-time history data used to compute metrics and (b) integration of angular rate-time history data

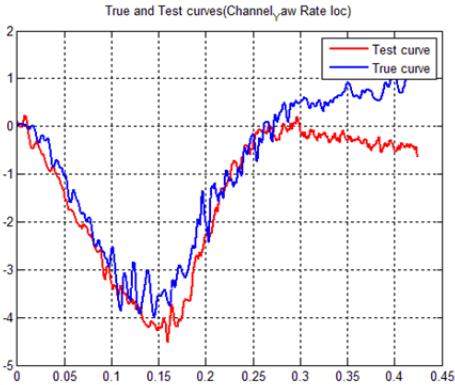


(a)

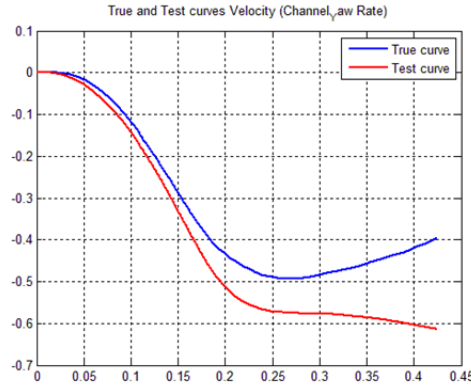


(b)

Figure G-5. Pitch Channel (a) angular rate-time history data used to compute metrics and (b) integration of angular rate-time history data



(a)



(b)

Figure G-6. Yaw Channel (a) angular rate-time history data used to compute metrics and (b) integration of angular rate-time history data

**END OF DOCUMENT**